1

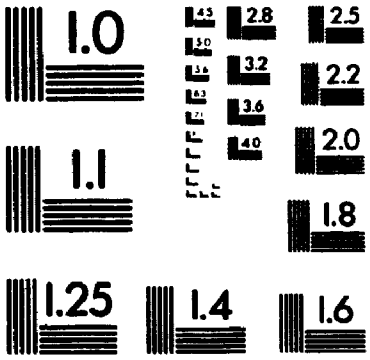

A Dynamic Model of the F404 Engine for Engine Health Monitoring Purposes

by

© Captain Brian D. Lewis, B.Eng., P.Eng.

A thesis submitted to the Faculty of Graduate Studies and Research in partial fulfillment of the requirements for the degree of Master of Engineering

Ottawa-Carleton Institute for
Mechanical and Aerospace Engineering

Department of Mechanical and Aeronautical Engineering
Carleton University
Ottawa, Ontario
Canada

May 1989

ISBN 0-315-54381-7

The undersigned hereby recommend to the Faculty of Graduate Studies and Research, acceptance of the thesis: "A Dynamic Model of the F404 engine for Engine Health Monitoring Purposes" submitted by Capt. B.D. Lewis, in partial fulfillment of the requirements for the degree of Master of Engineering.

Thesis Supervisor

Chairman
Department of Mechanical and
Aeronautical Engineering

ABSTRACT

Because the Canadian Forces have adopted an On-Condition Maintenance philosophy for the F404 engine installed in the CF-18 fighter aircraft, the development of reliable and effective methods of Engine Health Monitoring (EHM) is essential. One EHM technique is Module Performance Analysis which requires the use of a thermodynamic model in order to develop a fault library. Due to the nature of CF-18 operations, steady-state conditions are rarely sustained and therefore a model capable of simulating engine dynamic behaviour is necessary.

A component-based thermodynamic model that predicts the behaviour of the F404 during a transient has been developed. Steady-state component characteristics are utilized and, given ambient and flight conditions as well as inputs of fuel flow and exhaust nozzle area as functions of time, a series of module calculations are performed to determine the engine operating point at each time interval.

It is anticipated that the model will prove highly effective in investigating the effects that a wide range of faults have on the transient performance characteristics of the engine.

ACKNOWLEDGEMENTS

The model presented in this thesis was developed exclusively at GasTOPS Ltd., where free use of facilities, resources and expertise was generously provided. The cooperation, support and unending encouragment that I received from all GasTOPS personnel were most appreciated.

Most notably, I would like to thank the following individuals at GasTOPS who were integral in the success of the development of the model: Dr. B. D. MacIsaac, President of GasTOPS Ltd., who allowed me complete access to his facilities; Mr. D. E. Muir, who implemented and oversaw the project; Mr K. J. Kirkhope for his insightful suggestions and experienced analysis of problems that arose; and, Mr. B.I. Forsyth, whose infectious enthusiasm and regular brilliance were continual sources of inspiration.

I would also like to express my appreciation to Professor H.I.H. Saravanamuttoo for the advice and direction he provided as thesis supervisor.

Finally, I would like to thank my wife, Pamela, for her patience, understanding and encouragement.

TABLE OF CONTENTS

LIST OF TABLES

LIST OF FIGURES

NOMENCLATURE

A_i	-	flow area at station i
Cp_i	-	specific heat at station i
ECV_4	-	effective calorific value of combustor fuel
ECV_r	-	effective calorific value at reference temperature
EPR	-	engine pressure ratio
f	-	fuel/air ratio
F_g	-	gross thrust
F_{gb}	-	baseline thrust
F_{gc}	-	corrected gross thrust
g_c	-	gravitational constant
G	-	torque
h_i	-	enthalpy of gas at station i
h_{ref}	-	enthalpy at reference temperature
I	-	polar moment of inertia
I_1	-	polar moment of inertia of LP rotor
I_2	-	polar moment of inertia of HP rotor
k_{BL1}	-	bleed factor - HP turbine bleed flow
k_{BL2}	-	bleed factor - LP turbine bleed flow
k_{BL3}	-	bleed factor - HP rotor torque calculation
k_{BL4}	-	bleed factor - LP rotor torque calculation
k_{h16}	-	bypass duct heat injection factor
k_{L01}	-	intake pressure loss factor
k_{L34}	-	combustor pressure loss factor
k_{L6}	-	mixer pressure loss factor
k_{LF}	-	fan leakage flow factor
k_{LN}	-	nozzle leakage flow factor
k_{wAI}	-	engine anti-ice bleed flow factor
M_i	-	Mach number at station i
N	-	rotational speed
N_1	-	LP rotor speed
N_2	-	HP rotor speed
PLA	-	power lever angle
P_i	-	total pressure at station i
P_{si}	-	static pressure at station i

P_{ref}	-	reference pressure (14.7 psia)
Q	-	flow parameter, $W\sqrt{T}/P$
R	-	gas constant
t	-	time
$TSFC_c$	-	corrected thrust specific fuel consumption
T_i	-	total temperature at station i
T_{si}	-	static temperature at station i
T_{ref}	-	reference temperature (519 °R)
V	-	intercomponent volume
V_2	-	bypass duct and intercompressor volume
V_3	-	combustor volume
V_4	-	inter-turbine duct volume
V_6	-	tailpipe volume
W_i	-	mass flow at station i
W_{f3}	-	combustor fuel flow
W_{f3c}	-	corrected combustor fuel flow
W_{BL1}	-	bleed flow to HP turbine
W_{BL2}	-	bleed flow to LP turbine
W_{LF}	-	fan leakage flow
β_L	-	fan variable geometry setting
β_H	-	HP compressor variable geometry setting
γ_i	-	isentropic index at station i
θ_h	-	theta function for enthalpy
θ_r	-	theta function at reference temperature
θ_i	-	corrected temperature at station i (T_i/T_{ref})
δ_i	-	corrected pressure at station i (P_i/P_{ref})
η	-	isentropic efficiency
η_{a1}	-	intake efficiency
η_{34}	-	combustor efficiency
η_{m1}	-	mechanical efficiency of LP spool
η_{m2}	-	mechanical efficiency of HP spool
ϕ_i	-	momentum balance term at station i
Δt	-	integration time step

Station Numbers (refer to figure 4)

a	-	ambient
1	-	fan inlet
2.1	-	fan exit
2.5	-	compressor inlet
3	-	compressor exit/combustor inlet
4	-	combustor exit/HP turbine inlet
4.4	-	HP turbine exit
4.6	-	LP turbine inlet
5.6	-	LP turbine exit (at mixer inlet)
1.4	-	Bypass duct inlet
1.6	-	Bypass duct exit (at mixer inlet)
6	-	Mixer exit, ideal (before pressure losses)
6.1	-	Mixer exit, actual (after pressure losses)
7	-	Exhaust nozzle inlet
8	-	Exhaust nozzle throat
9	-	Exhaust nozzle exit

Subscripts

FAN	-	fan
g	-	guess
HPC	-	high pressure compressor
HPT	-	high pressure turbine
LPT	-	low pressure turbine
N	-	exhaust nozzle
R	-	inlet ram condition
ref	-	reference condition
x	-	extraction

Chapter 1

INTRODUCTION

1.1 General

The traditional maintenance philosophy for gas turbine engines of Canadian Forces fighter aircraft is based on scheduled inspections and subsequent engine/component repair or removal/replacement. First and second line maintenance actions (servicing or "snag" repairs and periodic inspections) are usually carried out at the field level; third-line work (engine overhaul and component repair) is performed by a contractor. The intervals between each of these actions, which are based on engine operating hours, are set initially by the engine manufacturer and periodically revised by the operator or manufacturer according to subsequent maintenance experience. In support of this overall engine maintenance concept, a spare engine reserve equal to 50 - 60% of the total engine fleet is typically required [1].

As the costs associated with fighter engines increase and the size of fighter aircraft fleets decrease, ways of reducing operating expenditures while improving aircraft availability and airworthiness gain increasing importance. As a result, the practice of fixing the time between overhauls has gradually been dropped by military operators (as well as some civilian operators) in favour of a potentially much more efficient engine maintenance program based on the On-Condition Maintenance (OCM) approach. This approach has been adopted for the F404 engines of the Canadian Forces main fighter aircraft, the CF-18.

1.2 The OCM Approach

The OCM philosophy, which can reduce an operator's spare engine requirement to just 5 - 10% of the total engine fleet size [1], is characterized by:

a) short, frequent inspections of the engine at the first-line level to assess its overall health and suitability for further operations;

b) no scheduled overhauls and (ideally) no complete engine overhauls for engines of modular construction;

c) the use of a system to identify certain critical life-limited components, assign "lives" to these components, and track their life consumption in order to minimize the probability of catastrophic failure; and,

d) a comprehensive Engine Health Monitoring (EHM) program, to be used for early detection of progressive engine deterioration and for diagnosis of engine faults.

The OCM approach is being readily adopted by several gas turbine engine maintainers mainly due to the realization that the wide variance in timing of various gas turbine engine failures makes setting fixed overhaul intervals based on expected mean time between failures (MTBF's) ineffective.

If it is assumed that all parts have a high enough strength upon installation to operate at the required stress level with some margin of safety, then gas turbine engine failure modes can generally be classified into three categories, as shown in figure 1 [2]:

a) Instantaneous;

b) Time dependent; and.

c) Delayed time dependent.

Failure mode (a) is instantaneous and occurs at random and without warning - any gradual deterioration is not considered detectable and, therefore, no degree of monitoring can be of any

practical use in preventing such failures. Fatigue failures, for example, are included in this category.

Since mandatory periodic inspections and overhauls are eliminated as part of the OCM approach, Engine Health Monitoring (EHM) is used to detect and diagnose developing problems such as those depicted by failure modes (b) and (c). The rate of degradation, whether delayed or not, is considered slow enough that a monitoring scheme could provide sufficient advanced warning of an impending failure. Furthermore, if the rate of degradation is definable (parameter trending), it may also be possible to predict the remaining useful life of the component. The early detection of faults should help to reduce operating costs since maintenance personnel will be able to replace components before repairable limits are exceeded. Also, the timely rectification of a fault should reduce the amount of secondary damage caused by that fault. Hence, effective EHM is considered to be a cornerstone of any successful OCM approach.

1.3 Available EHM Techniques

A number of wide-ranging EHM techniques are presently in use or under development, including:

a) Vibration Analysis (VA);
b) Sonic Analysis (SA);
c) Contaminant Analysis (CA)
    (1) Spectrometric Oil Analysis Program (SOAP)
    (2) Magnetic chip detectors and filters
    (3) Ferrography
    (4) Seta Flash
d) Borescope Inspections; and,
e) Engine Performance Monitoring (EPM).

Based on the results achieved versus the intended objective of each technique, however, only borescope inspections have thus far

been successful on the F404 engine and further development of the remaining techniques is required before their practical use can be fully implemented [3].

Gradual deterioration in performance, while usually the result of mechanical degradation (such as erosion, corrosion, dirt build-up, worn seals, loss of tolerances, temperature distortions, plugged nozzles, tip wear, leakages, etc.) is extremely difficult to assess using mechanical monitoring techniques. However, Engine Performance Monitoring (EPM), which includes Trend Analysis (TA) and Module Performance Analysis (MPA) (also known as Gas Path Analysis or GPA), is a very promising technique for identifying this type of engine health deterioration.

Trend Analysis is the simplest form of EPM. It consists of periodically determining any deterioration in engine health by plotting actual engine performance parameters versus time and comparing the results to established nominal, or baseline, plots. A sudden change in deviation or a rapidly rising trend indicates that a fault has probably occurred and maintenance action is required.

The basic premise underlying Module Performance Analysis is that the overall performance of an engine (in other words, the ability of the engine to produce a specified thrust/power output for a given fuel flow input or throttle demand) is directly related to the condition of its mechanical components which, in turn, can be defined by the thermodynamic relationships which govern engine operation. MPA is a technique by which a mathematical model is developed and utilized to investigate this coupling between the thermodynamic behaviour and mechanical health of the engine modules. The model can then be used to systematically develop a "fault library" for the engine. A schematic of the OCM approach showing where engine modelling fits in is included as figure 2. Figure 3 illustrates the use of a model in the development of a fault library.

1.4 The F404 Engine

Each CF-18 fighter aircraft in the Canadian Forces inventory is powered by two F404-GE-400 engines. The F404 is a modern, high performance, variable geometry, low bypass, twin-spool, turbofan engine with a mixed flow exhaust and afterburner. It consists of six major modules: the fan, high pressure compressor, combustor, high pressure turbine, low pressure turbine, and afterburner. A schematic of the engine showing the station numbering, which is based on standard S.A.E. practices and employed in this thesis, is presented in figure 4. Due to the F404's modularity, it has been readily adapted to an OCM program, a primary objective of which is to be able to isolate all engine faults to either an external component (such as the Electronic Control Unit (ECU), fuel pump, oil cooler, etc.) or to a major module [1].

EPM techniques for this engine have, to date, been focussed mainly on its steady-state performance. Consistent with the MPA technique, a component-based thermodynamic steady-state computer model capable of accepting implanted faults has been developed [4]. Using this model, a module performance "fault library" associated with steady-state operation has been derived as shown in figure 3.

Due to the nature of fighter aircraft operations, engine steady state conditions are rarely achieved for any length of time and generally must be investigated when the engine is in an Engine Test Facility (ETF). Furthermore, in-flight dynamic performance is not considered repeatable, except during take-off rolls. Therefore, if on-wing, operational F404 engine performance is to be monitored on a continual basis, two requirements are necessary:

a) suitable, readily available, engine take-off data; and,

b) a thorough understanding of the engine's dynamic behaviour in order to develop a fault library to assess transient response.

Fortunately, the CF-18 was delivered to the Canadian Forces with the capability to record appropriate engine parameters in flight, as will be discussed in the next section.

1.5 The In-Flight Engine Condition Monitoring System (IECMS)

A current practice amongst fighter aircraft/engine manufacturers is to incorporate a fully integrated on board engine condition monitoring system and this applies to the CF-18/F404 airframe/engine combination. The In-Flight Engine Condition Monitoring System (IECMS) aboard each CF-18 continuously records 13 different engine parameters and several additional aircraft parameters. Table 1 provides a listing of engine parameters recorded by the IECMS and the recording frequency.

The IECMS automatically records engine performance data during each take-off roll and whenever an engine operating limit (fan speed, compressor speed, exhaust gas temperature, oil pressure or vibration) is exceeded. The IECMS recordings can also be activated by a pilot record button located in the cockpit. The take-off recordings are typically 6 - 10 seconds in duration, starting when the throttle lever is advanced to the take-off power setting (a power lever angle (PLA) of 100°) and ending when the aircraft lifts off (weight off wheels). The exceedance and pilot-activated recordings consist of 5 seconds of pre-event and 35 seconds of post-event data.

The IECMS take-off data is probably the most attractive source of EPM data, since the recording of take-off data is software-initiated (hence there is minimal involvement of personnel in the data collection process) and all IECMS take-off recordings are archived and available for analysis. Hence, due to the vast amount of this data

already collected, its ready availability after each flight for monitoring purposes, and the nature of CF-18 operations, operational Engine Performance Monitoring procedures should centre on the take-off recordings provided by the IECMS.

1.6 Purpose

As each take-off is transient in nature, a clear understanding of the expected dynamic behaviour of the F404 is required in order to assess the current state of health of the engine based on the most recent IECMS take-off recordings. It has been concluded by Henry [3] that, provided repeatability factors are considered, the use of IECMS data for operational EPM purposes is viable. To date, however, only a limited number of statistically based engine health indices have been derived from IECMS take-off recordings [5]. Thus, the development of a dynamic model capable of operating with embedded faults is required in order to augment the existing fault library by investigating the effects that a wide range of engine faults would have on the transient performance characteristics of the engine. It is within this context that this thesis topic was selected.

1.7 Scope

This thesis will present a digital computer dynamic model of the F404 engine, as installed in the CF-18 aircraft. The model will be used to predict the engine's dynamic behaviour during take-off accelerations (from idle to military power). An investigation of the various modelling techniques used by other authors in previous studies of engine dynamic behaviour will be conducted and the reasons for choosing the method to be used in this thesis will be discussed.

All first-order effects will be included in the model; any second- and third-order effects, such as engine metal thermal absorption rates, clearance changes, seal openings, etc. will not be incorporated. The model will, however, be developed in modular

fashion such that ready inclusion of these effects (if deemed necessary) will be possible in the future. Similarly, only a basic open-loop consideration of the control system will be included as a discrete module which will allow a more in-depth description of the control dynamics to be developed in future model refinements.

Using data available from the In-Flight Engine Condition Monitoring System, the model will be validated as follows:

a) a comparison of the model's steady-state predictions with IECMS steady-state ground run data; and,

b) a comparison of dynamic results predicted by the model with the parameter data provided by IECMS for two separate aircraft take-offs (four different engines).

A further verification of the model's accuracy will be a comparison with the data presented by the existing F404 steady-state computer model [4].

As already mentioned, the model is intended to be used primarily as a tool for Engine Health Monitoring purposes and, therefore, will be designed to accept implanted faults as part of follow-on EHM analysis. Because of this application, modelling of the engine dynamics in real time is not considered a requirement, although minimizing computation time is clearly desirable.

Chapter 2

BACKGROUND

2.1 General

Analytical and experimental investigations of the dynamic behaviour of gas turbines have progressed steadily since they began in the late 1940's when computers were in their infancy. Throughout four decades of development mathematical models, or simulations, of gas turbine dynamic response have been derived almost exclusively for three main purposes:

a) To help minimize control system design/development time and costs;

b) To investigate means of improving the thrust response of developmental and in-service engines: and,

c) To provide engine manufacturers with the capability to guarantee thrust response rates to customers as early as the proposal stage.

It has not been until recently that dynamic modelling as a fault detection and diagnostic tool for Engine Health Monitoring purposes has been considered [3, 6, 10].

2.2 The Linear System Approach

The first published work on the dynamic behaviour of gas turbines was probably that of Otto and Taylor [11]. They derived equations for small perturbations about an equilibrium point by assuming the gas turbine could be approximated by a linear first-order system with the response of rotor speed to a step change in fuel flow being a simple lag. The engine was considered as a "black box" with defined input parameters, transfer functions and output

parameters. The output dynamic response was obtained by linearizing the response over a small range of given equilibrium points. Several simulations of the dynamics of single spool engines based on this simple approach then followed; for example [12, 13].

Emphasis was soon placed on improved methods of calculating the rotor-speed time constant based on available steady-state data [14]. An important advancement in this analysis was made by Lawrence and Powell of the Lucas Company [15] when they assumed that, following a step change in fuel flow, the turbine torque would change instantaneously whereas the compressor torque would briefly remain unchanged. As a result of this simplified analysis, the rotor time constant could be expressed in terms of thermodynamic parameters that could be easily obtained from steady-state data, making the method relatively quick, convenient and accurate.

In the midst of these studies on the dynamic behaviour of single-spool gas turbines was an analysis by Novik [16] on the dynamics of a twin-spool engine for small perturbations. While treating the engine as a linear system, time constants for the rotors were obtained in terms of partial derivatives; however, because of the number of derivations involved, it was cumbersome to predict engine dynamics.

The main disadvantage in modelling the dynamic behaviour of gas turbines based on the linear system approach was that, due to the highly non-linear nature of the gas turbine, the method was limited to small changes in speed (approximately ±5% [17]) from the equilibrium state and did not give much insight into the physical operation of the engine beyond the rotor speed response. Nevertheless, this somewhat elementary early approach was very successful in identifying and explaining the parameters which affect the response rate of gas turbines.

2.3 The Non-Linear System Approach

The shortcomings of the linear system approach prompted Saravanamuttoo and Fawke [18] to define the requirements for a successful mathematical model of gas turbine dynamic behaviour. The prime requirement was that the model/simulation must accurately represent the engine response over the entire running range. The other important requirements were broken down in reference 18 as follows:

"a) Flexibility - The simulation must be able to represent all modes of transient behaviour such as scheduled accelerations and decelerations, step changes, frequency response tests and the operation of variable geometry devices. It must also be capable of arbitrary selection of ambient or flight conditions and revision of component characteristics as the development program proceeds.

b) Credibility - The simulation must be readily understandable to performance, development and management engineers, producing results in a form similar to a real engine and making use of commonly available data.

c) Availability - The simulation, once proved in operation, must be capable of being rapidly brought into use whenever required.

d) Reliability - A high degree of reliability and repeatability is clearly essential and it must be easy to verify that the simulation is functioning correctly."

Long before these requirements were formally identified, treatment of the gas turbine as a non-linear system was considered in order to overcome the limitations of the linear system approach. The method involved the application of a necessary matching condition with a knowledge of the compressor, turbine and nozzle

characteristics as well as engine layout, so that the engine dynamics could be accurately predicted. Reference [19] provides the most comprehensive treatment of component matching and off-design operation.

A fundamental assumption used in the component-based thermodynamic approach was that of quasi-steady flow in each major component. Since the mechanical inertia of the system was large relative to the aerodynamic inertias, it tended to dominate the transient response. Therefore, the use of established steady-state component characteristics in the dynamic model was considered acceptable.

In addition to meeting the requirements of dynamic modelling laid down by Saravanamuttoo and Fawke, this approach has several other advantages. Models of this type provide a better description of the thermodynamic processes within the engine and allow the behaviour of any engine parameter to be "tracked" throughout a transient. The model's flexibility allows conditions such as airflow bleeds, engine variable geometry and operating limits to be incorporated. Second-order effects, such as the influence of the thermal capacity of the compressors and turbines on the transient response, can be readily included. The effects that specific modes of component degradation have on overall engine performance can be determined by appropriately modifying the individual component characteristics.

Dugan and Filippi [20], who considered accelerations of a twin-spool turbojet engine following a large step change in fuel flow, were amongst the first to publish work based on the non-linear system approach. Their method consisted of finding a series of engine operating points for which flow compatibility but not work compatibility was satisfied and from the resulting rotor torque imbalance at these points, the spool acceleration rates were predicted. For each time increment, an updated rotor speed was obtained and an

iteration loop was then followed to balance the flows. This was the genesis of the Iterative Method.

Fawke and Saravanamuttoo [21] pointed out that the assumption of flow compatibility in the Iterative Method was physically unrealistic, as it implied that pressures and mass flows within the engine can change instantaneously. They developed a component-based thermodynamic model that has been widely adopted [22] which includes the dynamics of the pressure changes in the engine. The major components maintain a quasi-steady flow throughout the transient such that the steady-state characteristics can be used. Flow imbalances are accounted for in the volumes between the components where all the non-steady flow is considered concentrated. By taking a value for these "intercomponent volumes" and applying the gas laws, time-dependent pressure derivatives can be evaluated and the flow balance iteration loop can be avoided [23, 24].

The Method of Intercomponent Volumes differs from the Iterative Method mainly in the transient predicted immediately following a rapid change in fuel flow or nozzle area, as shown in Figure 5 [21]. It is readily apparent that the Method of Intercomponent Volumes more closely represents actual engine dynamic response in the low speed range than the Iterative Method. For a complex engine, the overall computing time required for short term transients will be somewhat less for the Method of Intercomponent Volumes than for the Iterative Method. Although fewer points in time are required for a given transient calculated with the Iterative Method since larger time steps can be used, much more computation time per point is needed as several passes through the engine calculation are required before flow compatibility is achieved. Hence, the main advantage of the Iterative Method is that it is more efficient in calculating long-term transients as very large steps in time are acceptable.

The model to be developed in this thesis will be used to predict relatively short term transients experienced during a take-off roll. Therefore, to maintain the best computing efficiency possible while obtaining an excellent physical representation of the engine dynamics, the Method of Intercomponent Volumes will be used in this thesis and will be discussed in more detail in Chapter Three.

2.4 Second-Order Effects

The development of methods for synthesizing transient response since the widespread acceptance of component-based thermodynamic models has centered on pinpointing the accuracy of the results. Investigations have been focussed on second-order effects that are considered by some analysts to be important enough to be included in a model of an engine's dynamic behaviour in order to obtain results that are in closer agreement with actual engine data. The first to identify some of these effects was Bauerfeind [25] who considered the following:

a) the heat exchange between the gas stream in the engine and the material of the components, together with concurrent tip clearance changes, and their combined effect on the component characteristics and performance;

b) the "packing lag" for filling up volumes in the engine whenever the pressure and temperature change; and,

c) the transient performance of the combustion system (the "combustion lag").

The "packing lag" has since been accounted for by the pressure derivative formulation in Fawke and Saravanamuttoo's inter-component volume method. It was concluded in [18] that the "combustion lag" is significant for vaporizing type combustors but does not seem to be a necessary consideration for atomizing type

combustors; in any event, the combustion process is considered so rapid that the combustion lag can almost always be neglected [26].

Since Bauerfeind, considerable effort has been expended in improving the modelling of the heat transfer effects and tip/seal clearance changes during a transient and investigating their influence on the accuracy of the overall dynamic model under various acceleration/deceleration conditions. The salient results of studies of these effects by Fawke and Saravanamuttoo [27], Maccallum et al [28 - 33] and others [34, 35] can be summarized as follows:

a) During an acceleration, some of the energy from the increasing fuel flow will be absorbed as the component metal heats up and this will lead to a slower response rate. However, this appears to affect only the attainment of the last few percent of demanded thrust as most of the heat is transferred very rapidly and some 95% of the desired thrust will be achieved in about the first 3 seconds. It takes between thirty seconds and five minutes for the engine metal to reach thermal equilibrium. An appropriate reduction in the fuel flow rate is a simple method that can be used to account for this effect

b) Heat transfer has a greater effect on decelerations than on accelerations because on decelerations the fuel flow is low and the flow of heat from the engine metal to the working fluid has a more significant effect on the energy transfers within the engine.

c) Heat transfer has a greater effect at altitude than at sea level because at altitude the fuel flow must be reduced due to the lower air mass flow but the thermal capacity of the engine components remains unchanged. Again, the component heat capacity has a more significant effect on the energy transfers within the engine.

d) There is a considerable decrease in acceleration time for a "hot reslam" compared to a normal acceleration. A hot reslam occurs when an engine is run at maximum rating, for example, decelerated and then re-accelerated almost immediately. The metal temperatures will be higher at the start of this acceleration than for a normal acceleration and, therefore, smaller amounts of heat energy will be extracted from the working fluid.

e) During an acceleration, the tip clearances in the HP compressor and HP turbine initially decrease slightly during the short term transient because the centrifugal and thermal growth of the blades is greater than the thermal growth of the component casing. After approximately five seconds, as the thermal expansion of the casing becomes dominant, the tip clearances increase beyond their steady-state values by a significant amount, and then gradually return to their stabilized values as thermal equilibrium is re-established. This variance in tip clearances results in small component efficiency changes throughout a transient.

f) Possibly the strongest influence on the accuracy of dynamic models for some engine designs lies in the response of seals which control cooling air flows. Seals may exhibit openings during an acceleration which are up to double those at steady-state conditions and increases in cooling air flows are directly proportional to the amount the seals open.

As mentioned previously, these effects are not included in the dynamic model developed herein. However, the model has been designed in modular fashion such that if, after careful analysis, it is determined that inclusion of these effects is necessary in order to better the accuracy of the model results, they can be readily incorporated.

Chapter 3

THEORY

3.1 General

A component-based thermodynamic approach based on the Method of Intercomponent Volumes will be used in this thesis to model the dynamic behaviour of the F404 engine during CF-18 take-offs. This chapter will first describe a typical F404 take-off acceleration profile and then explain the theory behind this modelling procedure.

3.2 F404 Accelerations

When the pilot commences a CF-18 take-off roll by "slamming" the throttle forward to a power lever angle (PLA) of at least 100°, a series of control system inputs results in the following sequence of events within the engine [3, 36]:

a) An immediate closing of the nozzle throat area to its fully shut position occurs in order to avoid overspeeding and subsequent surging of the fan.

b) As the high pressure (HP) turbine is choked over most of its operating range, the flow parameter ($W\sqrt{T}/P$) at the turbine entrance (combustor exit) is fixed. If it is assumed that the addition of energy due to the increased fuel flow is instantaneous, there will be an instantaneous rise in total temperature at the HP turbine entrance which must be offset by a corresponding decrease in mass flow such that the flow parameter remains constant.

c) The decrease in mass flow at the HP turbine entrance produces a relatively large flow imbalance in the combustor,

causing the HP compressor delivery pressure to rise rapidly. Concurrently, torque (or power) imbalances occur between the turbines and the compressors but the heavy mechanical inertias of the rotors result in a comparatively slower rotor speed response.

d) Therefore, during the start of a transient, the rapid rise in HP compressor pressure ratio is due mainly to the initial increase in fuel flow and must be limited by a modulation of the fuel flow in order to avoid HP compressor surge. Eventually, the rotors begin to accelerate as they overcome inertia effects and fuel is controlled in order to maintain the HP compressor operating line as close to the surge line as possible (within a reasonable margin of safety, or surge margin) as this produces the quickest rotor speed, and hence thrust, response. At the same time, the control system also ensures that no other engine operating limit, for instance maximum allowable turbine inlet temperature (TIT), maximum allowable rotor speeds, etc., is exceeded.

e) Once the torque/power balance between the compressors and turbines is restored, steady-state operation at a new speed is achieved.

3.3 Gas Turbine Engine Modelling Theory - General

For a given engine, if the details of the engine layout and component characteristics are known, then the gas turbine is precisely defined and a model of the engine can be developed. Any model of gas turbine dynamic behaviour is generally mathematical and usually consists of a number of equations which are solved for a variety of conditions. If the model is proven to be sufficiently accurate for its application, then the actual behaviour of the engine can be inferred from that of the model.

3.4 Component-Based Thermodynamic Models

Because the mechanical inertia of the system is large relative to the aerodynamic inertias, the rotor speed dynamics tend to dominate the transient response of a gas turbine engine. This leads to a fundamental assumption used in component-based thermodynamic models which states that quasi-steady flow occurs in each of the major components during a transient. This assumption permits the use of standard steady-state performance characteristics, or maps, to define component operation. The maps describe the flow and temperature rise or drop (or efficiency) for each component in terms of the corrected speed ($N/\sqrt{\theta}$) and the pressure ratio. Given inlet conditions, outlet pressure and the rotor speed for each component, its map, which can be readily stored in tabular form in the memory of a digital computer, can be accessed to produce component flow and outlet temperature. Thus, component maps provide a means of calculating the torque absorbed or generated by each component.

If the compressor and turbine torques on each rotor are not equal (allowing for minor mechanical losses in the shaft bearings), there will be a net torque acting to accelerate or decelerate the rotor, depending on the relative magnitudes of the torques. Increments of net torque associated with time increments of fuel flow and/or nozzle area change result in increments of rotor acceleration which are then continuously integrated to find the change of rotor speed for each time interval until work compatibility is re-established. Considering the HP rotor, in general the net torque is given by (refer to figure 4 for station numbering):

$$\Delta G = \frac{\eta_{m2} W_4 Cp_4 (T_4 - T_{4A}) - W_{2.5} Cp_{2.5} (T_3 - T_{2.5})}{2\pi N_2} - G_x$$

From this equation and a knowledge of the rotor moment of inertia, the rotor rotational speed derivative can be calculated:

$$\frac{dN_2}{dt} = \frac{\Delta G}{2\pi I_2}$$

When a gas turbine is in a state of torque imbalance there is often, but not always, an imbalance in the flows at one or more locations within the engine. As discussed in Chapter Two, one way this flow mismatch may be modelled is by using the Method of Intercomponent Volumes.

3.5 The Method of Intercomponent Volumes

One of the first requirements for the design of a dynamic model based on the Method of Intercomponent Volumes is the selection of a set of engine parameters such that when the externally controlled variables of fuel flow, exhaust nozzle area, flight conditions and bleed and power extractions are specified, the operation of each engine component and hence the overall engine can be determined. Fawke and Saravanamuttoo [21] named this set of engine parameters the state vector, $\vec{x}$, and assigned it the following parameters for a twin-spool turbojet:

$$\vec{x} = (N_1, N_2, P_2, P_3, P_5, P_6)$$

where N_1 = Low pressure spool speed
N_2 = High pressure spool speed
P_2 = Intercompressor total pressure
P_3 = High pressure compressor exit total pressure
P_5 = Inter-turbine total pressure
P_6 = Low pressure turbine exit total pressure

In a later paper on the dynamic modelling of a twin-spool turbofan with mixed exhausts [27], they chose a total of eight parameters for the engine state vector:

$$\vec{x} = (N_1, N_2, P_2, P_3, P_5, P_{6s}, P_7, T_7)$$

The first six parameters were similar to those chosen for the twin-spool turbojet, with the exception that P_{6s}, the static pressure at the LP turbine exit, was selected to make use of the Kutta requirement of equal static pressures of the hot and cold streams at the mixer inlet. The additional two parameters, P_7 and T_7, the total pressure and temperature at the mixer exit, were included to account for the dynamics within the mixer. For a given engine, however, several possible combinations of parameters exists and it is simply a matter of choosing a set that gives the greatest ease of computation.

Once the state vector $\vec{x}$ has been selected, $\vec{x}_0$ can be defined as the state vector corresponding to an overall engine steady-state condition. If one or more of the externally controlled conditions is changed and the engine operation calculation is repeated using $\vec{x}_0$, the engine will be determined to be in a transient state, since there will be a work and flow imbalance. As previously discussed, the work imbalance is used to calculate the rotor rotational speed time derivatives. The flow imbalance is used to determine the rate of change of pressure within each intercomponent volume in the engine by considering the rate of accumulation or depletion of mass within each volume and applying the gas law. To illustrate, consider a volume, V, with a gas density, ρ . If the inlet mass flow is W_1, and the exit mass flow is W_2, then the rate of change of physical mass within the volume will be:

$$\frac{d(\rho V)}{dt} = W_1 - W_2 \qquad (1)$$

Applying the gas law,

$$P_1 = \rho_1 R T_1$$

a second equation can be developed:

$$\frac{dP_1}{dt} = RT_1\frac{d\rho_1}{dt} + R\rho_1\frac{dT_1}{dt} \qquad (2)$$

Fawke pointed out in his thesis [23] that, the magnitude of the effects of the pressure dynamics on the change in mass flow are considerably greater than the magnitude of the temperature dynamics effects and the term $\rho dT/dt$ generally amounts to only about 15% of the term $Td\rho/dt$. It is therefore a second-order effect which can be neglected in this equation; its effect can be indirectly accounted for by adjusting the intercomponent volume size. Equation (1) and a simplified equation (2) can now be combined to yield the general intercomponent volume pressure derivative equation:

$$\frac{dP_1}{dt} = \frac{RT}{V}(W_1 - W_2)$$

Where intercomponent volumes will be located within the engine is usually decided at the same time that the state vector is selected and is generally a relatively simple determination; however, it is a somewhat more difficult task to assign values to these volumes. Although it is assumed that the mass storage property of the engine is concentrated between the engine components, it is desirable to account for some of the physical reality that it is actually a distributed property. Therefore, some allowance should be made to include part of the volumes of the components adjacent to the intercomponent volumes chosen. Furthermore, the volume should be adjusted to account for the exclusion of the $\rho dT/dt$ term in equation (2), as discussed above.

Fortunately, Fawke et al [23, 27, 36, etc.] found that engine dynamic behaviour predicted by the model is rather insensitive to the volume sizes used. The rotor dynamics (which have a relatively long time constant) predominate over the pressure dynamics (which

have a comparatively short time constant) and therefore determine the overall transient behaviour of the engine. Hence, relatively large changes in the pressure dynamics will have only a slight effect on the system as a whole. It was illustrated in reference [36] that a doubling of the intercomponent volume sizes had no effect on the rotor speed responses of a twin-spool turbojet. Indeed, reference [27] states that for most engines, volumes of the order of three times greater than the physical sizes on the engine can be used. However, for the turbofan with mixed exhausts, it was found to be necessary to use the physical volume size for the intercompressor space combined with the bypass duct because the flow split between the hot and cold streams was sensitive to changes in P_2 and P_6.

It is interesting to note that in his model of a turbofan engine with mixed exhausts, Fawke increased his value representing the inter-turbine volume by a factor of five [23]. Since the inter-turbine volume was the smallest volume considered, it dictated the length of the integration time step that could be used. The larger this volume could be made without significantly affecting the overall engine dynamics, the longer the time step could be extended and the shorter the computing time became.

Once the rotor rotational speed derivatives and the pressure derivatives have been evaluated, the derivative of the engine state vector at a given time has been established. Hence, the dynamic behaviour of gas turbine engines can be described by the following set of equations:

$$\dot{\vec{x}} = f(\vec{x}, \vec{u}, t)$$

where $\vec{u}$ = the set of time- or parameter- dependent externally controlled variables

A wide variety of numerical methods is available for solving this set of differential equations. However, with the short integration time step that must be used with the Method of Intercomponent

Volumes to maintain equation stability, it may be assumed that each derivative remains constant during each time interval. Therefore, a simple integration routine based on Euler's Method is considered sufficient, such that if $\vec{x}_t$ is evaluated from the value of $\vec{x}$ at time t, then at time $t + \Delta t$,

$$\vec{X}_{(t+\Delta t)} = \vec{X}_t + \frac{d\vec{X}_t}{dt}\Delta t$$

If the initial steady-state state vector, $\vec{x}_0$, is not known, then a "steady-state search transient" must be performed. This is accomplished by simply guessing values for each parameter in the initial state vector, $\vec{x}_0$, and allowing the model to run at a constant value for the control vector, $\vec{u}$, until a steady-state point is reached where the rotor rotational speed derivatives and the pressure derivatives are approximately zero. The accuracy of the initial guess is generally not critical provided that, as a result, the range of the component characteristics is not exceeded.

Chapter 4

MODEL DESIGN

4.1 General

The model used to simulate the dynamic behaviour of the F404 engine was developed in modular fashion such that the modules represent major engine components and interact with each other in the same way as they would in the actual engine. General constants, which are listed in Appendix A, and steady-state component maps have been adopted from the F404 steady-state model previously developed at GasTOPS Ltd [4] and are utilized along with a set of thermodynamic equations to describe each module. This approach makes the simulation flexible in use, easy to understand and provides a means to simulate several component faults by appropriately modifying the component char-acteristics.

4.2 Input Vector Parameters, State Vector Parameters, and Intercomponent Volumes

The input vector consists of time- or parameter-dependent externally controlled variables. For the installed F404 engine, this includes the fuel flow, variable exhaust nozzle throat area, ambient temperature and pressure, flight Mach number, customer bleed and torque extraction, and engine anti-ice flow, or:

$$\vec{U}_{F404} = (W_{f3}, A_8, T_a, P_a, M_a, G_x, W_{BLx}, W_{AI})$$

Since the mixer is considered to be a steady-state component during transient F404 operation, as will be discussed later, the following set of six parameters for the engine state vector is sufficient:

$$\vec{X}_{F404} = (N_1, N_2, P_{2.1}, P_3, P_{4.4}, P_{5.6})$$

Figure 4 shows the station numbering designated for the F404.

The intercomponent volumes were selected as follows:

a) the intercompressor volume and the bypass duct (V_2);

b) the combustor (V_3);

c) the inter-turbine duct (V_4); and,

d) the tailpipe volume (V_6);

The physical values of each of the volumes was used except for the inter-turbine volume. It was found that increasing its actual value by a factor of six had virtually no effect on the overall engine dynamics but allowed a significant increase in the integration time step.

4.3 Model Calculation Routines

For ease of comprehension, the model calculation routines are presented in figures 9 - 21 as Input, Process and Output (IPO) diagrams. The following calculation routines were required to model the transient response of the F404 engine:

a) the inlet module;

b) the fan module;

c) the high pressure compressor module;

d) the combustor module;

e) the high pressure turbine module;

f) the low pressure turbine module;

g) the bypass duct module;

h) the mixer module;

i) the variable exhaust nozzle module;

j) the engine performance calculations;

k) the state vector derivative calculations; and,

l) the integration routine.

The modules are separate component descriptions that are not related to any form of implementation. An additional routine, reserved for future work, which would involve the modelling of the control system, could readily be incorporated.

The program hierarchy diagram and the overall program flow chart are included as figures 6 and 7. An outline of the information flow and component interaction during model module execution is shown in figure 8. Details of the individual calculation routines are given in the following sections.

4.3.1 The Inlet Module

As indicated in figure 9, with inputs of ambient temperature and pressure and flight Mach number, compressible flow relationships can be used to obtain the total temperature and the ram pressure (P_{1R}) at the inlet to the fan. A variable pressure loss relationship based on the flow parameter, as suggested in reference [19], is then applied to the ram pressure to obtain the actual total pressure at inlet to the fan. Since ambient pressure is not available in the IECMS engine take-off data files, fixed values of P_{amb} = 14.696 psia have been assumed for all take-offs at CFB Bagotville and CFB Baden and P_{amb} = 13.8 psia has been assumed for CFB Cold Lake.

Although not significant at the low Mach numbers experienced during take-offs, ram pressure and temperature rise calculations have been included in the model to add to its flexibility. A constant

value for the intake efficiency of 0.93 was taken for take-off runs, as this was the value selected in reference [19] for subsonic conditions and calculated in reference [37] for a flight Mach number of 0.1. It is, nevertheless, easy to vary the intake efficiency whenever necessary, such as when investigating engine dynamics at altitude.

An estimate of a typical take-off Mach number versus time is plotted in figure 22 and is used whenever a take-off run is performed. While it is recognized that aircraft Mach numbers versus time will vary from take-off to take-off due to varying ambient conditions, aircraft external loading (drag), etc., the ram temperature and pressure rise experienced during a take-off roll will have a very minor effect on the engine dynamics and are calculated only to slightly improve the accuracy of the conditions inputted to the fan. Their calculation becomes more significant after the aircraft lifts off and continues to increase its velocity. The model has been developed to allow the user to select the typical take-off Mach number versus time curve (which is activated when the engine commences a transient), or to input a constant Mach number of his/her own choice, depending on the type of run under investigation.

4.3.2 The Fan Module

With N_1 given as a state vector parameter and T_1 determined by the inlet module, the corrected low pressure (LP) rotor speed $N_1/\sqrt{\theta_1}$ can be evaluated and then used to look up the fan variable geometry setting β_L from the schedule. Knowing P_1 from the inlet module calculations and since $P_{2.1}$ is input as a state vector parameter, the fan pressure ratio can be established and, together with the corrected LP rotor speed and variable geometry setting, used to access the fan thermodynamic performance maps to obtain values of the flow parameter and temperature rise ratio. The fan inlet flow, W_1, and exit temperature, $T_{2.1}$, can then be readily computed.

Since the fan is considered a quasi-steady component for the purposes of these calculations, the fan exit flow, $W_{2.5}$, is simply the

fan inlet flow minus a "leakage" flow. The leakage flow is actually a seal pressurization flow that is bled off the fan exit and returned at the exit to the low pressure turbine.

The torque required by the fan is calculated using the component torque equation developed in Chapter Three. It should be noted at this point that constant values of specific heat at constant pressure (Cp) and constant values of the isentropic index (γ) have been assumed throughout the model calculations in order to greatly simplify the computations without any significant loss in accuracy, as explained in reference [19].

Each of the maps used in the fan module and subsequent modules has been generated by a generalized stage-stacking technique based on mean-line conditions [4]. However, due to the split in the flow at the fan exit to the bypass duct and high pressure compressor, radial variations in parameters at the fan exit must be considered. A set of empirical correlations defining the radial non-uniformity of parameters at the fan exit as developed in reference [4] and used in this model is shown in figure 11. From this data, the temperature and pressure at the inlet to the bypass duct and high pressure compressor, which are not equal to the fan exit mean-line conditions, can be determined.

4.3.3 The High Pressure Compressor Module

The high pressure (HP) compressor module calculations are very similar to the fan module calculations. The HP rotor corrected speed is used to obtain the HP compressor variable geometry setting which, combined together with the HP compressor pressure ratio, are used to look up values of the flow parameter and temperature rise ratio. The inlet mass flow and exit temperature can then be evaluated.

Because the IECMS records static pressure instead of total pressure at the HP compressor exit, a conversion from total to static pressure at that location is required for comparison purposes. A

very simple empirical correlation where the static pressure equals 0.9375 times the total pressure was observed by GasTOPS Ltd. using data supplied by the engine manufacturer, and is shown in figure 23.

A number of bleed flows are extracted from the HP compressor:

a) the HP turbine cooling flow (8.59% of $W_{2.5}$ [4]) is routed from the HP compressor exit to the HP turbine rotor blades;

b) the LP turbine cooling flow (3.66% of $W_{2.5}$ [4]) is routed from the HP compressor fourth stage exit to the nozzle vanes of the LP turbine;

c) engine anti-ice flow (2% of $W_{2.5}$ [38]) is drawn off the HP compressor fourth stage and re-inserted in the fan inlet guide vanes. According to reference [39], the pilot will activate engine anti-ice whenever an engine inlet ice detection light illuminates in the cockpit and/or whenever the ambient temperature drops below 505 °R; and,

d) customer bleed air (1.05 lbm/sec [40]) is extracted from the HP compressor exit for cockpit and avionics conditioned air. The value of 1.05 lbm/sec was used as an estimate by McDonnell Douglas during CF-18 flight testing for flight Mach numbers less than 0.2 and for one place cockpits. Such an estimate is required because there is no instrumentation on board to measure customer bleed air. According to reference [3], customer bleed air is extracted equally from both engines.

The combustor inlet flow, W_3, is calculated by subtracting each of these bleed air flows from the HP compressor inlet mass flow.

Similar to the computation of the torque required by the fan, the HP compressor torque requirement is evaluated knowing the

inlet mass flow, the HP rotor speed and the temperature drop across the component. This is actually an approximation of the torque required to drive the HP compressor as the two bleed flows off the fourth stage exit will have a modulating effect. However, this effect will be modelled by "absorbing" the torque difference in the HP rotor torque calculation factor, as will be discussed in the section on the HP turbine module.

4.3.4 The Combustor Module

Having determined the combustor inlet conditions in the HP compressor module, the combustor exit pressure may be calculated as a function of the dynamic head at the combustor inlet.

If the heat release due to fuel injection is considered instantaneous, then a steady-state form of the energy equation can be used to determine the temperature at the combustor exit. However, since the exit temperature is calculated from the exit enthalpy and the effective calorific value of the fuel, both of which are looked up in tables [41] using the exit temperature, an iteration is required as shown in figure 13. This iteration routine is very stable and converges to 0.1 °R within four to five iterations.

4.3.5 The High Pressure Turbine Module

Typical turbine maps generally show the flow parameter and temperature rise ratio as functions of the turbine pressure ratio and turbine speed. Often, however, especially in the case of the high pressure (HP) turbine whose operating region is restricted by the LP turbine downstream of it, the speed dependence can be neglected as a small effect, as explained in reference [19], and it was determined that this could be done with the HP turbine on the F404 with minimal inaccuracy [4].

The single line HP turbine maps presented irrespective of HP rotor speed are shown in figure 14. From these, the inlet mass flow and exit temperature may be calculated. The HP turbine exit mass

flow is computed by adding the rotor blade cooling flow (as determined in the HP compressor module) to the inlet mass flow. If negligible losses in the small inter-turbine duct are assumed, then the LP turbine inlet pressure and temperature will simply be equal to the HP turbine exit pressure and temperature.

The HP turbine torque output is calculated in a manner similar to the HP compressor and fan torque requirement calculations, with the exception that a factor has been added to account for the effects of cooling airflow. The turbine maps have been developed using an average value of temperature within the inter-turbine duct. The drop in temperature from the turbine inlet to this value is not due solely to work being extracted from the gas stream, but is also caused by the heat transfer due to the cooling flow. Additionally, the effect that the extraction of the LP turbine cooling flow from the HP compressor fourth stage exit has on the HP rotor torque calculations must be "absorbed" by this factor.

4.3.6 The Low Pressure Turbine Module

It was determined in reference [4] that the LP turbine on the F404 has a sufficiently large speed dependence to warrant its inclusion on the LP turbine maps. These maps are accessed by the LP turbine pressure ratio to yield values of the flow parameter and temperature ratio which allow the inlet mass flow and exit temperature to be calculated. The exit mass flow is computed by adding the LP turbine cooling flow and the fan "leakage" flow to the inlet mass flow. Calculation of the torque generated by the LP turbine is then performed using an equation similar to the HP turbine torque calculation.

Considerable model "tuning" based on the rotor torque calculation factors, k_{BL3} and k_{BL4}, was carried out and it was found that the best results were obtained with k_{BL3} equal to 1.02 and k_{BL4} equal to 0.925.

The mixer module calculations require that the Mach number at the LP turbine and bypass duct exits be known. Since the static temperature at the LP turbine exit is not known, and since the Mach number cannot be determined directly from a knowledge of the flow parameter at the LP turbine exit, $Q_{5.6}$, an iteration based on $Q_{5.6}$ is required to find $M_{5.6}$ as shown in figure 15. This iteration routine is very stable and converges to a difference between the flow parameters of just 0.0001 within six to seven iterations.

4.3.7 The Bypass Duct Module

Since the intercompressor volume amounts to only 8.5% of the total of the intercompressor volume and the bypass duct volume, it can be assumed that mass accumulation or depletion in this intercomponent volume (V_2) occurs exclusively in the bypass duct. Then, from continuity, the mass flow entering the bypass duct, $W_{1.4}$, may be calculated simply as the difference between the fan exit flow and the HP compressor inlet flow.

To determine the temperature and pressure at the bypass duct exit, it must be realized that heat transfer to the bypass duct from the nearby combustion process has an effect. GasTOPS Ltd. has developed a correlation [4] that is used to determine the exit pressure based on the combustor exit temperature and the bypass duct inlet temperature and flow, as shown in figure 16. The bypass duct exit temperature can be determined by using a simple "heat injection factor" developed specifically for this thesis, multiplying it by the combustor exit temperature and adding it to the bypass duct inlet temperature. It was found, utilizing data supplied by the engine manufacturer, that a maximum error of just 0.23% was incurred using this relationship.

Assuming the Kutta condition of equal static pressures of the hot and cold streams at the mixer splitter and employing compressible flow relationships, the Mach number at the bypass duct exit can be calculated. From this and a knowledge of the exit pressure, temperature and flow area, the mass flow exiting the

bypass duct can be calculated. Developments of the equations used to calculate the bypass duct exit Mach number and mass flow are included as Appendix B.

4.3.8 The Mixer Module

Figure 17 indicates the equations used to model the mixer. Knowing the exit flow conditions from the bypass duct and LP turbine, the mixed total temperature, Mach number, flow parameter and hence total pressure are obtained by solving in succession the continuity, energy and momentum balance equations for the mixer control volume. For computational convenience, complete mixing is assumed to occur by station 6.1, the actual mixer exit. Development of these equations is presented in Appendix C.

4.3.9 The Variable Exhaust Nozzle Module

For non-afterburning operation, the nozzle inlet and throat temperatures and pressures will be equal to the actual mixer exit temperature and pressure, assuming negligible losses. The nozzle inlet pressure sets the nozzle pressure ratio which is used to look up the nozzle flow parameter. Since the nozzle throat area is given as a control input, the throat mass flow can then be evaluated. In order to determine the nozzle inlet flow, the throat flow is modified by a factor that accounts for a small amount of leakage through the nozzle petals.

4.3.10 The Engine Performance Calculations

The engine performance calculations presented in figure 19 are identical to those used by the IECMS [42]. Corrected engine airflow and corrected fuel flow are calculated based on available IECMS parameters. The thrust calculations take into account whether the nozzle is choked by calculating the engine pressure ratio (EPR) and then applying an appropriate "force-area-pressure function". Thrust, corrected for ambient conditions, is then computed and from this and

the corrected fuel flow, the thrust specific fuel consumption may be evaluated.

4.3.11 The State Vector Derivative Calculations

The state vector derivative calculations, shown in figure 20, evaluate the pressure dynamics within each intercomponent volume and the rotor dynamics for each spool. Each derivative is assumed to remain constant for each time step.

The derivation of the general pressure derivative equation from the ideal gas law was presented in Chapter Three and is used in these calculations, with volume representative temperatures used where necessary. As discussed in Section 4.2, the values used for the intercomponent volumes selected for this model are the actual values, with the exception that the inter-turbine duct volume has been increased by a factor of six. This allowed a significant increase in the integration time step and a consequent dramatic decrease in the model computation time, with virtually no effect on the overall engine dynamics. The reason for this, as stated by Fawke and Saravanamuttoo in reference [23], is that the rotor dynamics have a considerably longer time constant than the pressure dynamics and tend to dominate the transient response. Therefore, comparatively large changes in the time constant of the pressure dynamics will have little effect on the system as a whole.

Pressure disturbances in the mixer are assumed to be generated instantaneously to the LP turbine exit, since they travel unimpeded at a Mach number of unity. The rate of change of pressure at the LP turbine exit is thus assumed equal to the rate of change of pressure at the mixer exit; therefore, the temperature and mass flow at the mixer exit are used to determine the pressure derivative at the LP turbine exit.

The rotor dynamics are evaluated using the torque difference equations developed in Chapter Three. The polar moments of inertia were obtained from the engine installation manual [38] and the

mechanical efficiencies are identical to those used in the F404 steady-state model [4]. Consideration must be given to the torque that is extracted from the HP rotor to power certain aircraft components (hydraulics, electric generators, fuel boost pumps, etc.). A constant value of allowable normal operating torque extraction of 37.5 ft-lbf, as indicated in reference [38], was used.

4.3.12 The Integration Routine

The simple Euler integration method was considered sufficiently accurate for this application. After careful program optimization and manipulation of the inter-turbine volume size, a constant integration time step of 0.02 seconds was established. This allowed very stable running of the model, in real time. It was found that the model often went unstable whenever the time step was increased over 0.025 seconds. Since the control update interval used was 0.1 seconds, this is consistent with the results of reference [43], where it was reported that "for proper stability and accuracy a good rule of thumb is that a numerical (Euler) integration time of not more than one quarter of the control interval should be used in the simulation".

With the state vector updated for the given time step, the model modules can be re-executed. This process will continue until the user terminates program execution by selecting the appropriate keypad on the keyboard.

Chapter 5

VALIDATION

5.1 General

Confidence in any mathematical model is only established when it is proven to be an adequate representation of the real physical system for its intended application. The processes used to achieve the required degree of confidence are called verification and validation.

Verification occurs after the analysis and subsequent mathematical model have been implemented to produce a computer model. "Hand" calculations are compared to computer-generated results to ensure that the computer is actually solving the required equations. Model verification also involves comparison of predicted results with other similar models that may be available.

The more difficult task of validating the model against actual engine data is then carried out. Any differences between the two sets of data must be accounted for and minimized by suitable adjustments to the model. It is also necessary that all changes to the model be verified and the model re-validated against the complete set of engine data. As pointed out by MacIsaac in his PhD thesis [22] :

> "Sound engineering judgement must be applied to the validation procedure in view of the fact that there will be some variation of performance from engine to engine built to the same design. This variation in performance is due to minor variations in areas and turbomachinery blade dimensions that are within the production tolerances required. In view of these variations, it makes good engineering sense to validate a model only to the extent that its behaviour falls within the band of performance found to exist over a range of production engines rather than to

search for and model detailed secondary effects that will bring it exactly in line with one specific case."

The following sections will discuss the verification, steady-state validation and dynamic validation of the model presented in this thesis. Reasons for discrepancies between the model and comparative data will be examined, followed by a relatively simple case study that will demonstrate the model's utility and provide a further degree of confidence in the results.

5.2 Model Verification

Since the model was developed in modular fashion, its verification was a rather quick and simple process. Each module was considered separately and calculations were performed by hand and on the computer using identical input values. Corrections to the computer model were made until the outputs of each module matched the results from the hand calculations. Then, the modules were integrated and a complete computation was performed which matched the hand calculations for the overall model.

A further verification of the basic model involved a comparison with the results predicted by the existing F404 steady-state model. This was considered necessary since, although the constants, performance maps and several of the equations used in the two models are identical, the dynamic model utilizes a different mixer model, new T_4 and M_{56} iterations, revised pressure loss determinations and an improved bypass duct exit temperature calculation based on a new heat injection factor, k_{h16}. At identical values for fuel flow and nozzle area, excellent agreement between the two sets of predictions was obtained, with a maximum discrepancy of 0.24%.

5.3 Steady-State Validation

In order to establish the steady-state operating line of the F404 engine as installed in the CF-18 aircraft, successive ground runs of each engine of a dedicated CF-18 were performed at CFB Cold Lake in July 1986. The procedure used to obtain the required data was as follows:

a) the throttle was advanced to give $N_1 = 75 \pm 1\%$ RPM, allowed to stabilize for at least five minutes, and then the IECMS pilot record button was depressed;

b) the throttle was adjusted to the following settings, allowed to stabilize for three minutes, and then the IECMS pilot record button was depressed:

i) $N_1 = 80 \pm 1\%$ RPM
ii) N1 = 85 ± 1% RPM
iii) $N_1 = 90 \pm 1\%$ RPM
iv) $N_1 = 95 \pm 1\%$ RPM
v) $N_1 = 100 \pm 1\%$ RPM
vi) $N_1 = 95 \pm 1\%$ RPM
vii) $N_1 = 90 \pm 1\%$ RPM
viii) $N_1 = 85 \pm 1\%$ RPM
ix) $N_1 = 80 \pm 1\%$ RPM
x) $N_1 = 75 \pm 1\%$ RPM

c) the barometric pressure and ambient temperature at the time of the test runs were recorded.

Thus, the IECMS was able to record two sets of operating point data for both engines. A four point average of this data was then taken to establish the operating line for the F404 engine installed in the CF-18 aircraft.

Since the fuel flow, variable exhaust nozzle area and ambient pressure and temperature are the parameters taken from the test data that are used to drive the dynamic model, a "control input parameter", $W_{f3}/(A_8 P_a \sqrt{T_a})$, has been taken as the independent variable for comparison purposes. It is simply an adaptation of the fuel flow parameter, $W_f/P_a\sqrt{T_a}$, described in reference [19]. When N_1, N_2, P_{s3}, $P_{5.6}$, and $T_{5.6}$ recorded by IECMS and predicted by the model are plotted versus this parameter, as shown in figures 24 - 28, it can be seen that good agreement is obtained, the maximum error being 2.88% on $T_{5.6}$ at the highest temperature.

5.4 Dynamic Validation

5.4.1 IECMS Data

As discussed in Chapter One, the In-Flight Engine Condition Monitoring System data is recorded during each CF-18 take-off, whenever the pilot record button in the cockpit is selected or whenever an engine operating limit is exceeded. The parameters recorded by the IECMS are listed in Table 1.

The IECMS data processing is a somewhat involved procedure that is well described in reference [44]. One of the final products is the engine data file produced by a take-off analysis program [45]; the parameters contained in the engine take-off data file are listed in Table 2.

Figures 29, 30 and 31 show examples of the "raw" data recorded by the IECMS during a typical take-off. It is readily apparent that a smoothing and filtering process is required in order to reduce the inaccuracies in the raw data. This procedure is described in Appendix D and an example of the smoothed data produced is shown in these figures as well.

In order to gain as much information concerning the engines as possible, a recent amendment to the standard operating procedures

for CF-18 aircraft requires the pilot to activate IECMS pilot recordings at the point that he slams the throttle forward to initiate the take-off roll. This allows the accumulation of five seconds of pre-take-off steady-state data followed by the take-off transient and a significant amount of post-take-off data. Data collected in this way provides the analyst with significantly more information than is available from the automatic take-off recordings that are typically only 6 - 10 seconds in duration and do not provide any pre-take-off steady-state data.

5.4.2 Engine Take-Off Data File Selection

Selection of engine take-off data files for the dynamic validation of the model was restricted to files whose initial steady-state operating point corresponded to corrected fan speeds greater than 50%, which is the lower limit of the fan maps used in the model. Since most engine take-off data files commence at ground idle, which corresponds to corrected fan speeds that are lower than 50%, only four suitable files where the initial steady-state operating point was at a high enough corrected fan speed were available.

The four files selected for the dynamic validation of the model have been named 716LB, 716RB, 711LI, 711RI. The three digits identify the tail number of the aircraft the engine was installed on at the time of the recording, the first letter refers to the left-hand or right-hand installation and the last letter indicates the event number. Tail numbers beginning with a seven indicate single-seat aircraft; those beginning with a nine designate dual-seaters. The complete nomenclature for each engine data file also includes the engine serial number and the type of recording (pilot record, automatic take-off record (called a "thrust check"), or an in-flight incident).

5.4.3 Comparison of Predicted Results with IECMS Data

Figures 32 - 44, 45 - 55, 56 - 66, and 67 - 77 show the results predicted by the model compared to the data presented by the engine take-off data files for 716LB, 716RB, 711LI and 711RI respectively.

A very good match between the model and IECMS data was obtained for each parameter during the initial steady-state operating point and throughout the approximately three second transient. However, it seems that the engine and the model have settled to what are apparently different steady-state conditions after the transient has taken place. In reality, the model had indeed reached a steady-state condition but the engine had not; as figures 78 and 79 indicate, it takes the F404 approximately 150 seconds to stabilize after a transient from idle to a corrected fan speed of 89%. This behaviour may be attributed to the long term heat transfer effects that were discussed in Chapter Two but were not represented in the model.

The data presented in figures 78 and 79 were obtained from a run of an F404 engine at the CFB Baden Engine Test Facility. The engine was accelerated rapidly from "cold" ground idle to an engine pressure ratio (EPR) of 2.7, which corresponds to a corrected fan speed of approximately 89%. When the engine reached this value for EPR, successive readings of N_1, N_2, and fuel flow at 30 second intervals were then taken in order to roughly determine the thermal stabilization period for the engine.

The dynamic results compare very favourably with the results obtained by similar work done elsewhere, such as at the National Gas Turbine Establishment in the United Kingdom where an engine similar to the F404 was modelled with and without heat transfer effects represented [46]. Since their engine took five to ten minutes to fully stabilize, they also found that unless heat soakage effects were modelled, the rotor speeds predicted by their model during a slam acceleration settled to comparably higher steady-state values.

Table 4 lists the IECMS precision errors, as estimated by Henry [4]. Tables 5 and 6 show the sensitivity of the parameters to the maximum precision error for the fuel flow and exhaust nozzle area measurements, respectively. Steady-state conditions corresponding to W_{f3} = 6635 lbm/hr and A_8 = 19.5% have been taken as the baseline for comparison. Even with these possible measurement

precision errors, the model gives good agreement with the IECMS recordings.

Validating temperatures during dynamic analysis is difficult due to the poor response characteristics of the thermocouple probes, as figure 40 indicates, for instance. If the F404 control system is to be modelled in the future, an accurate representation of the exhaust gas temperature ($T_{5.6}$) thermocouple variable time constant will be required.

The plots of fuel ratio units (W_{f3c}/P_{s3}) versus N_2, which correspond to the main fuel control schedule, have been included to illustrate that the model is considered accurate enough for a good description of the control system to be developed as a future model extension. Standard fan and high pressure compressor maps for 716LB, figures 43 and 44, have been included simply for illustrative purposes.

5.5 Case Study - 912LB

Although not an analysis of the F404 during a CF-18 take-off, the following case study involving an in-flight incident of an F404 overtemperature above CFB Cold Lake was selected to illustrate the flexibility and usefulness of the model and to provide a further degree of confidence in its predictions.

As figures 80 and 81 indicate, when the pilot was aware that the exhaust gas temperature (EGT) limit of 812 °C had been exceeded, he quickly pulled back on the throttle, allowed the EGT to lower considerably, then slammed the throttle back to the full power setting in two steps. Once full power was re-established, the EGT again went beyond its limit, causing the pilot to chop his throttle once again.

It is apparent from figure 82 that a variable exhaust nozzle (VEN) fault occurred on the left-hand engine. It appears as though

the nozzle slammed itself fully opened, since the recordings show it to be well above 100%. However, this is immediately suspect since an opening of the nozzle should have caused the EGT to lower considerably. The model was then used to investigate the possibility of a faulty VEN actuator position reading which may have subsequently activated the nozzle failsafe logic. The VEN failsafe logic forces the nozzle to fully close whenever the VEN position reading exceeds 100%.

The model was run for 912LB with the VEN failsafe logic implemented directly after A_8 was read in. A constant value of Mach number, M=0.6, was assumed throughout the run. Because the corrected fan speed dipped below 50% at approximately 10 seconds into the recording, the run had to be split into two parts: 0 - 10 seconds (figures 84 - 88) and 22.3 - 40 seconds (figures 89 - 93). It can be concluded from these figures that indeed the nozzle had shut to its fully closed position, and that the model was very effective in confirming this suspicion.

Chapter 6

RECOMMENDATIONS FOR FUTURE WORK

The development of a basic dynamic model of the F404 engine as presented in this thesis can only be considered the first of a number of tasks required to develop a comprehensive dynamic fault library for the engine based on the Module Performance Analysis technique. The work that remains is listed below, most of which can be performed concurrently.

a) The model should be extended to allow for the thermal capacity of the engine components. This will require the determination of the thermal time constant, either analytically or experimentally, and will require the integration of a new energy absorption derivative.

b) The fan map should be extended down to a corrected fan speed of 30%, which corresponds approximately to engine ground idle. It is recognized that the accuracy of the stage stacking technique diminishes with decreasing rotor speed. However, this extension of the map is recommended in order to permit an analysis of the large quantity of engine take-off data files that commence at ground idle. Only rough accuracy in the low speed range is required, since the initial steady-state point simply positions the model close enough to the actual engine operating point at the start of the transient such that the transient itself may be accurately predicted.

c) The dynamic response characteristics of the $T_{5.6}$ thermocouple should be represented in the model as a further derivative to be integrated over time.

d) A complete closed-loop model of the engine control system should be designed as a stand-alone module that may be

readily incorporated into the engine dynamic model. The ultimate goal would be to provide predictions of the engine dynamic response to changes in the power lever angle position. This would allow the expansion of the dynamic fault library to include control system anomalies.

e) Software revisions to the IECMS data processing should be performed in order to include the following items in future engine take-off data files:

(1) Pressure altitude;
(2) Aircraft Mach number;
(3) Engine anti-ice flag; and,
(4) Bleed air door open flag.

Appropriate revisions to the dynamic model should then be made to better account for ambient pressure, inlet ram effects, engine anti-ice flow, and customer bleed air extractions.

f) The dynamic model should be utilized to augment the dynamic fault library currently in existence.

Chapter 7

CONCLUSIONS

The On-Condition Maintenance philosophy adopted for the F404 engine in the CF-18 requires the development of effective Engine Health Monitoring techniques. One very promising and potentially powerful technique is Module Performance Analysis, which utilizes a thermodynamic model to assist in developing a fault library for the engine. A steady-state model of the F404 has already been developed; however, due to the nature of CF-18 operations, sustained steady-state conditions are rare and therefore a dynamic model of the engine is required.

A component-based thermodynamic model of the F404 engine has been developed to predict the engine's dynamic behaviour during take-off accelerations. In order to obtain an excellent physical representation of the engine dynamics while maintaining the best computing efficiency possible, the model has been designed based on the Method of Intercomponent Volumes. Given the ambient conditions and aircraft Mach number, the model is driven by inputs of fuel flow and exhaust nozzle area as functions of time. A series of module calculations are performed to determine the engine operating point at a specified time, followed by an integration of two rotor speed derivatives (which are determined by rotor torque mismatches) and four pressure derivatives (which are calculated from flow incompatibilities in the intercomponent volumes). This process is repeated for each integration time increment until a program termination command is received from the user.

The model has been implemented on a Digital Microvax II computer at GasTOPS Ltd and has the capability to operate in real time. The VAX/VMS version 4.5 operating system and the VAX Fortran version 4.5 language have been utilized, producing a program of approximately 3500 lines requiring 600 K of storage.

An extensive steady-state and dynamic validation of the model has been carried out, utilizing operational engine data obtained from the In-Flight Engine Condition Monitoring System (IECMS). Good agreement between the results predicted by the model and the IECMS data has generally been obtained, with the exception of the "steady-state" condition found immediately after a transient. Secondary effects have not been represented in the model and, consequently, this has resulted in some inaccuracies in the predictions for this "steady-state" condition, which is actually a long-term transient due to the relatively slow engine metal heat absorption rate that extracts energy from the gas stream.

Although the model was developed specifically to predict the dynamic behaviour of the F404 during take-off accelerations, a case study of the engine at altitude has been included to show the flexibility and adaptability of the model and to gain a further degree of confidence in its predicted results.

It is anticipated that the model will prove highly effective in investigating the effects that a variety of faults will have on the dynamic operation of the engine. Considerable follow-on work is now required in order to develop a comprehensive dynamic fault library for the F404.

REFERENCES

1. MacIsaac, B.D. and Muir, D.E.,
"CF-18 EHM Management Plan and Methodologies - Implementation Plan",
GasTOPS Ltd. Report No. GTL-7-9-TR.4
January, 1984.

2. MacIsaac, B.D.,
"Controls, Transients and Engine Health Monitoring" in "Gas Turbine Performance and Design Supplementary Notes".
Course taught at Carleton University,
May 1986.

3. Henry, J.R.,
"CF-18/F404 Transient Performance Trending",
MEng Thesis, RMC, April 1987
and AGARD-CP-448, Paper No. 37,
Quebec, 1988.

4. Muir, D.E. and Kitaljevich, D.,
"Computer Model of the F404-GE-400 Turbofan Engine - Thermodynamic Analysis and System Design",
GasTOPS Ltd. Report No. GTL-19-15.1-TR.1
March, 1984.

5. Muir, D.E., Rudnitski, D.M. and Cue, R.W.,
"CF-18 Engine Performance Monitoring",
AGARD-CP-448 Paper No. 7
Quebec, 1988.

6. Muir, D.E.,
"CF-18 Engine Performance Monitoring",
GasTOPS Ltd. Report No. GTL-19-26.7-TR.1
March, 1986.

7. MacIsaac, B.D. and Muir, D.E.,
"CF-18 EHM Management Plan and Methodologies - IECMS Utilization Plan",
GasTOPS Ltd. Report No. GTL-7-9-TR.4
March 1984.

8. Schofield, C. et al,
"Canadian Forces Aircraft Engine Condition/Health Monitoring - Policy, Plans and Experience",
AGARD-CP-448 Paper No. 4
Quebec, 1988.

9. "F404 EMS Program - EPLTS/EHM Research Engineers",
DND internal letter
May, 1988.

10. Merrington, G.L.,
"Identification of Dynamic Characteristics for Fault Isolation Purposes in a Gas Turbine Using Closed-Loop Measurements",
AGARD-CP-448 Paper No. 36
Quebec, 1988.

11. Otto, E.W. and Taylor, B.L.,
"Dynamics of a Turbojet Engine Considered as a Quasi-Static System",
NACA TN 2091
1950.

12. Ketchum, J.R. and Craig, R.T.,
"Simulation of Linearized Dynamics of Gas Turbine Engines",
NACA TN 2826
1952.

13. Pack, G.J. and Phillips, W.E.,
"Analog Study of Interacting and Non-interacting Multiple-Loop Control Systems for Turbojet Engines",
NACA TN 3112
1954.

14. Gold, H. and Rosenzweig, S.,
"A Method for Estimating Speed Response of Gas Turbine Engines",
NACA RM E51 K21
1952.

15. Laurence, J.O.N. and Powell, R.D.,
"The Application of Servo-Mechanism Analysis to Fuel Control Problems",
Proc. Inst. Mech. Engrs., Vol. 172
1958.

16. Novik, D.,
"Some Linear Dynamics of Two-Spool Turbojet Engines",
NACA TN 3274
1956.

17. Saravanamuttoo, H.I.H. and MacIsaac, B.D.,
"An Overview of Engine Dynamic Response and Mathematical Modelling Concepts",
AGARD-CP-324, Paper No. 25
Greece, 1982.

18. Saravanamuttoo, H.I.H. and Fawke, A.J.,
"Simulation of Gas Turbine Dynamic Performance",
ASME 70-GT-23
1970.

19. Cohen, H., Rogers, G.F.C., and Saravanamuttoo, H.I.H.,
Gas Turbine Theory , 3rd edition,
Longman Group UK Ltd and John Wiley & Sons, Inc., New York,
1987.

20. Filippi, R.E. and Dugan, J.F.,
"Effect of Design Overall Compressor Pressure Ratio Division on Acceleration Characteristics of Three Hypothetical Two-Spool Turbojet Engines",
NACA RM E56 D13
1956.

21. Fawke, A.J. and Saravanamuttoo, H.I.H.,
"Digital Computer Methods for Prediction of Gas Turbine Dynamic Response",
Trans. S.A.E., 80 [iii],
1971, pp. 1805-13.

22. MacIsaac, B.D.,
"Techniques for Improving the Dynamic Response of the Gas Turbine; A Comparative Study Using a Hybrid Computer Model",
Ph.D. thesis, Carleton University
1974.

23. Fawke, A.J.,
"Digital Computer Simulation of Gas Turbine Dynamic Behaviour",
Ph.D. thesis, University of Bristol
March, 1970.

24. MacIsaac, B.D. and Saravanamuttoo, H.I.H.,
"An Investigation into the Dynamic Performance of a Variable Pitch Turbofan Using a Hybrid Computer",
ASME 76-GT-31
1976.

25. Bauerfeind, K.,
"A New Method for the Determination of Transient Jet Engine Performance Based on the Nonstationary Characteristics of the Components",
AGARD-CP-34, Paper No. 32,
September, 1968.

26. Saravanamuttoo, H.I.H. and MacIsaac, B.D.,
"The Use of a Hybrid Computer in the Optimization of Gas Turbine Control Parameters",
Trans. ASME, Journal of Engineering for Power,
July, 1973.

27. Fawke, A.J. and Saravanamuttoo, H.I.H.,
"Digital Computer Simulation of the Dynamic Response of a Twin-Spool Turbofan with Mixed Exhausts",
Aeronautical Journal, Vol. 77, pp. 471 - 478,
September, 1973.

28. Maccallum, N.R.L.,
"The Performance of Turbojet Engines During the Thermal Soak Transient",
Proc. Inst. Mech. Engrs., Vol. 184, pp.23 - 29,
1969.

29. Maccallum, N.R.L.,
"Effect of Bulk Heat Transfer in Aircraft Gas Turbines on Compressor Surge Margins",
Proc. Inst. Mech. Engrs., pp. 94 - 100
1974.

30. Maccallum, N.R.L.,
"Thermal Influences in Gas Turbine Transients - Effects of Changes in Compressor Characteristics",
ASME 79-GT-143
1979.

31. Maccallum, N.R.L.,
"Further Studies of the Influence of Thermal Effects on the Predicted Acceleration of Gas Turbines",
ASME 81-GT-21
1981.

32. Pilidis, P. and Maccallum, N.R.L.,
"A Study of the Prediction of Tip and Seal Clearances and their Effects on Gas Turbine Transients",
ASME 84-GT-245
1984.

33. Pilidis, P. and Maccallum, N.R.L.,
"The Effect of Heat Transfer on Gas Turbine Transients",
ASME 86-GT-275
1986.

34. Thomson, B.,
"Basic Transient Effects of Aero Gas Turbines",
AGARD-CP-151
February, 1975.

35. Larjola, J.,
"Simulation of Surge Margin Changes due to Heat Transfer Effects in Gas Turbine Transients",
ASME 84-GT-129
1984.

36. Fawke, A.J., Saravanamuttoo, H.I.H. and Holmes, M.,
"Experimental Verification of a Digital Computer Simulation Method for Predicting Gas Turbine Dynamic Behaviour",
Proc. Inst. Mech. Engrs., Volume 186, pp. 323 - 329,
1972.

37. Fishback, L.H. and Koenig, R.W.,
"GENENG - A Program for Calculating Design and Off-Design Performance for Turbojet and Turbofan Engines",
NASA TN D-6552,
February, 1972.

38. F404-GE-400 Afterburning Turbofan Engine Installation Manual,
General Electric Company,
I vnn, Massachusetts,
June, 1980.

39. Discussion with Mr. J. Miller,
General Electric Field Services Representative with the Department of National Defence,
10 January, 1989.

40. "F/A-18 Flight Test Performance Data Reduction Procedures",
McDonell Aircraft Company,
St. Louis, Missouri,
January, 1981.

41. Chappell, M.S. and Cockshutt, E.P.,
Gas Turbine Cycle Calculations: Thermodynamic Data Tables for Air and Combustion Products for Three Systems of Units,
National Research Council of Canada no. 14300,
Ottawa,
August, 1974.

42. Brennan, W.H. and Stanko, M.S.,
F404 - F/A-18 IECMS Handbook,
General Electric Company,
Lynn, Massachusetts,
October, 1982.

43. DeLatt, J.C., Litt, J.S., and Merrill, W.C.,
"A Microprocessor-Based Real-Time Simulator of a Turbofan Engine",
NASA-TM-100889,
May, 1988.

44. Kirkhope, K.J. and Muir. D.E.,
"Development of IECMS Data Analysis Procedures",
GasTOPS Ltd. Report No. GTL-7-17.4-TR.2,
March, 1989.

45. Brouse, D.,
"IECMS Take-Off Data Analysis - Computer Program User's Manual",
GasTOPS Ltd. Report No. GTL-7-17.4-TR.9
September, 1988.

46. Onions, R.A. and Foss, A.M.,
"Improvements in the Dynamic Simulation of Gas Turbines",
National Gas Turbine Establishment, U.K.,
AGARD-CP-324, Paper No. 27,
October, 1982.

47. Mattingly, J.D., Heiser, W.H., and Daley, D.H.,
Aircraft Engine Design,
AIAA Education Series,
New York, 1987.

Appendix A

General Constants

R	Gas constant (ft-lbf/lbm-°R)	53.3
g_c	Gravitational constant (ft-lbm/lbf-sec^2)	32.174
π	Pi	3.14159
P_{ref}	Reference pressure (psia)	14.7
T_{ref}	Reference temperature (°R)	519
h_{ref}	Enthalpy at reference temp. (BTU/lbm)	124.04
θ_{ref}	Theta function at reference temp. (BTU/lbm)	55.2
ECV_r	Eff. calorific value at ref. temp. (BTU/lbm)	18540
Cp_1	Specific heat (BTU/lbm-°R) - Fan	0.240
Cp_{16}	Specific heat (BTU/lbm-°R) - Bypass duct exit	0.249
Cp_{25}	Specific heat (BTU/lbm-°R) - HP compressor	0.260
Cp_4	Specific heat (BTU/lbm-°R) - HP turbine	0.274
Cp_{46}	Specific heat (BTU/lbm-°R) - LP turbine	0.265
Cp_{56}	Specific heat (BTU/lbm-°R) - LP turbine exit	0.258
γ_1	Isentropic index - Inlet and fan	1.4000
γ_{16}	Isentropic index - Bypass duct exit	1.3796
γ_2	Isentropic index - HP compressor	1.3755
γ_4	Isentropic index - HP turbine	1.3459
γ_{46}	Isentropic index - LP turbine	1.3569
γ_{56}	Isentropic index - LP turbine exit	1.3615
γ_6	Isentropic index - Mixer	1.3300
η_i	Inlet efficiency	0.93
η_{m1}	LP rotor mechanical efficiency	0.98
η_{m2}	HP rotor mechanical efficiency	0.98
η_{34}	Combustor efficiency	0.9875
K_{BL1}	Bleed flow factor - HP turbine cooling	0.0859
K_{BL2}	Bleed flow factor - LP turbine cooling	0.0366
K_{BL3}	Bleed flow factor - HP rotor torque calculation	1.02
K_{BL4}	Bleed flow factor - LP rotor torque calculation	0.925

K_{WAI}	Bleed flow factor - Engine anti-ice	0.02
K_{L01}	Pressure loss factor - Intake	$3.21*10^{-6}$
K_{L34}	Pressure loss factor - Combustor	$6.0*10^{-4}$
K_{L6}	Pressure loss factor - Mixer	0.0048727
K_{H16}	Heat injection factor - Bypass duct	0.030727
K_{LF}	Fan flow leakage factor	0.995
K_{LN}	Nozzle flow leakage factor	1.005
A_{16}	Area (in^2) - Bypass duct exit	59.0
A_{56}	Area (in^2) - LP turbine exit	365.
A_6	Area (in^2) - Mixer	424.
V_2	Volume (in^3) - Bypass duct and inter-compressor space (actual)	12196.
V_3	Volume (in^3) - combustor (actual)	3319
V_4	Volume (in^3) - interturbine duct (actual*6)	2190.
V_6	Volume (in^3) - tailpipe (actual)	28319.
I_1	Polar moment of inertia (slugs-ft^2) - LP rotor	2.44
I_2	Polar moment of inertia (slugs-ft^2) - HP rotor	2.50
G_x	Torque extraction (ft-lbf)	37.5
W_{BLx}	Customer bleed airflow extraction (lbm/sec)	1.05
Δt	Time step (sec)	0.02

Appendix B

Bypass Duct Exit Equations

In order to perform the mixer module calculations, the Mach number and mass flow of the cold stream exiting the bypass duct at the mixer entrance must be determined. The following is a development of the equations used to evaluate these two parameters [47].

Assuming the Kutta condition at the mixer inlet of equal static pressures, P_s, of the two streams, the conventional compressible flow functions used to relate the total pressures to the static pressure may be written as:

$$\frac{P_{1.6}}{P_S} = \left(1 + \frac{\gamma_{1.6} - 1}{2} M_{1.6}^2\right)^{\frac{\gamma_{1.6}}{\gamma_{1.6} - 1}} \qquad (1)$$

$$\frac{P_{5.6}}{P_S} = \left(1 + \frac{\gamma_{5.6} - 1}{2} M_{5.6}^2\right)^{\frac{\gamma_{5.6}}{\gamma_{5.6} - 1}} \qquad (2)$$

Dividing equation (1) by equation (2) yields:

$$\frac{P_{1.6}}{P_{5.6}} = \frac{\left(1 + \frac{\gamma_{1.6} - 1}{2} M_{1.6}^2\right)^{\frac{\gamma_{1.6}}{\gamma_{1.6} - 1}}}{\left(1 + \frac{\gamma_{5.6} - 1}{2} M_{5.6}^2\right)^{\frac{\gamma_{5.6}}{\gamma_{5.6} - 1}}}$$

Solving for $M_{1.6}$:

$$M_{1.6} = \left\{\frac{2}{\gamma_{1.6} - 1}\left(\left[\frac{P_{1.6}}{P_{5.6}}\left(1 + \frac{\gamma_{5.6} - 1}{2} M_{5.6}^2\right)^{\frac{\gamma_{5.6}}{\gamma_{5.6} - 1}}\right]^{\frac{\gamma_{1.6} - 1}{\gamma_{1.6}}} - 1\right)\right\}^{\frac{1}{2}}$$

The non-dimensional flow at the bypass duct exit may be expressed as:

$$\frac{W_{1.6}\sqrt{T_{1.6}}}{P_{1.6} A_{1.6}} = \frac{\rho_{1.6} A_{1.6} V_{1.6} \sqrt{T_{1.6}}}{P_{1.6} A_{1.6}}$$

Substituting the ideal gas law,

$$\rho_{1.6} = \frac{P_{s1.6}}{R\,T_{s1.6}}$$

and the Mach number relationship,

$$V_{1.6} = M_{1.6}\sqrt{\gamma_{1.6}\,g_c\,R\,T_{s1.6}}$$

and isolating $W_{1.6}$ yields:

$$W_{1.6} = \frac{M_{1.6}\,A_{1.6}\,P_{s1.6}\sqrt{\dfrac{\gamma_{1.6}\,g_c}{R}}}{\sqrt{T_{s1.6}}}$$

Applying the compressible flow functions,

$$\frac{P_{1.6}}{P_{s1.6}} = \left(1 + \frac{\gamma_{1.6} - 1}{2} M_{1.6}^2\right)^{\frac{\gamma_{1.6}}{\gamma_{1.6} - 1}}$$

$$\frac{T_{1.6}}{T_{s1.6}} = \left(1 + \frac{\gamma_{1.6} - 1}{2} M_{1.6}^2\right)$$

and simplifying results in the expression for the mass flow at the bypass duct exit:

$$W_{1.6} = \frac{M_{1.6}\,P_{1.6}\,A_{1.6}\sqrt{\dfrac{\gamma_{1.6}\,g_c}{R}}}{\sqrt{T_{1.6}}\left(1 + \dfrac{\gamma_{1.6} - 1}{2} M_{1.6}^2\right)^{\frac{\gamma_{1.6} + 1}{2(\gamma_{1.6} - 1)}}}$$

Appendix C

STEADY-STATE MIXER MODEL

Steady-State Assumption

If it is assumed that complete mixing of the hot and cold gas streams occurs by the time they reach the mixer exit, then the kinetic energy of each of the molecules of gas leaving the mixer will be equal. Even at low power settings where, for example, the Mach number and static temperature of the cold gas stream entering the mixer are just 0.14 and 580 °R, the velocity of the gas stream would be:

$$V_{1.6} = M_{1.6}\sqrt{\gamma_{1.6}\, g_c\, R\, T_{s1.6}}$$

$$= 0.14\sqrt{1.3796 \cdot 32.2 \cdot 53.3 \cdot 580}$$

$$= 164.0 \text{ ft/sec}$$

If the mixing duct length is 1 foot, then the resident time of a molecule in the mixer would be just 0.006 seconds which, since each molecule leaves the mixer with the same kinetic energy, represents the maximum stabilization time for the mixer under dynamic engine conditions. The velocity of the gas stream doubles as design conditions are approached and therefore the stabilization time is halved. Quite clearly, the dynamics of the mixer can be considered instantaneous when compared to the overall engine dynamics.

Mixer Model

The mixer model that follows was adapted from Mattingly et al [47] and is applicable under the following conditions:

a) A constant area mixer of known geometry with no heat transfer losses;

b) The static pressures of the hot and cold streams at the inlet to the mixer are equal;

c) Mixing is complete with a uniform stream of gas leaving the mixer;

d) The gases follow the perfect gas laws and the gas constant (R) remains constant;

e) The fluid properties (Cp, γ) at each station are known and remain constant;

f) The mass flow rates (W) and Mach numbers (M) at the bypass duct exit and core exit are known;

g) Uni-dimensional, axial-flow conditions in which mass continuity is maintained.

The following diagram illustrates the mixer control volume and station designations.

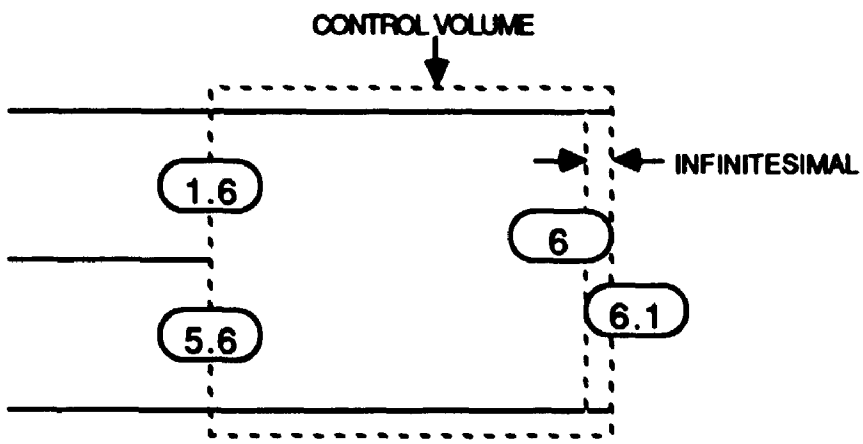

STATION	DESIGNATION
1.6	Bypass duct exit
5.6	Core exit
6	Ideal mixer plane
6.1	Actual mixer plane *

* Accounts for pressure losses due to wall/fluid friction.

The mixed total temperature, Mach number, non-dimensional flow and hence total pressure are obtained by solving in succession the energy, continuity, and momentum balance equations for the mixer control volume.

The ideal mixed total temperature (T_6) can be calculated from the following energy (heat) balance:

$$W_6 Cp_6 T_6 = W_{16} Cp_{16} T_{16} + W_{56} Cp_{56} T_{56}$$

Assuming continuity,

$$W_6 = W_{16} + W_{56}$$

$$\therefore \; T_6 = \frac{W_{16} Cp_{16} T_{16} + W_{56} Cp_{56} T_{56}}{(W_{16} + W_{56}) Cp_6}$$

where,

$$Cp_6 = \frac{W_{16} Cp_{16} + W_{56} Cp_{56}}{W_{16} + W_{56}}$$

$$\therefore \; T_6 = \frac{W_{16} Cp_{16} T_{16} + W_{56} Cp_{56} T_{56}}{W_{16} Cp_{16} + W_{56} Cp_{56}}$$

Since negligible heat transfer losses are assumed, the actual mixed total temperature (T_{61}) is considered equal to the ideal mixed total temperature (T_6) :

$$T_{61} = T_6 = \frac{W_{16} Cp_{16} T_{16} + W_{56} Cp_{56} T_{56}}{W_{16} Cp_{16} + W_{56} Cp_{56}} \qquad (1)$$

To determine the ideal mixed pressure (P_6), a momentum balance is performed. Since all the gas properties (Cp, γ, R) at each station are known and the mass flow rates (W) and Mach numbers (M) at the bypass duct exit and core exit (i.e. at inlet to the mixer) are known, the equations can be derived as follows.

The general non-dimensional flow in terms of static pressure (P_s) can be written as:

$$\frac{W\sqrt{T}}{P_sA} = \frac{\rho AV\sqrt{T}}{P_sA}$$

$$= \frac{\rho M\sqrt{\gamma Rg_cT_s}\sqrt{T}}{P_s}$$

$$= \frac{P_sM\sqrt{\gamma Rg_cT_s}\sqrt{T}}{RT_sP_s}$$

$$= M\sqrt{\frac{\gamma g_c}{R}}\sqrt{\frac{T}{T_s}}$$

$$\frac{W\sqrt{T}}{P_sA} = M\sqrt{\frac{\gamma g_c}{R}}\left(1+\frac{\gamma-1}{2}M^2\right)^{\frac{1}{2}} \qquad (2)$$

For an ideal, constant area mixer, the momentum equation in terms of the impulse function (I) is:

$$I_6 = I_{16} + I_{56} \qquad (3)$$

where,

$$I = P_sA\left(1+\gamma M^2\right) \qquad (4)$$

Replacing P_sA in equation (4) with P_sA from equation (2):

$$I = \frac{W\sqrt{\frac{RT}{\gamma g_c}}\left(\frac{1+\gamma M^2}{M}\right)}{\left(1+\frac{\gamma-1}{2}M^2\right)^{\frac{1}{2}}}$$

or,

$$I = W\sqrt{\frac{RT}{\gamma g_c\phi}} \qquad (5)$$

where,

$$\phi = \frac{M^2}{\left(1+\gamma M^2\right)^2}\left(1+\frac{\gamma-1}{2}M^2\right) \qquad (6)$$

Substituting equation (5) for each term in equation (3):

$$W_6\sqrt{\frac{RT_6}{\gamma_6 g_c \phi_6}} = W_{16}\sqrt{\frac{RT_{16}}{\gamma_{16} g_c \phi_{16}}} + W_{56}\sqrt{\frac{RT_{56}}{\gamma_{56} g_c \phi_{56}}}$$

Solving for ϕ_6:

$$\phi_6 = \left[\frac{W_6}{W_{16}\sqrt{\frac{T_{16}}{\gamma_{16}\phi_{16}}} + W_{56}\sqrt{\frac{T_{56}}{\gamma_{56}\phi_{56}}}}\right]^2 \left(\frac{T_6}{\gamma_6}\right)$$

multiplying by:

$$\left(\frac{1}{\sqrt{\frac{\gamma_{56}}{T_{56}}}}\right)^2 \times \left(\frac{\gamma_{56}}{T_{56}}\right)$$

yields:

$$\phi_6 = \left[\frac{\frac{W_6}{W_{56}}}{\frac{W_{16}}{W_{56}}\sqrt{\frac{\gamma_{56}T_{16}}{\gamma_{16}T_{56}\phi_{16}}} + \frac{1}{\sqrt{\phi_{56}}}}\right]^2 \left(\frac{\gamma_{56}}{\gamma_6}\right)\left(\frac{T_6}{T_{56}}\right)$$

where, from continuity,

$$W_6 = W_{16} + W_{56}$$

$$\therefore \frac{W_6}{W_{56}} = 1 + \frac{W_{16}}{W_{56}}$$

and, since $T_{61} = T_6$, then $\gamma_{61} = \gamma_6$ and,

$$\phi_6 = \left[\frac{1 + \frac{W_{16}}{W_{56}}}{\frac{W_{16}}{W_{56}}\sqrt{\frac{\gamma_{56}T_{16}}{\gamma_{16}T_{56}\phi_{16}}} + \frac{1}{\sqrt{\phi_{56}}}}\right]^2 \left(\frac{\gamma_{56}}{\gamma_{61}}\right)\left(\frac{T_{61}}{T_{56}}\right) \qquad (7)$$

Placing equation (7) in equation (6) and solving the subsequent quadratic equation yields:

$$M_6^2 = \frac{(1 - 2\gamma_6\phi_6) \pm \sqrt{1 - 2(\gamma_6+1)\phi_6}}{2\gamma_6^2\phi_o - \gamma_6 + 1}$$

multplying by:

$$\frac{\left(1 - 2\gamma_6\phi_6\right) \pm \sqrt{1 - 2(\gamma_6+1)\phi_6}}{\left(1 - 2\gamma_6\phi_6\right) \pm \sqrt{1 - 2(\gamma_6+1)\phi_6}}$$

yields:

$$M_6 = \left[\frac{2\phi_6}{\left(1 - 2\gamma_6\phi_6\right) \pm \sqrt{1 - 2(\gamma_6+1)\phi_6}}\right]^{\frac{1}{2}} \qquad (8)$$

where the + sign corresponds to subsonic flow and the - sign corresponds to supersonic flow.

Similar to the development for equation (2), the non-dimensional flow in terms of total pressure at station 6 can be derived as follows:

$$Q_6 = \frac{W_6\sqrt{T_6}}{P_6A_6}$$

$$= M_6\sqrt{\frac{\gamma_6 g_c}{R}}\sqrt{\frac{T_6}{T_{6S}}}\frac{P_{6S}}{P_6}$$

$$= \frac{M_6\sqrt{\frac{\gamma_6 g_c}{R}}\left(1 + \frac{\gamma_6-1}{2}M_6^2\right)^{\frac{1}{2}}}{\left(1 + \frac{\gamma_6-1}{2}M_6^2\right)^{\frac{\gamma}{\gamma-1}}}$$

$$Q_6 = \frac{M_6\sqrt{\frac{\gamma_{61} g_c}{R}}}{\left(1 + \frac{\gamma_{61}-1}{2}M_6^2\right)^{\frac{\gamma_{61}+1}{2(\gamma_{61}-1)}}} \qquad (9)$$

And it follows that, since $W_{61} = W_6$ (continuity),

$$P_6 = \frac{W_{61}\sqrt{T_{61}}}{Q_6A_{61}} \qquad (10)$$

where $A_{61} = A_{56} + A_{16}$ (constant area mixer).

An extensive analysis of steady-state data from the engine manufacturer showed that the F404 mixer pressure loss could be very simply and accurately approximated by a 3% pressure loss, where,

$$P_{61} = P_6 - kP_6 \tag{11}$$

and k= 0.030727 for the F404 engine.

Appendix D

Data Smoothing and Filtering

Due to signal noise and sampling rate problems encountered in the collection of raw data, data smoothing and/or filtering techniques must be employed before any analysis is carried out. After investigating several data reduction and smoothing techniques, GasTOPS Ltd. concluded that a two-point moving average filtering method was the most effective and stable technique that could be used to smooth the N1 and N2 data. Examples of the raw and smoothed N_1 and N_2 data are shown in figures 29 and 30. The two-point moving average technique does not completely filter out the signal noise; however, it does reduce the magnitude of the scatter considerably. A two-point method is also employed on the more coherent P_{s3}, $P_{5.6}$, $T_{5.6}$ and Fg_c data to help reduce small noise levels and/or spikes in these parameters [44].

The engine fuel flow transducer outputs two pulse signals, the period between which is proportional to the mass flow rate. At high flow rates, the rotor within the transducer spins at only four revolutions per second. However, as noted by Henry [3], the IECMS samples the fuel flow measurement at 10 Hz and therefore samples the same value two or three times before receiving an updated reading from the transducer. This problem with the sampling rate results in fuel flow traces that are generally very irregular. The following three steps are undertaken in order to generate a more useable set of fuel flow data [44]:

a) any points corresponding to large spikes or flats in the trace are removed from data set;

b) new points for the removed data are inserted using linear interpolation between the adjoining saved points; and,

c) the two-point moving average technique is applied to smooth the resulting curve.

An example of raw and smoothed fuel flow data is presented in figure 31. Table 3 summarizes the smoothing and filtering techniques currently used to improve the IECMS data.

Table 1

IECMS Parameters and Recording Frequencies

Symbol	Description	Units	Recording Rate (Hz)
T_1	Inlet Temperature	°C	5/10*
N_1	Fan Speed	%	10
N_2	Compressor Speed	%	10
W_{fm}	Fuel Flow	lb/hr	10
T_{56}	Turbine Discharge Temperature	°C	10
P_{56}	Turbine Discharge Pressure	psi	5/10*
P_{s3}	Compressor Discharge Pressure	psi	5/10*
EOP	Engine Oil Pressure	psi	1
VF	Fan Vibration	ips	1
VC	Compressor Vibration	ips	1
VB	Broadband Vibration	ips	1
PLA	Power Lever Angle	deg.	10
$\%A_8$	Nozzle Position	%	10
BAD	Bleed Air Door Flag	--	1
APC	APC Flag	--	1
VCS	VCS Flag	--	1
N2L	N_2 Lock-up Flag	--	1
BP	Boost Pressure Flag	--	1
DER	Derich Flag	--	1
REC	Pilot Record Flag	--	1
SEN	Sensor Failure Flag	--	1
AI	Anti-ice Flag	--	1
F_c	Computed Thrust	%	10
M_o	Mach Number	--	5/10*
AOA	Angle of Attack	deg.	5/10*
T_o	Total Temperature	°C	5/10*
P_{alt}	Pressure Altitude	ft.	5/10*

* pre/post event recording rates

Table 2

Engine Take-Off Data File Parameters

Parameter	Description	Units
TIME	Event recording time	sec
T1	Fan inlet temperature (recorded)	°C
N1	LP rotor speed (recorded)	%
SN1	LP rotor speed (smoothed)	%
SN1C	Corrected LP rotor speed (smoothed)	%
N2	HP rotor speed (recorded)	%
SN2	HP rotor speed (smoothed)	%
SN2C	Corrected HP rotor speed (smoothed)	%
PS3	Compressor discharge pressure (recorded)	psia
SPS3	Compressor discharge pressure (smoothed)	psia
P56	LP turbine exit pressure (recorded)	psia
SP56	LP turbine exit pressure (smoothed)	psia
T56	LP turbine exit temperature (recorded)	°C
ST56	LP turbine exit temperature (smoothed)	°C
WFM	Core engine fuel flow (recorded)	pph
SWFM	Core engine fuel flow (smoothed)	pph
W_P3	Corrected fuel ratio units $W_{fm}/P_{s3}\sqrt{\theta_1}$	pph/psia
NOZ	Nozzle position (recorded)	%
PLA	Power lever angle (recorded)	deg
EOP	Engine oil pressure (recorded)	psi
VF	Fan vibration (recorded)	ips
VC	Compressor vibration (recorded)	ips
VB	Broadband vibration (recorded)	ips
SFCC	Corrected specific fuel consumption	pph/lb_f
QC	Computed flow parameter	lb_m/sec
THR	Computed thrust (recorded)	%

Table 3

Data Smoothing and Filtering Techniques

Parameter	Smoothing Technique
N_1	2 point moving average (10 iterations)
N_2	2 point moving average (20 iterations)
W_{fm}	Flats and spikes removed and 2 point moving average (2 iterations)
T_{56}	2 point moving average (2 iterations)
P_{56}	2 point moving average (2 iterations)
P_{s3}	2 point moving average (2 iterations)
EOP	Not smoothed
VF	Not smoothed
VC	Not smoothed
VB	Not smoothed
PLA	Not smoothed
$\%A_8$	Not smoothed
F_C	2 point moving average (1 iteration)
T_1	T_1 value when smoothed N_1 is equal to 90%

Table 4
Estimated IECMS Precision Errors [4]

Parameter	Target Value	Total Error	% Total Error
N_1	10000 rpm	+/-121 rpm	+/-1.2%
N_2	14000 rpm	+/-141 rpm	+/-1.0%
P_{S3}	300 psia	+/-12.4 psia	+/-4.1%
$P_{5.6}$	40 psia	+/-1.3 psia	+/-3.2%
$T_{5.6}$	1440°R	+/-58°R	+/-2.0%
W_{f3}	6000 lbm/hr	+/-161 lbm/hr	+/-2.7%
A_8	30%	+/-0.62%	+/-2.0%

Table 5
Predicted Parameter Sensitivity to W_{f3} Precision Error

Parameter	Sensitivity to Wf3 +/-2.7%*
N_1	+/-0.52%
N_2	+/-0.40%
P_{S3}	+/-1.93%
$P_{5.6}$	+/-1.69%
$T_{5.6}$	+/-0.73%

Table 6
Predicted Parameter Sensitivity to A_8 Precision Error

Parameter	Sensitivity to A8 +/-2.0%*
N_1	+/-0.12%
N_2	+/-0.01%
P_{S3}	+/-0.04%
$P_{5.6}$	+/-0.38%
$T_{5.6}$	+/-0.10%

* At W_{f3} = 6635 lbm/hr, A_8 = 19.5%

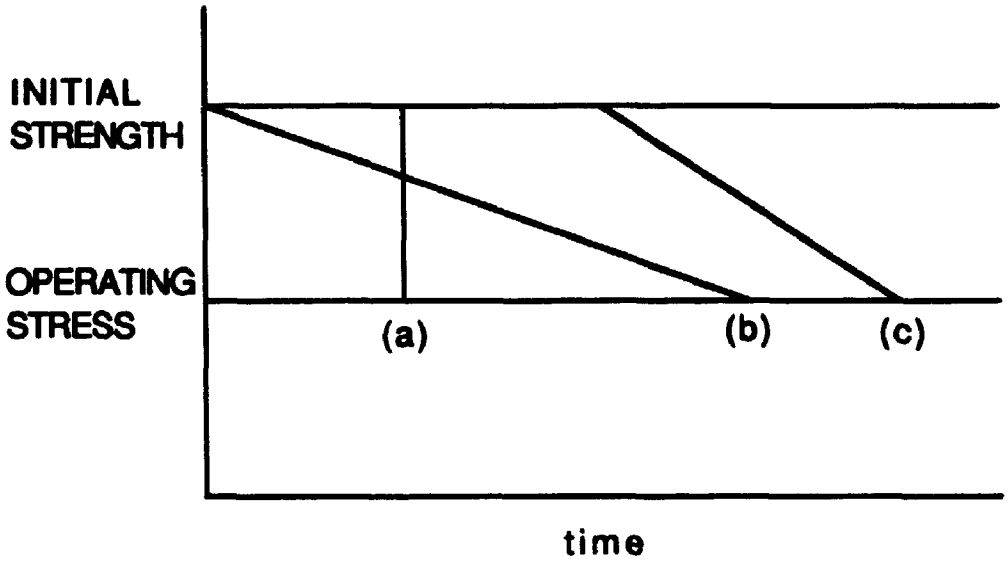

Figure 1: Failure Modes

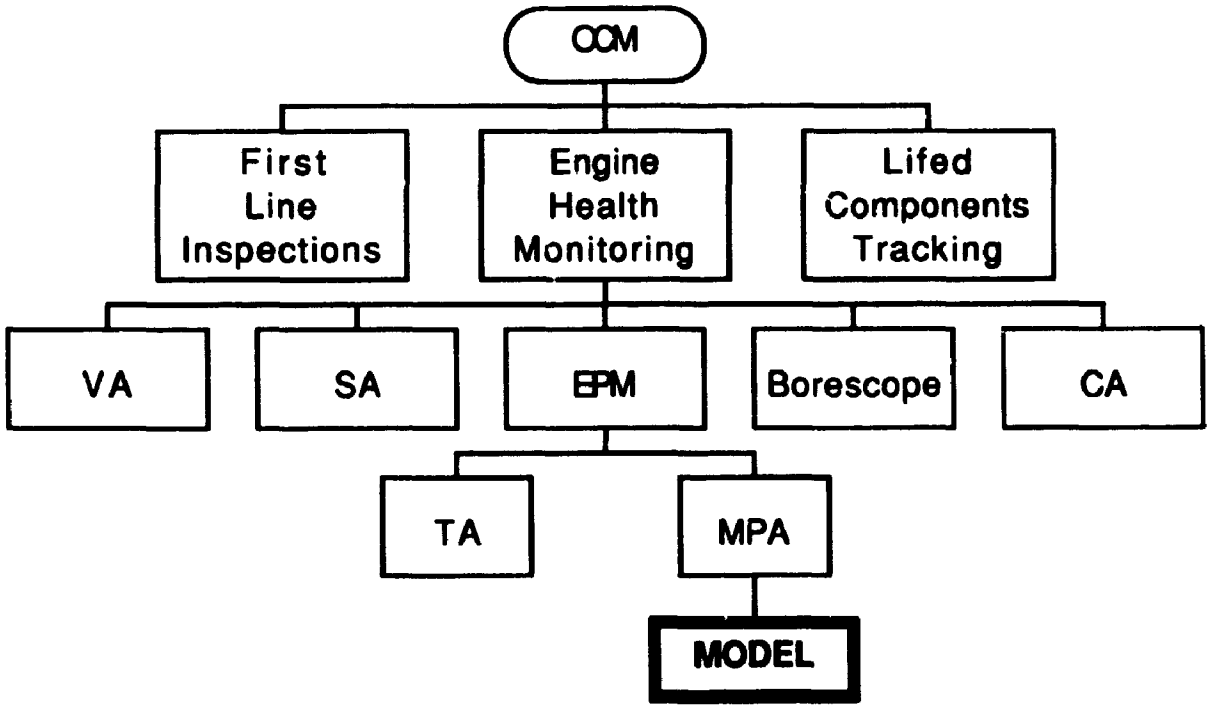

Figure 2: Thermodynamic Modelling Under the OCM Approach

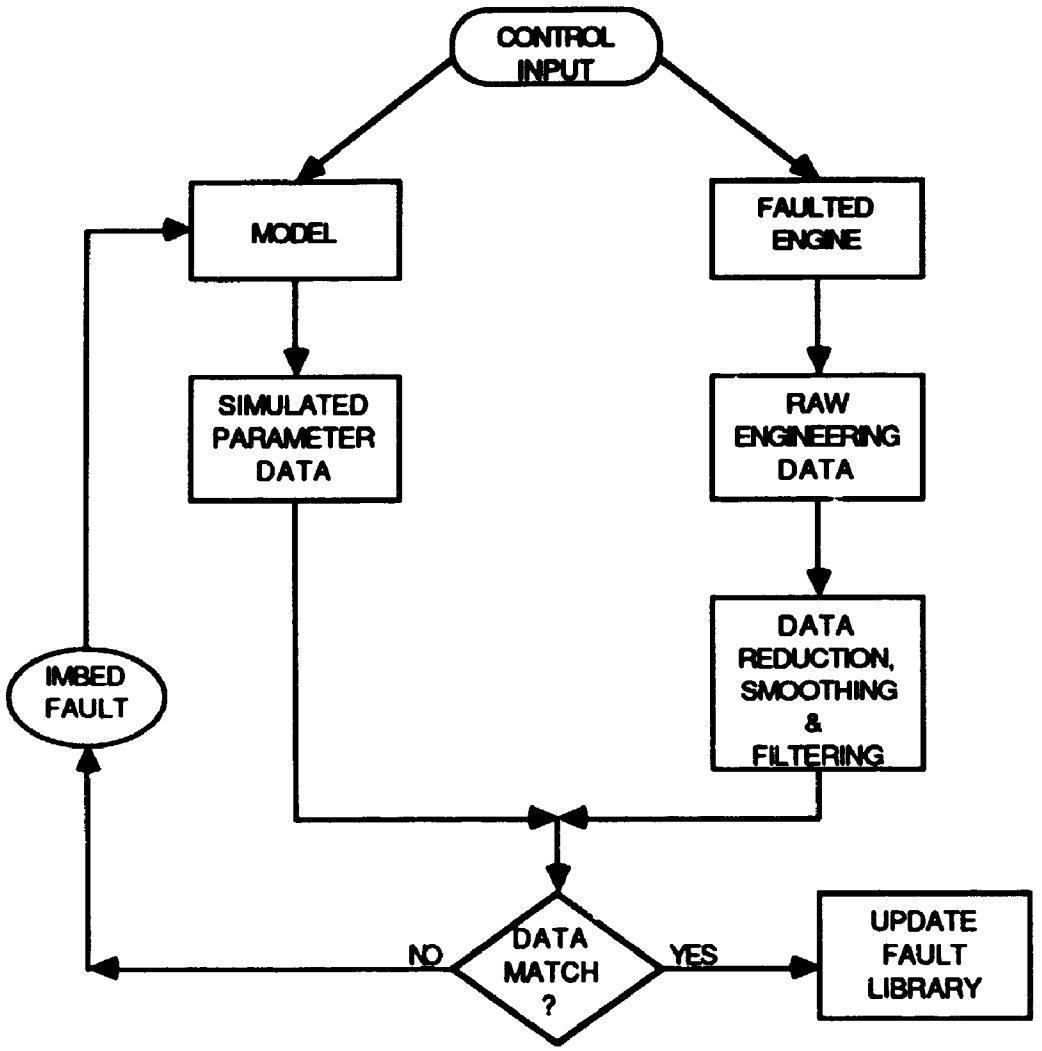

Figure 3: Fault Library Development

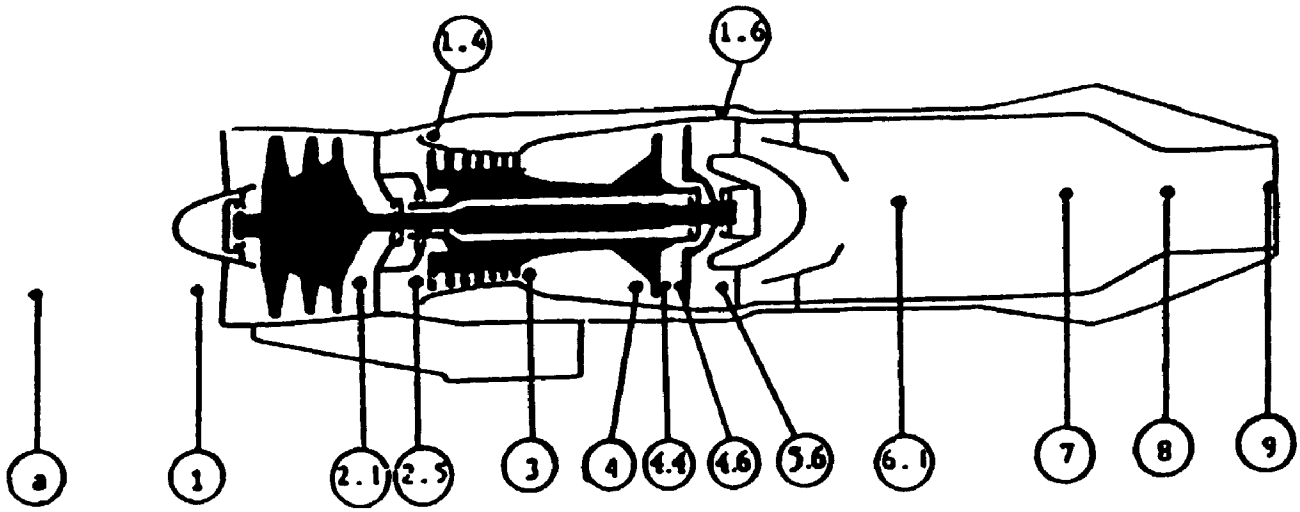

Figure 4: F404 Station Numbering

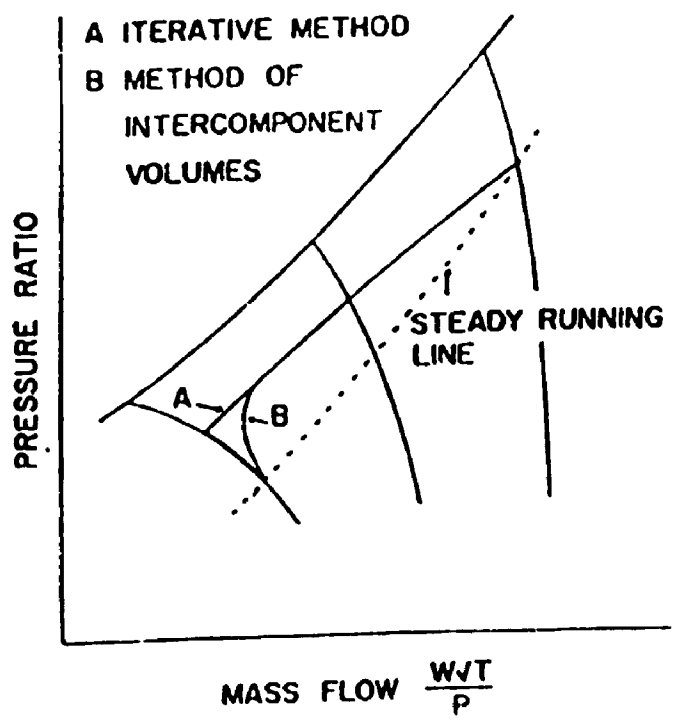

Figure 5: Single-Spool Compressor Operating Trajectories for Two Dynamic Modelling Methods [21]

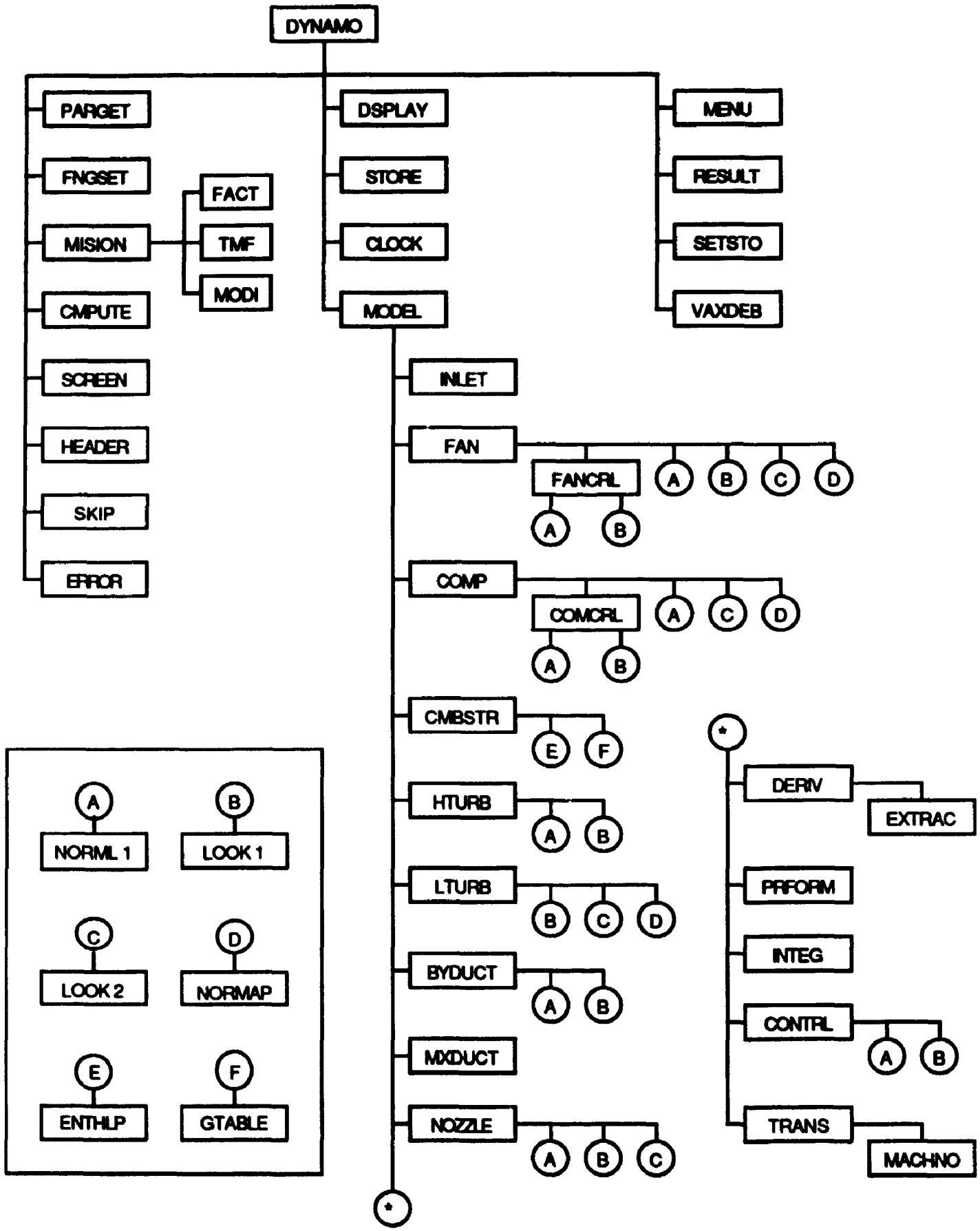

Figure 6: Program Hierarchy Diagram

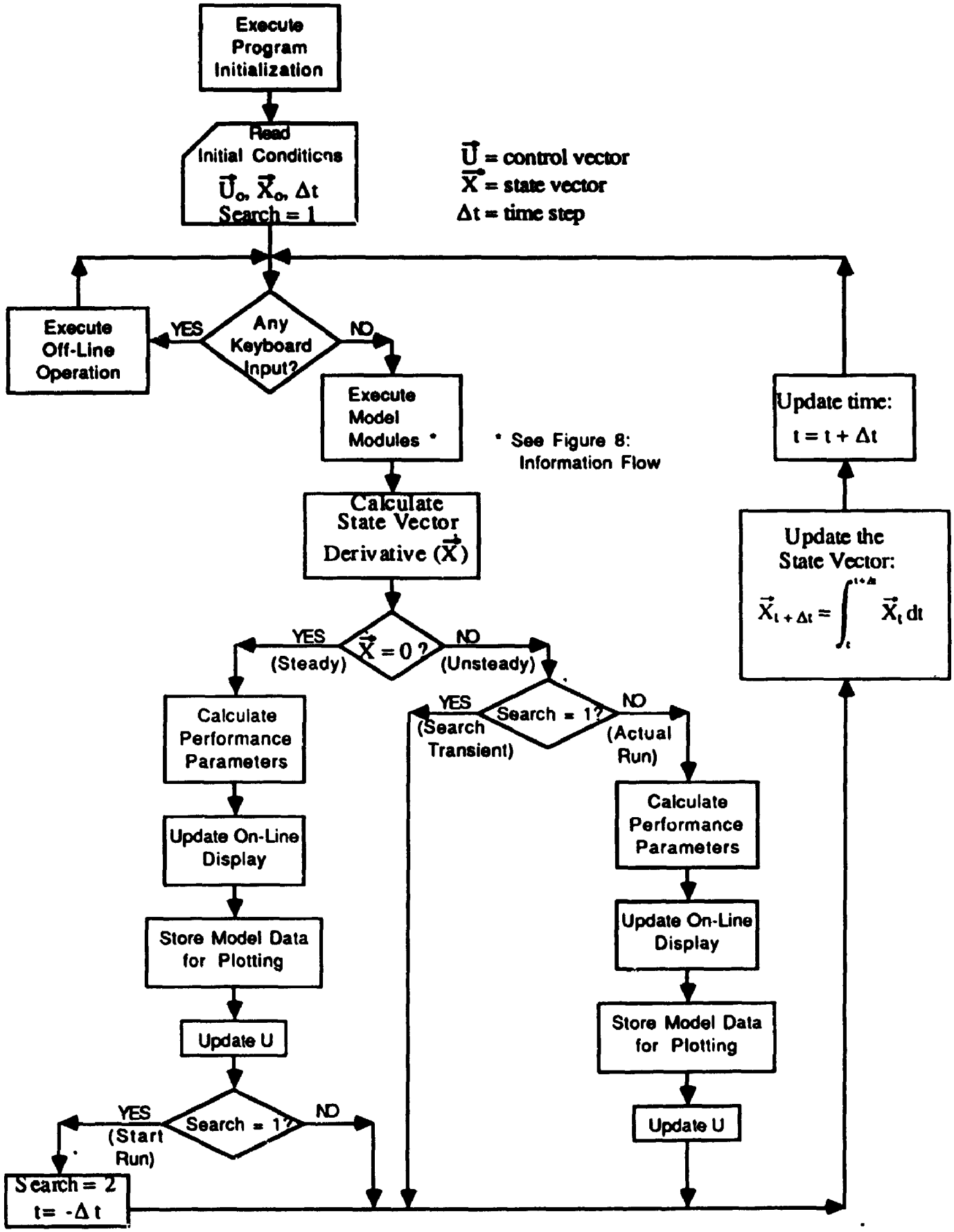

Figure 7: Program Flow Chart

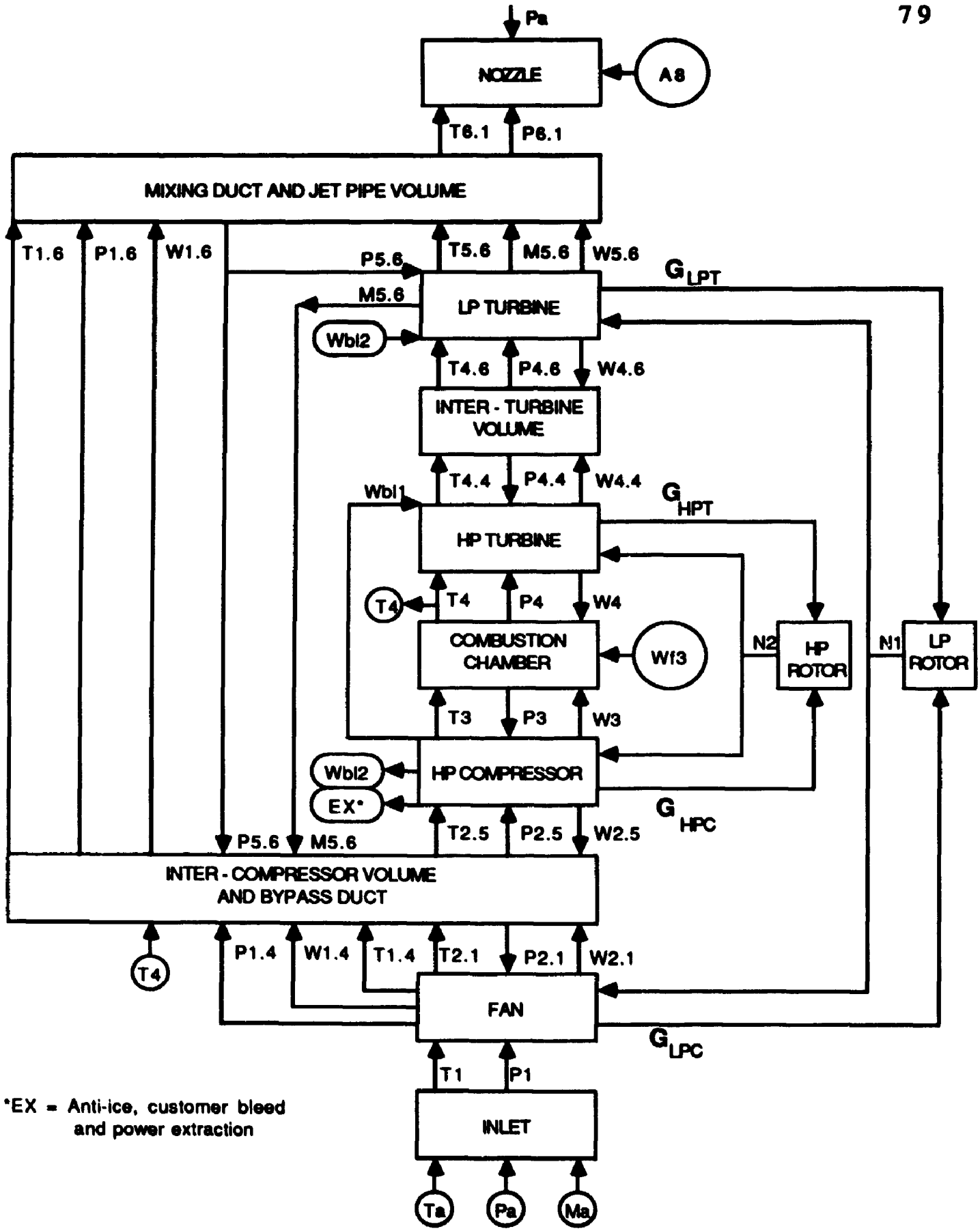

*EX = Anti-ice, customer bleed and power extraction

Figure 8: Model Information Flow

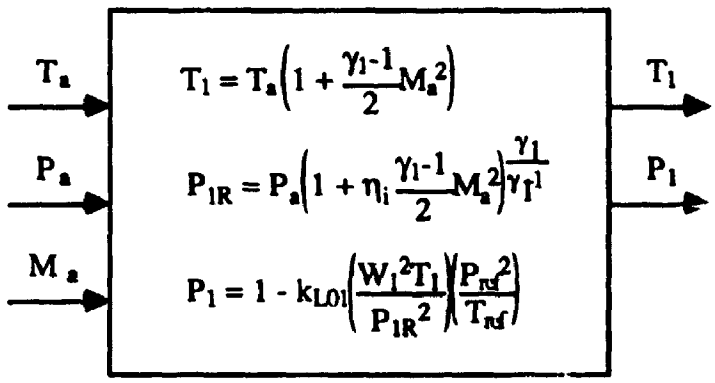

Figure 9: The Inlet Module

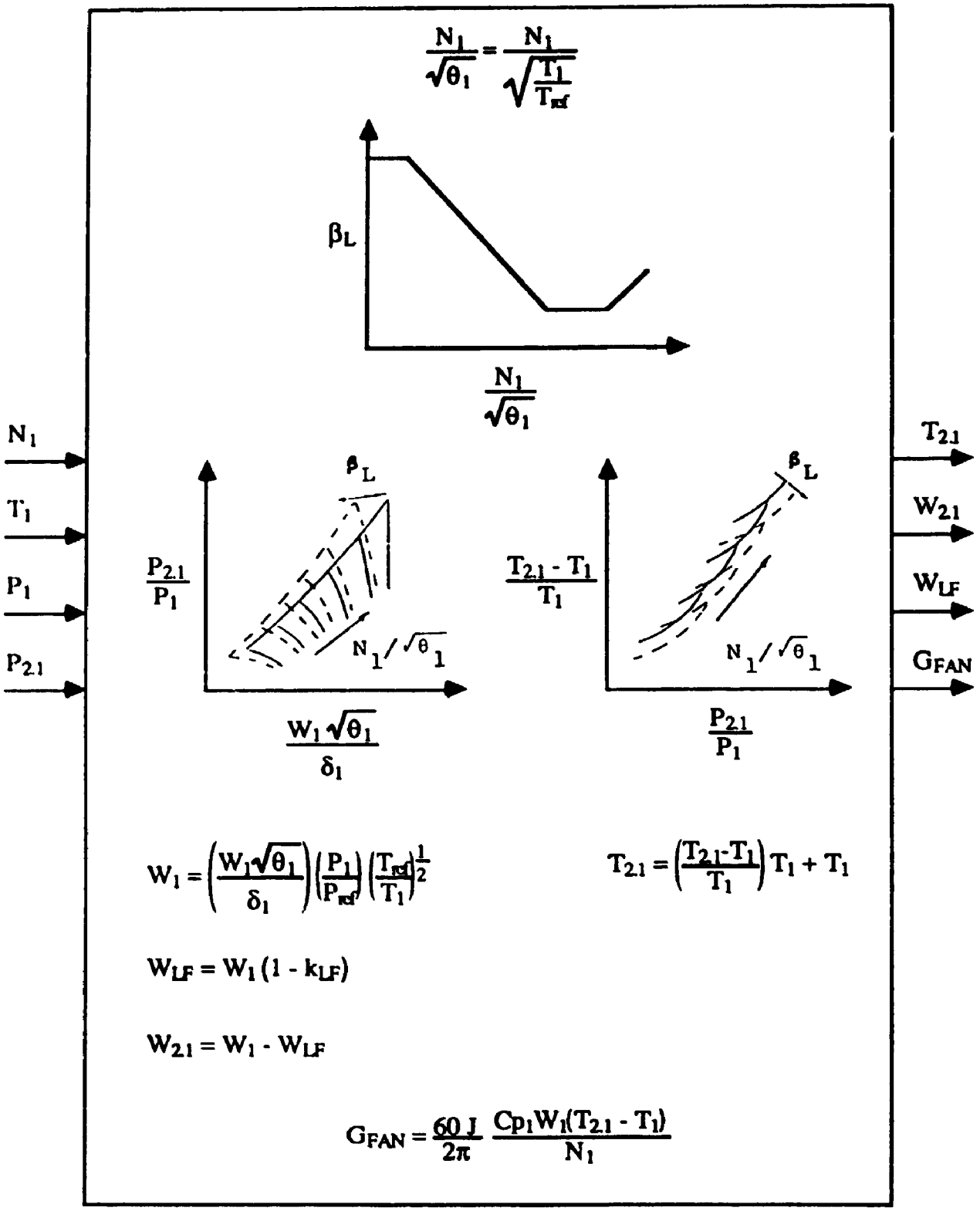

Figure 10: The Fan Module

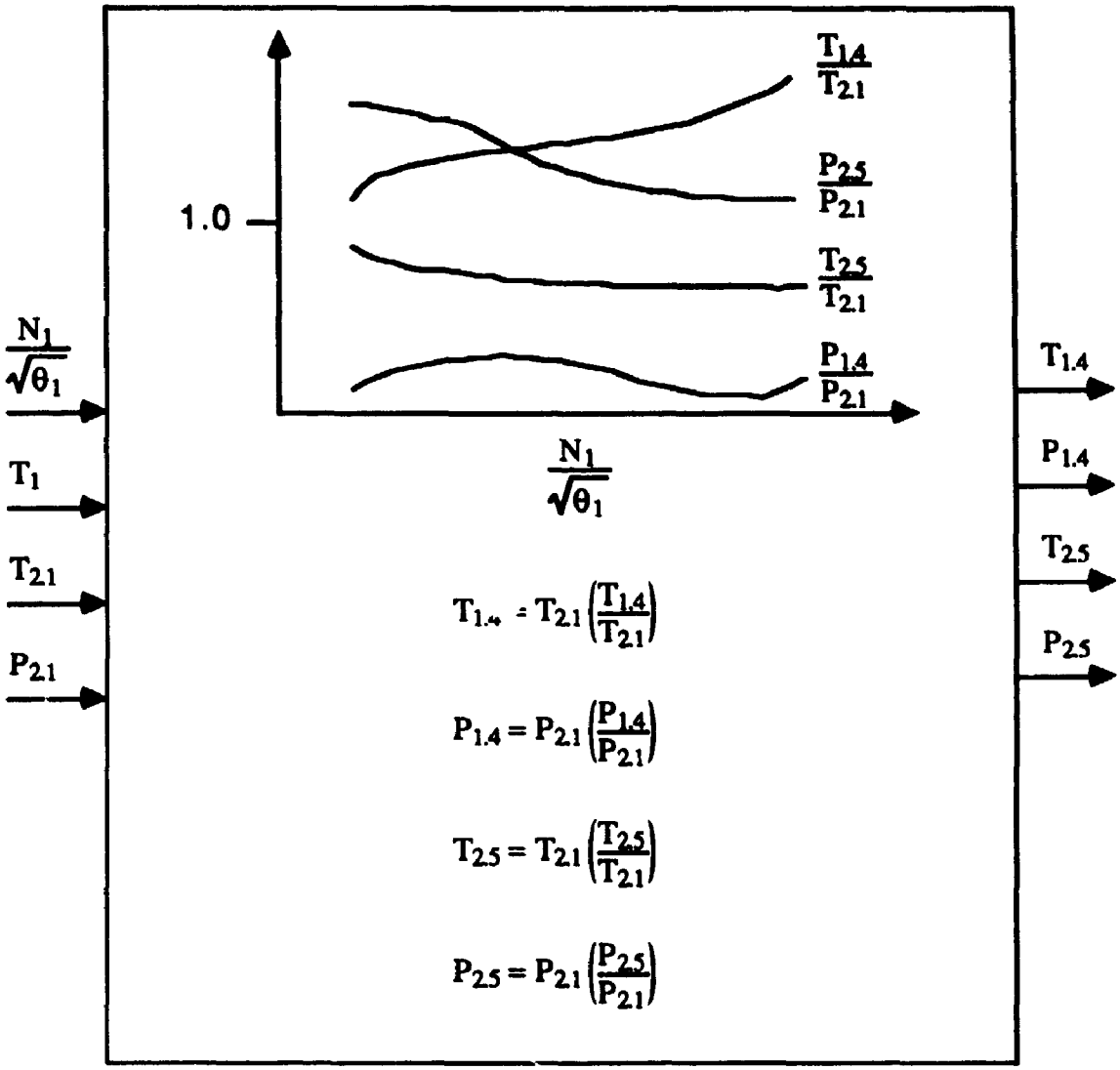

Figure 11: Radial Non-Uniformity of Parameters at the Fan Exit

2 OF/DE 2

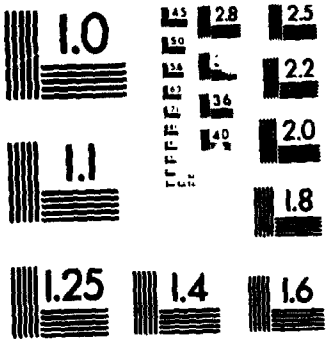

$$\frac{N_2}{\sqrt{\theta_{25}}} = \frac{N_2}{\sqrt{\frac{T_{25}}{T_{ref}}}}$$

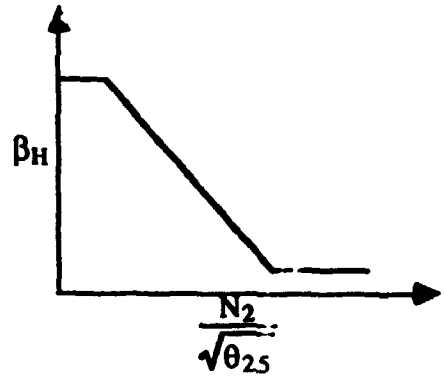

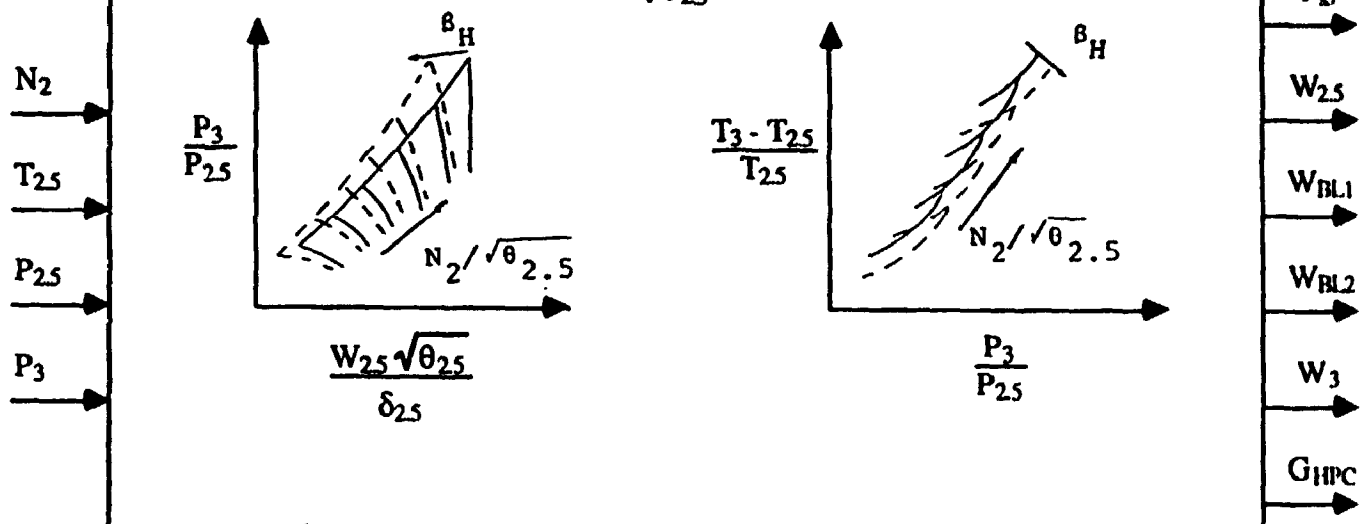

$$W_{25} = \left(\frac{W_{25}\sqrt{\theta_{25}}}{\delta_{25}}\right)\left(\frac{P_{25}}{P_{ref}}\right)\left(\frac{T_{ref}}{T_{25}}\right)^{\frac{1}{2}}$$

$$T_3 = \left(\frac{T_3 - T_{25}}{T_{25}}\right) T_{25} + T_{25}$$

$$W_{BL1} = k_{BL1} \cdot W_{25}$$

$$P_{s3} = P_3 \cdot 0.9375$$

$$W_{BL2} = k_{BL2} \cdot W_{25}$$

$$W_{AI} = W_{25} \cdot k_{WAI} \quad (\text{for } T_a < 505°R)$$

$$W_3 = W_{25} - W_{BL1} - W_{BL2} - W_{BLx} - W_{AI}$$

$$G_{HPC} = \frac{60\,J}{2\pi} \frac{Cp_{25} W_{25} (T_3 - T_{25})}{N_2}$$

Figure 12: The High Pressure Compressor Module

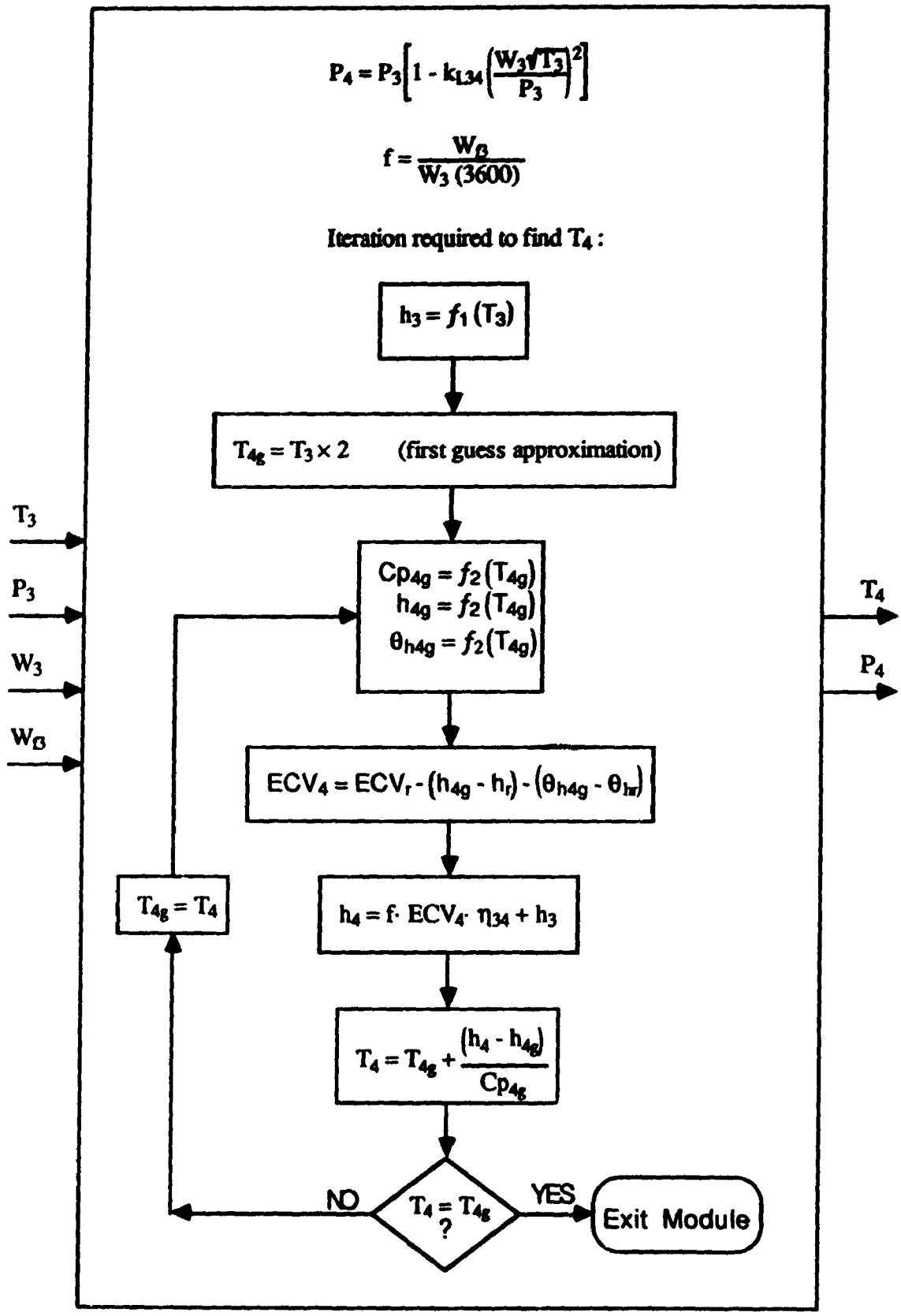

Figure 13: The Combustor Module

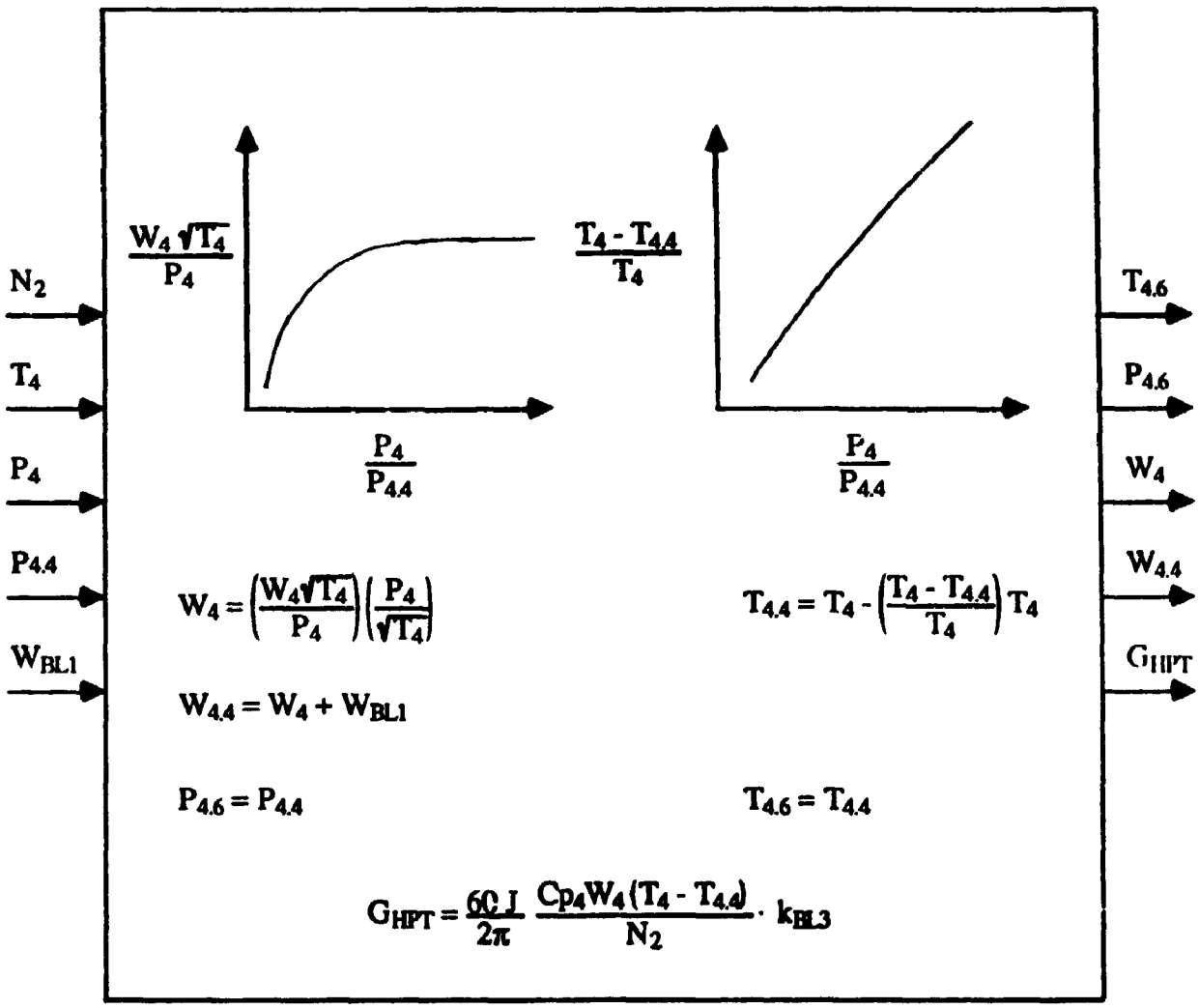

Figure 14: The High Pressure Turbine Module

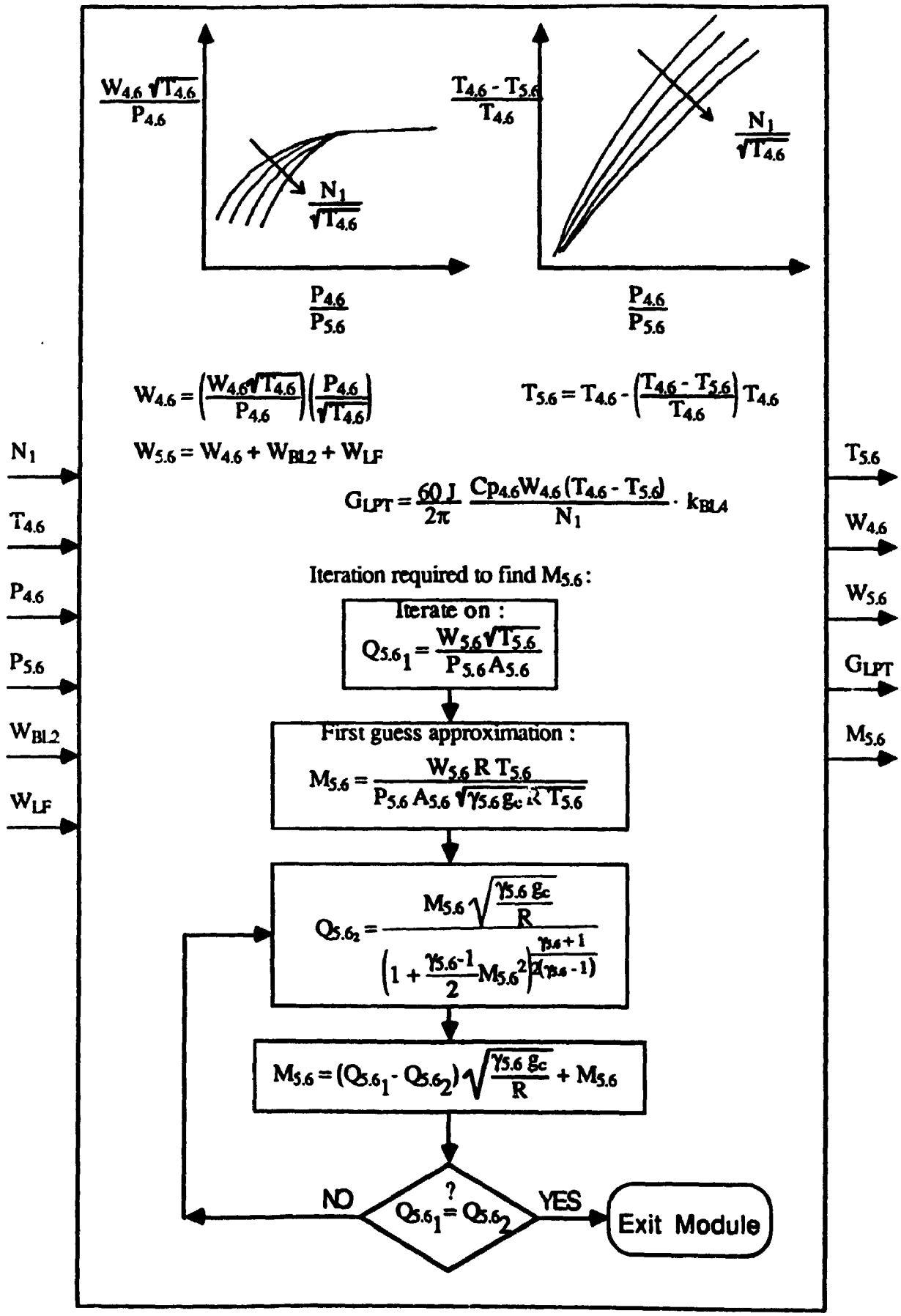

Figure 15: The Low Pressure Turbine Module

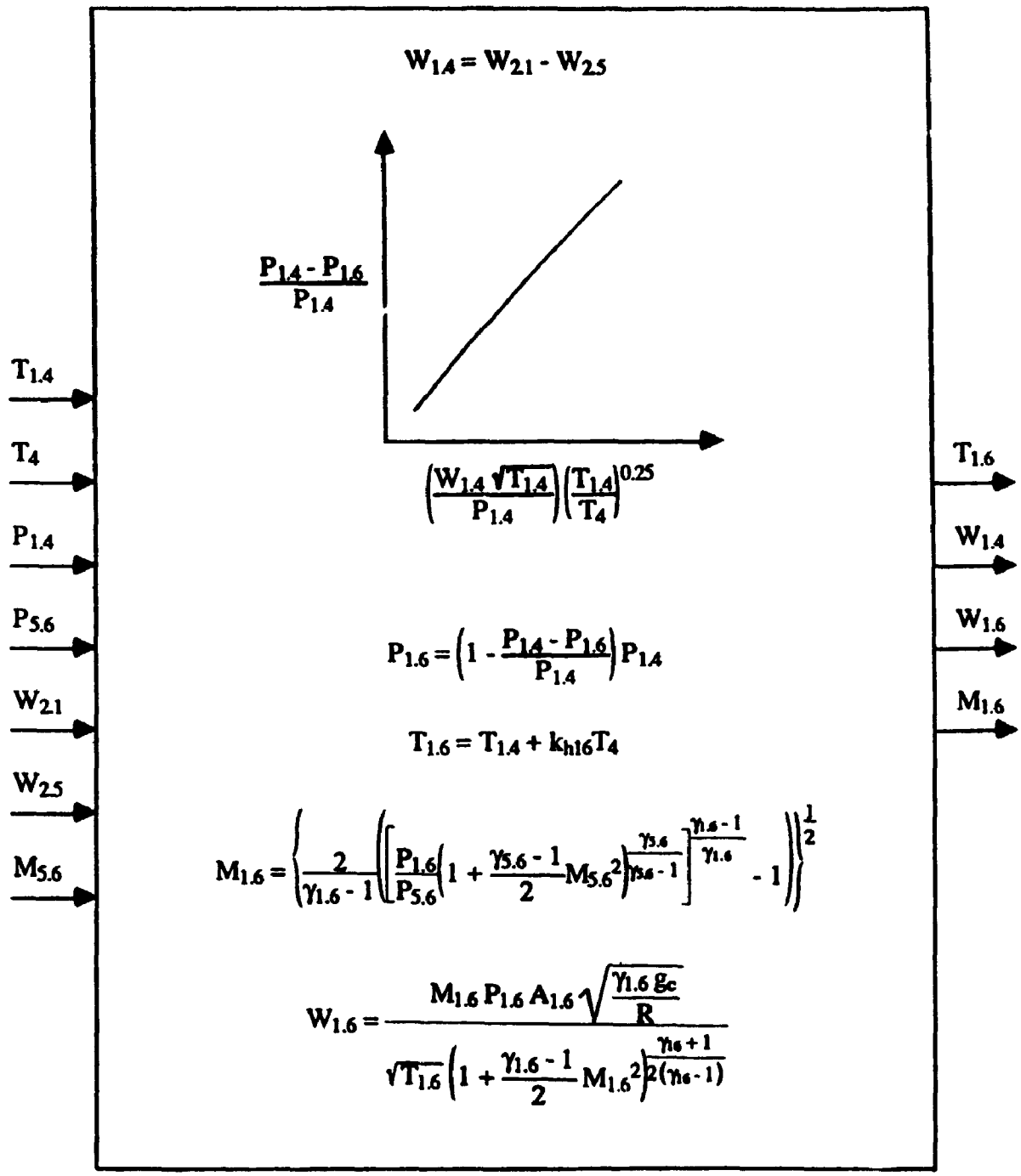

Figure 16: The Bypass Duct Module

$$W_6 = W_{1.6} + W_{5.6}$$

$$T_6 = \frac{W_{1.6}\, Cp_{1.6}\, T_{1.6} + W_{5.6}\, Cp_{5.6}\, T_{5.6}}{W_{1.6}\, Cp_{1.6} + W_{5.6}\, Cp_{5.6}}$$

$$M_6 = \left[\frac{2\,\Phi_6}{\left(1 - 2\,\gamma_6\,\Phi_6\right) + \sqrt{1 - 2\left(\gamma_6 + 1\right)\Phi_6}}\right]^{\frac{1}{2}}$$

where $$\Phi_6 = \left[\frac{1 + \frac{W_{1.6}}{W_{5.6}}}{\frac{1}{\sqrt{\phi_{5.6}}} + \frac{W_{1.6}}{W_{5.6}}\sqrt{\frac{\gamma_{5.6}\, T_{1.6}}{\gamma_{1.6}\, T_{5.6}\, \phi_{1.6}}}}\right]^2 \left(\frac{\gamma_{5.6}}{\gamma_{6.1}}\right)\left(\frac{T_6}{T_{5.6}}\right)$$

and $$\phi_{5.6} = \frac{M_{5.6}^2\left(1 + \frac{\gamma_{5.6} - 1}{2} M_{5.6}^2\right)}{\left(1 + \gamma_{5.6}\, M_{5.6}^2\right)^2}$$

$$\phi_{1.6} = \frac{M_{1.6}^2\left(1 + \frac{\gamma_{1.6} - 1}{2} M_{1.6}^2\right)}{\left(1 + \gamma_{1.6}\, M_{1.6}^2\right)^2}$$

$$Q_6 = \frac{M_6 \sqrt{\frac{\gamma_6\, g_c}{R}}}{\left(1 + \frac{\gamma_6 - 1}{2} M_6^2\right)^{\frac{\gamma_6 + 1}{2(\gamma_6 - 1)}}}$$

$$P_6 = \frac{W_6 \sqrt{T_6}}{Q_6\, A_6}$$

$$P_{6.1} = P_6 - k_{L6}\, P_6$$

$$T_{6.1} = T_6 \qquad W_{6.1} = W_6$$

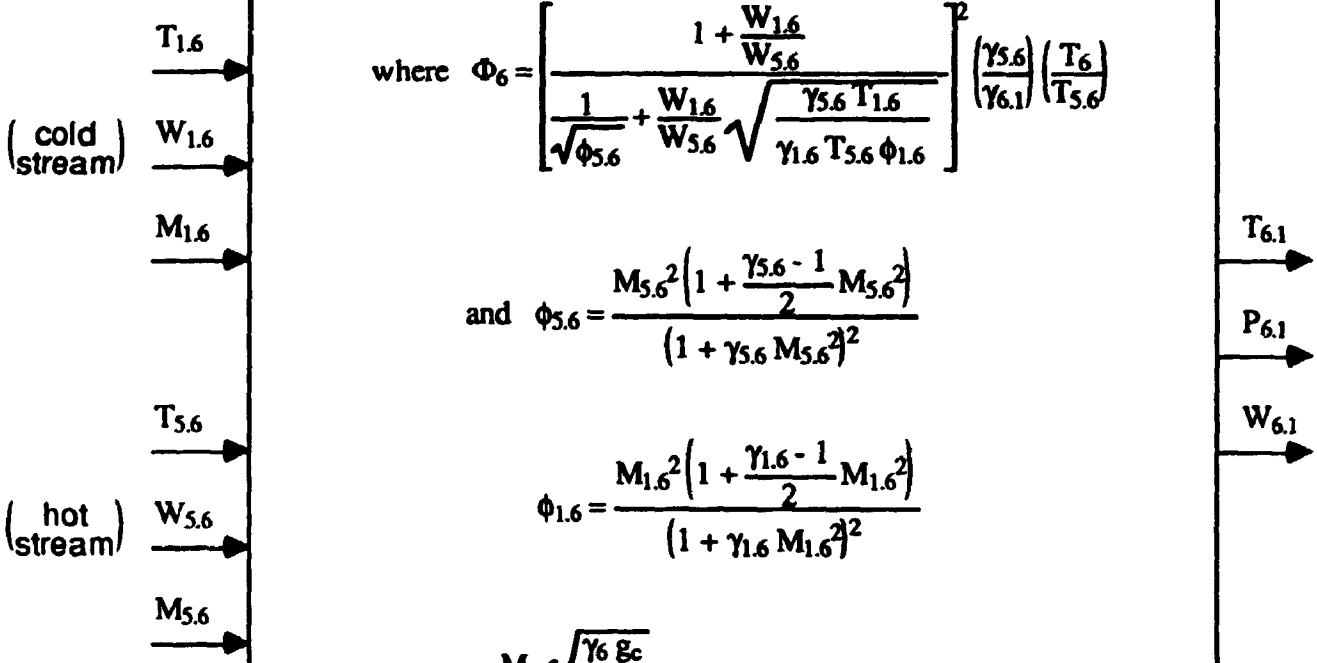

Figure 17: The Mixer Module

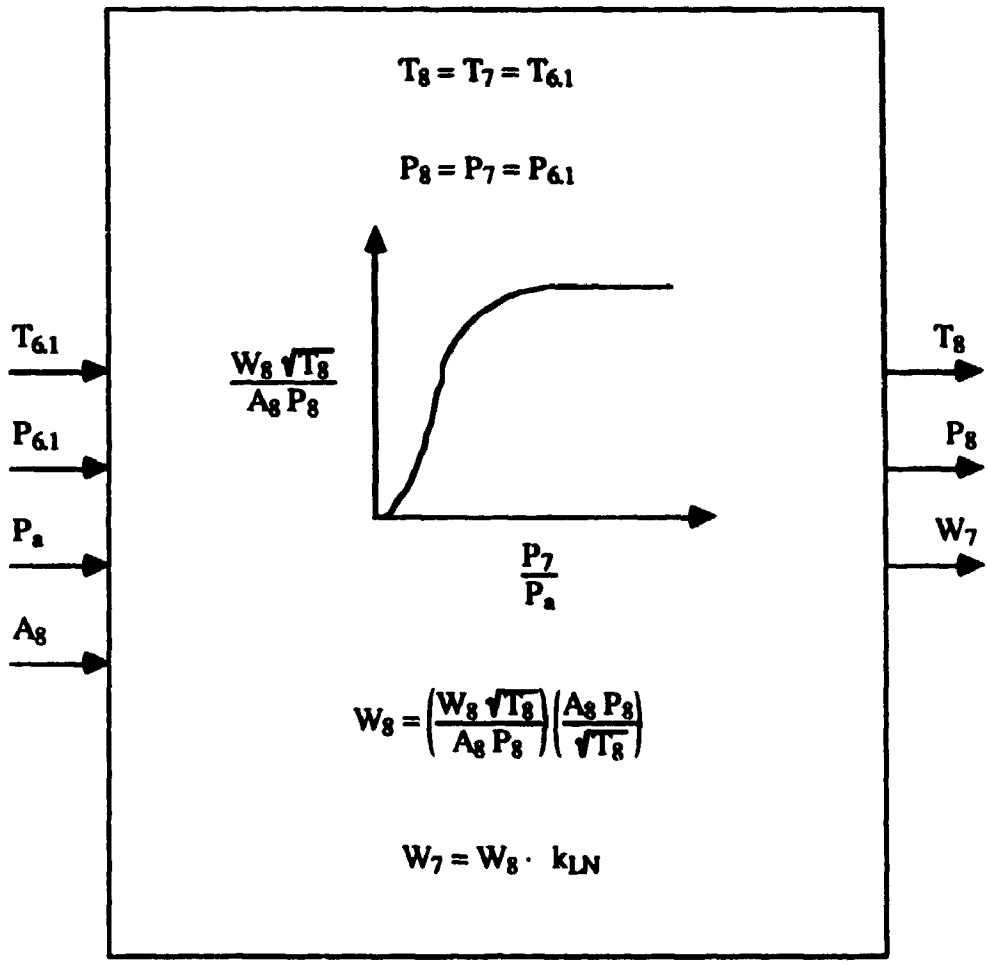

Figure 18: The Variable Exhaust Nozzle

Corrected Engine Airflow Parameter:

$$Q_c = \frac{0.509 \cdot P_{5.6} A_8 \sqrt{\frac{T_1}{T_{ref}}}}{\sqrt{T_{5.6}} \frac{P_a}{P_{ref}}}$$

Corrected fuel flow:

$$W_{\beta c} = W_\beta \cdot \sqrt{\frac{T_1}{T_{ref}}}$$

THRUST CALCULATIONS

Engine Pressure Ratio:

$$EPR = \frac{P_{5.6}}{P_a}$$

Force-Area-Pressure Function:

$$FAP = 1.4985 \cdot EPR - 2.10194 \quad (\text{for } EPR < 2.8789)$$

$$FAP = 1.2620 \cdot EPR - 1.42269 \quad (\text{for } EPR \geq 2.8789)$$

Nozzle Thrust (uncorrected):

$$F_g = FAP \cdot A_8 \cdot P_{ref}$$

T1 Correction Lapse Rate:

$$FNQ = 0.9556 + 0.001117\, T_1 - 2.43\times10^{-5}\, T_1^2 \quad (\text{for } T_1 < -6.7°C)$$

$$FNQ = 0.9550 + 0.001753\, T_1 + 8.31\times10^{-5}\, T_1^2 \quad (\text{for } T_1 \geq -6.7°C)$$

Corrected Thrust (%):

$$F_{gc} = \frac{F_g}{F_{gb}} \cdot FNQ \cdot 100$$

Corrected Thrust Specific Fuel Consumption:

$$TSFC_c = \frac{W_{\beta c}}{(F_{gc} \cdot 100)}$$

Inputs: P_a, T_1, W_β, $T_{5.6}$, $P_{5.6}$, A_8

Outputs: Q_c, $W_{\beta c}$, F_g, F_{gc}, $TSFC_c$

Figure 19: The Engine Performance Calculations

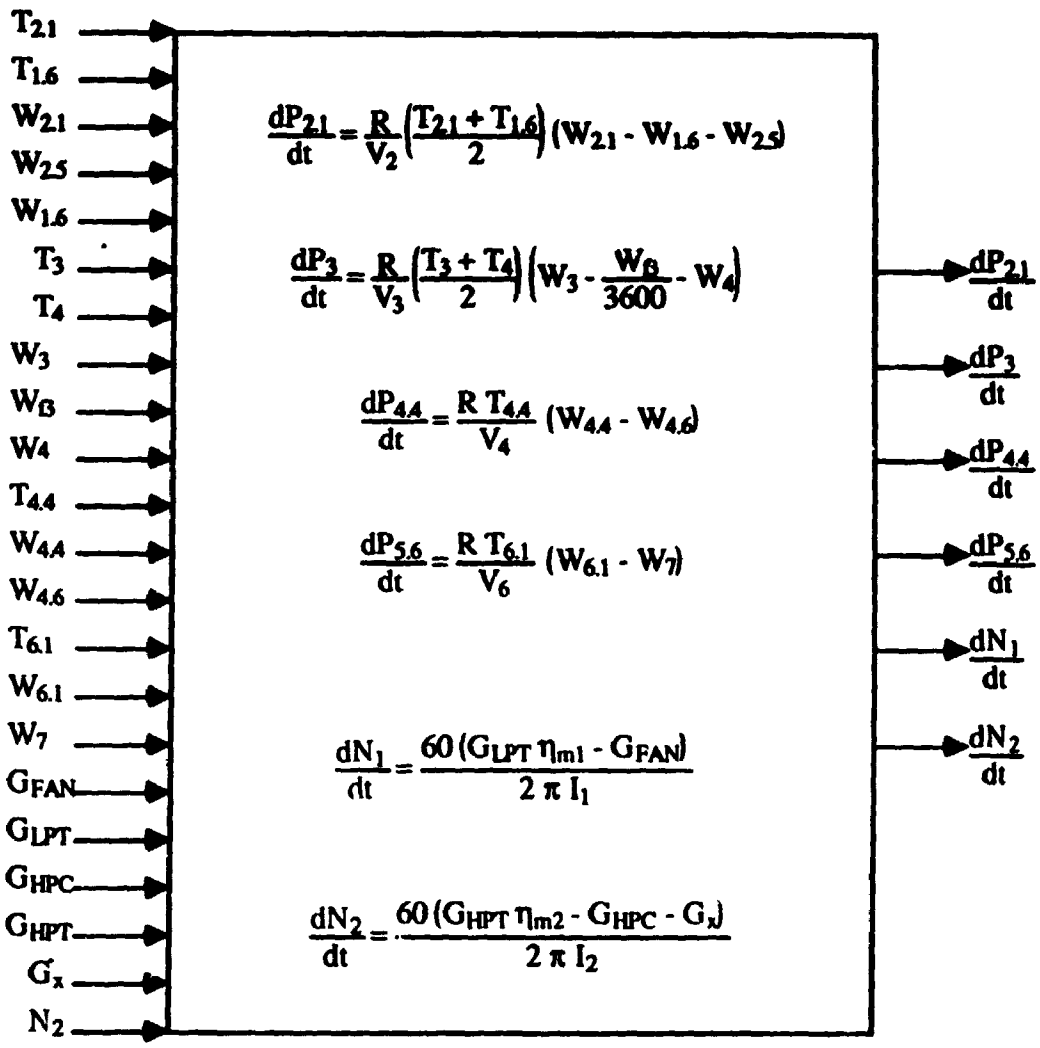

Figure 20: The State Vector Derivative Calculations

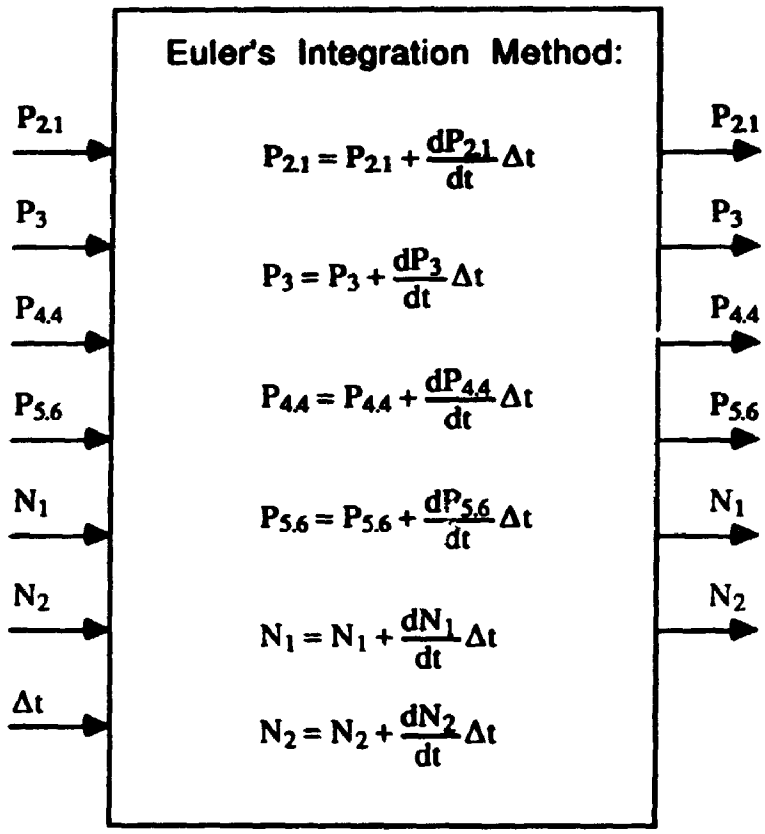

Figure 21: The Integration Routine

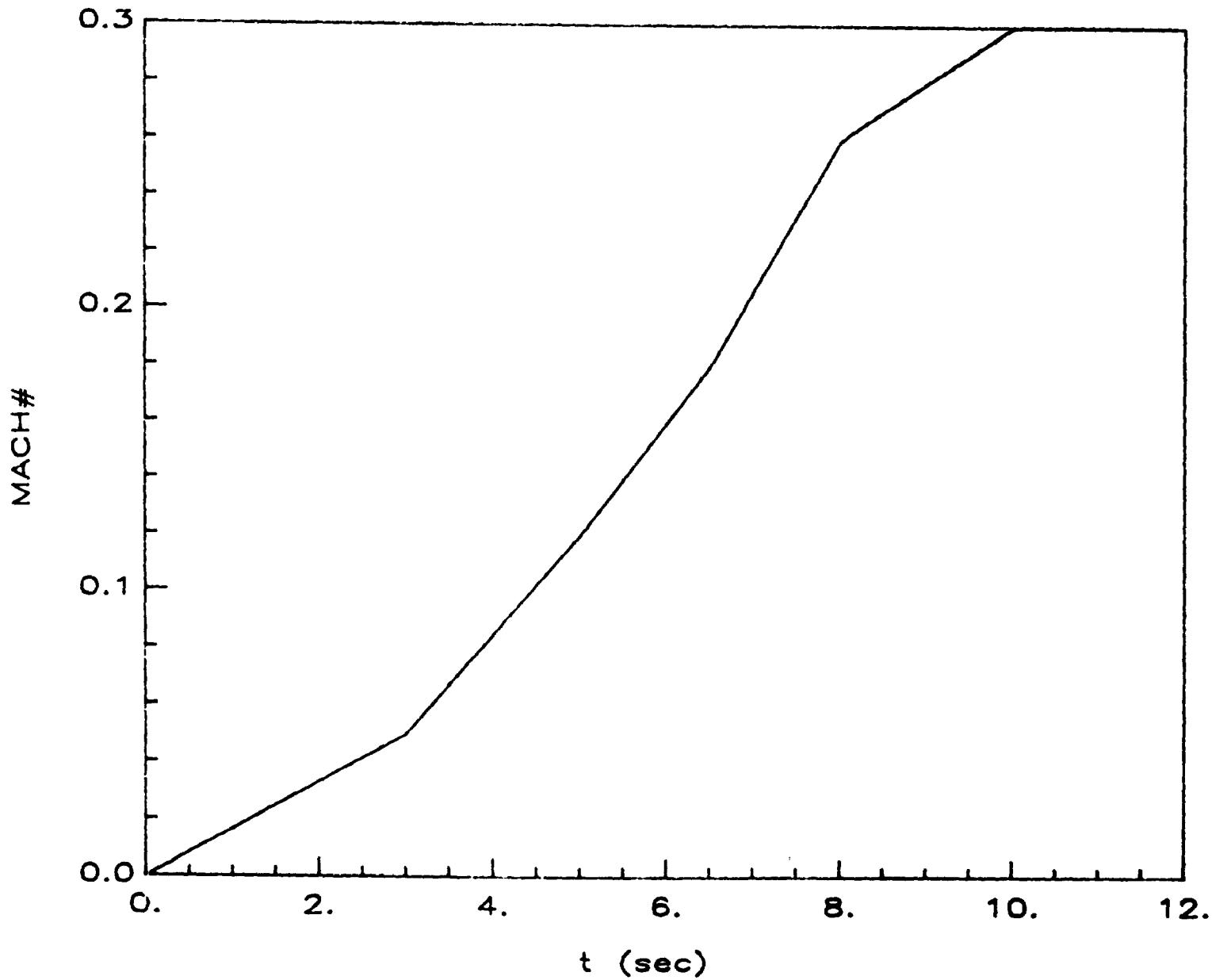

Figure **22** — Mach no. versus time — Typical Take—Off

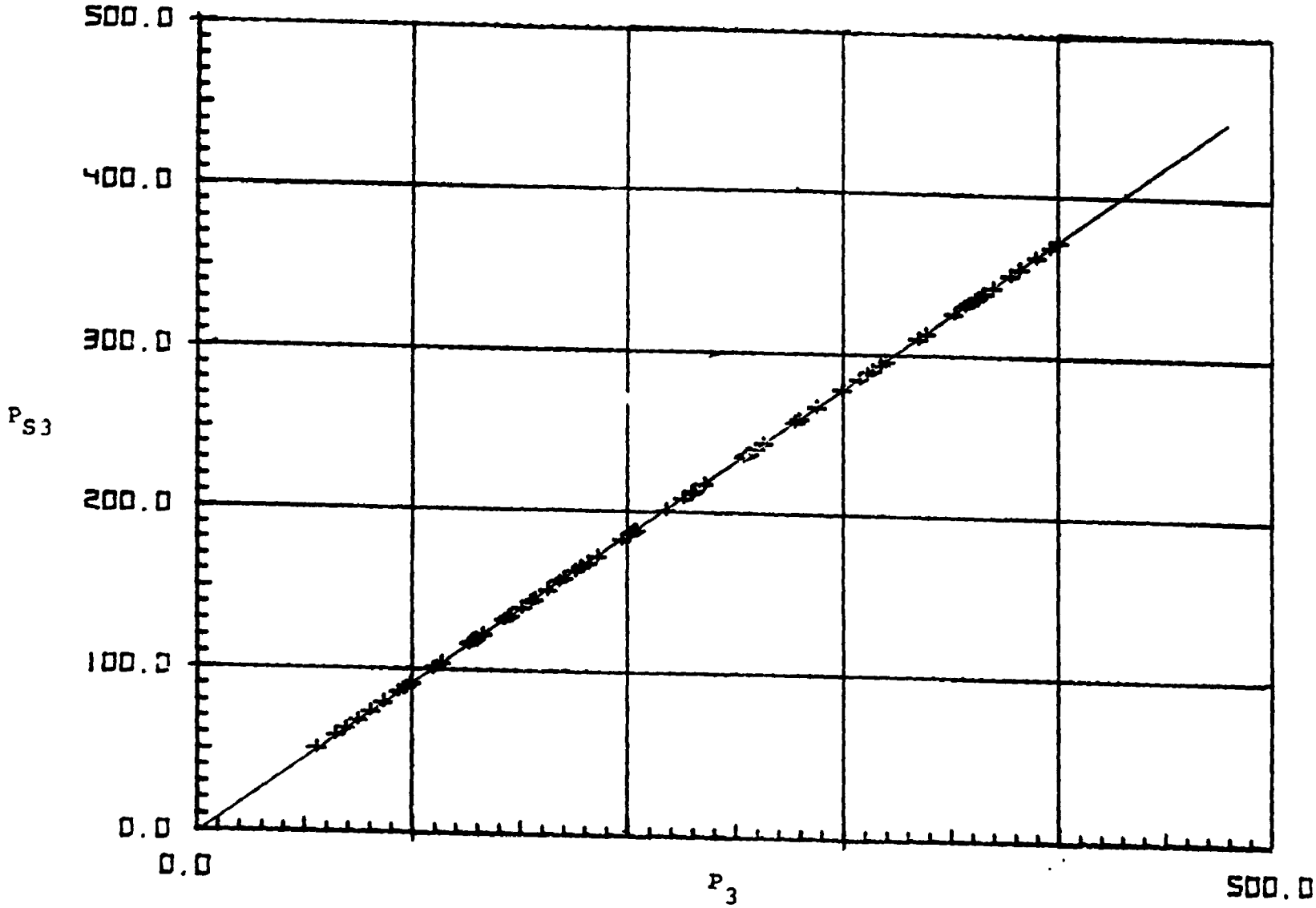

Figure 23: P_{S3} versus P_3 Relationship

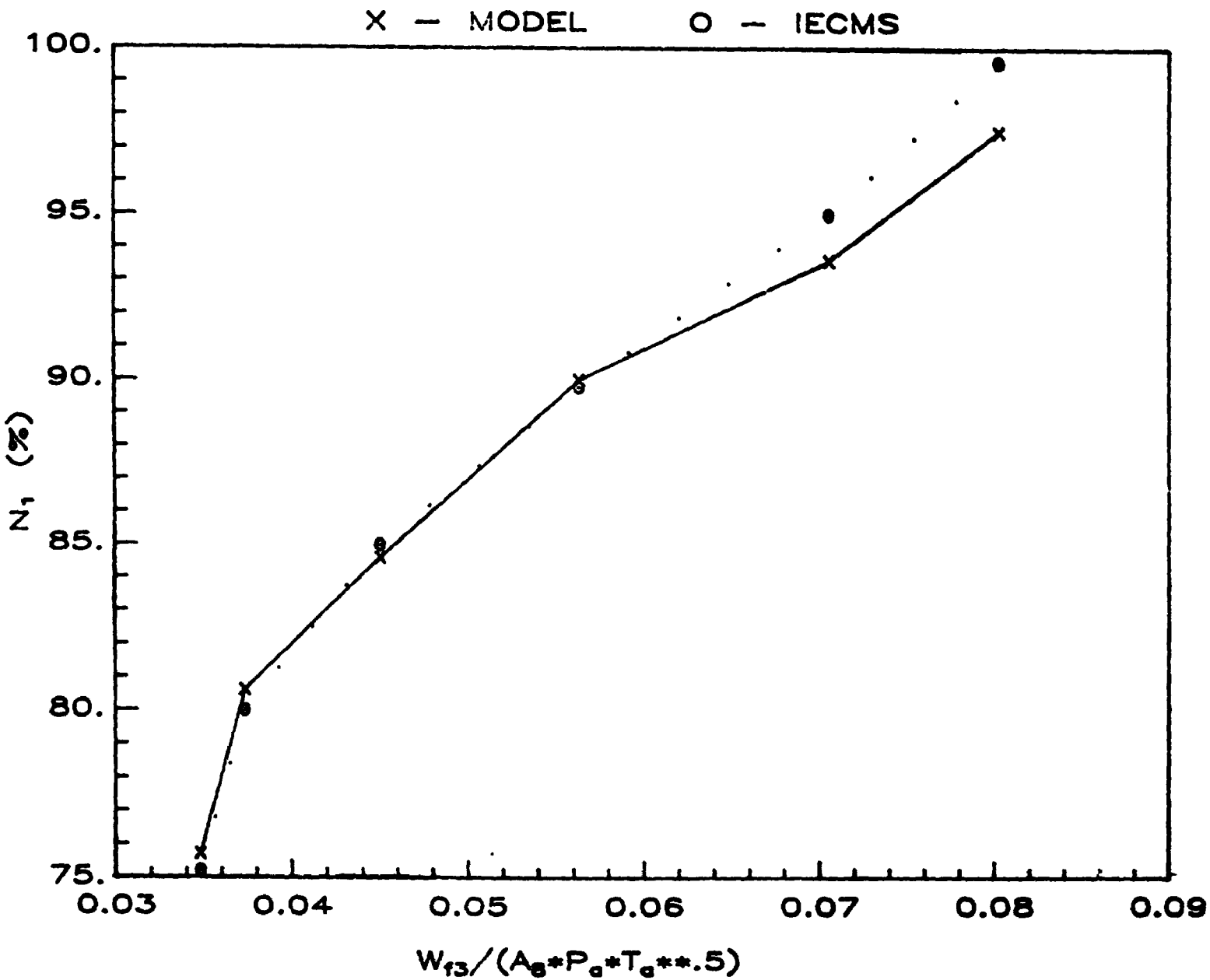

Figure **24** — STEADY—STATE VALIDATION

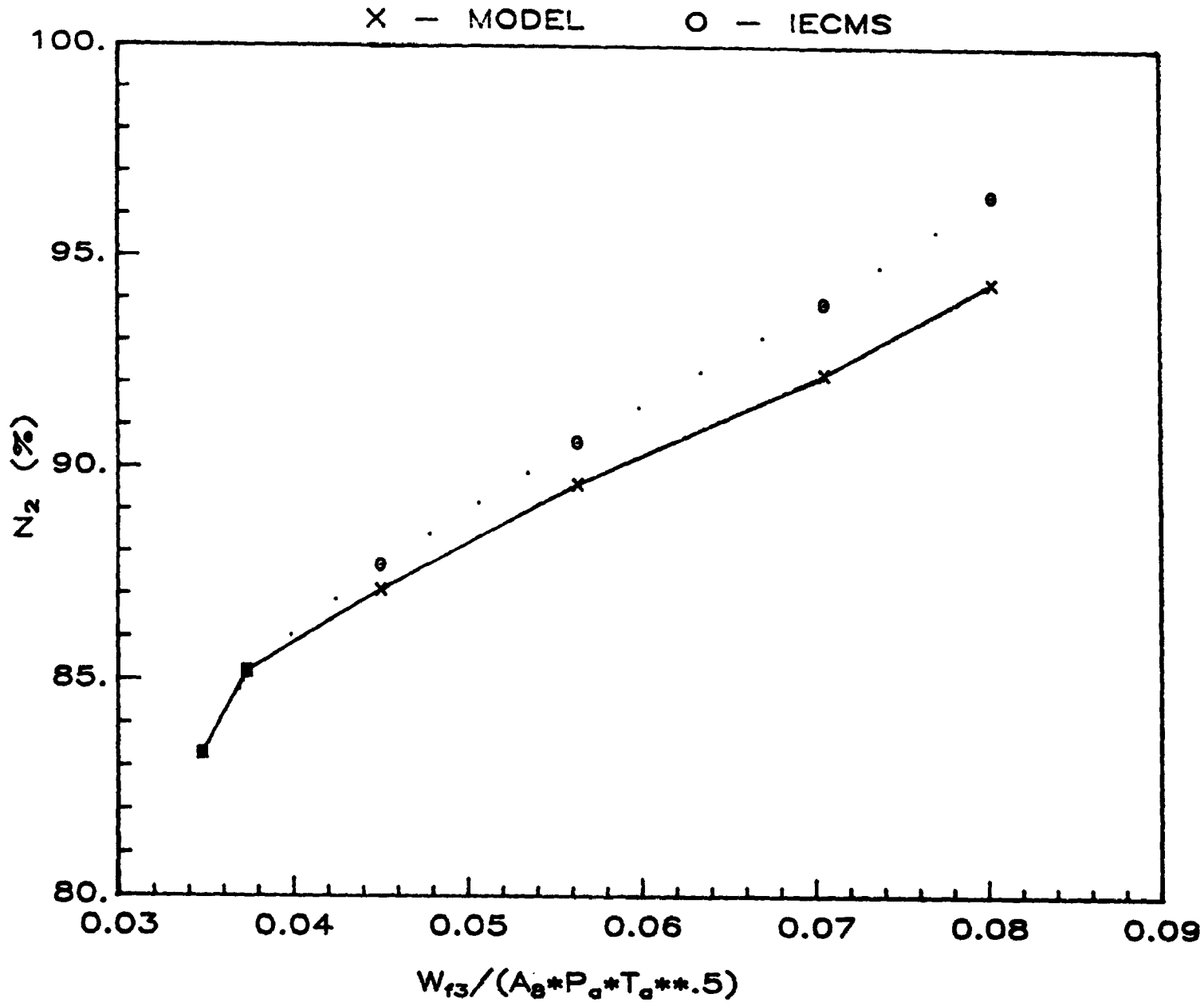

Figure **25** — STEADY—STATE VALIDATION

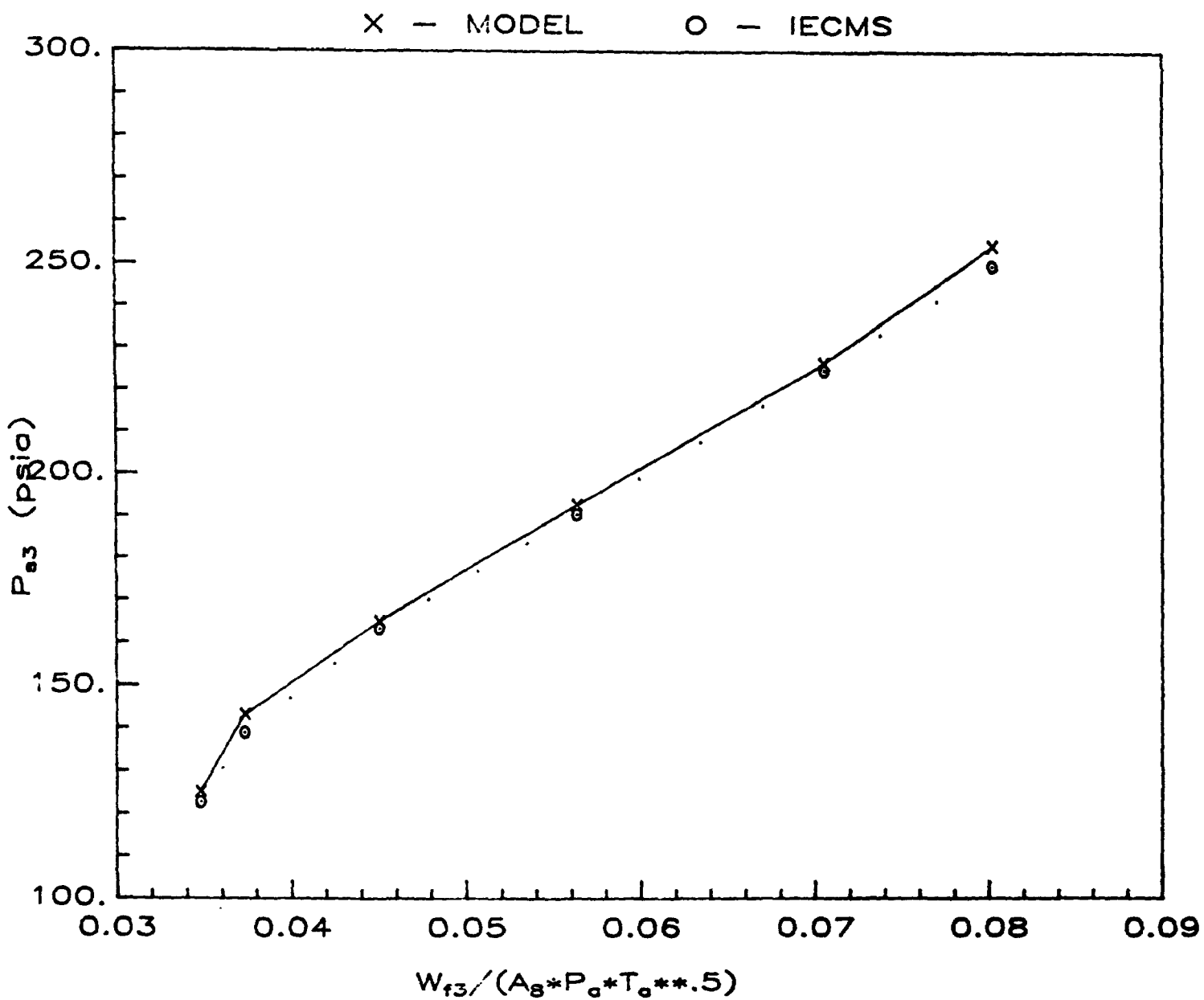

Figure **26** — STEADY—STATE VALIDATION

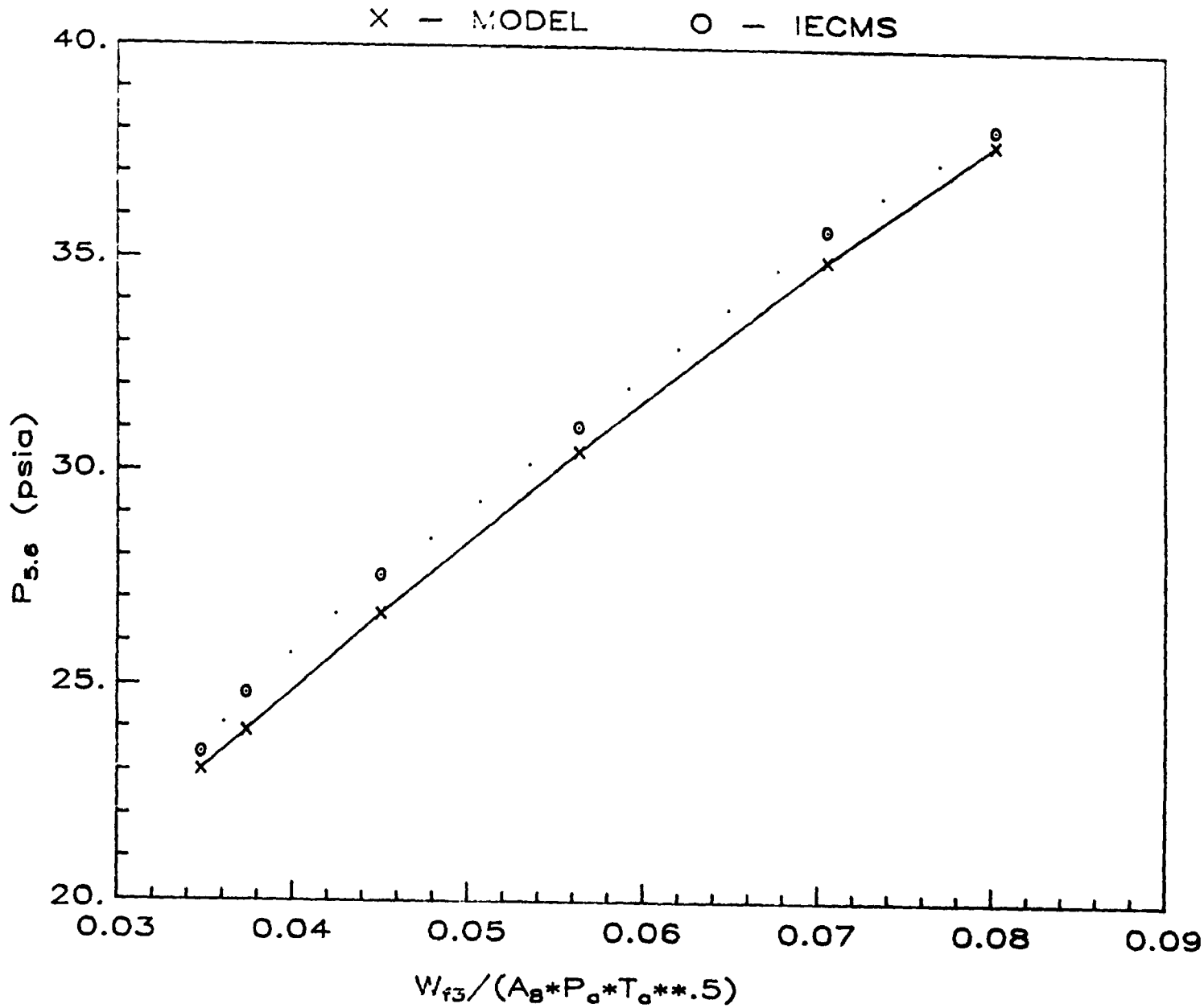

Figure **27** — STEADY—STATE VALIDATION

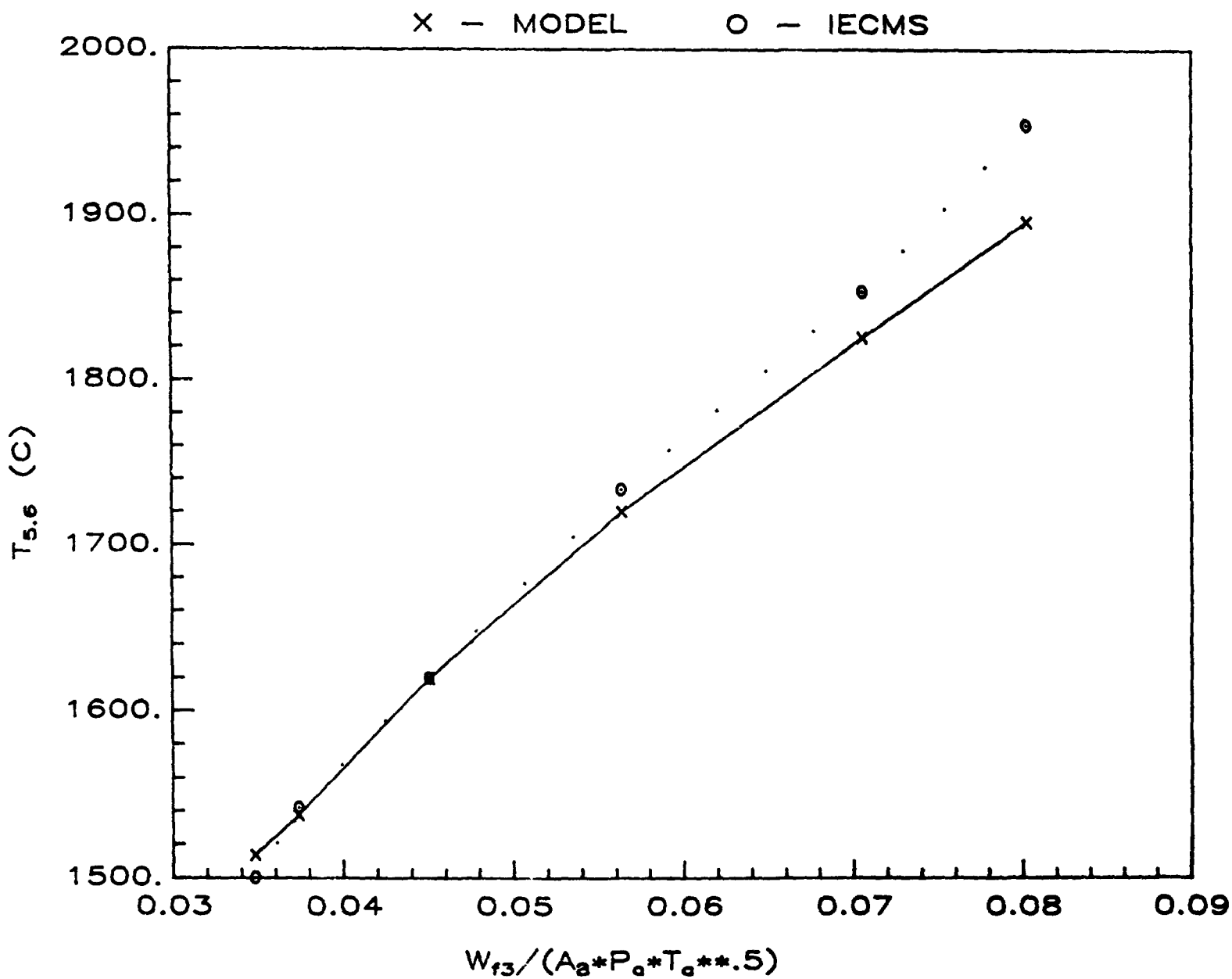

Figure **28** — STEADY-STATE VALIDATION

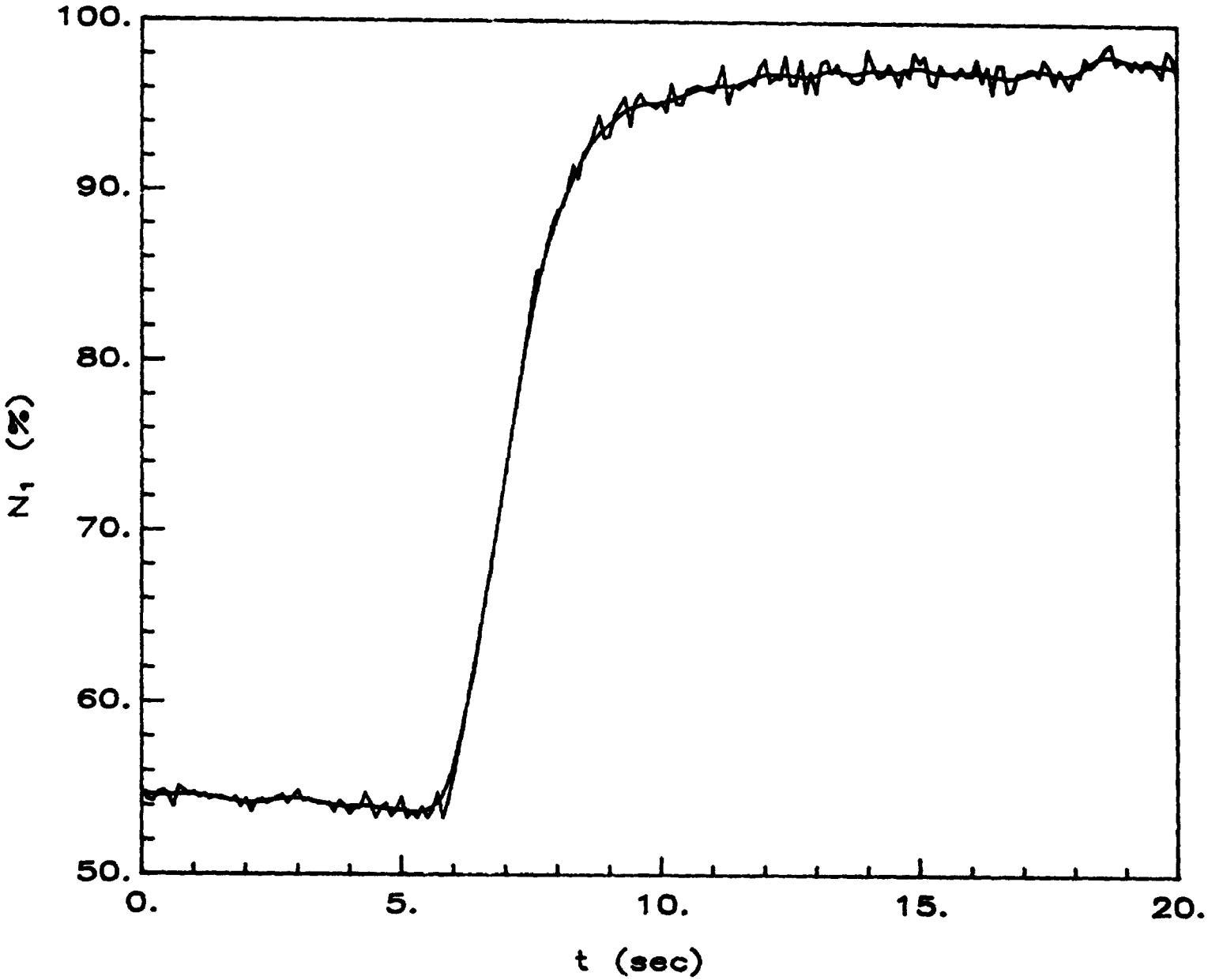

Figure 29 — Raw and Smoothed N1 Data

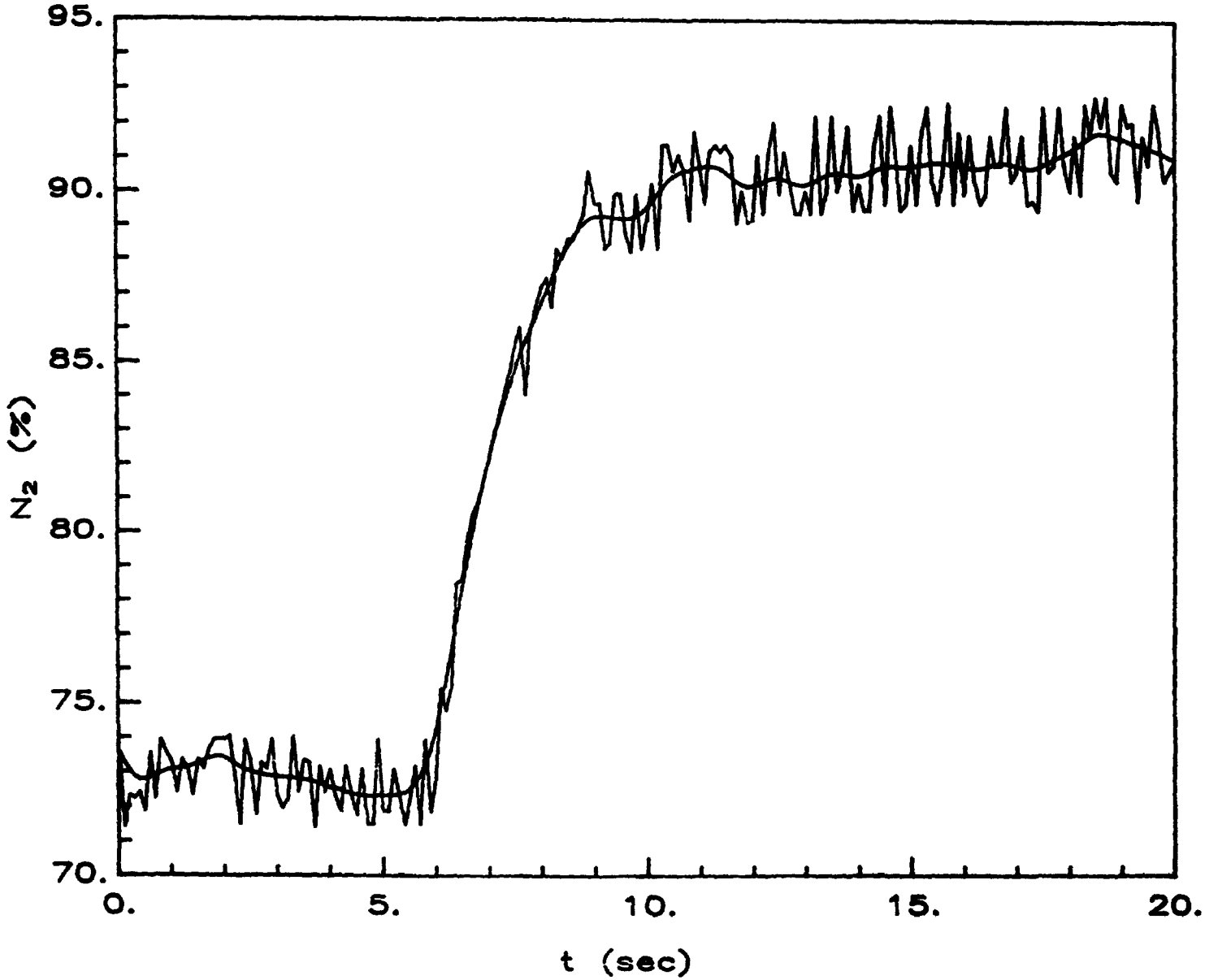

Figure 30 — Raw and Smoothed N2 Data

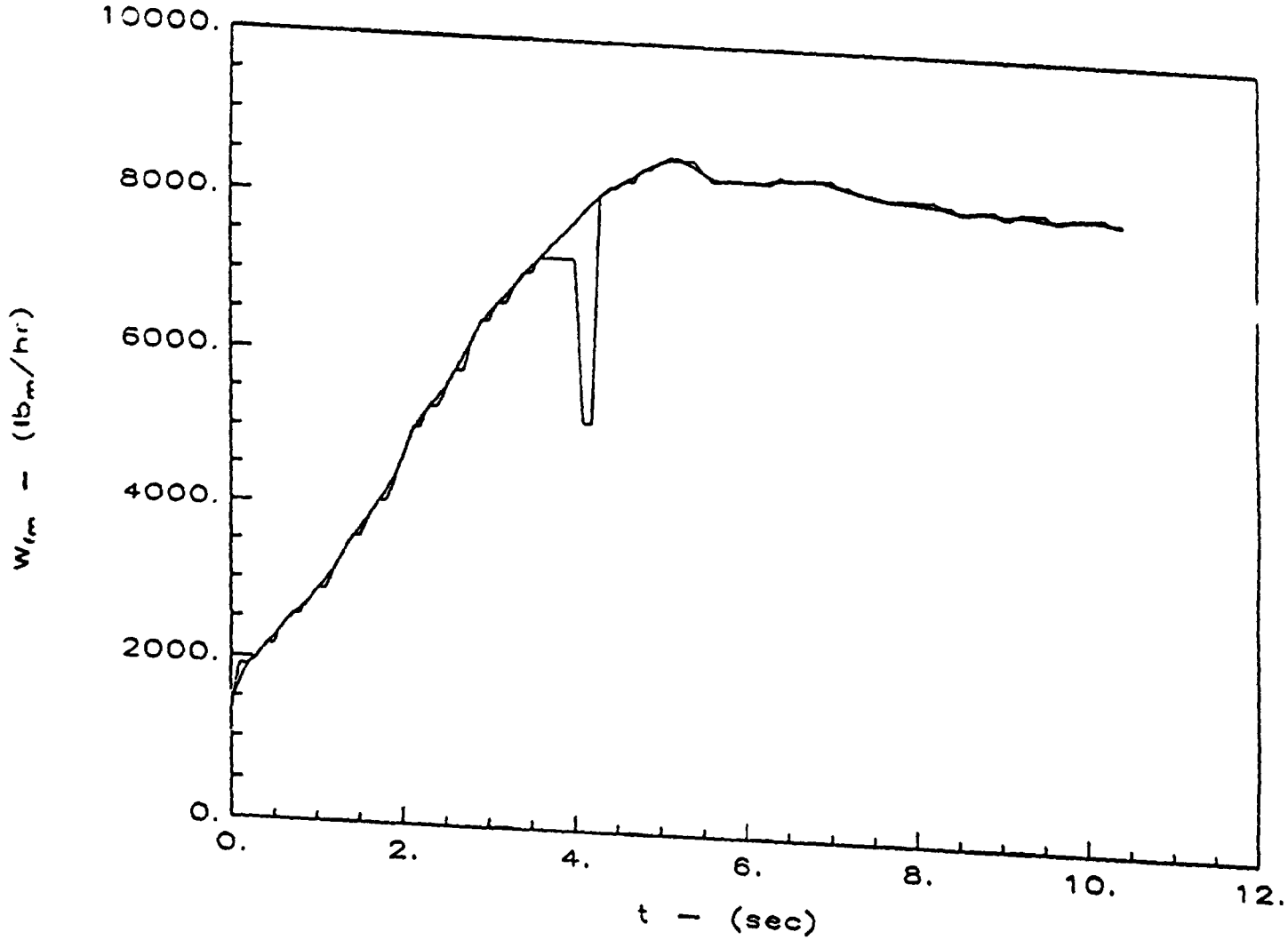

Figure **31** - Raw and Smoothed Fuel Flow Data [45]

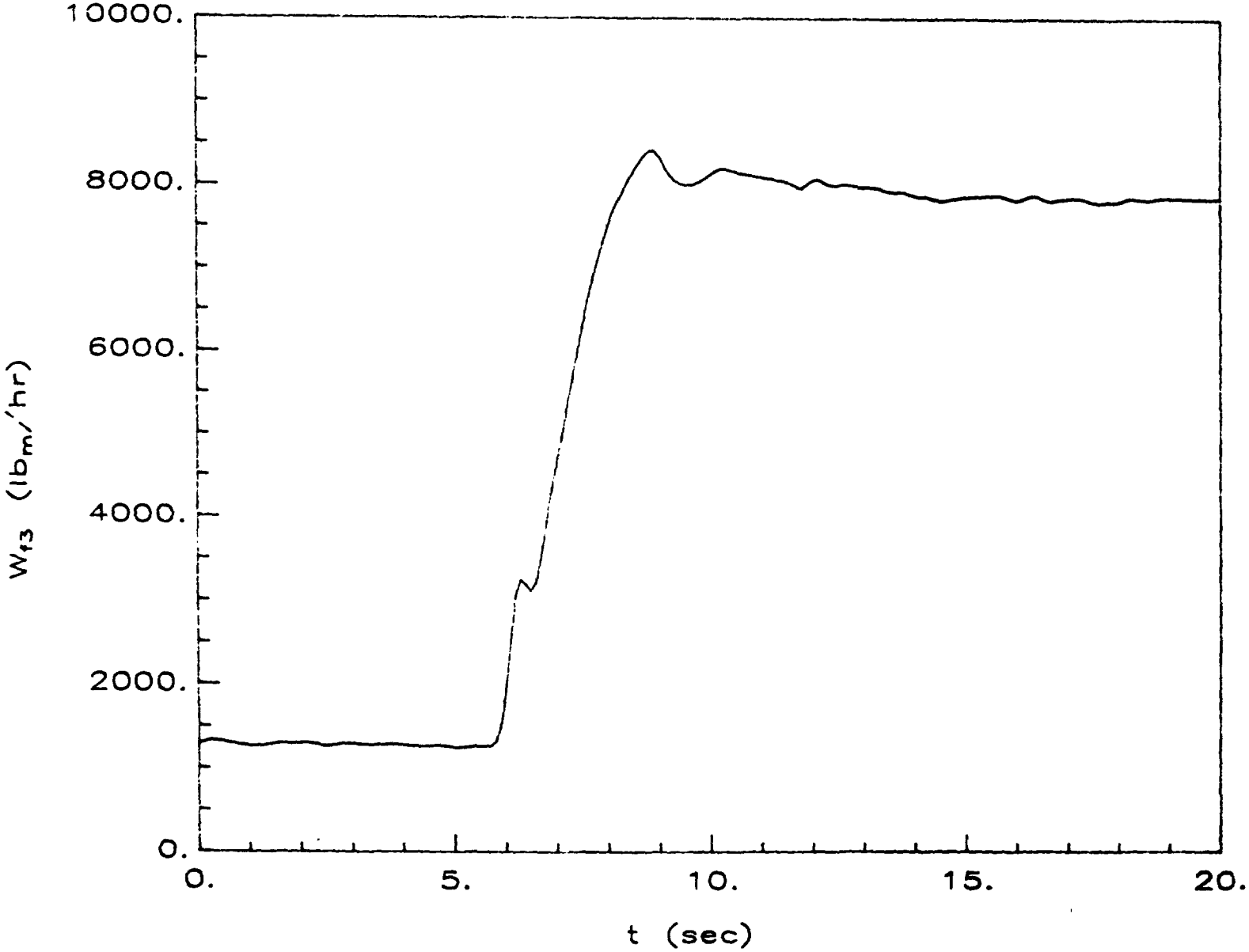

Figure **32** — WF3 versus time — 716LB

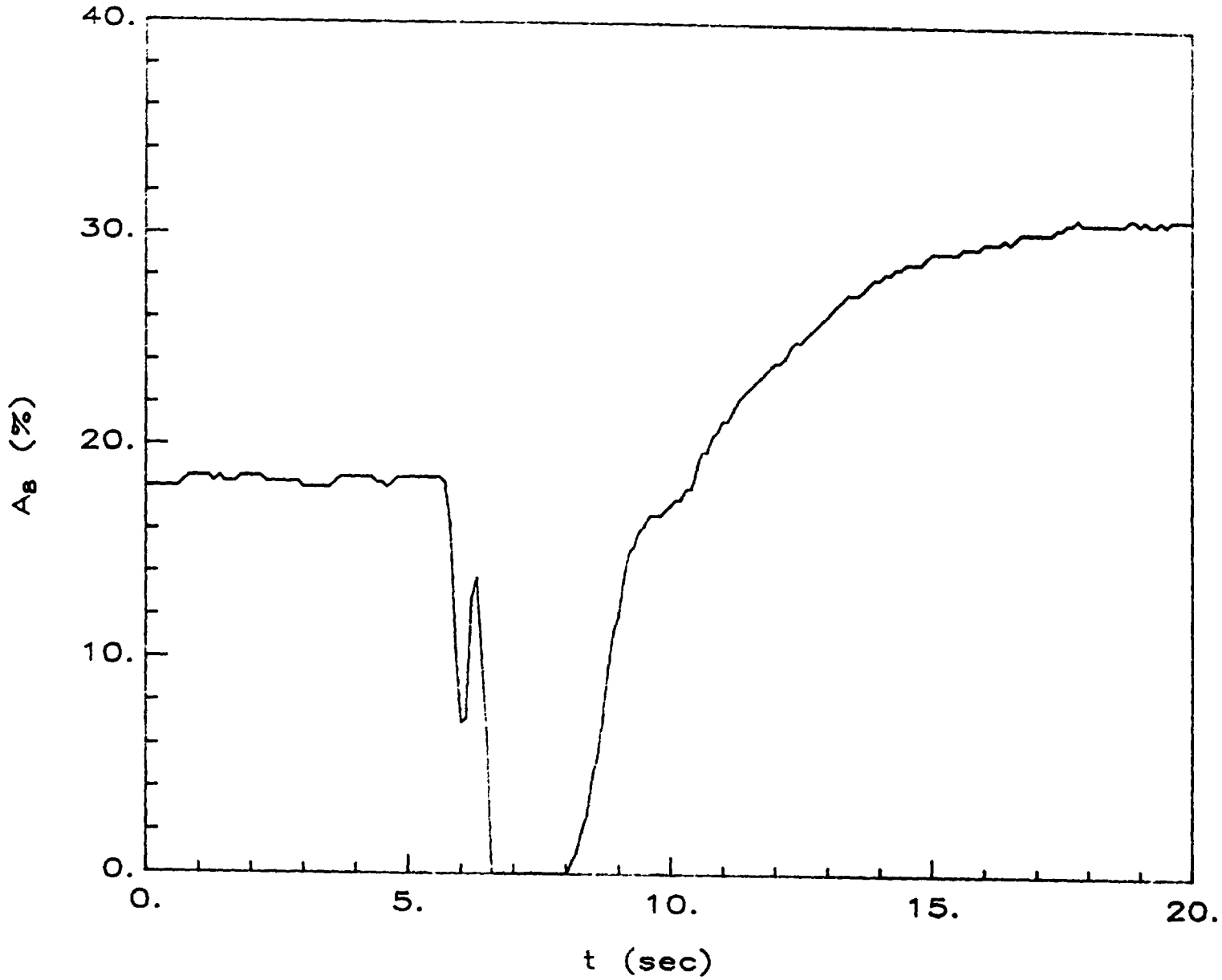

Figure **33** -- A8 versus time — 716LB

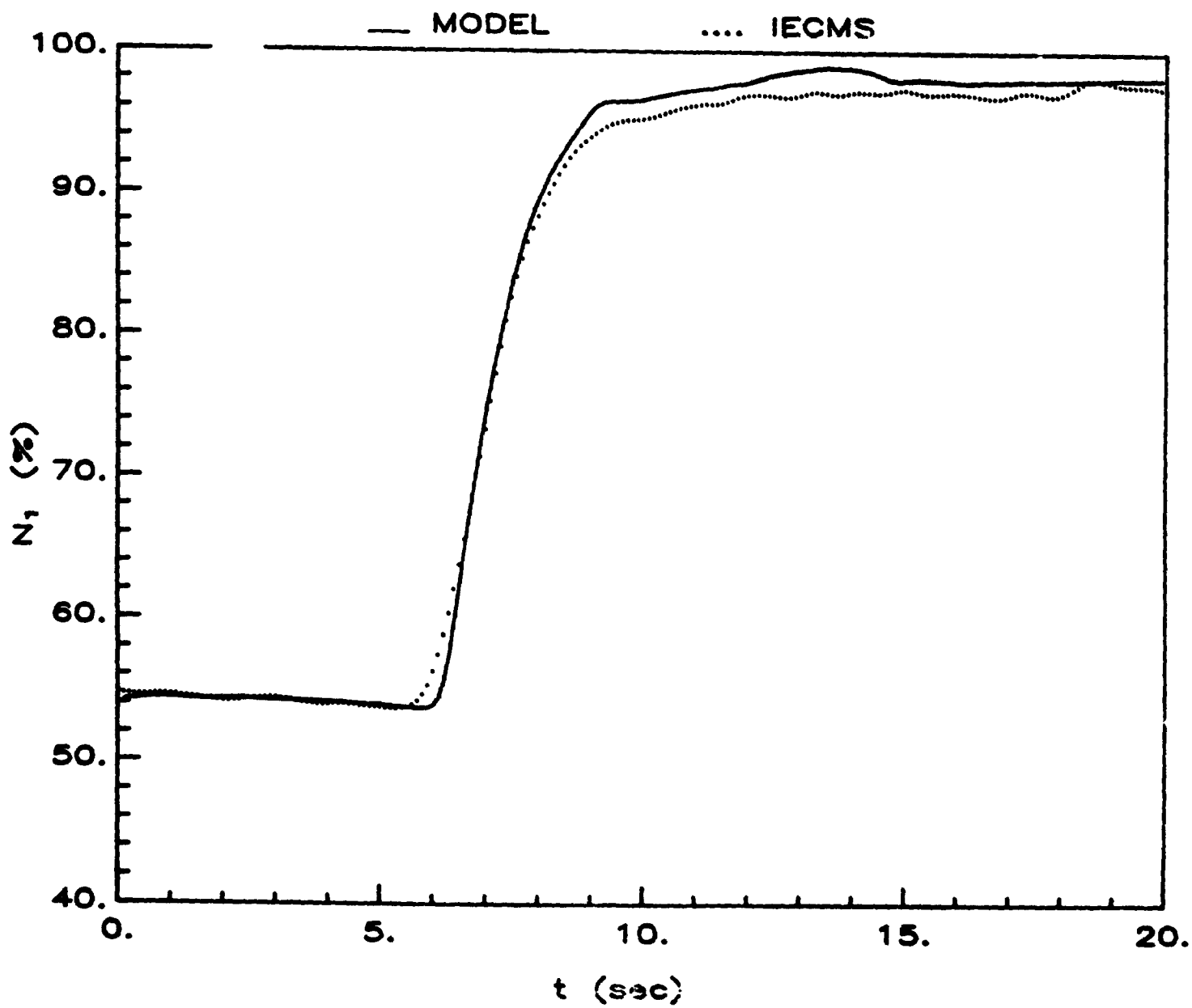

Figure 34 – N1 versus time – 716LB

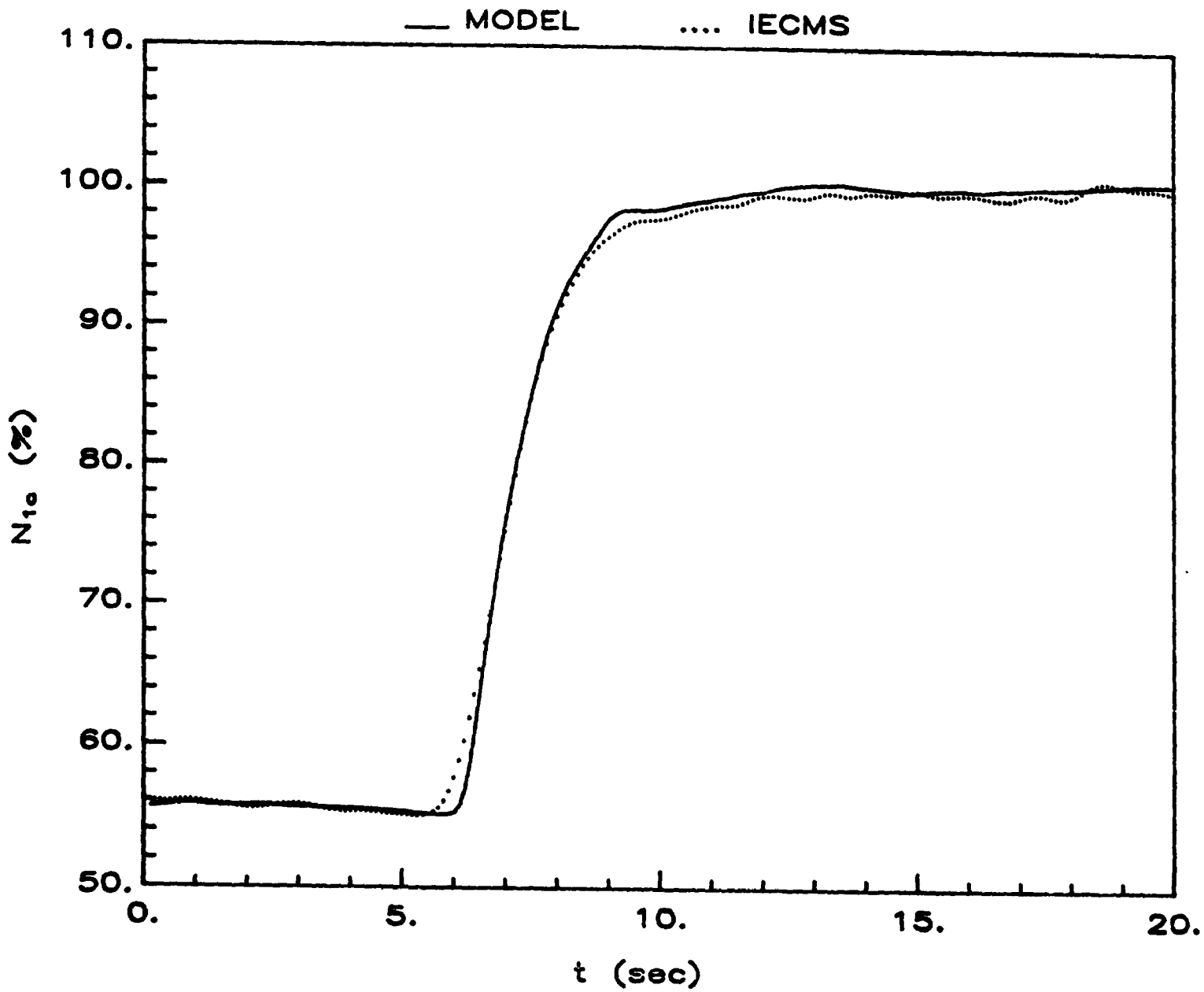

Figure 35 – N1C versus time – 716LB

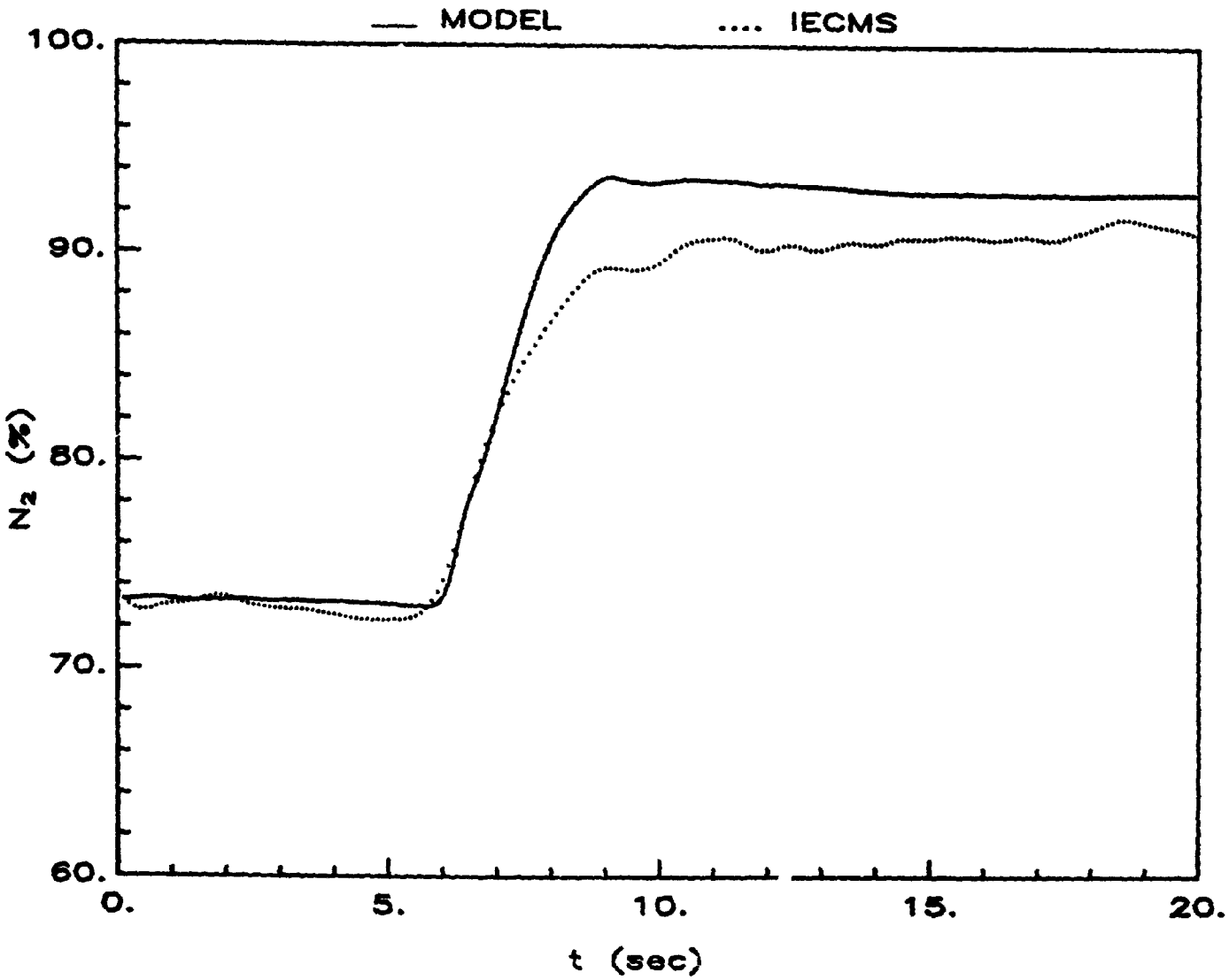

Figure 36 – N2 versus time – 716LB

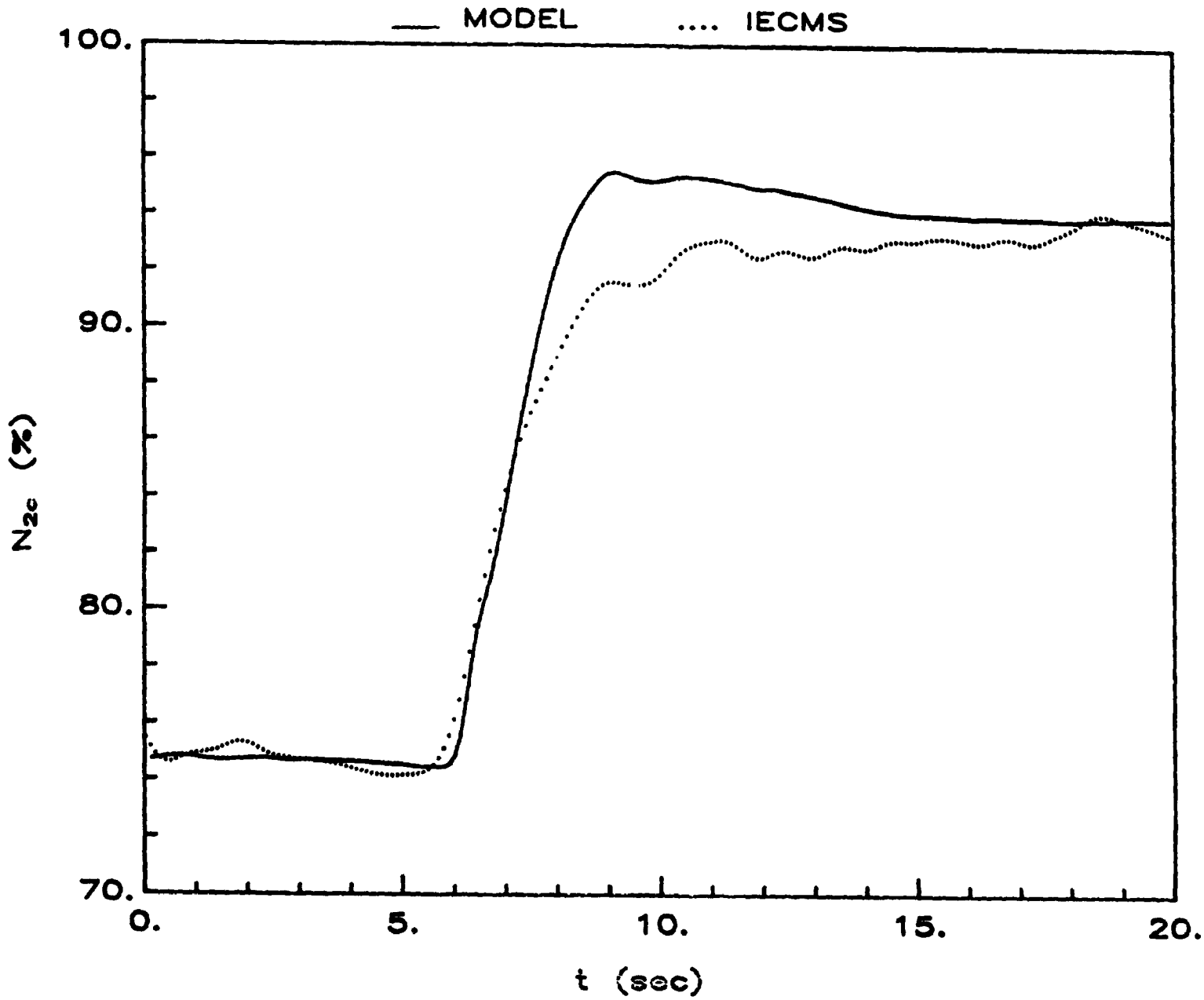

Figure 37 – N2C versus time – 716LB

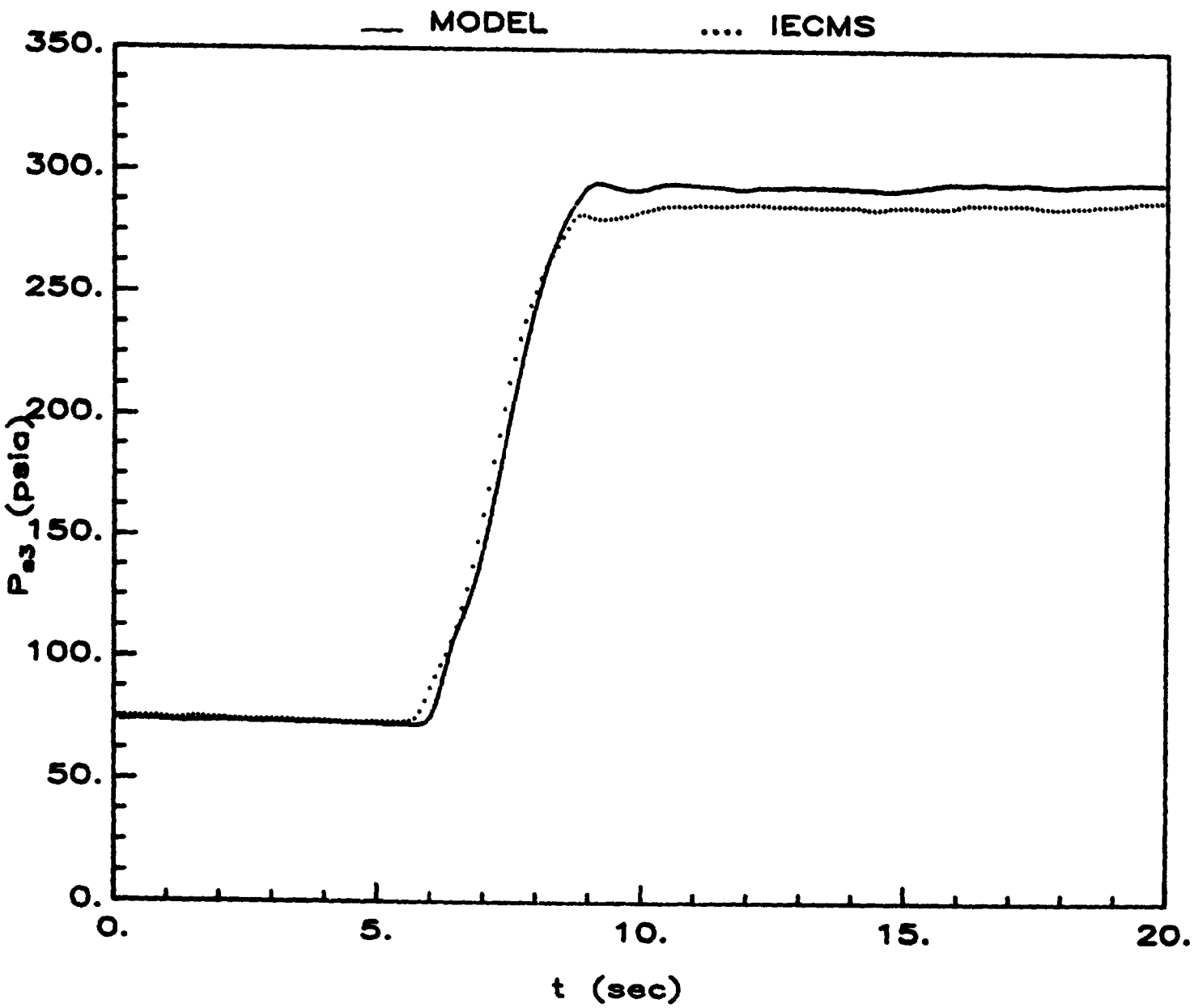

Figure 38 – PS3 versus time – 716LB

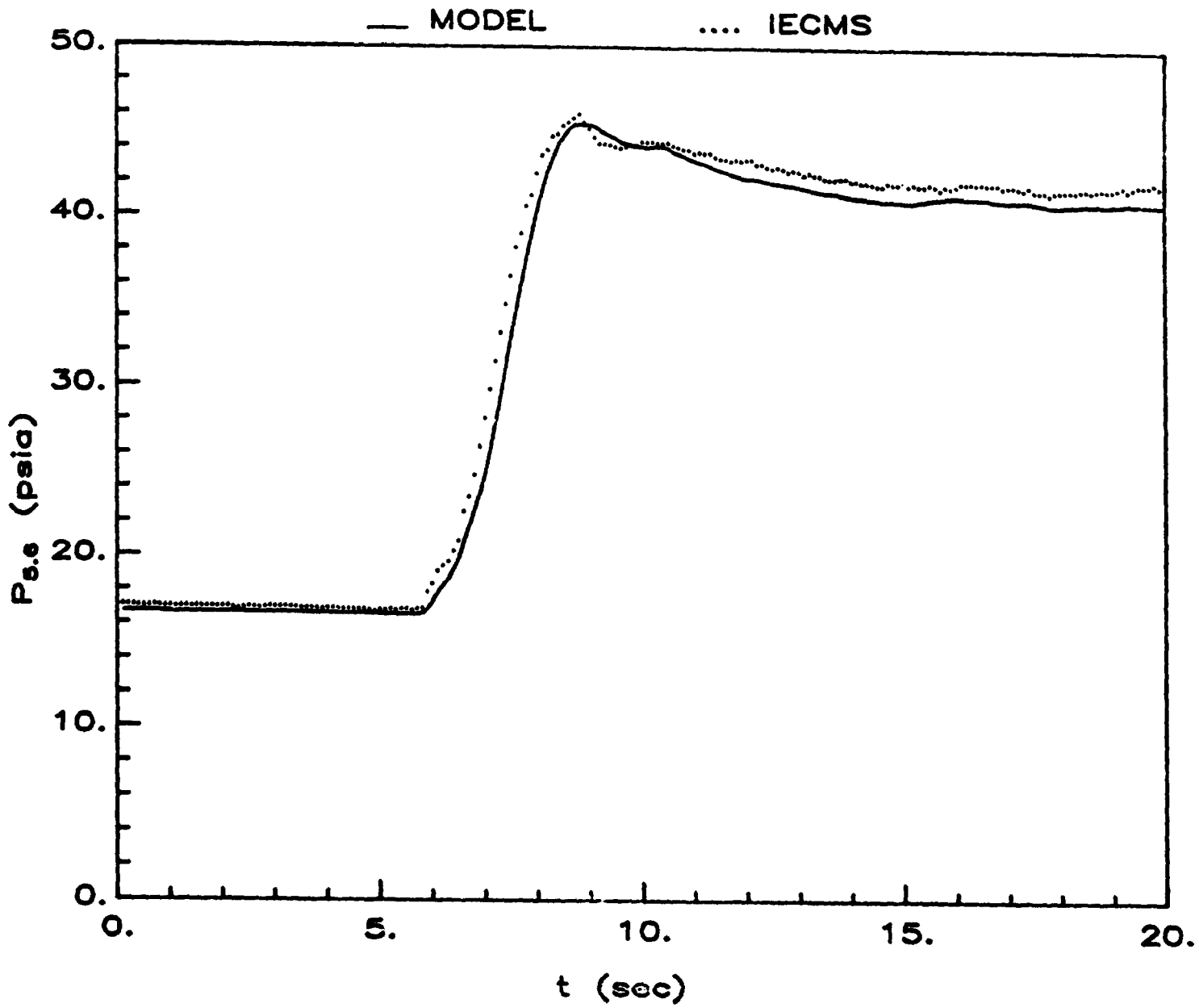

Figure 39 – P56 versus time – 716LB

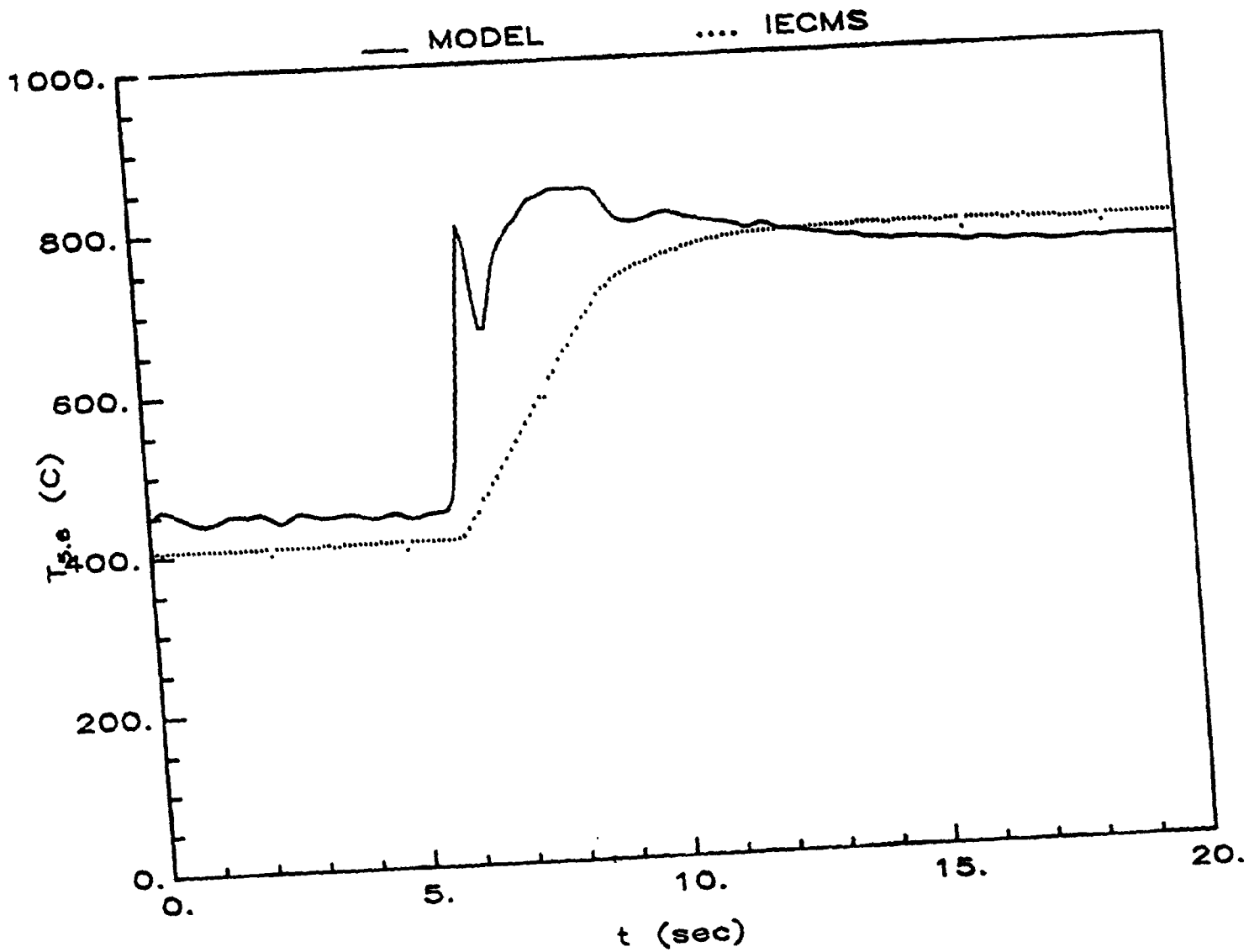

Figure 40 – T56 versus time – 716LB

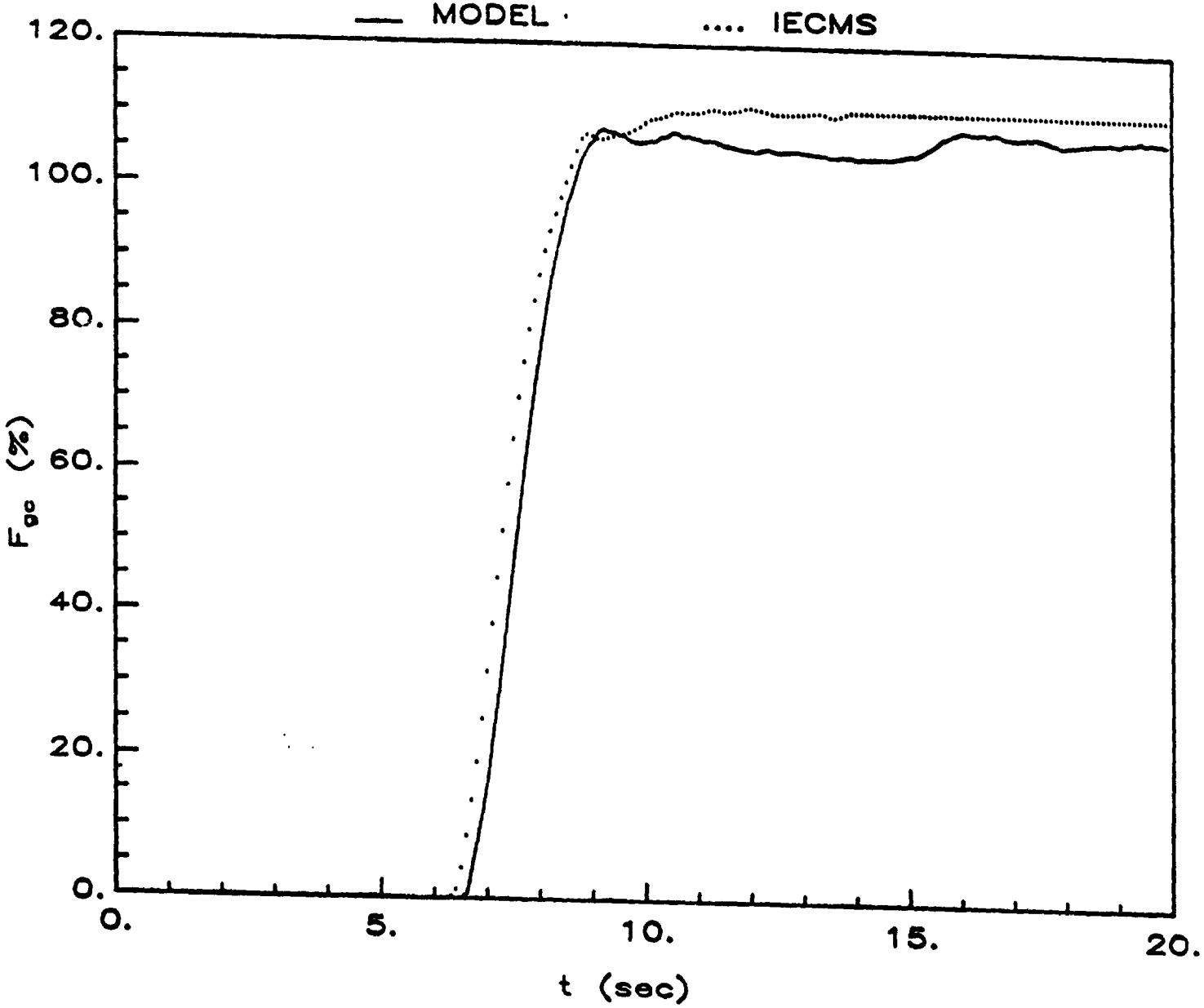

Figure 41 — Thrust versus time — 716LB

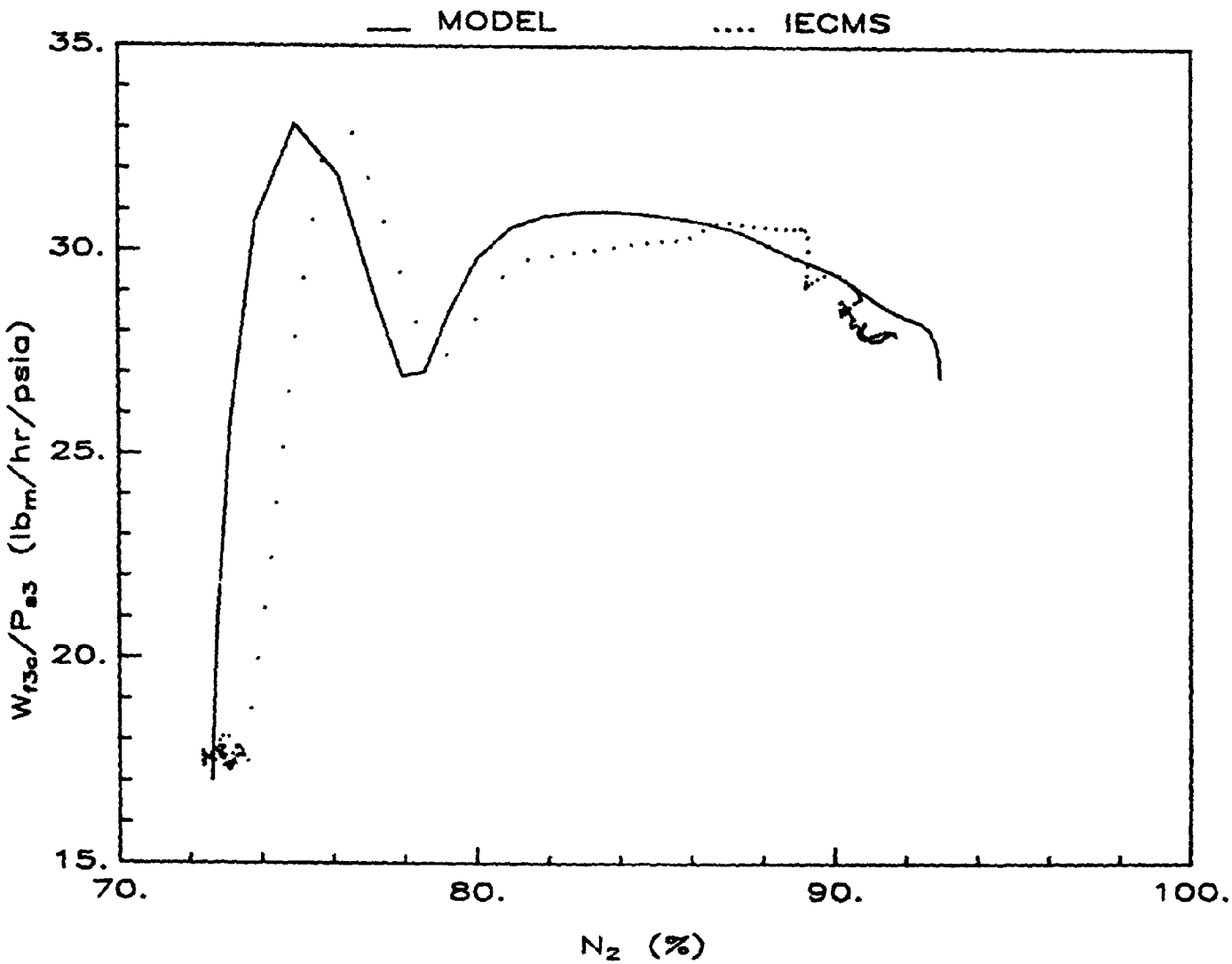

Figure **42** — WF3C/PS3 versus N2 — 716LB

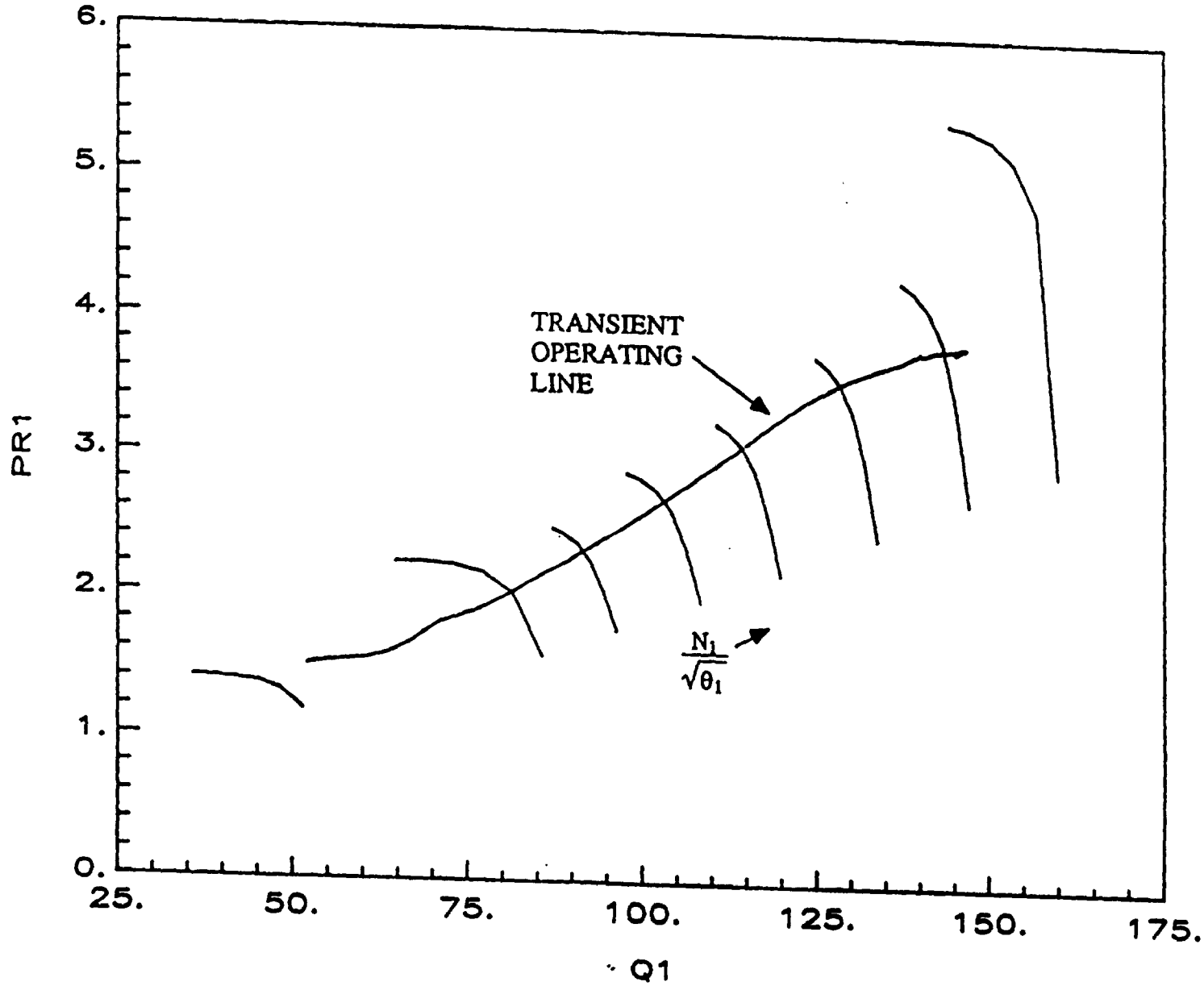

Figure 43 — Fan map — AC716LB

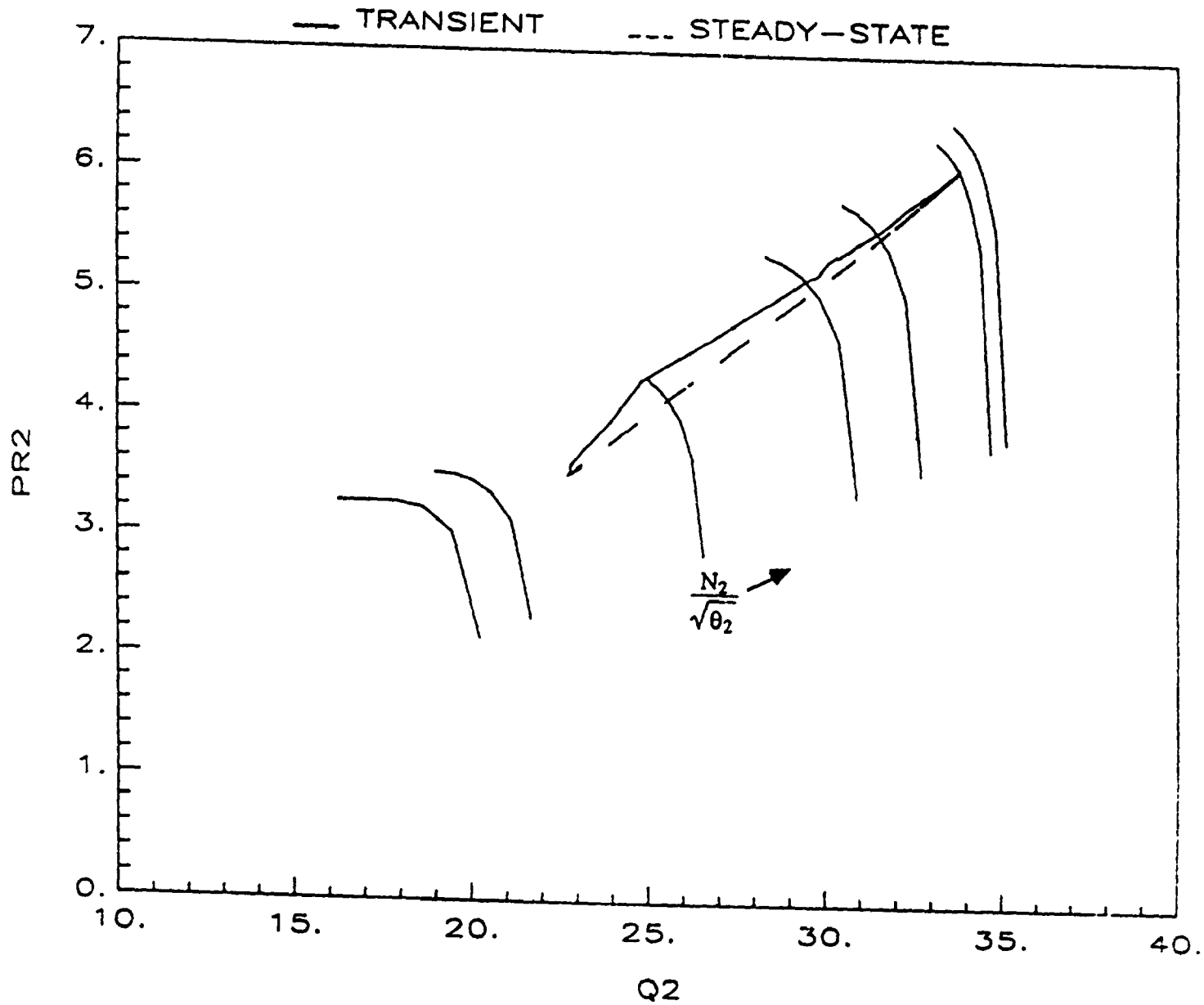

Figure **44** – Compressor map – AC716LB

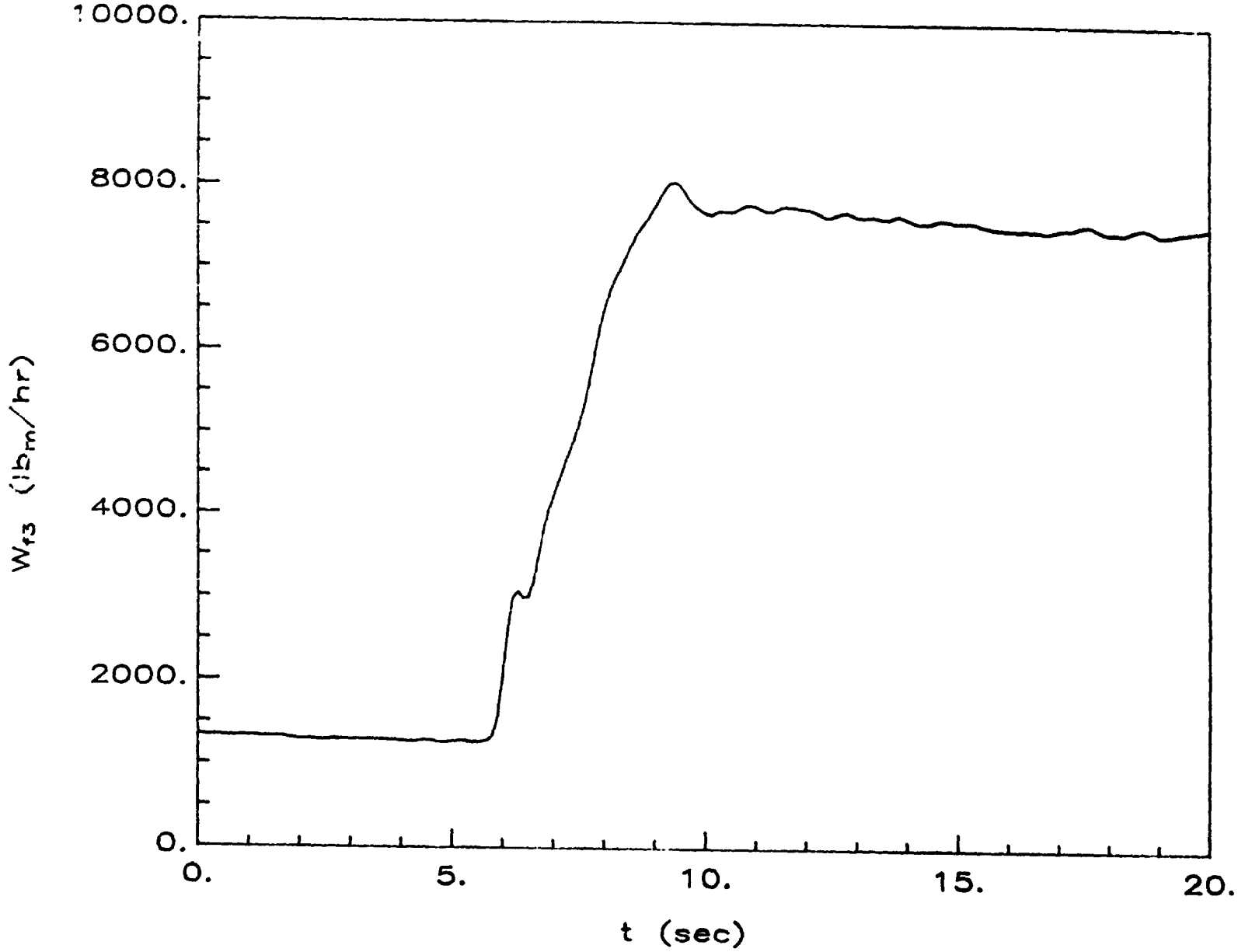

Figure **45** — WF3 versus time — 716RB

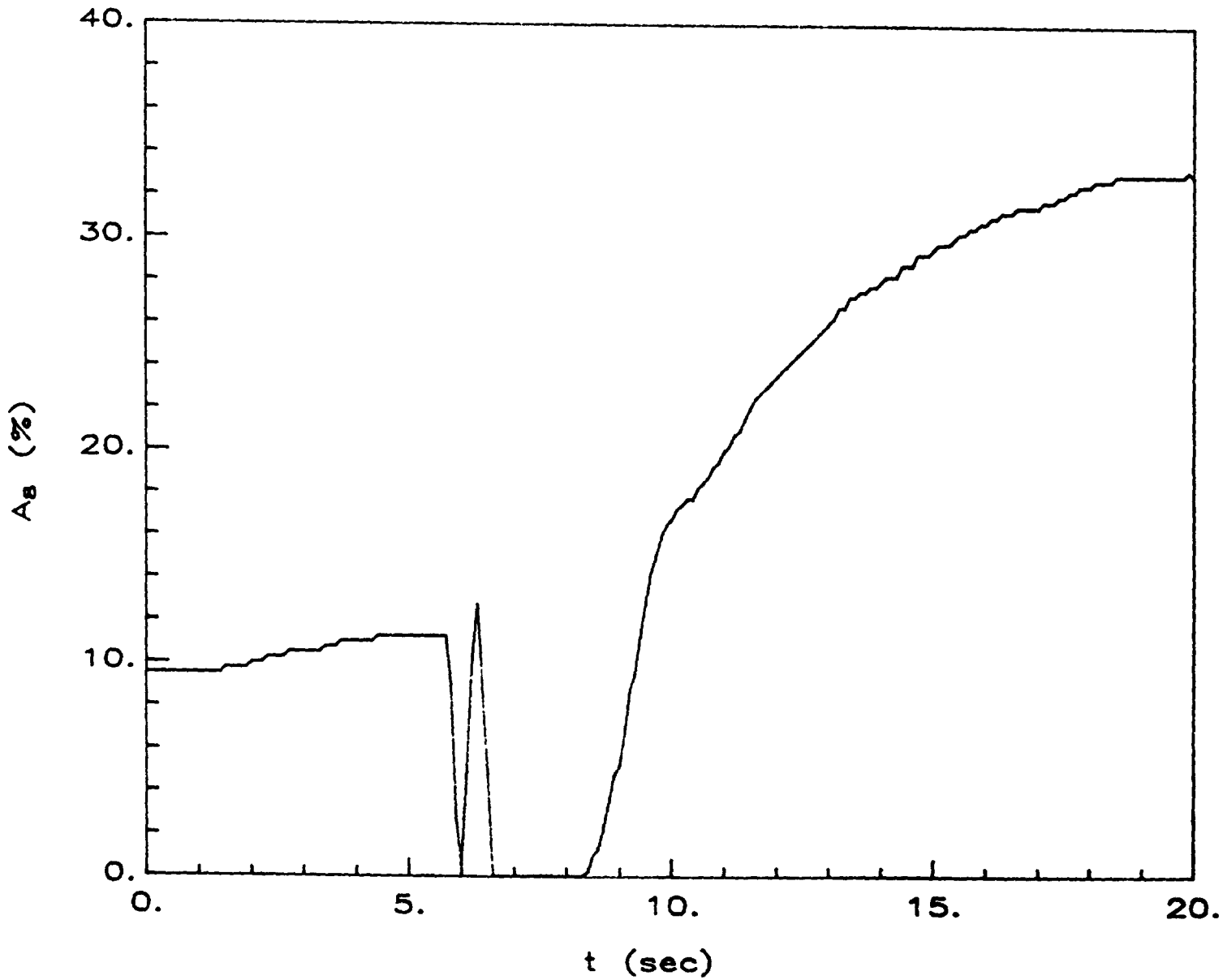

Figure **46** — A8 versus time — 716RB

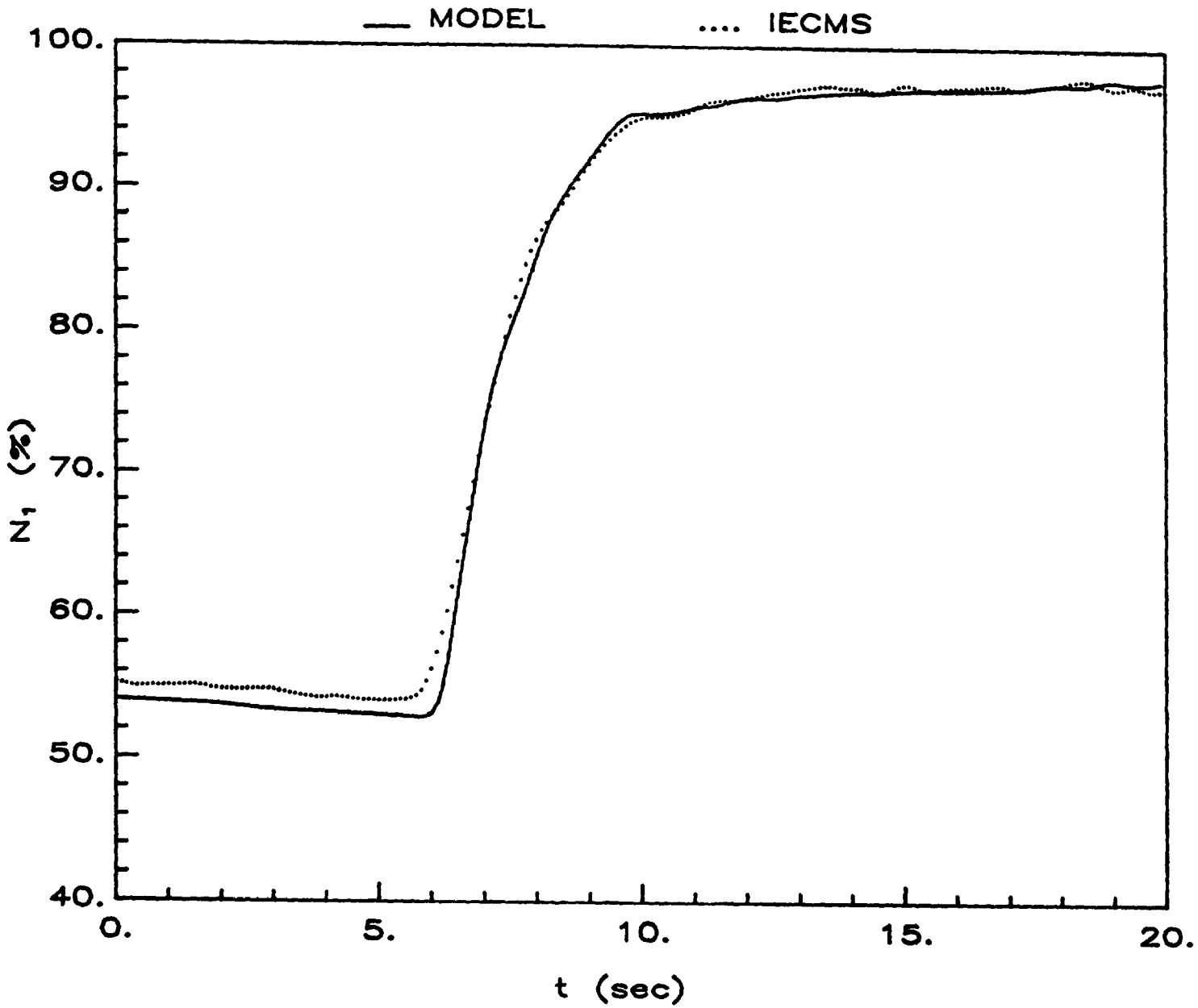

Figure 47 — N1 versus time — 716RB

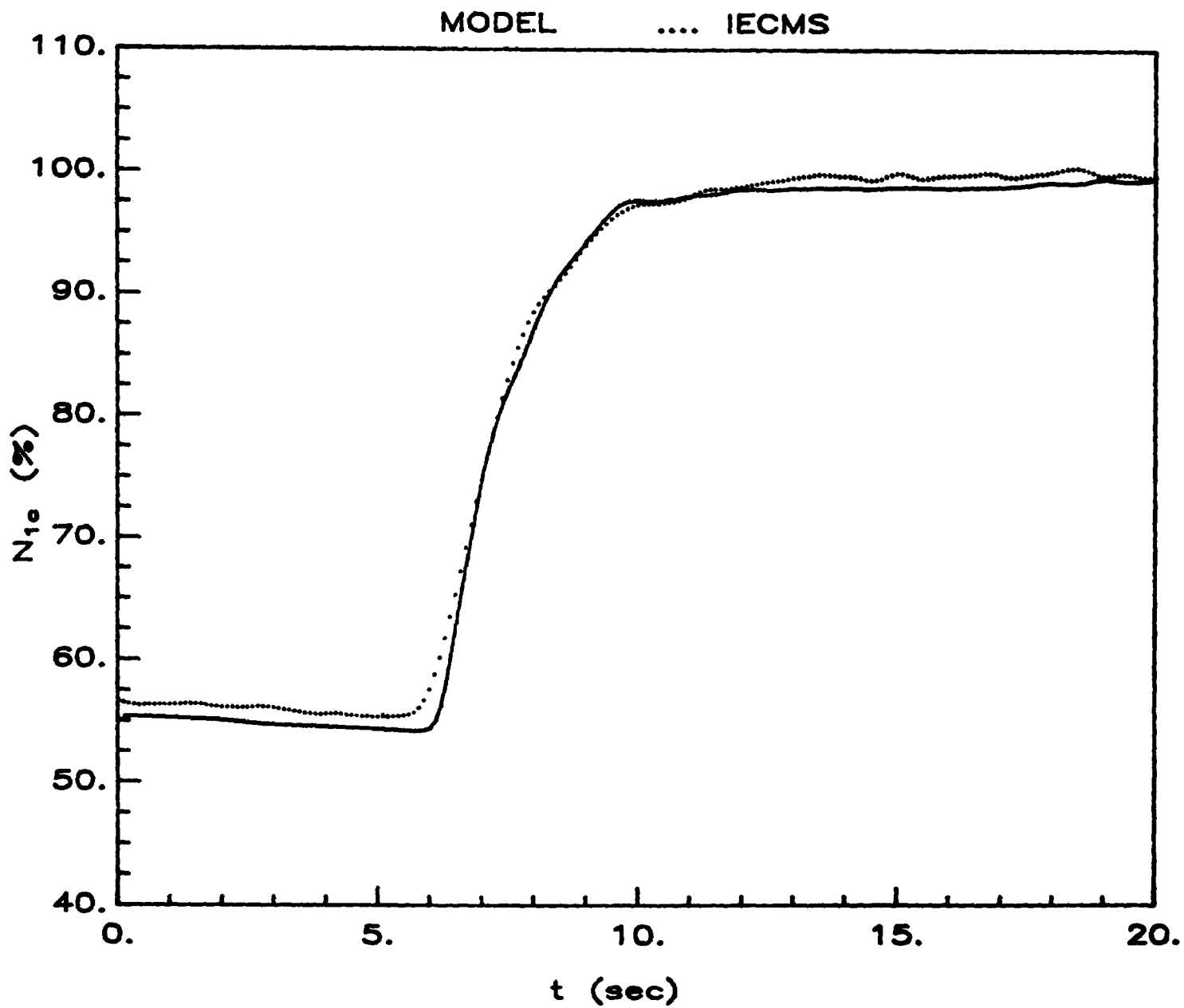

Figure 48 — N1C versus time — 716RB

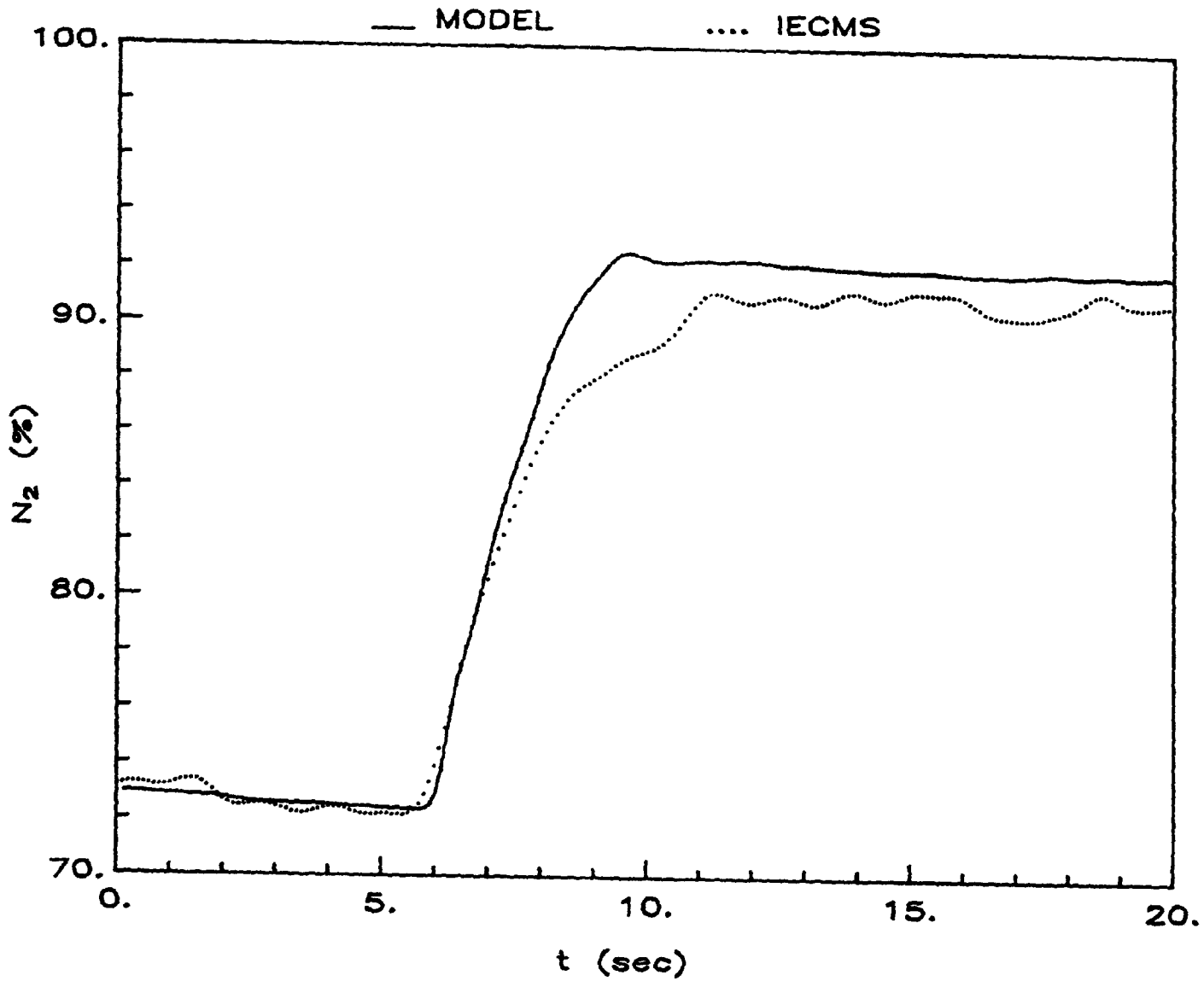

Figure 49 — N2 versus time — 716RB

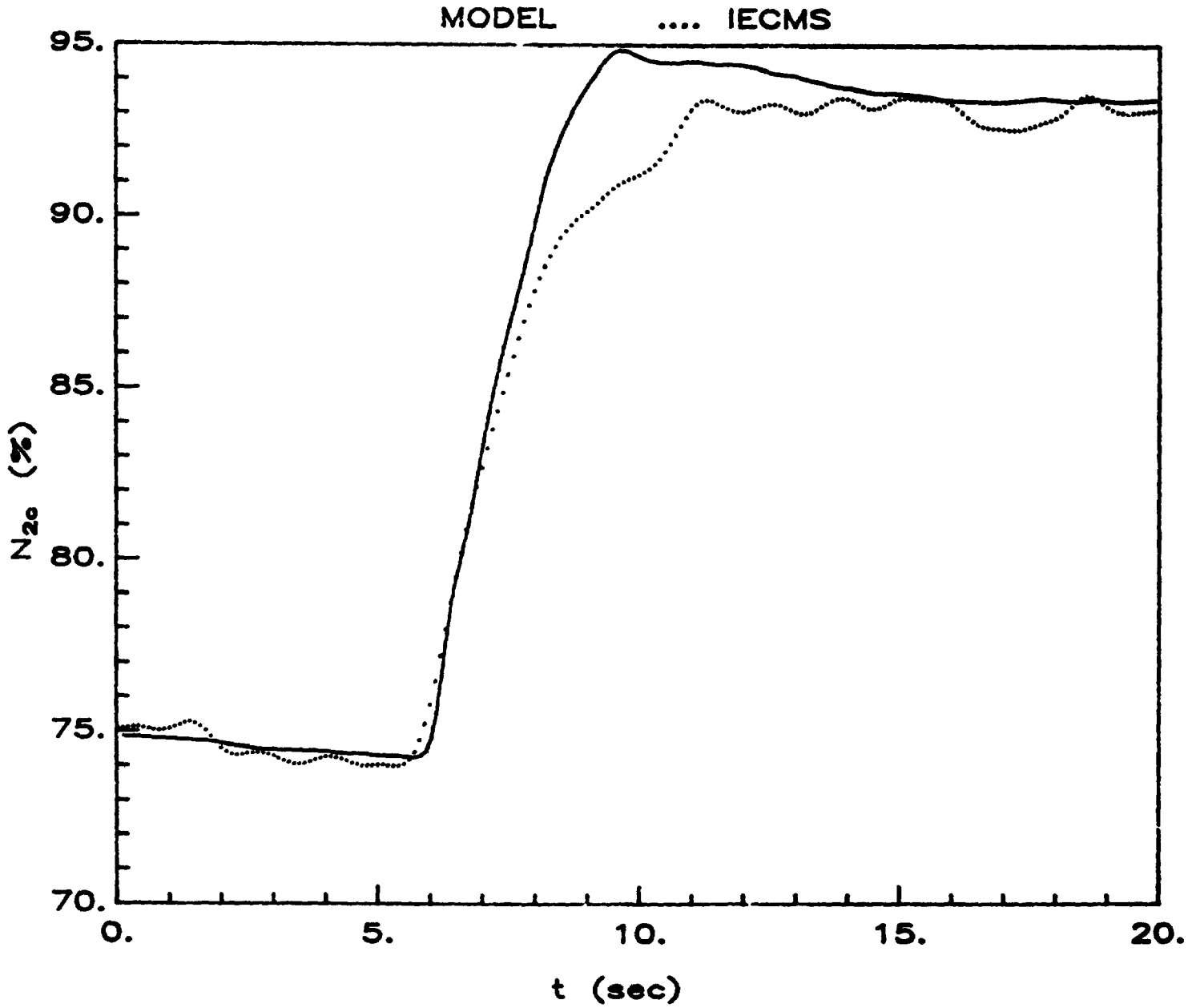

Figure 50 — N2C versus time — 716RB

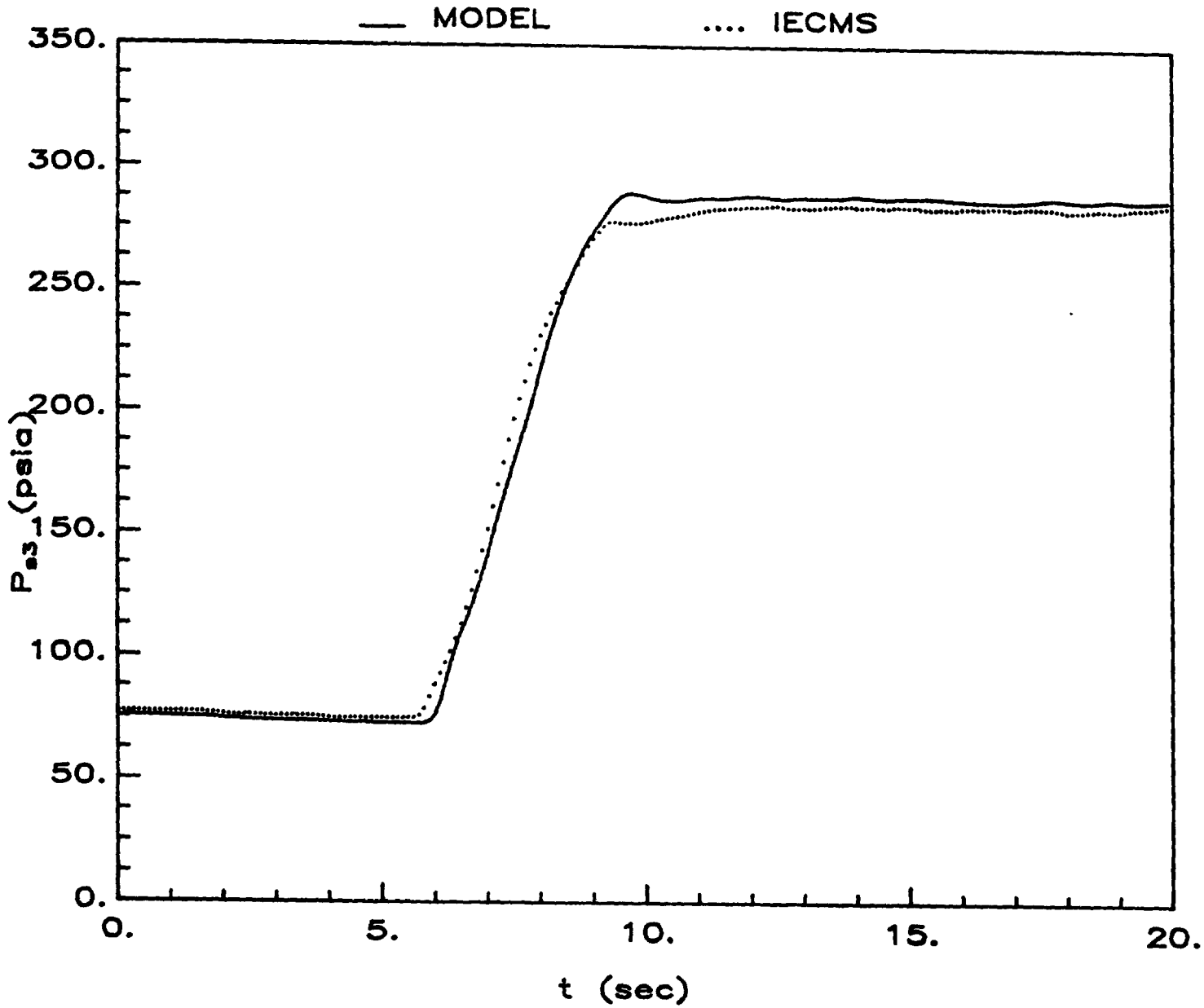

Figure 51 — PS3 versus time — 716RB

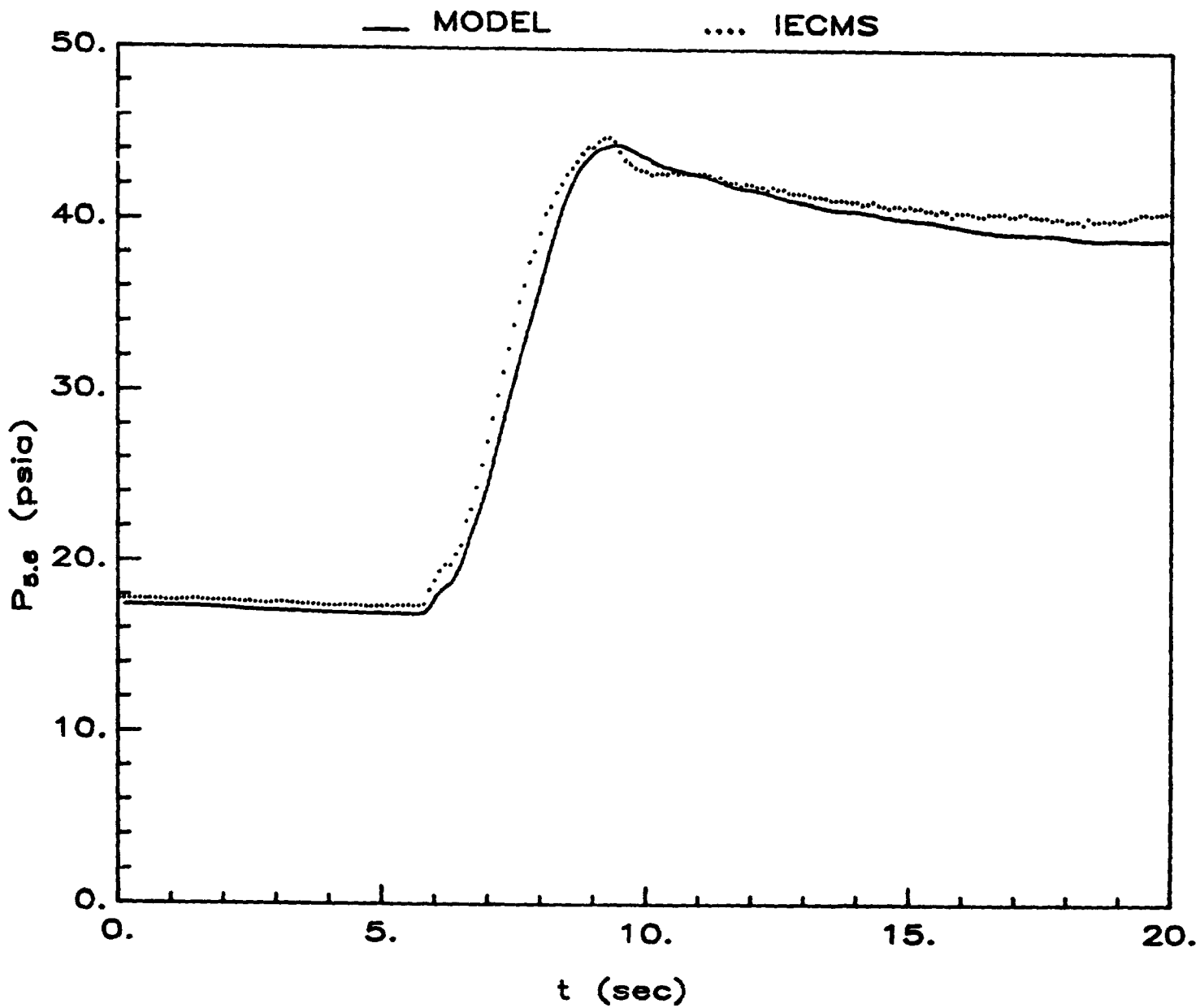

Figure 52 — P56 versus time — 716RB

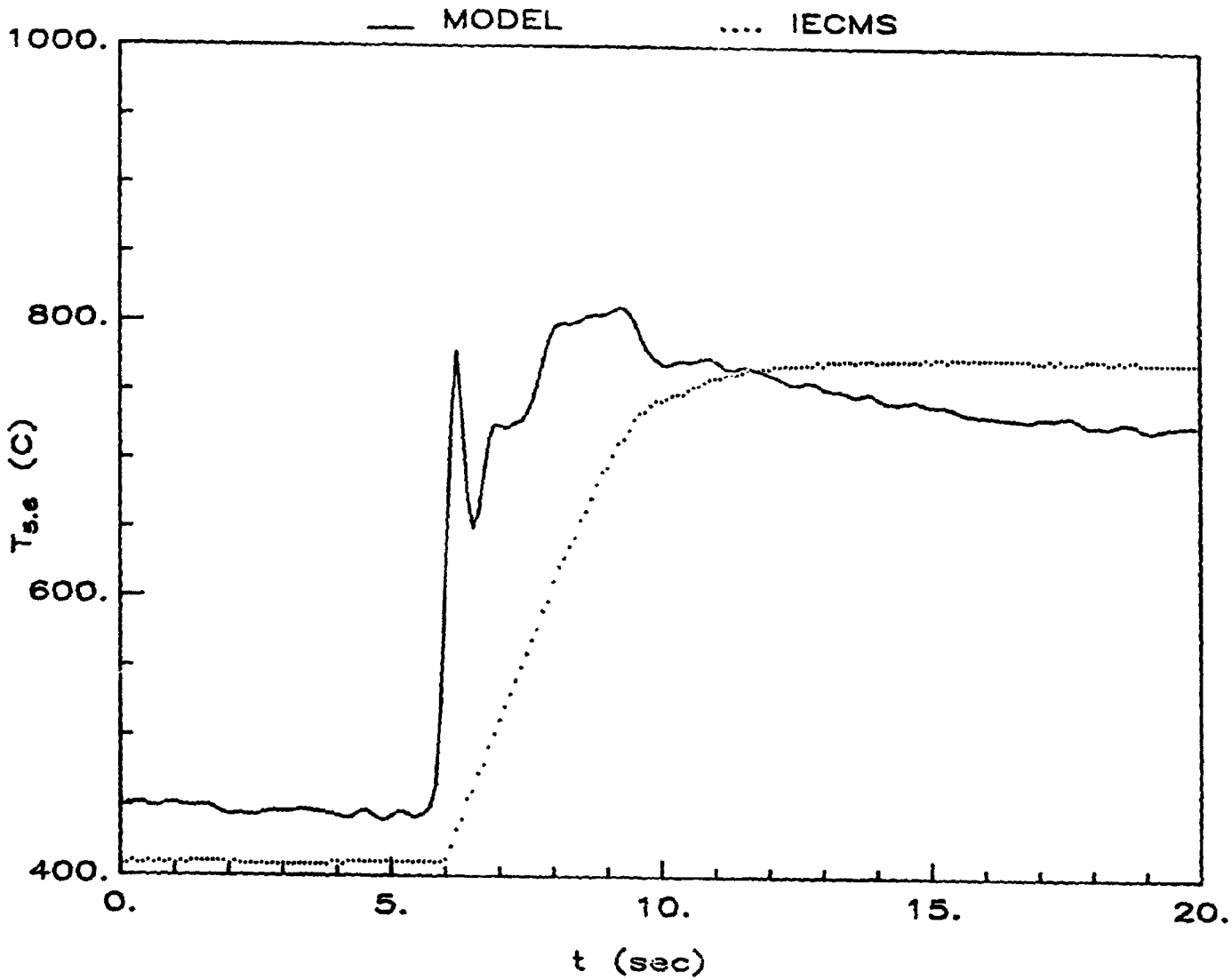

Figure 53 — T56 versus time — 716RB

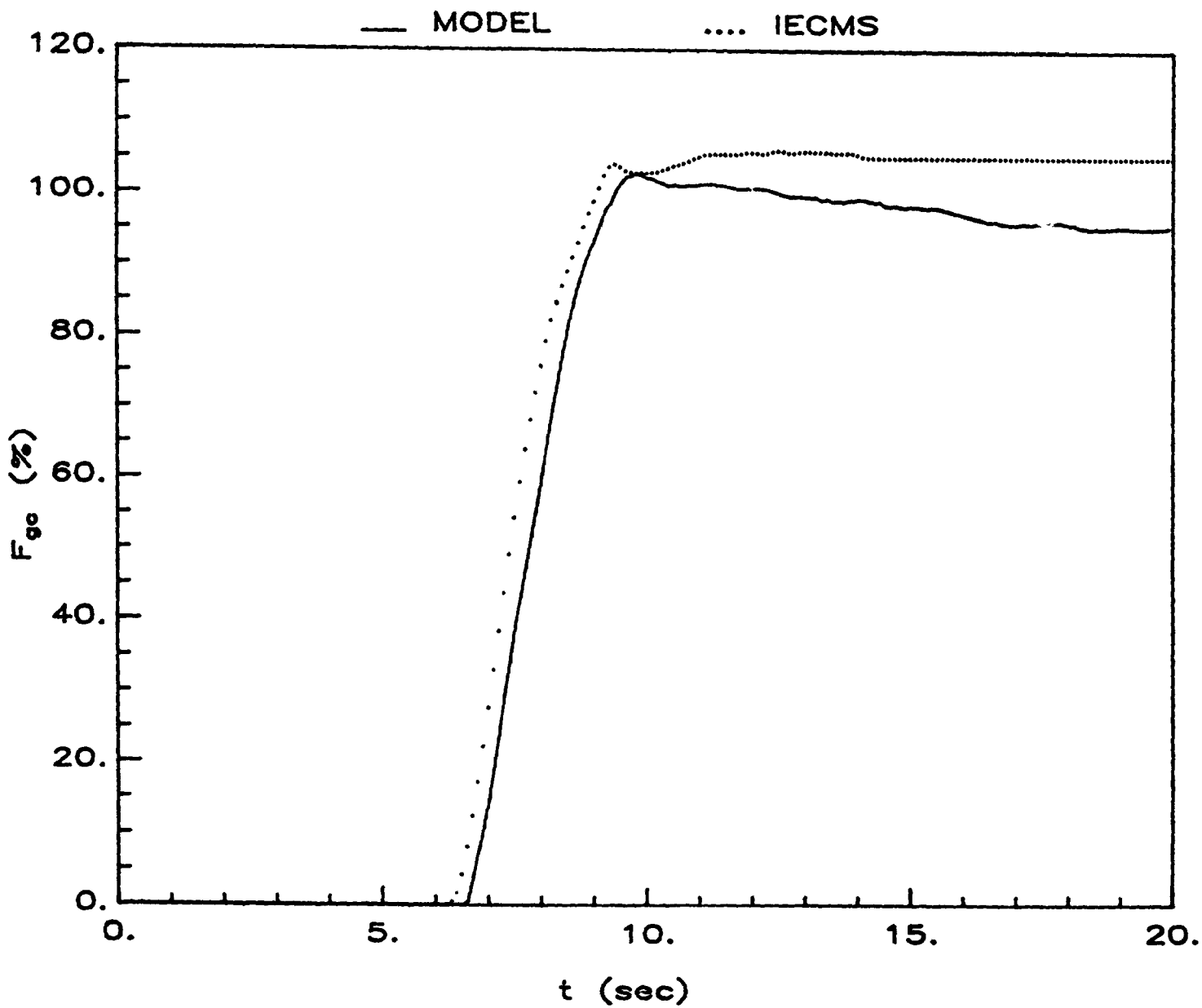

Figure 54 — Thrust versus time — 716RB

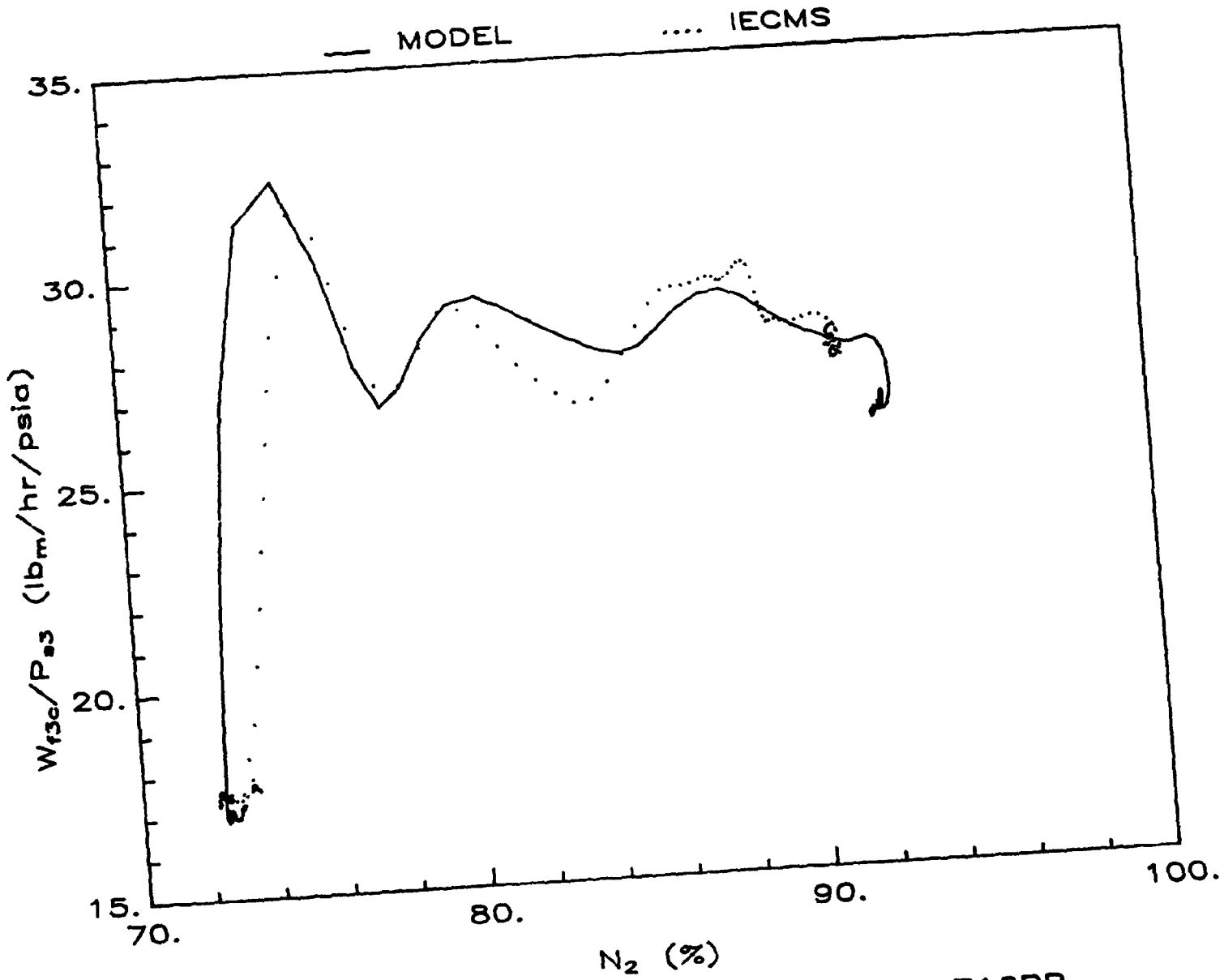

Figure **55** – WF3C/PS3 versus N2 – 716RB

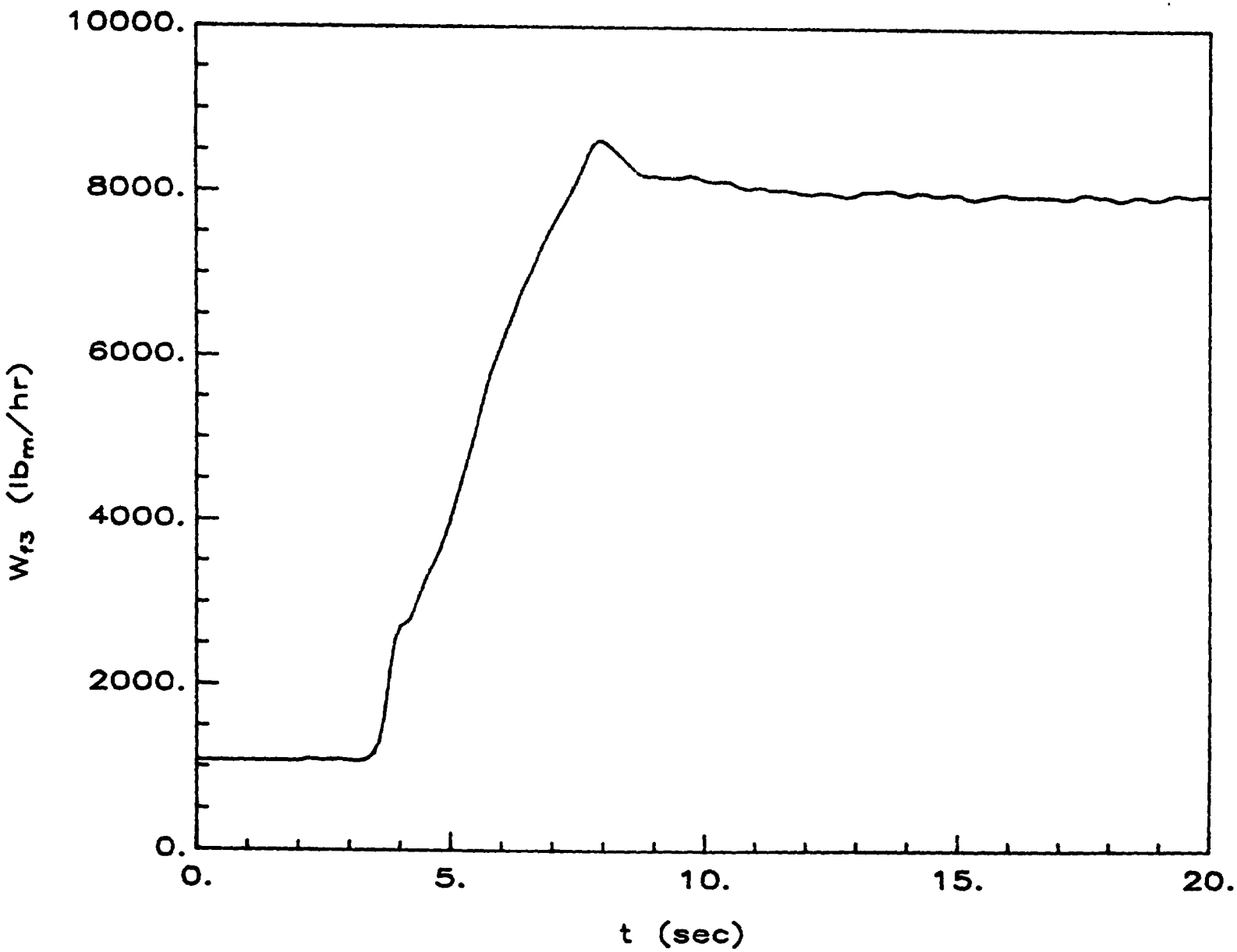

Figure 56 — WF3 versus time — 711LI

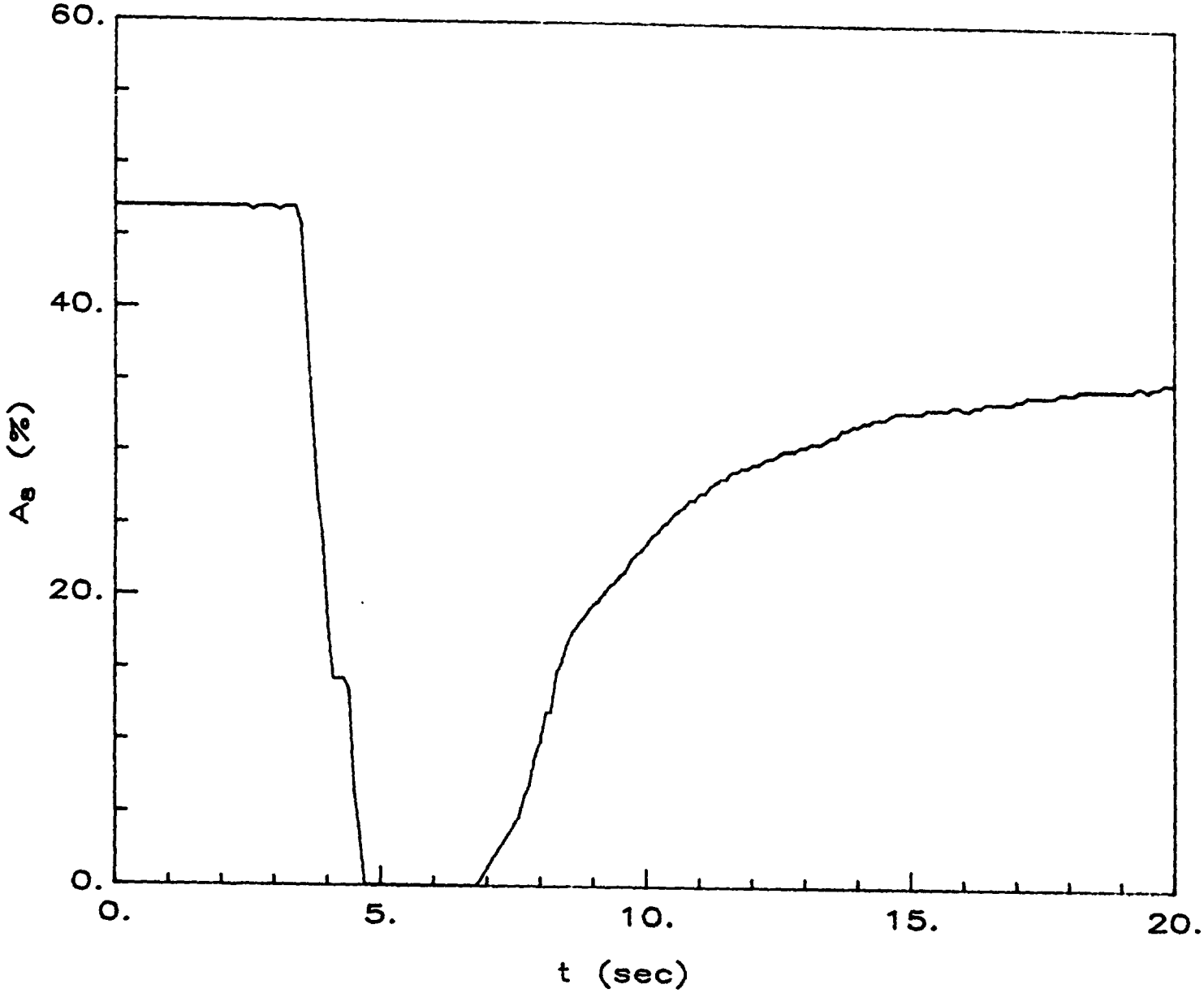

Figure **57** — A8 versus time — 711LI

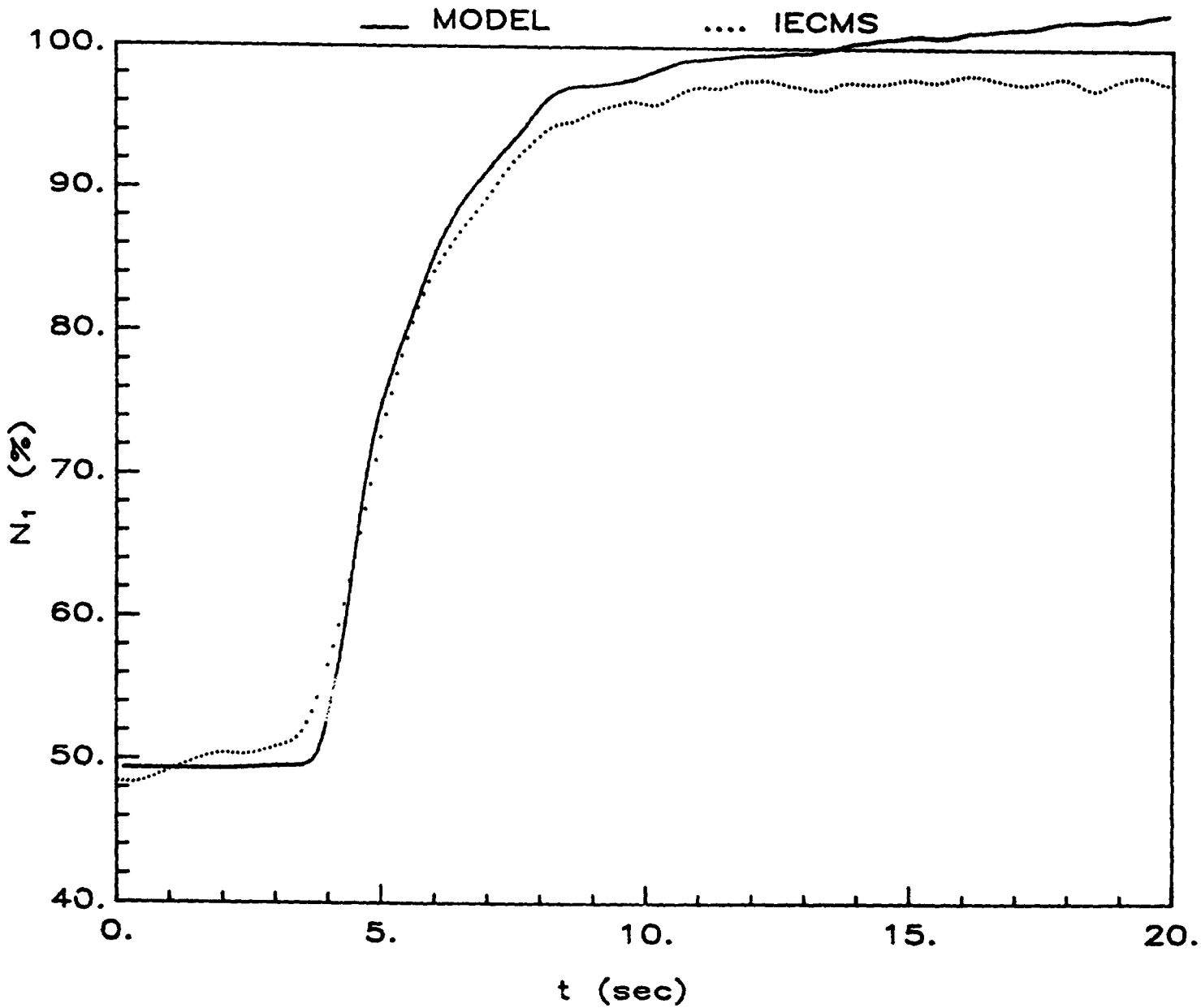

Figure **58** — N1 versus time — 711LI

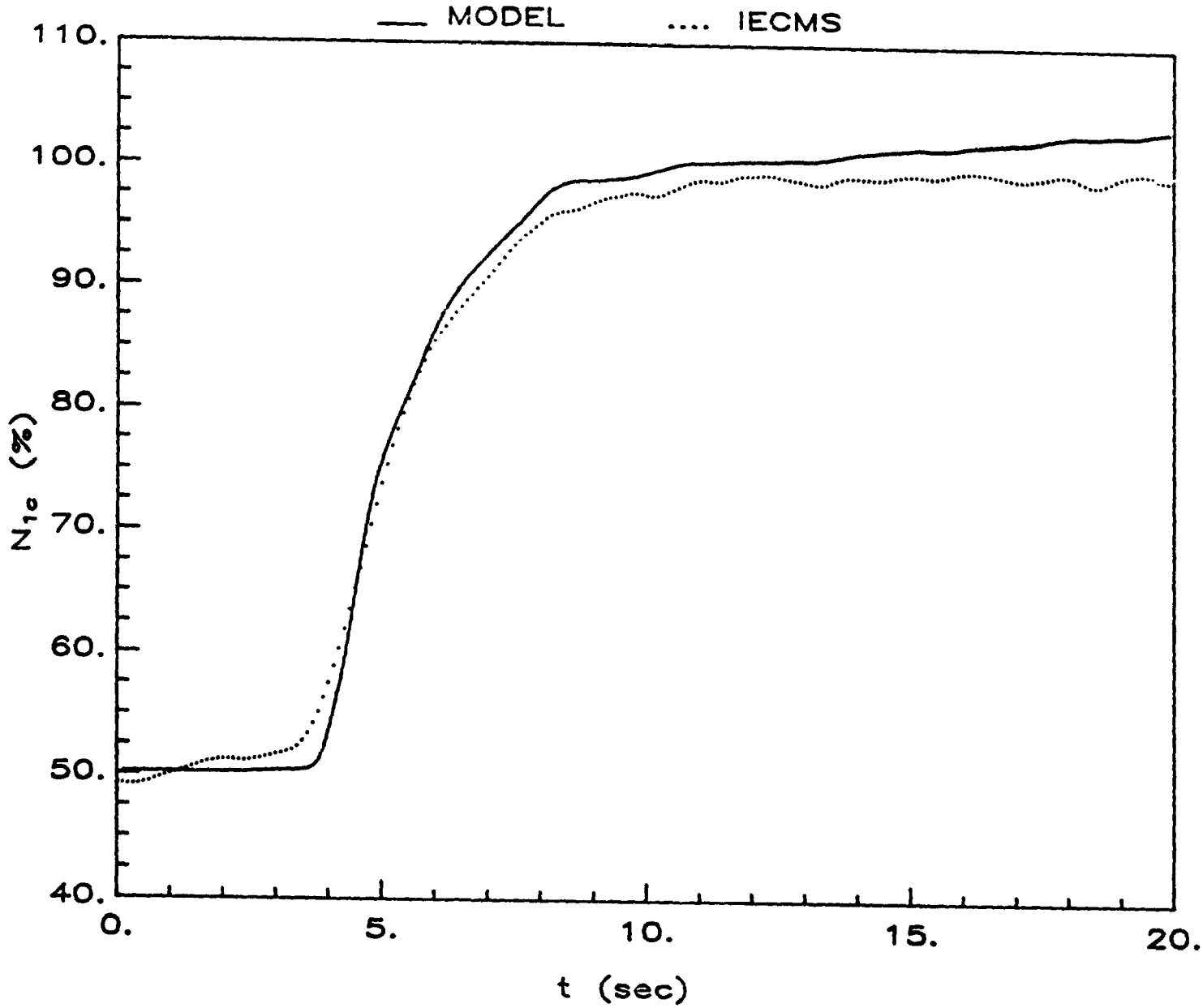

Figure **59** — N1C versus time — 711LI

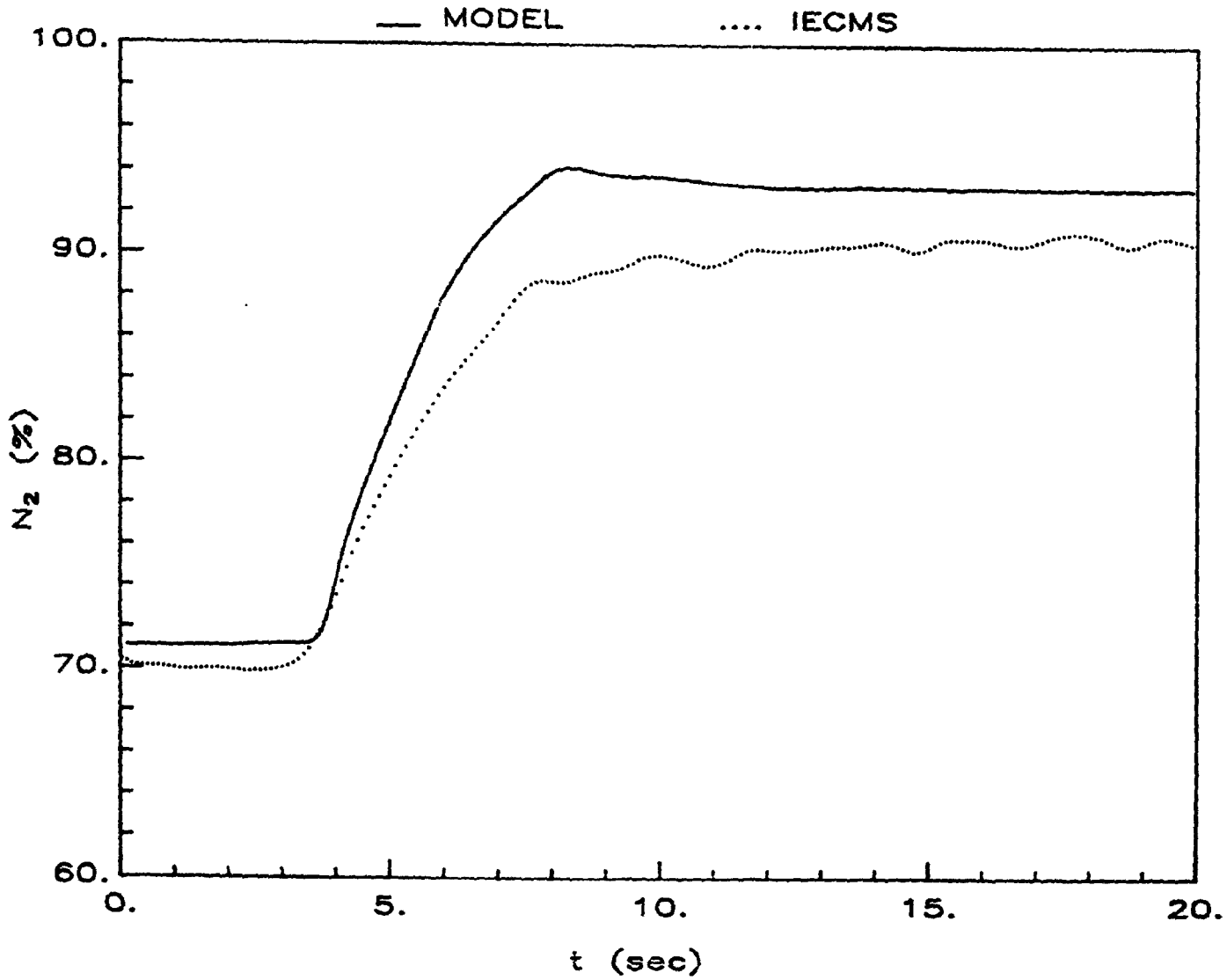

Figure **60** — N2 versus time — 711LI

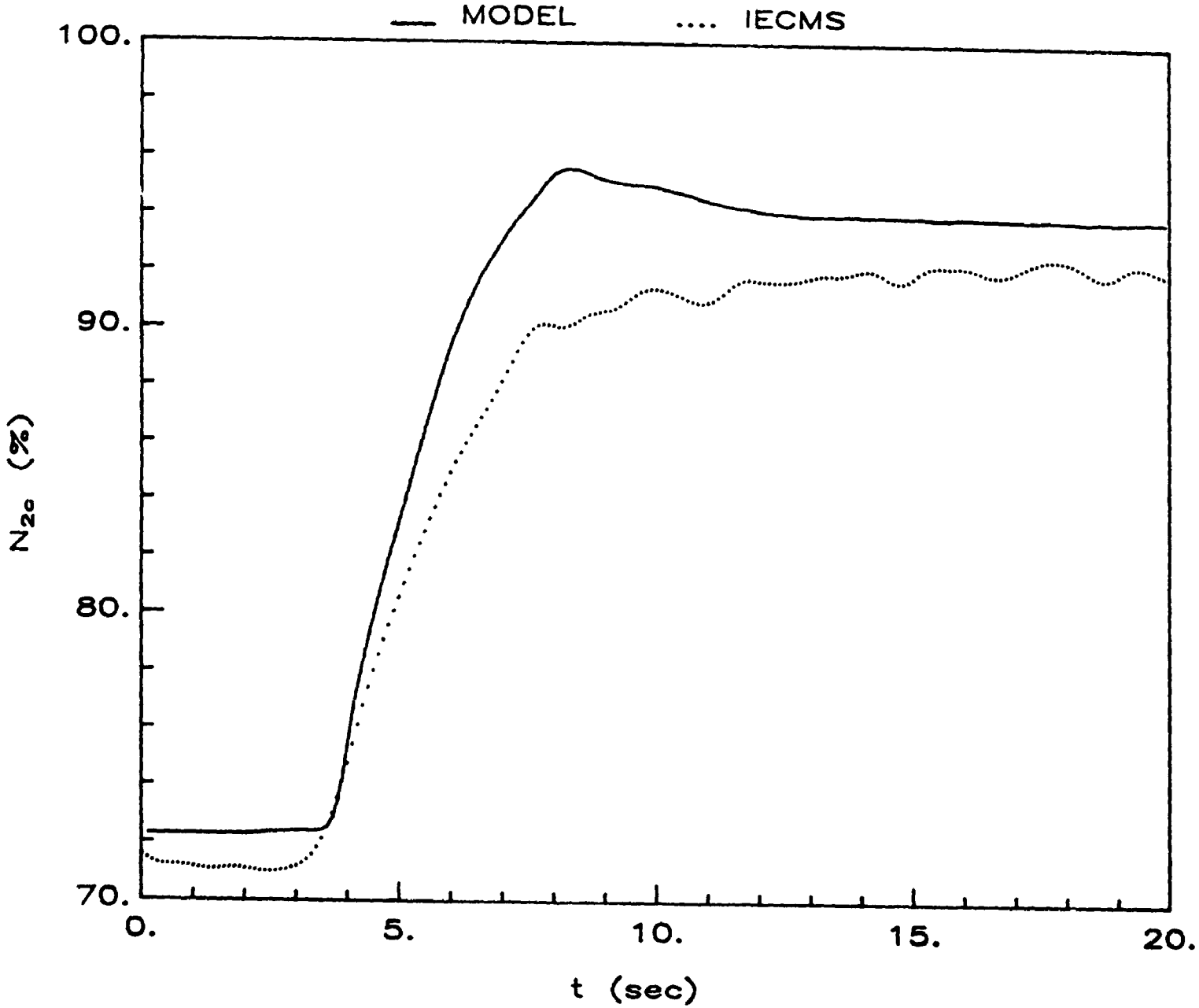

Figure **61** — N2C versus time — 711LI

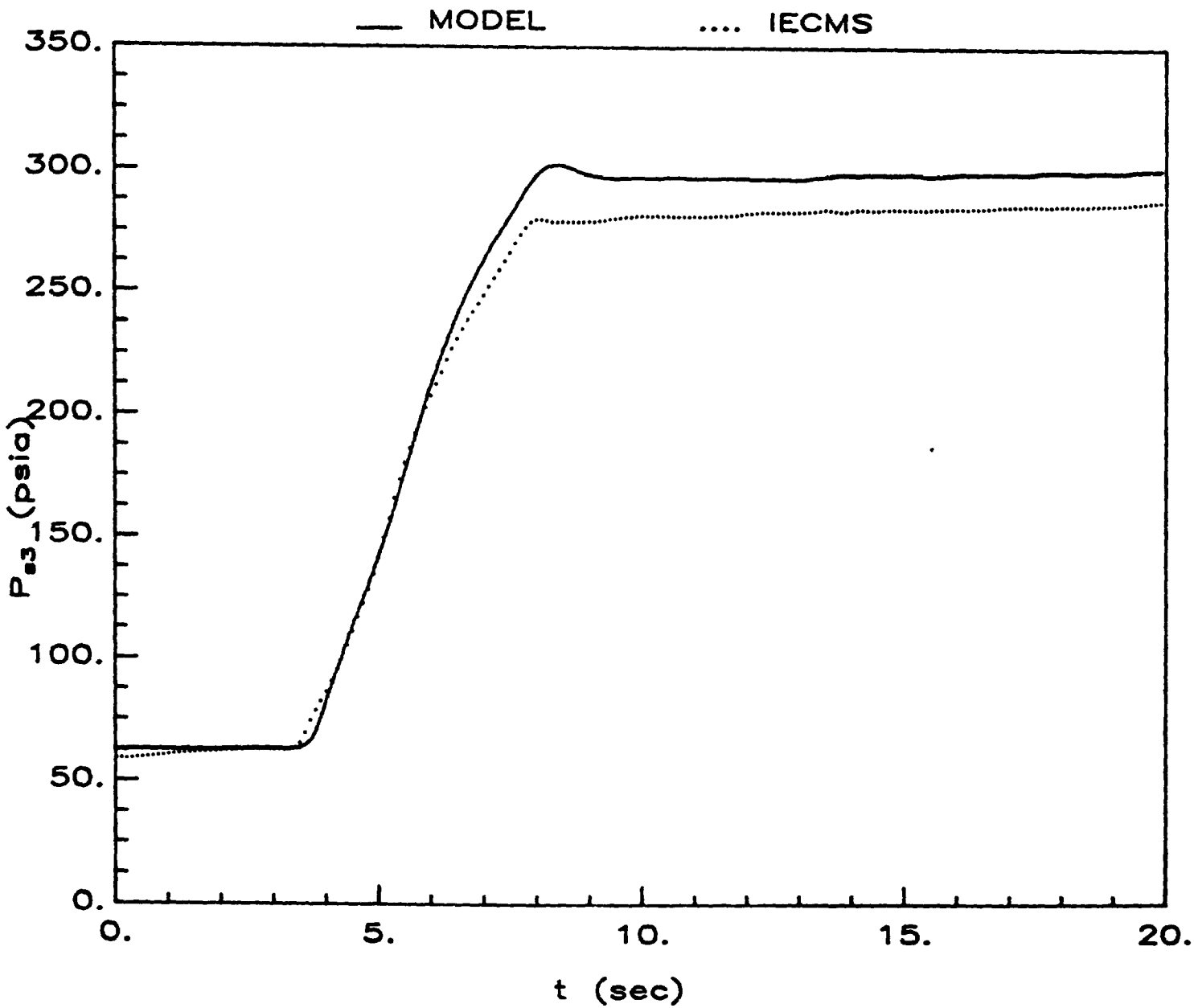

Figure 62 — PS3 versus time — 711LI

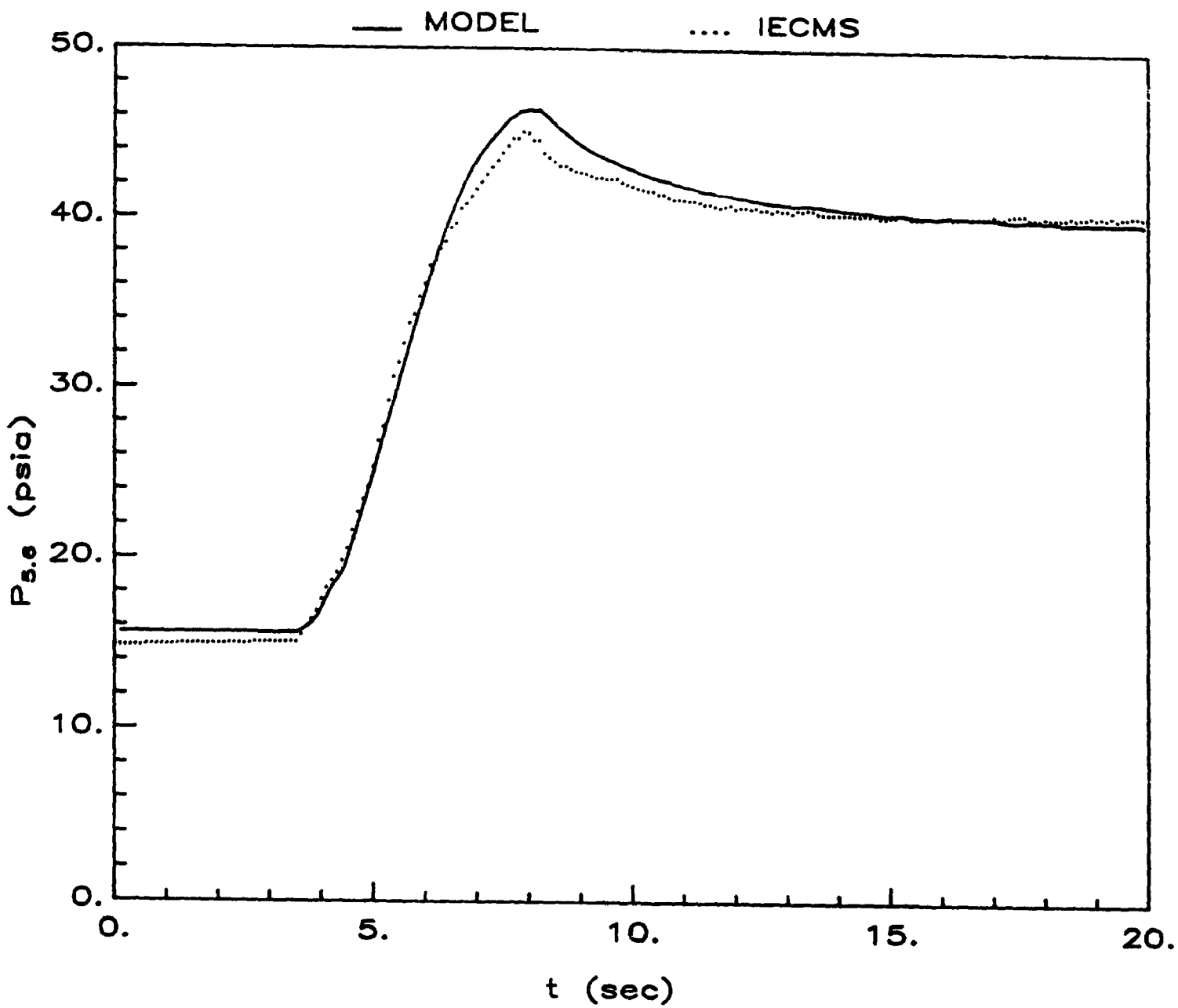

Figure **63** — P56 versus time — 711LI

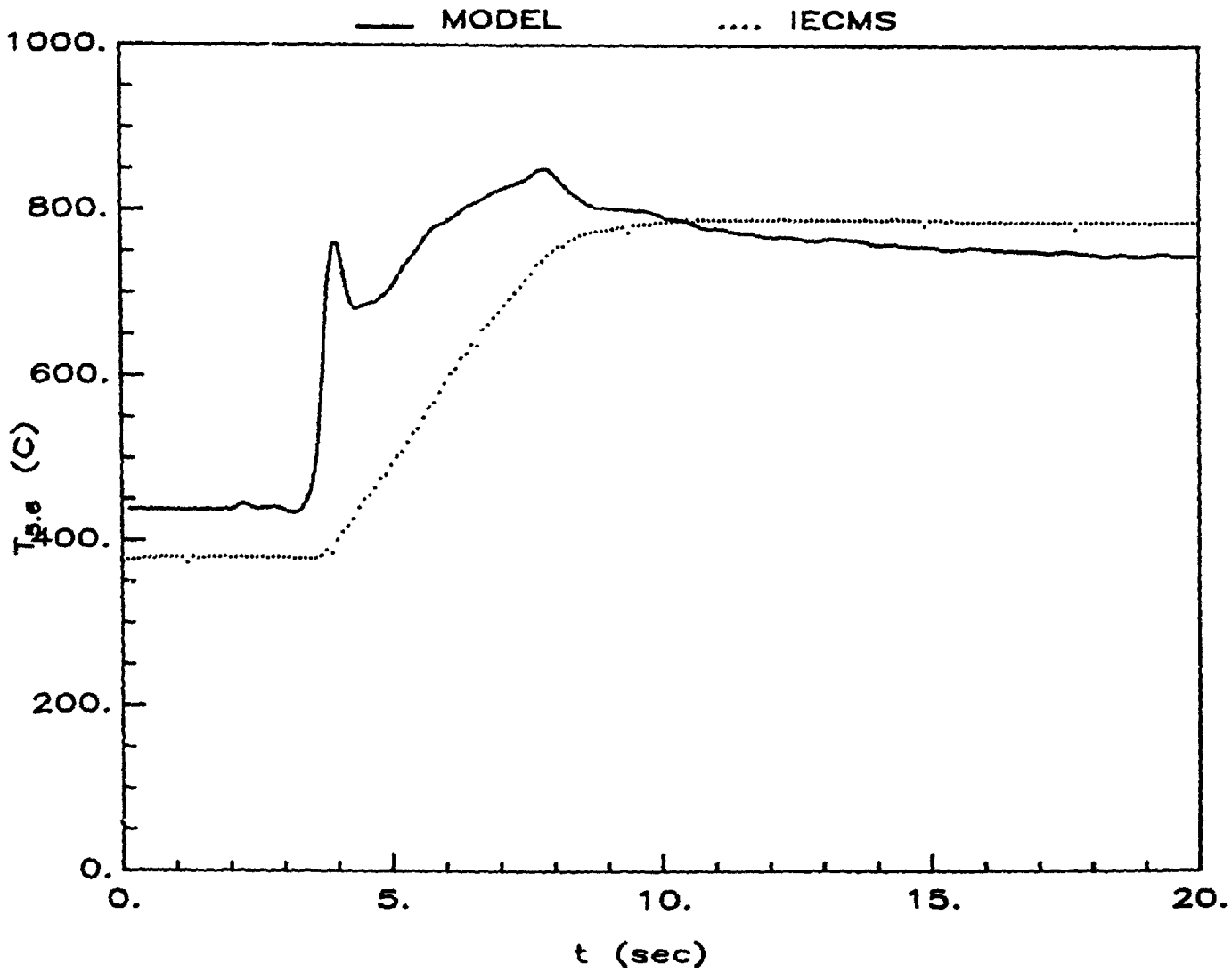

Figure 64 — T56 versus time — 711LI

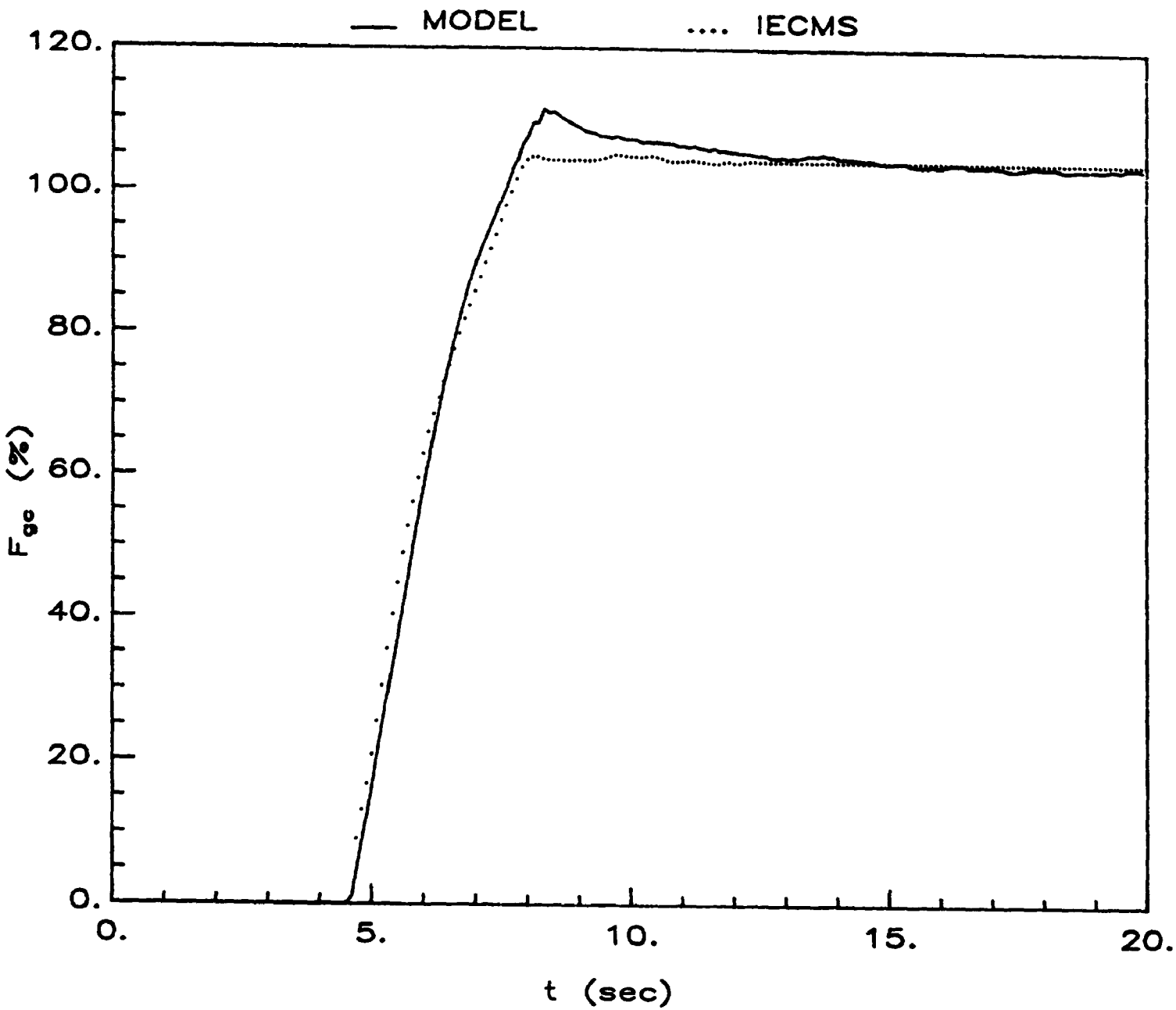

Figure **65** — Thrust versus time — 711LI

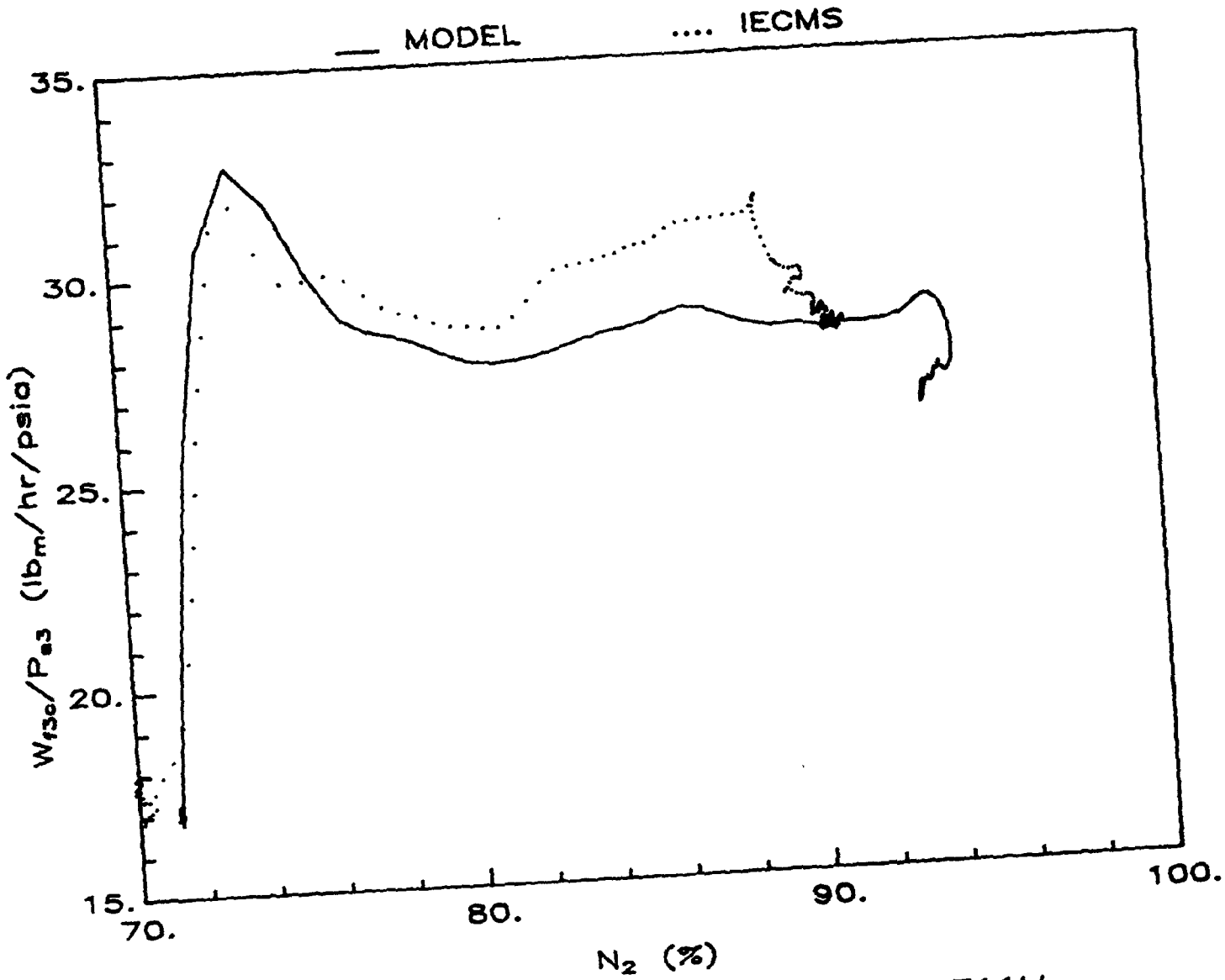

Figure **66** — WF3C/PS3 versus N2 — 711LI

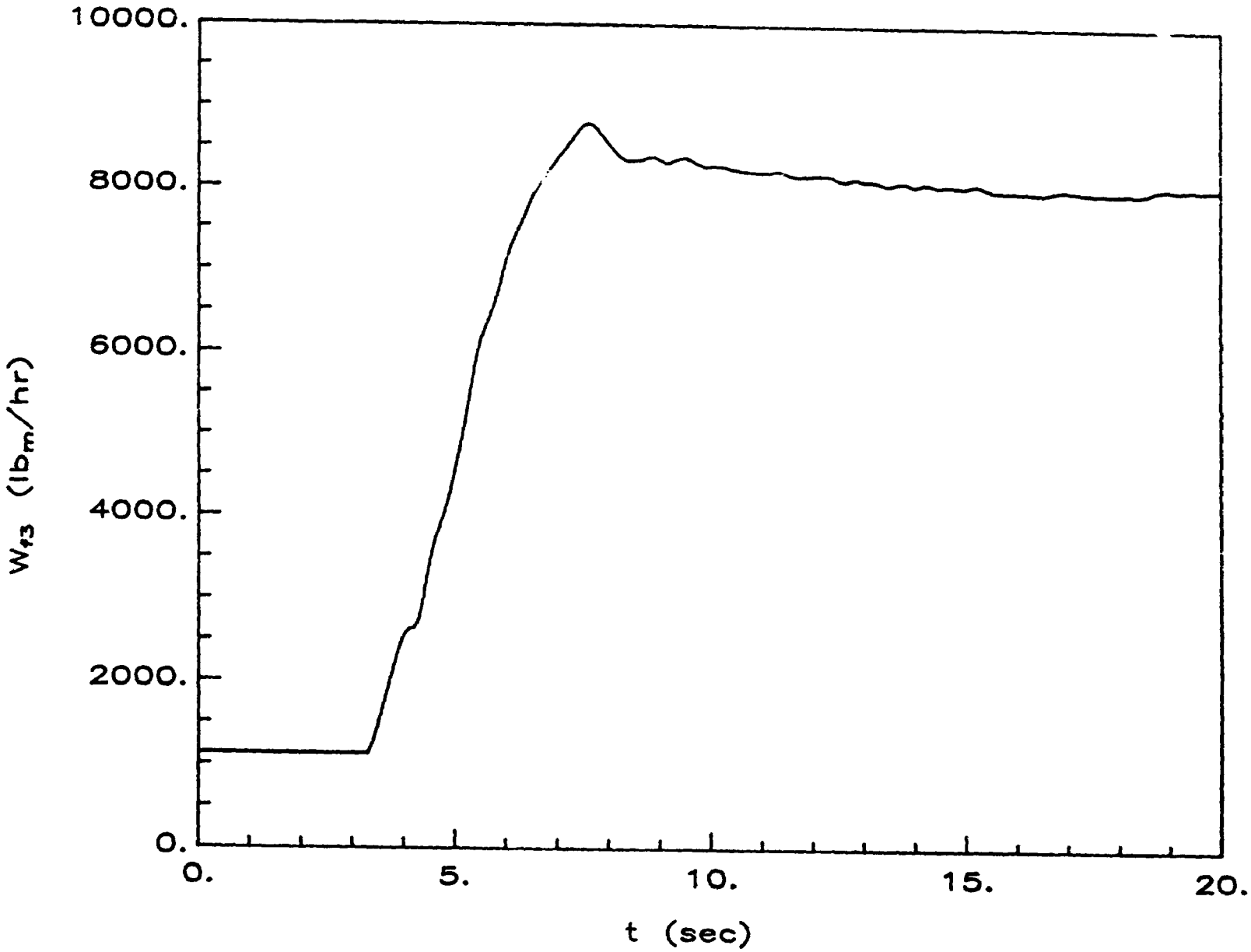

Figure 67 — WF3 versus time — 711RI

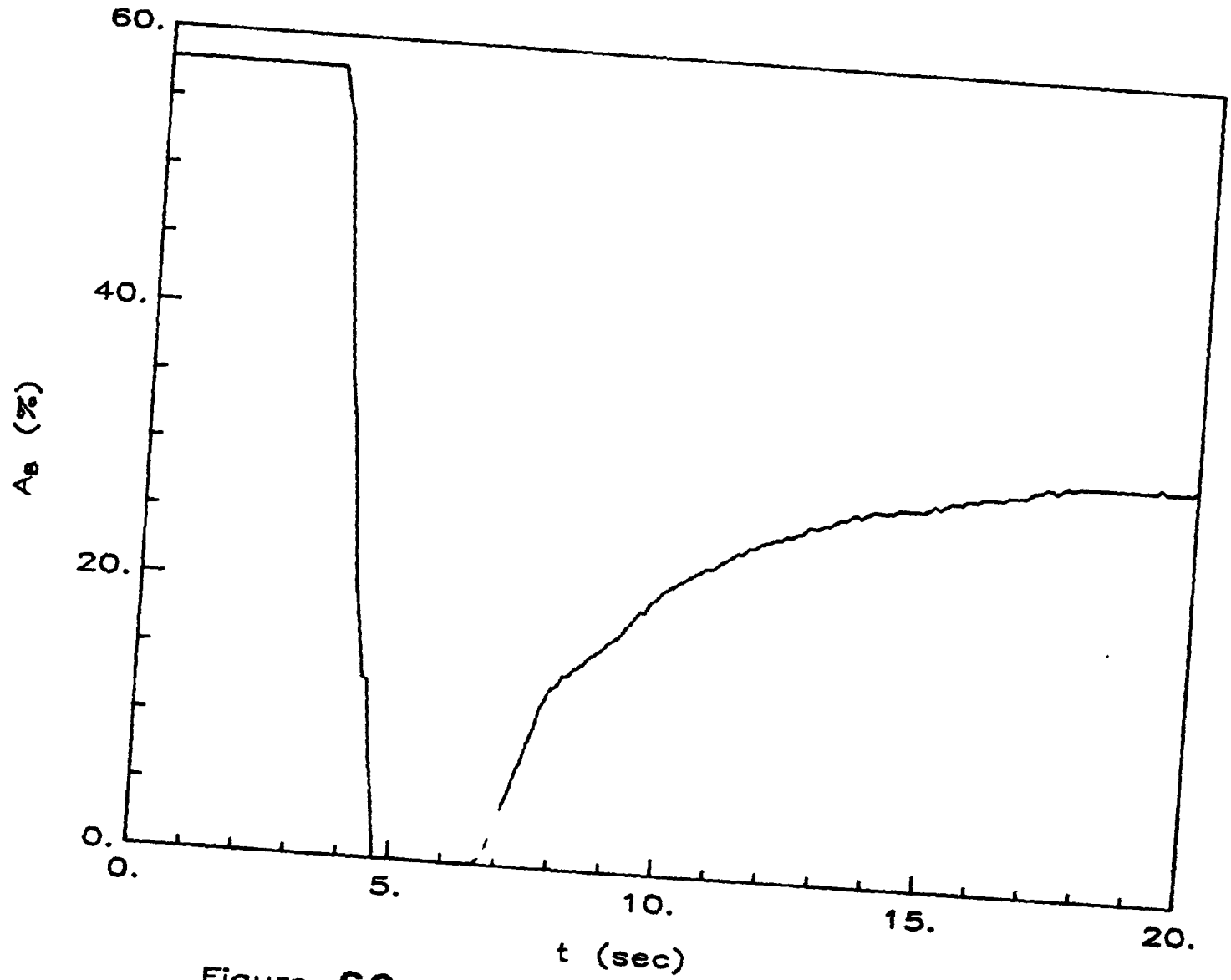

Figure **68** – A8 versus time – 711RI

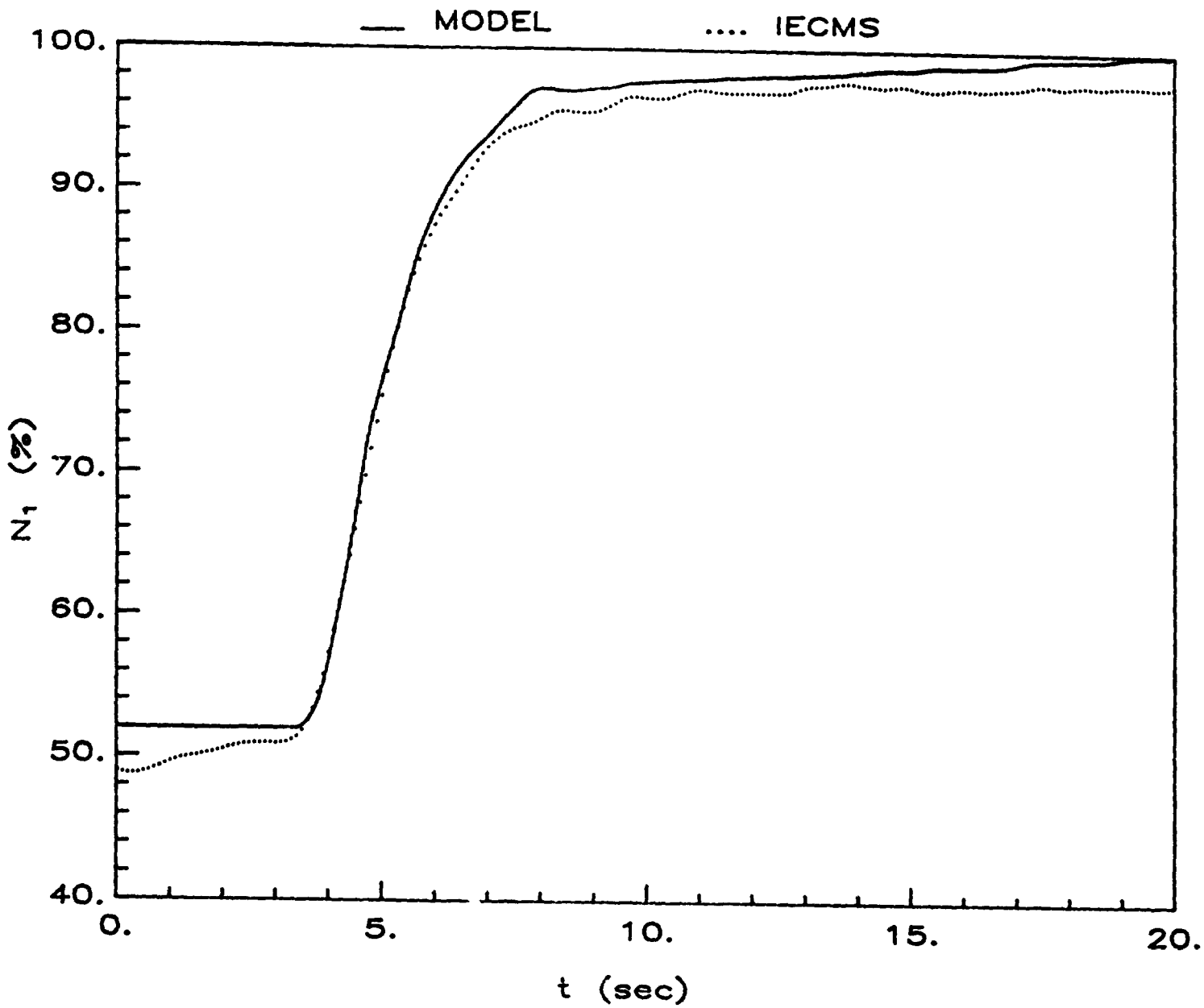

Figure **69** — N1 versus time — 711RI

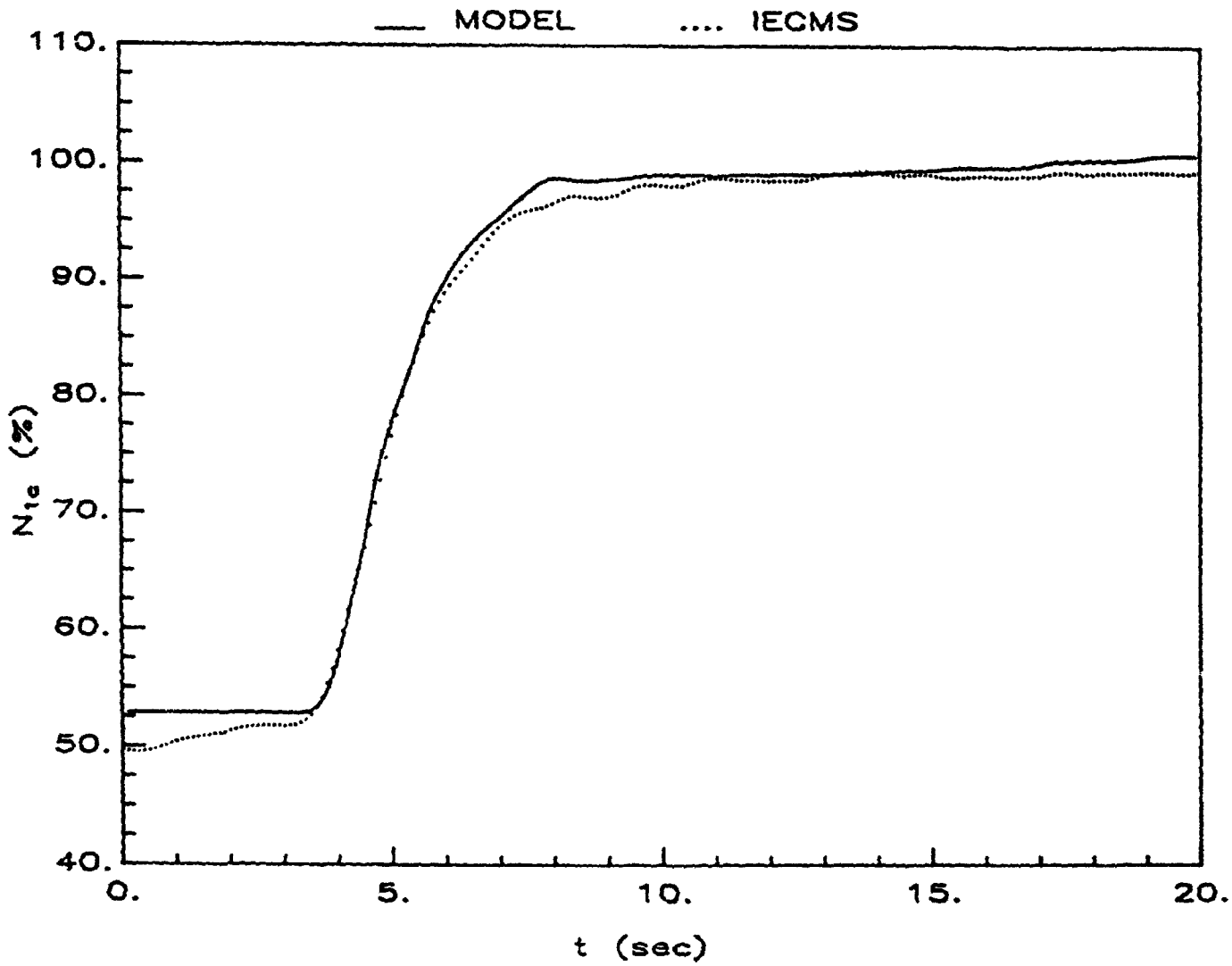

Figure 70 — N1C versus time — 711RI

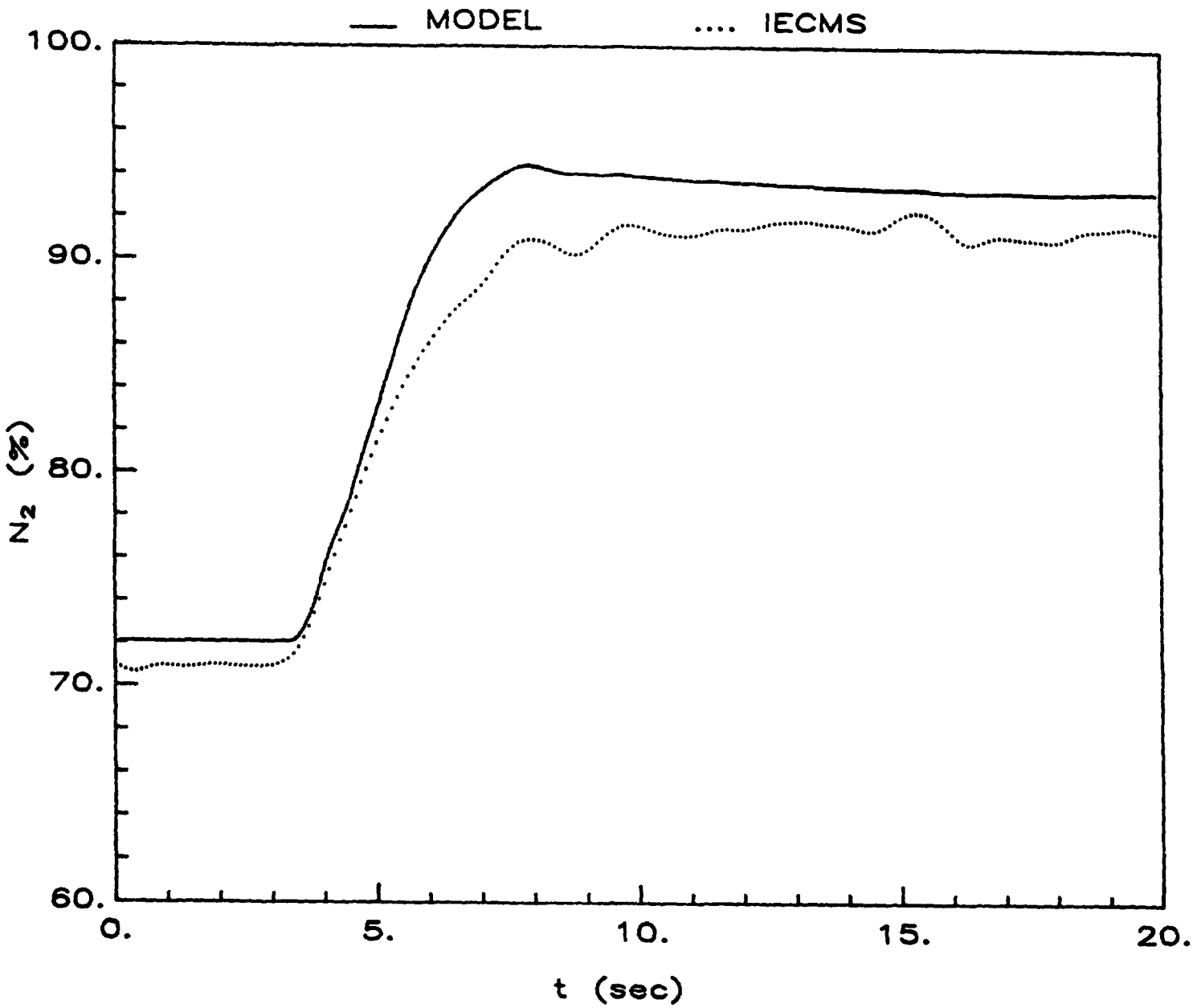

Figure **71** — N2 versus time — 711RI

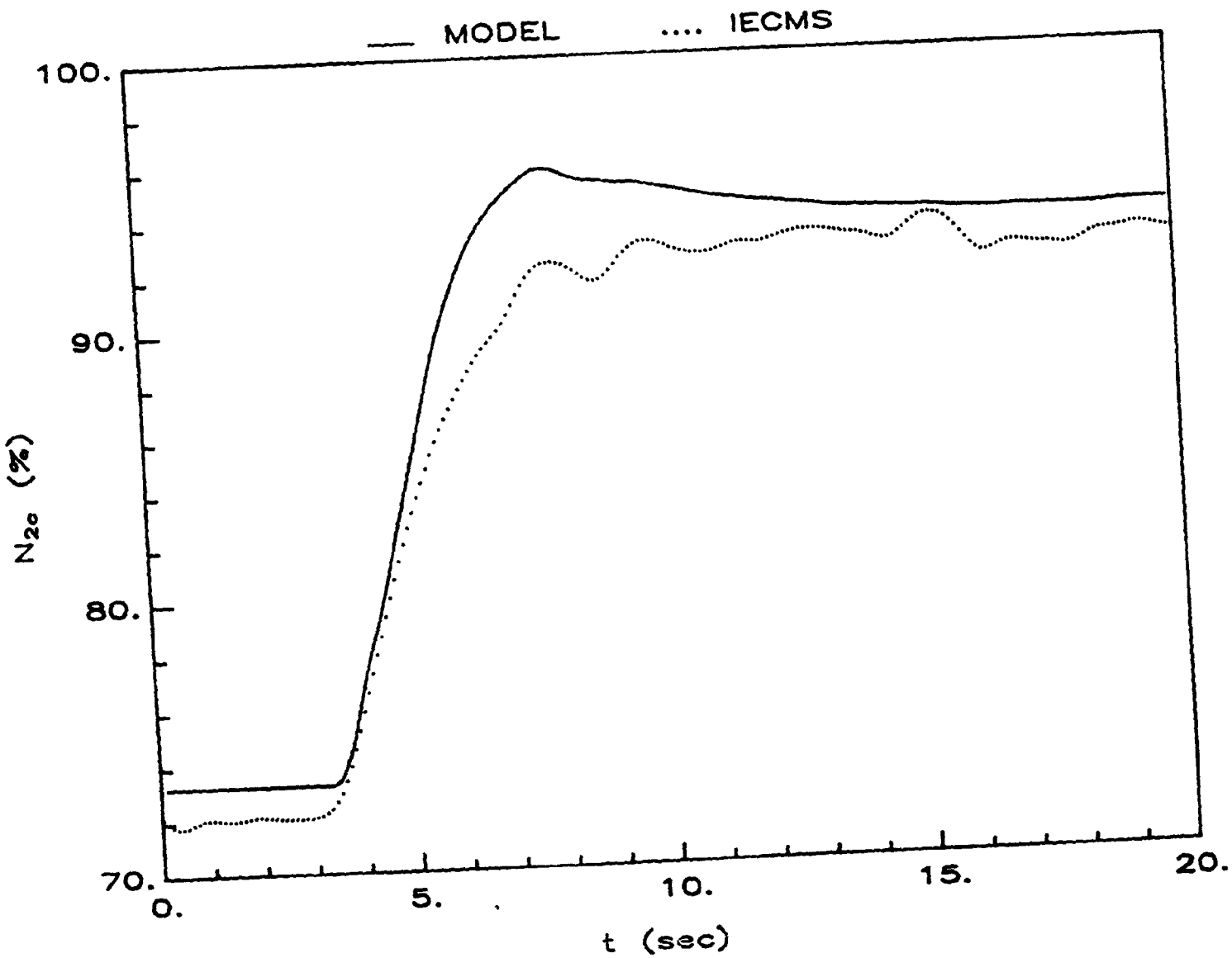

Figure **72** — N2C versus time — 711RI

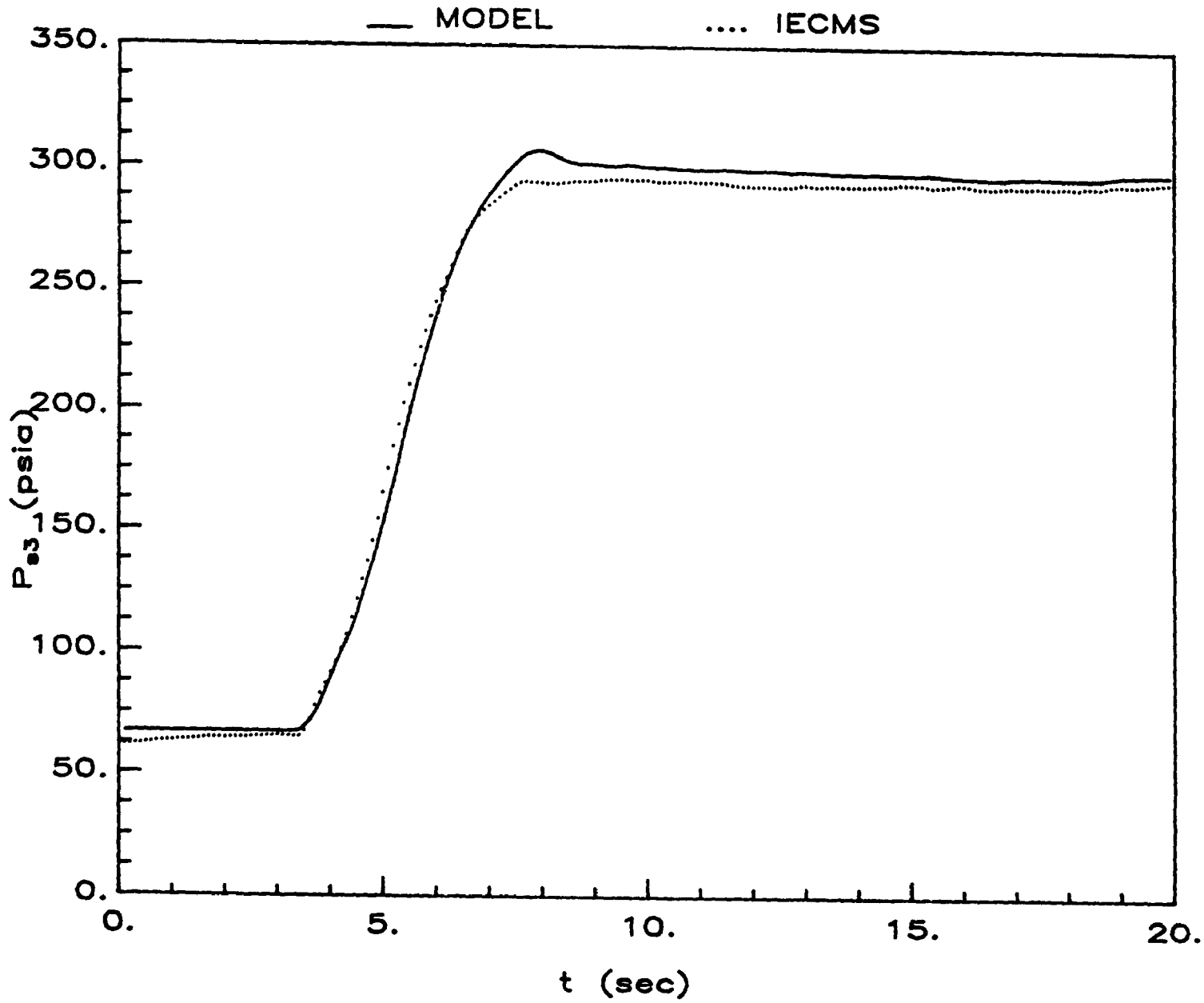

Figure 73 — PS3 versus time — 711RI

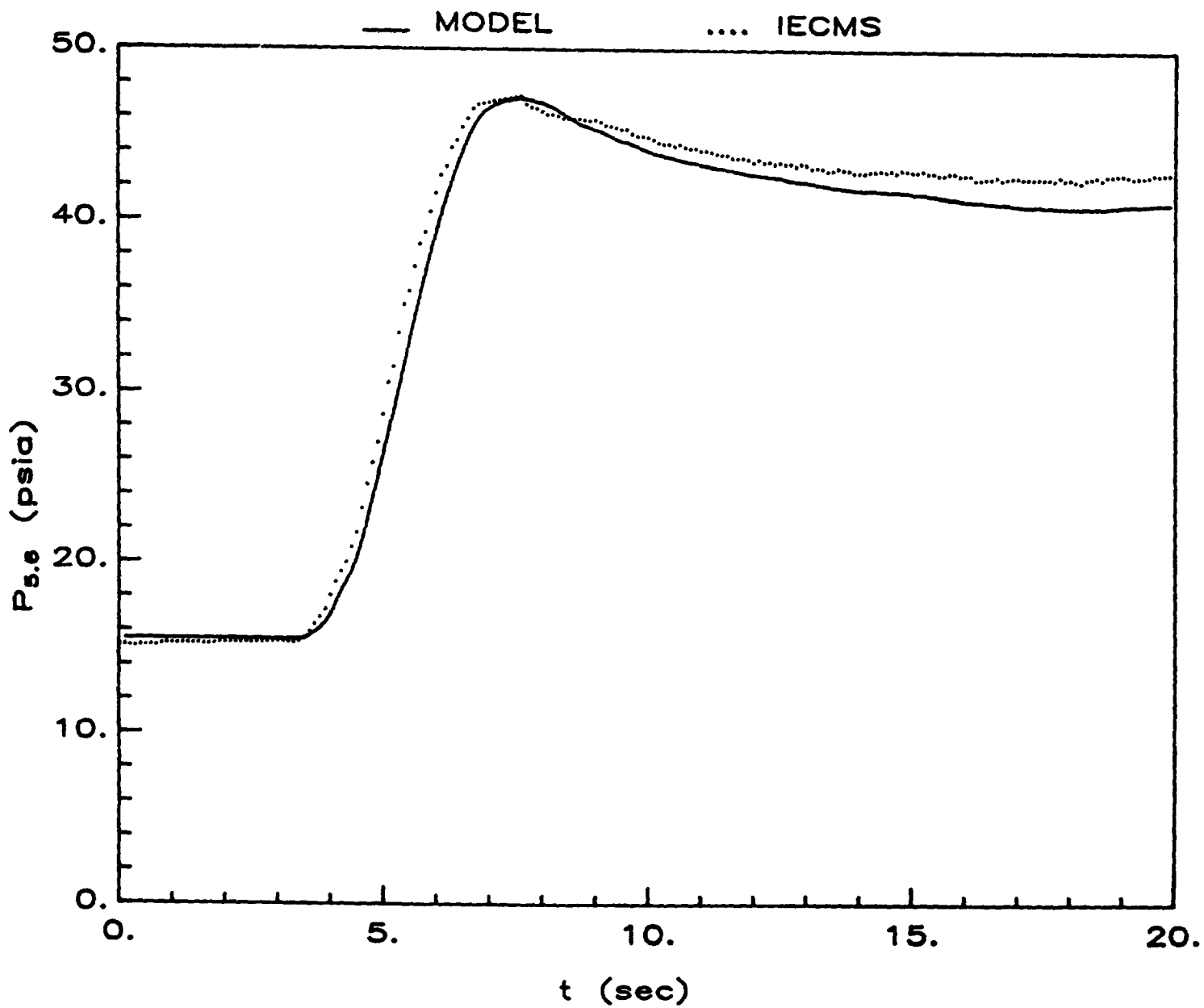

Figure 74 — P56 versus time — 711RI

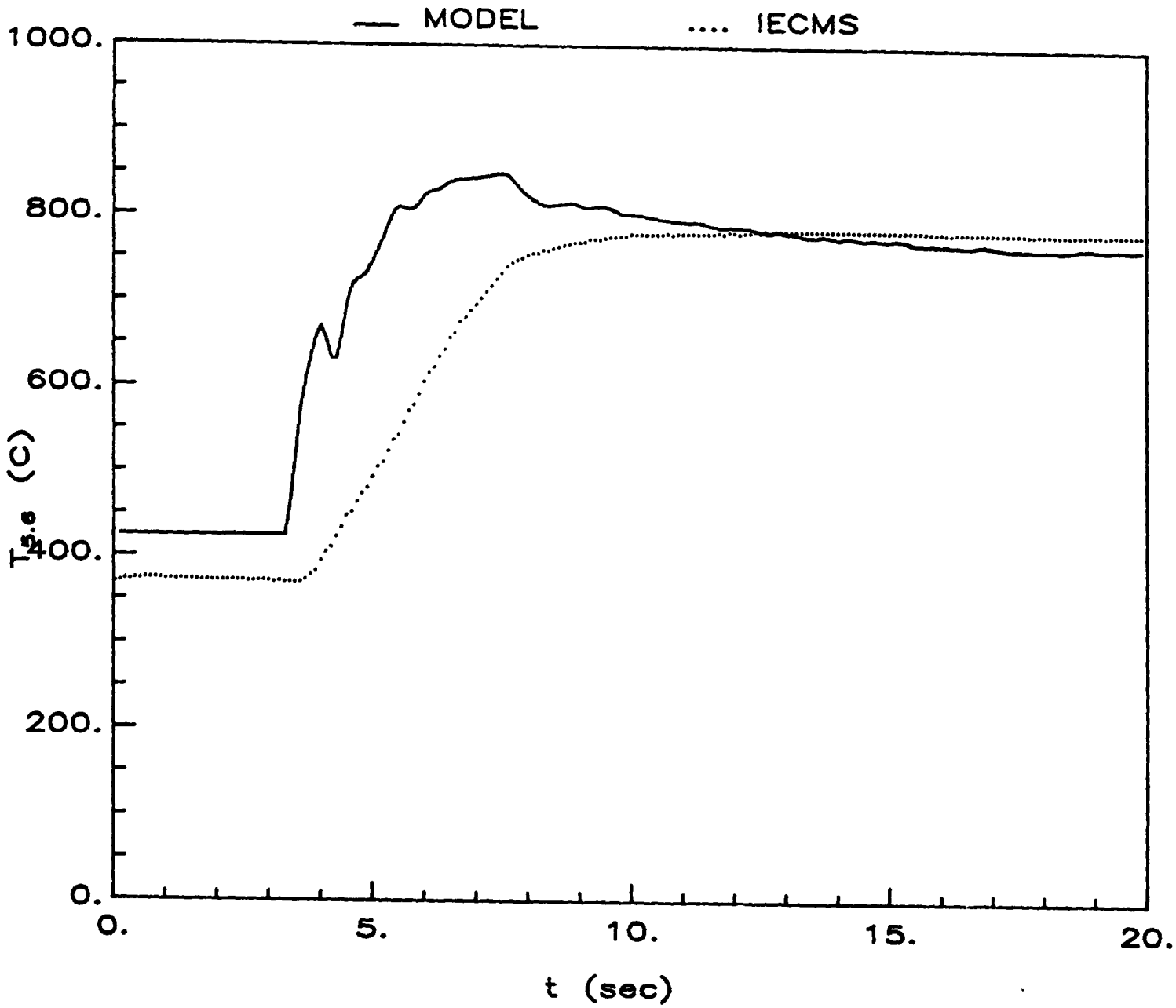

Figure 75 — T56 versus time — 711RI

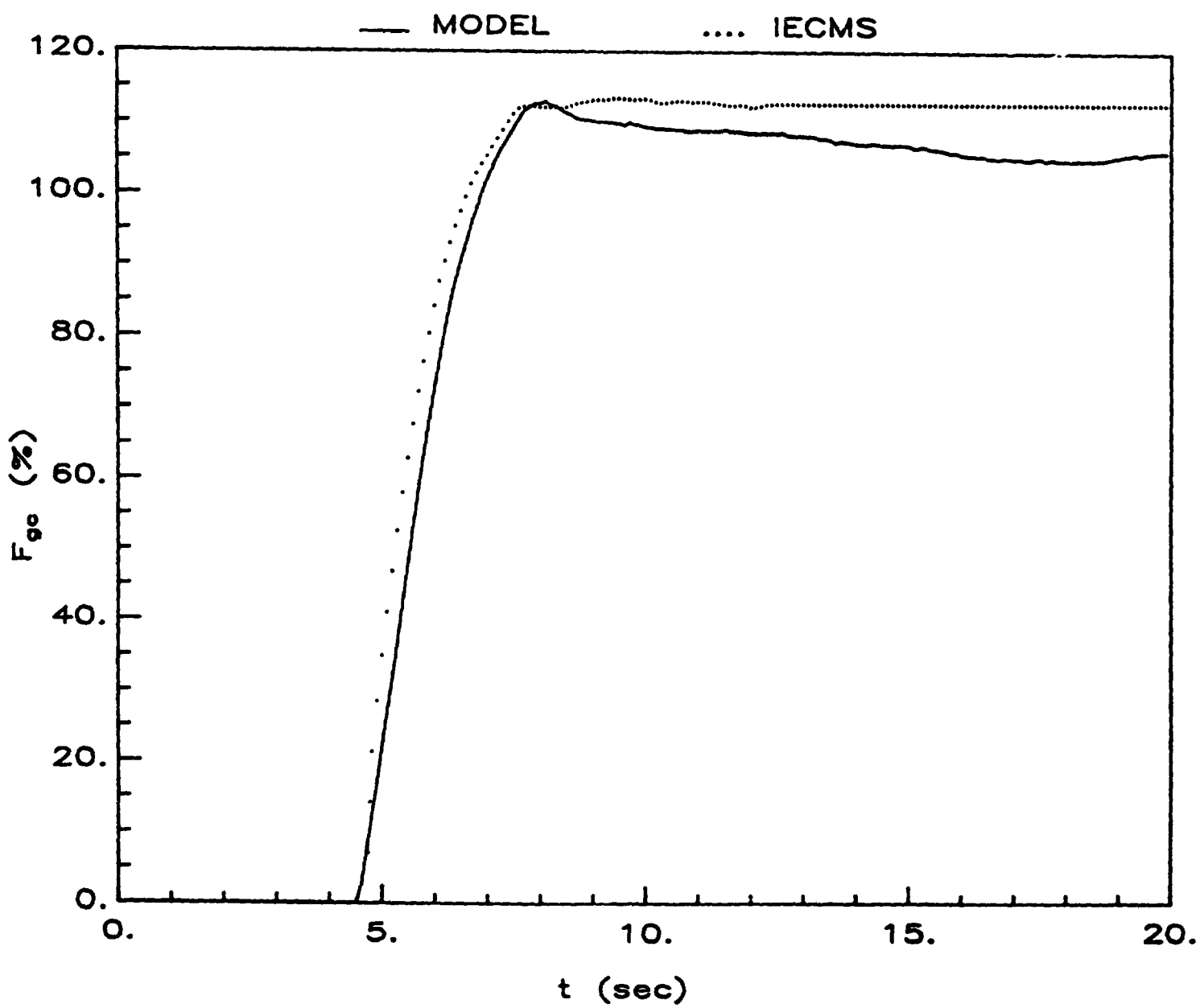

Figure 76 — Thrust versus time — 711RI

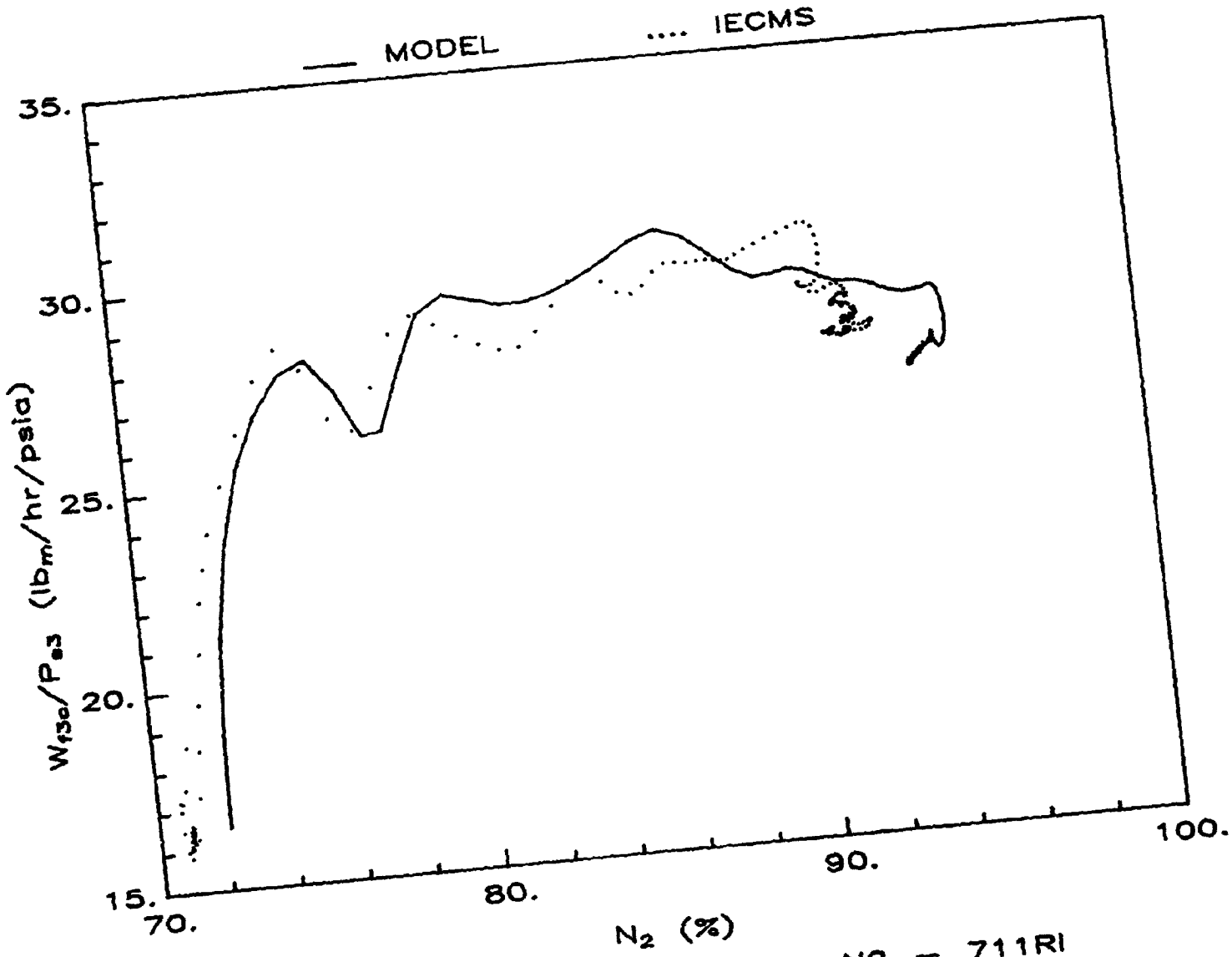

Figure 77 — WF3C/PS3 versus N2 — 711RI

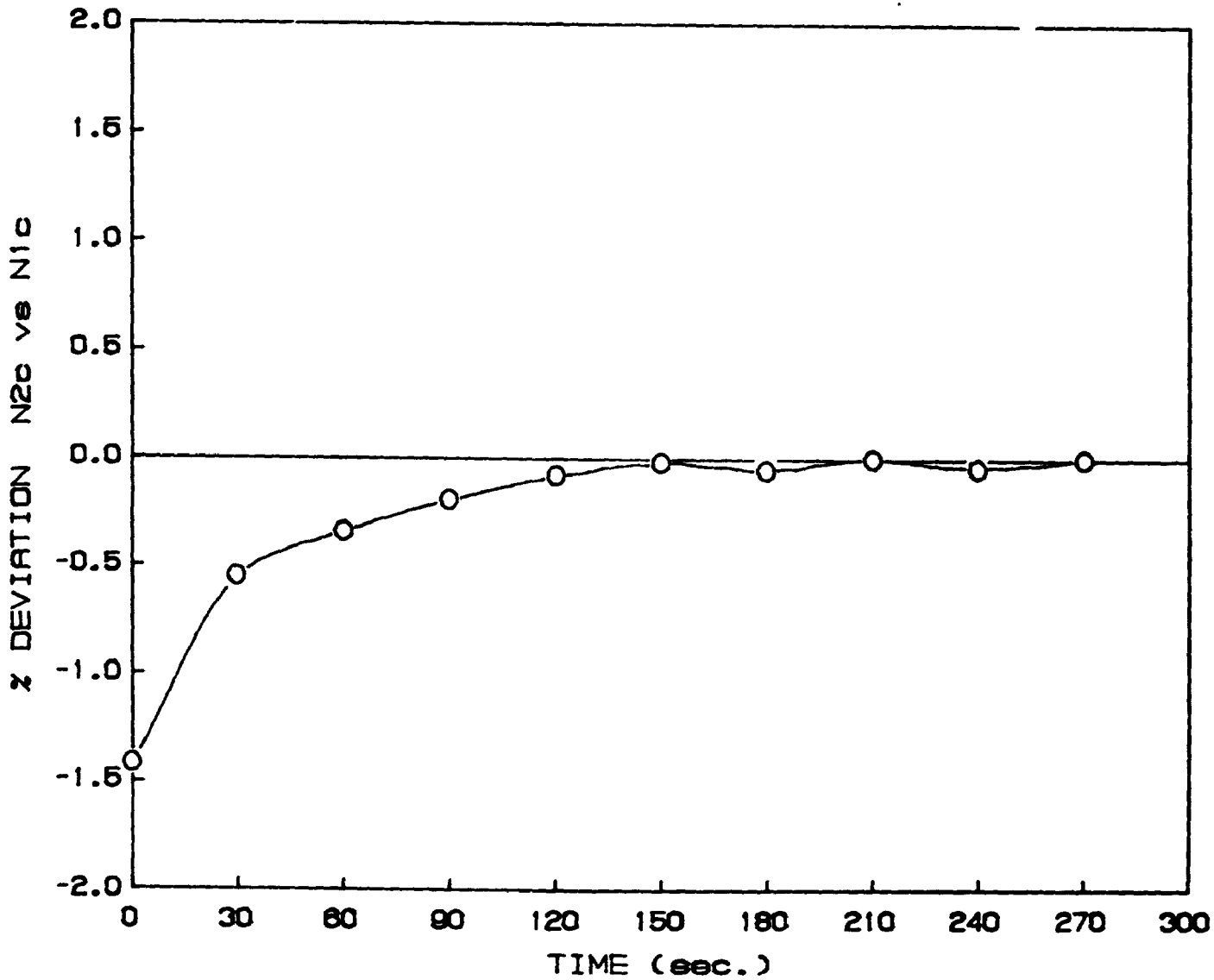

Figure 78 : Stablization from Idle to N_{1c} = 89%

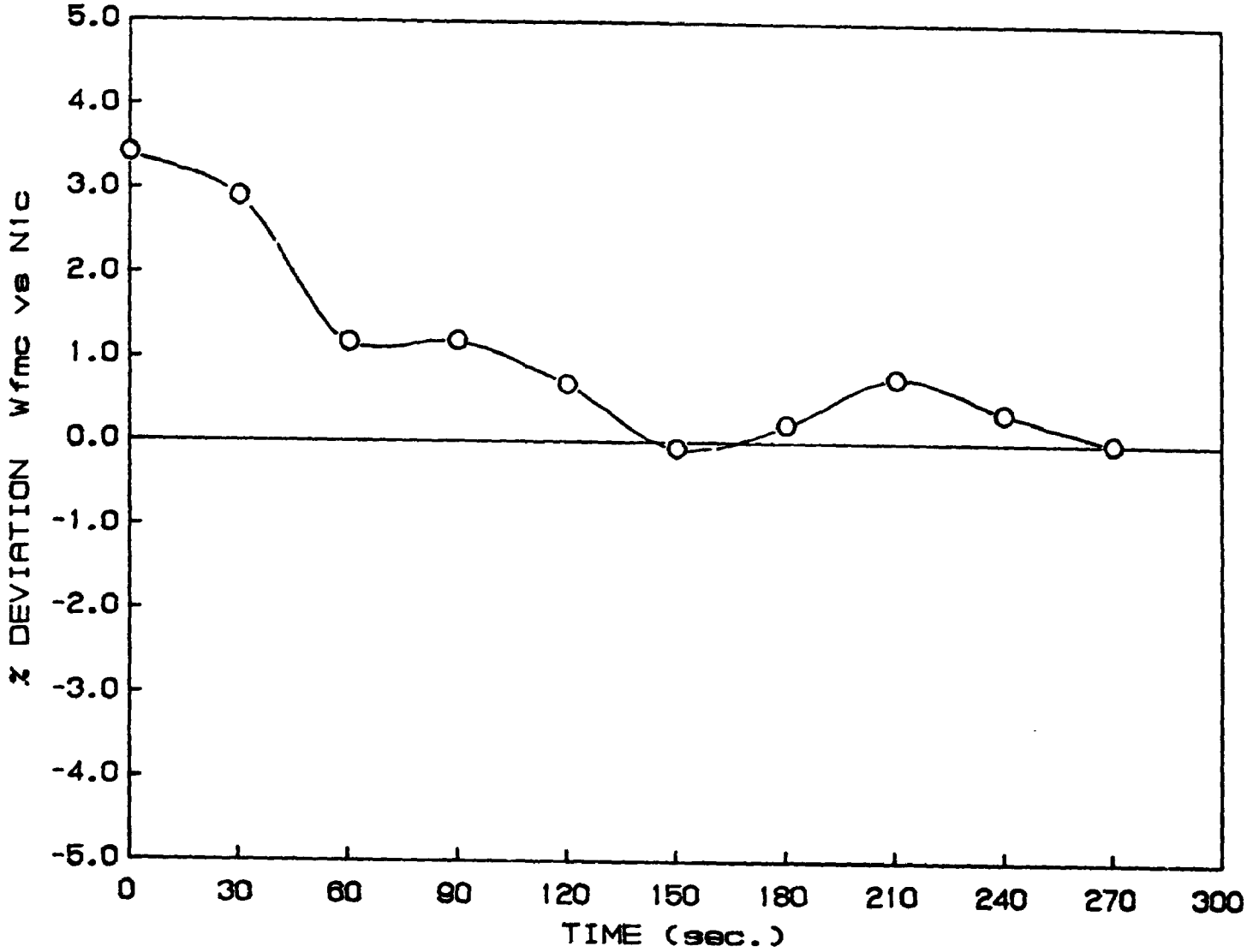

Figure **79**: Stablization from Idle to N_{1c}= 89%

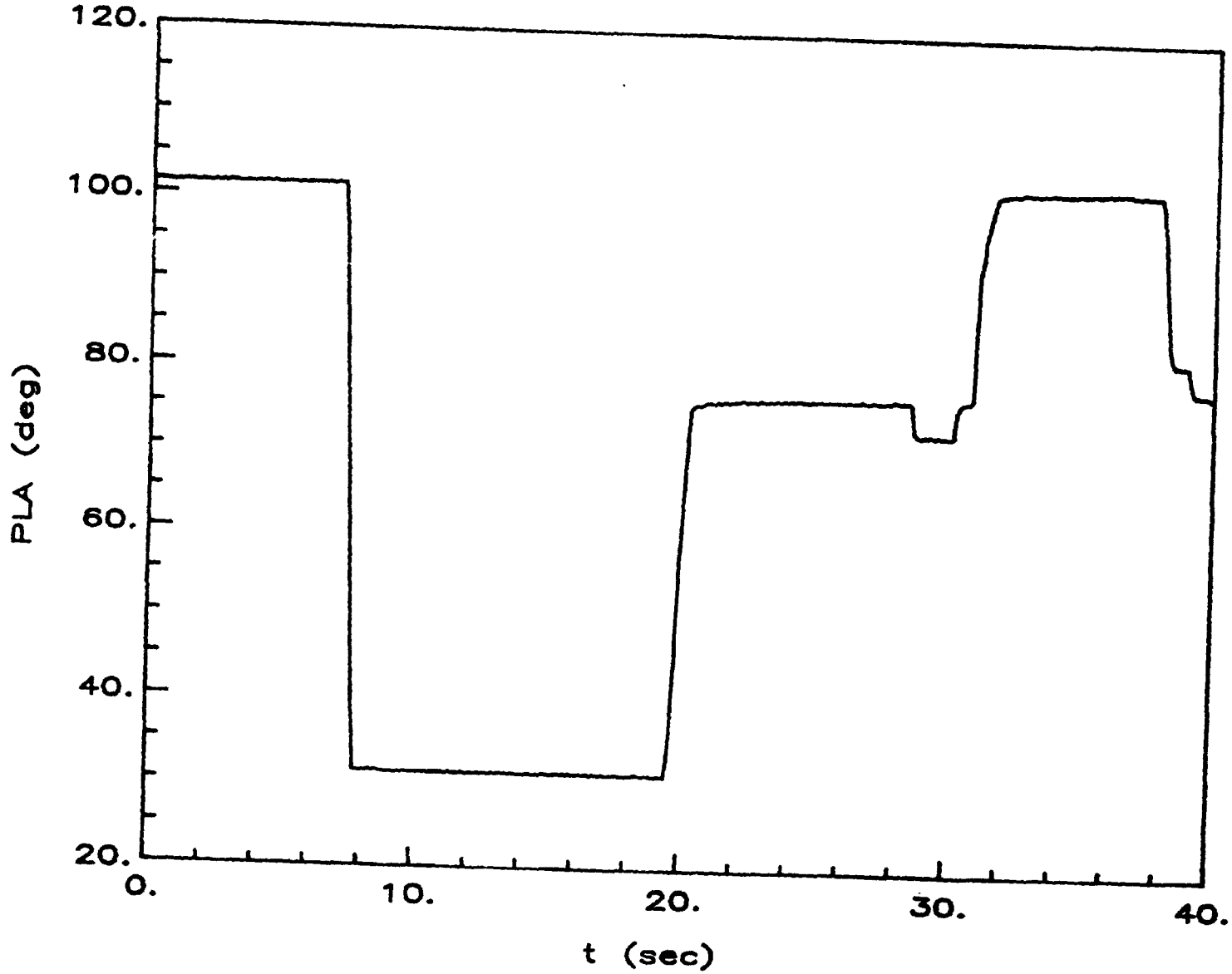

Figure 80 — PLA versus time — 912LB

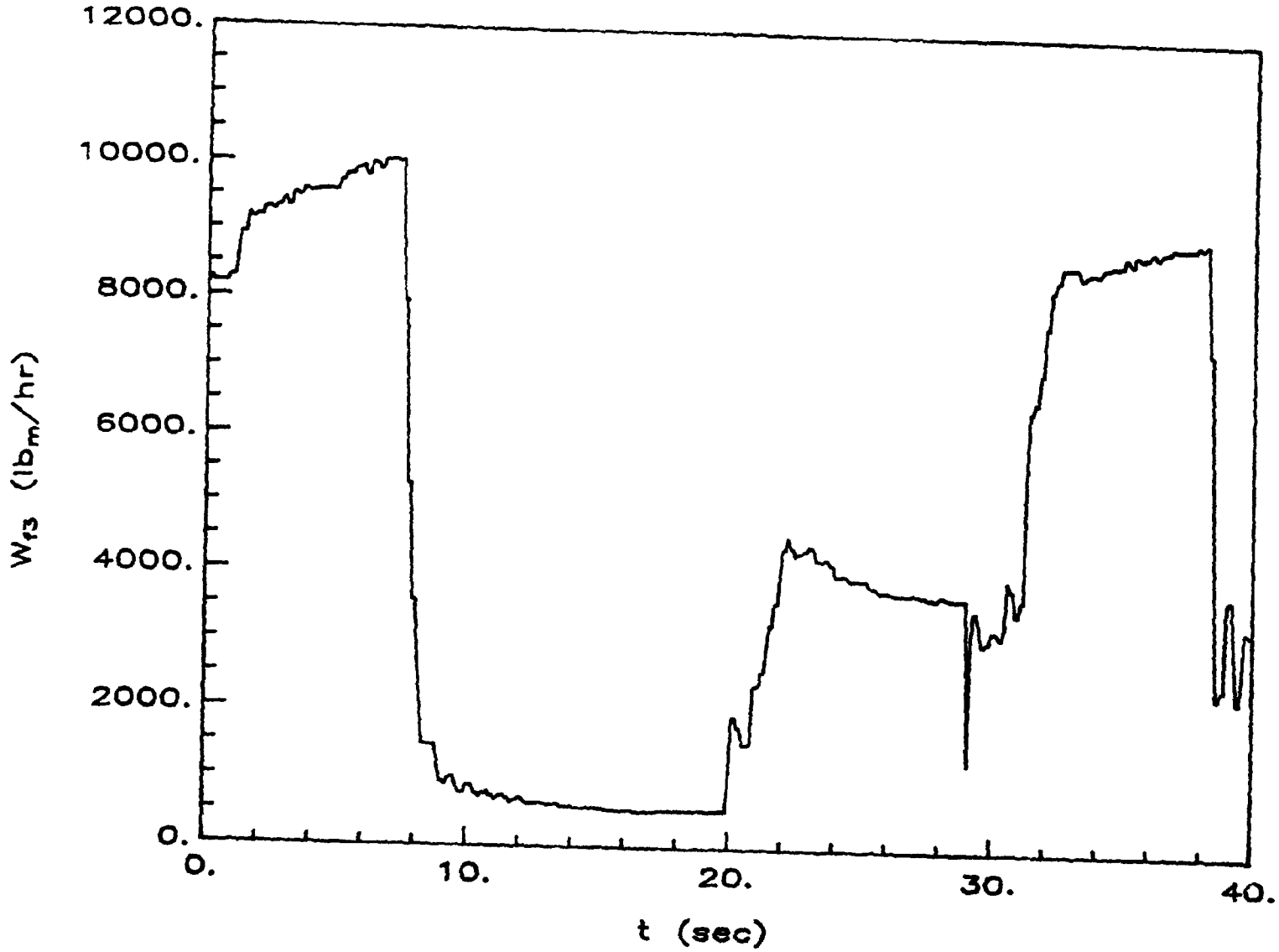

Figure 81 — Wf3 versus time — 912LB

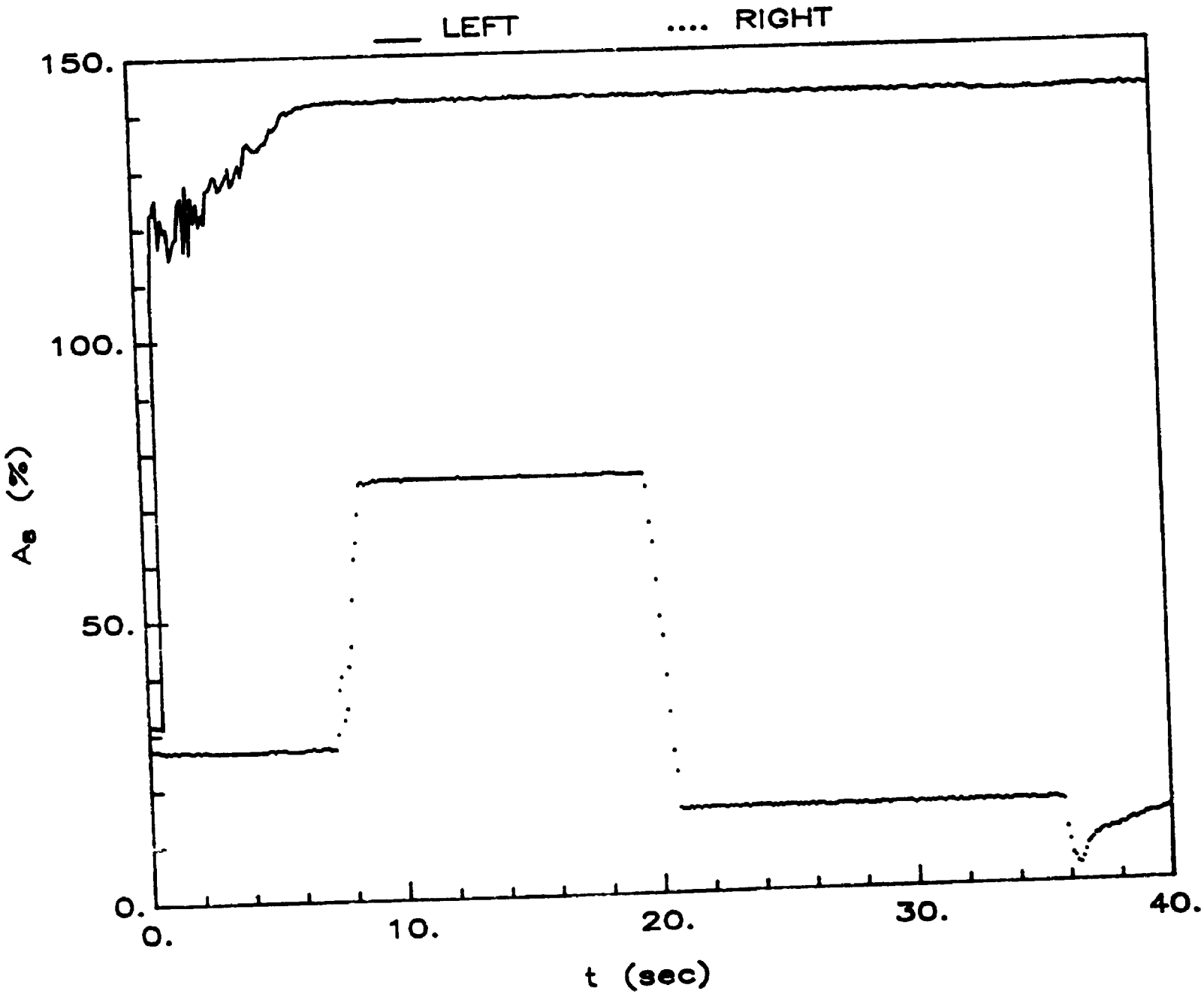

Figure 82 — A8 versus time — 912

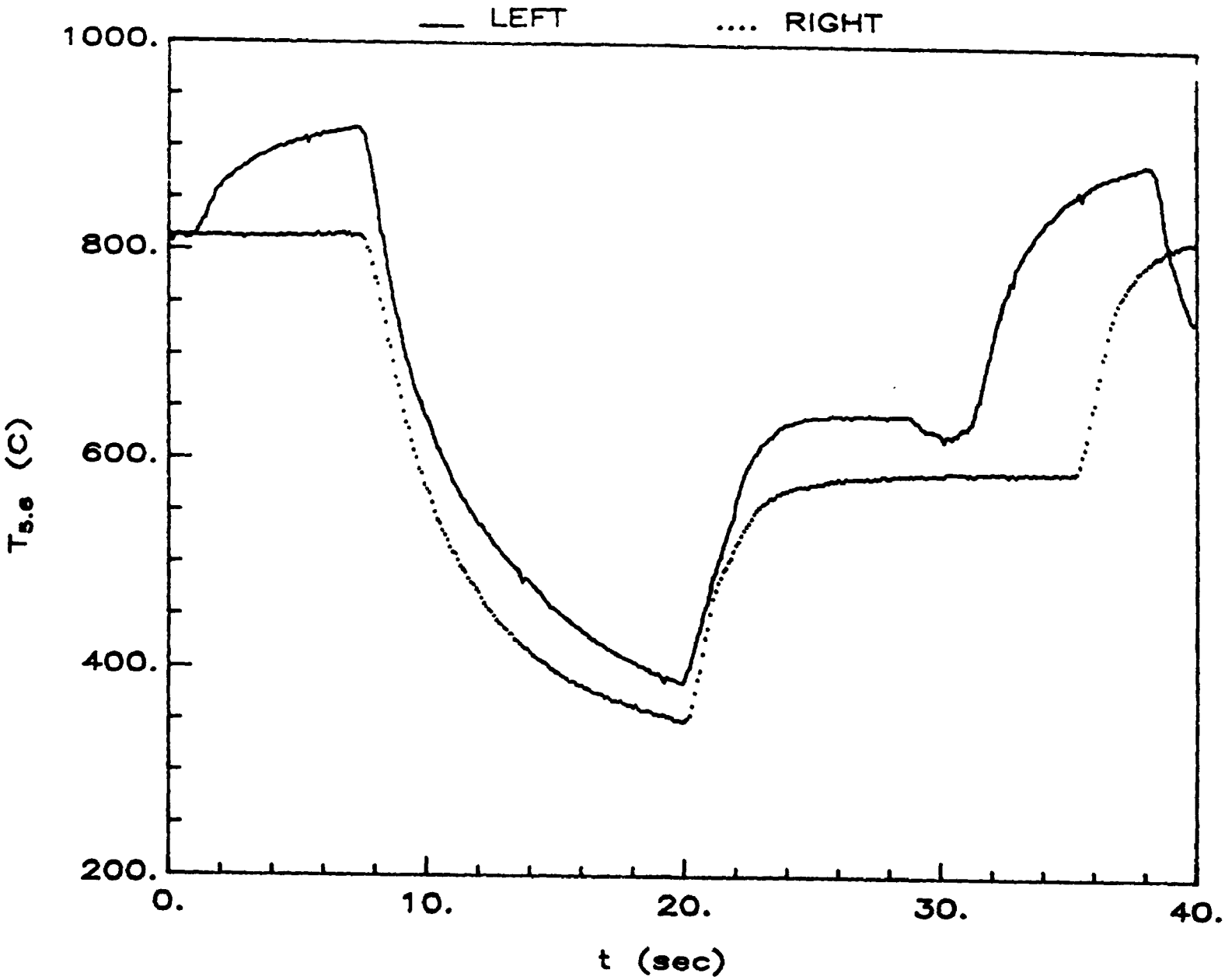

Figure **83** — T56 versus time — 912

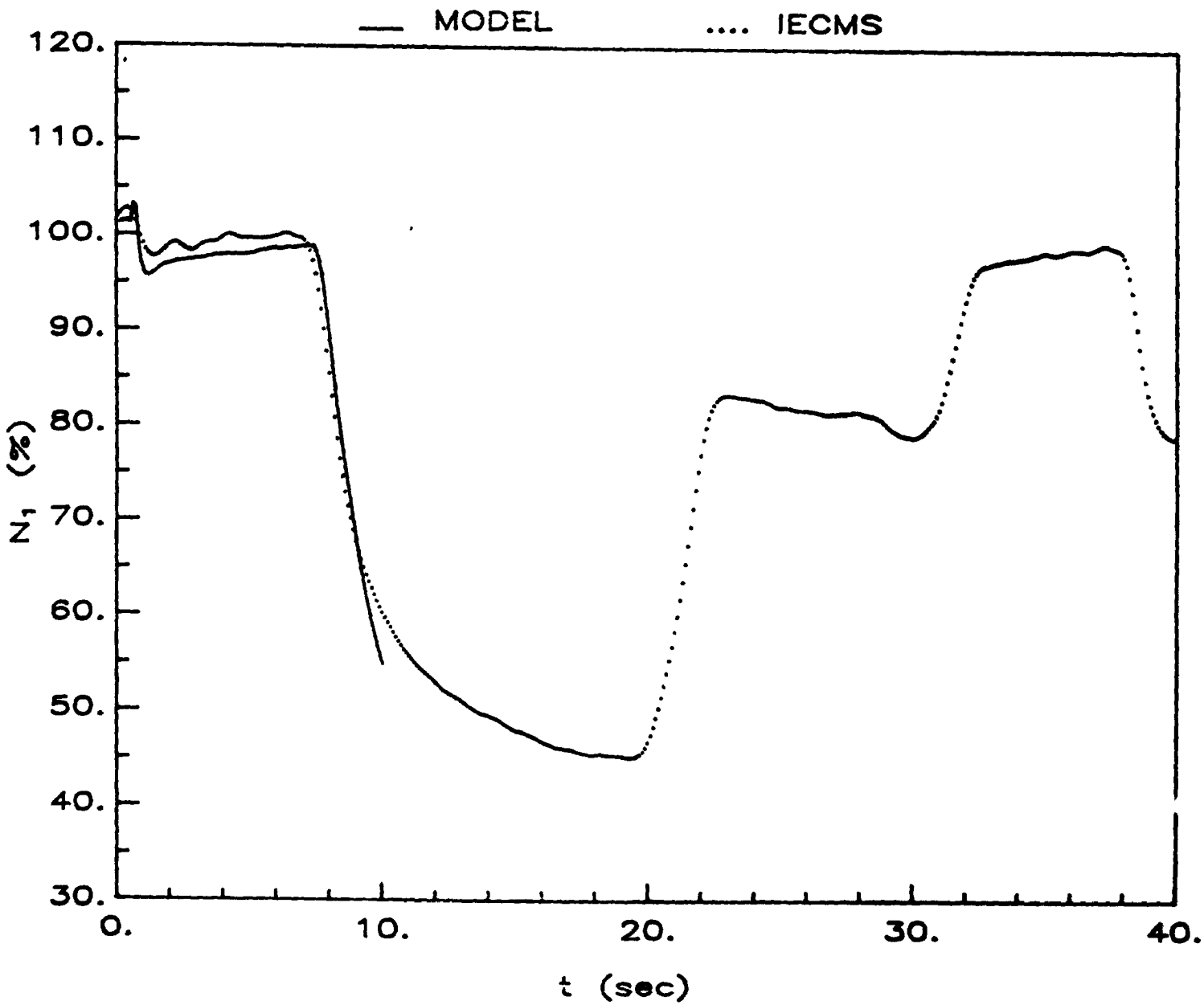

Figure **84** — N1 versus time — 912LB

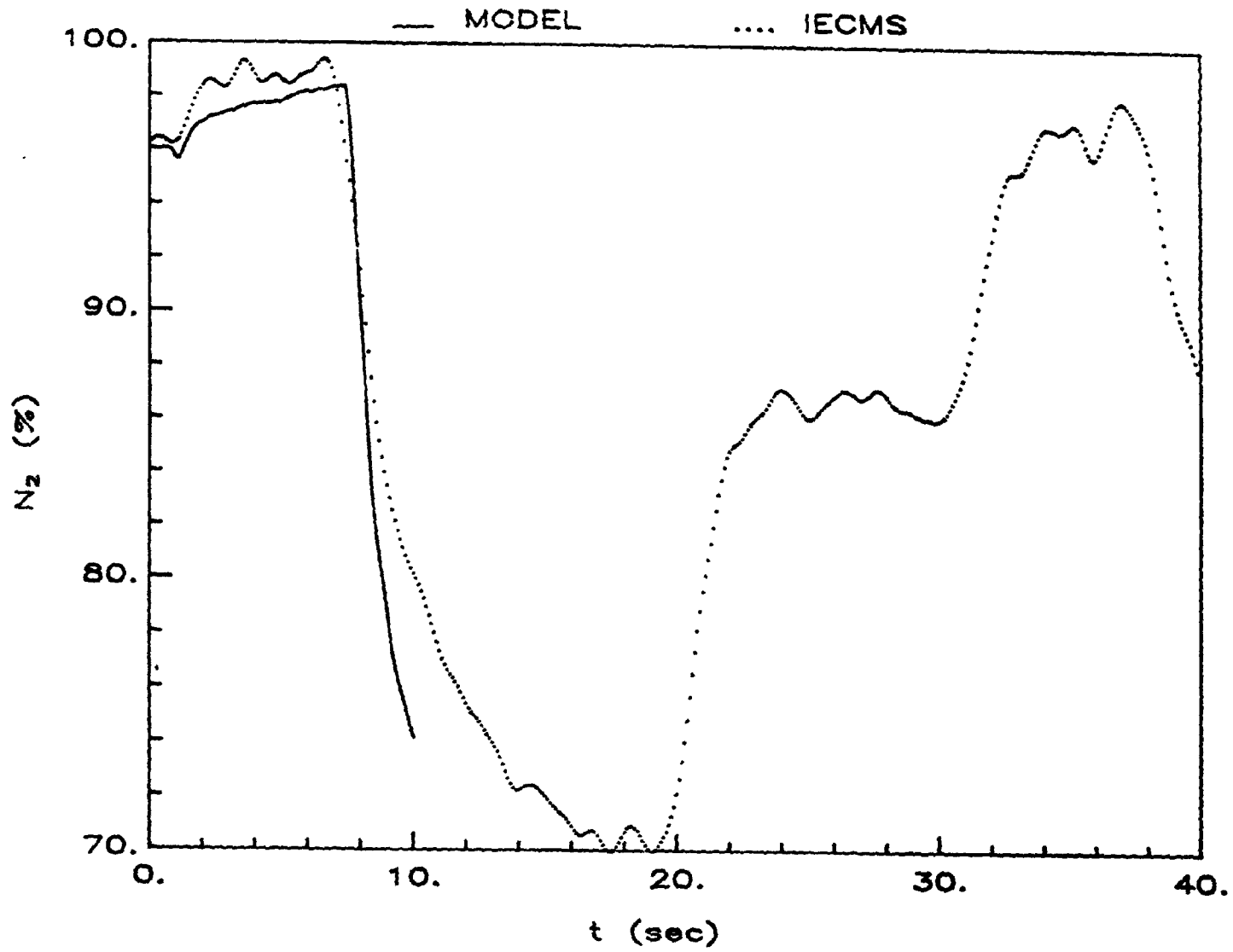

Figure **85** — N2 versus time — 912LB

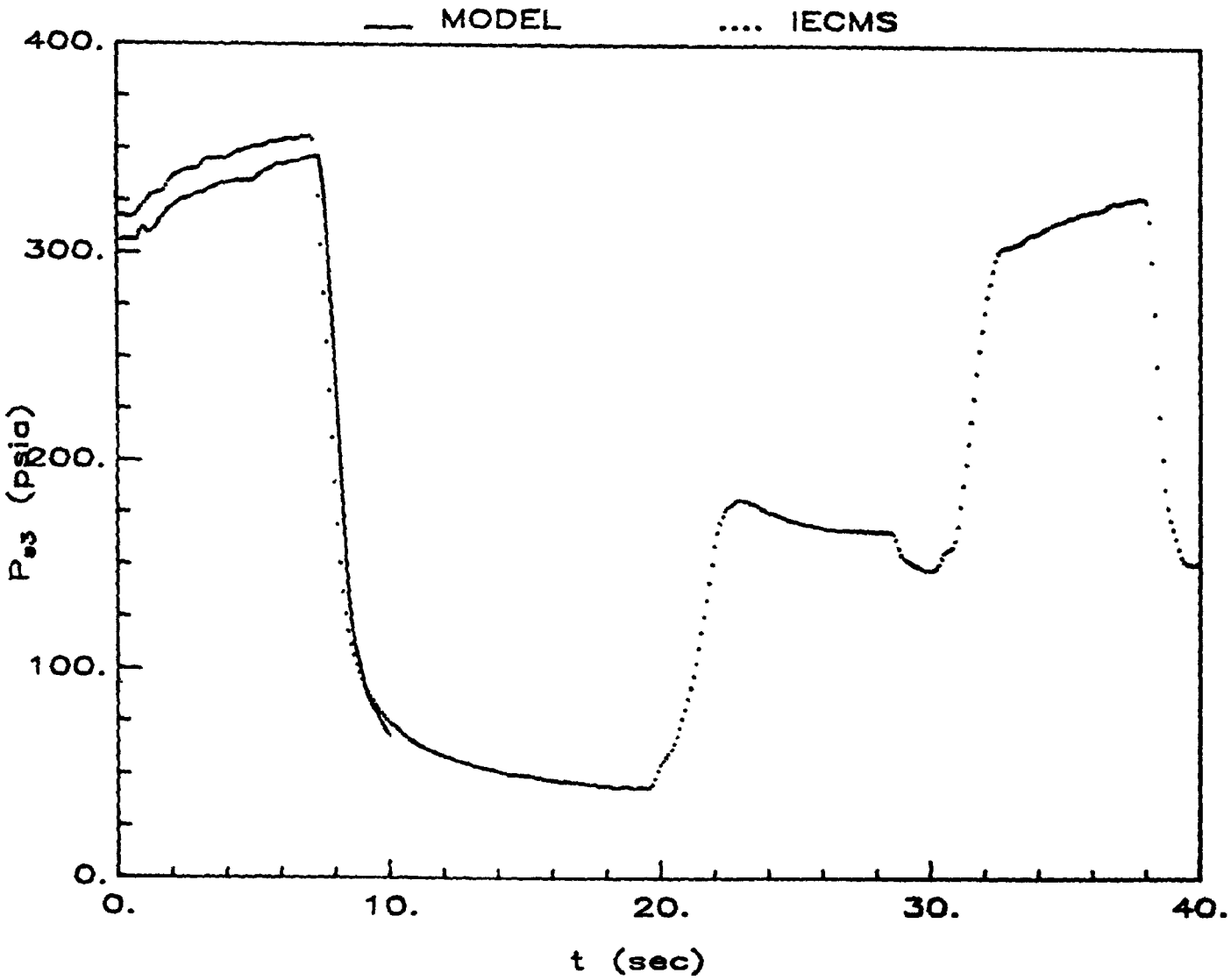

Figure 86 — PS3 versus time — 912LB

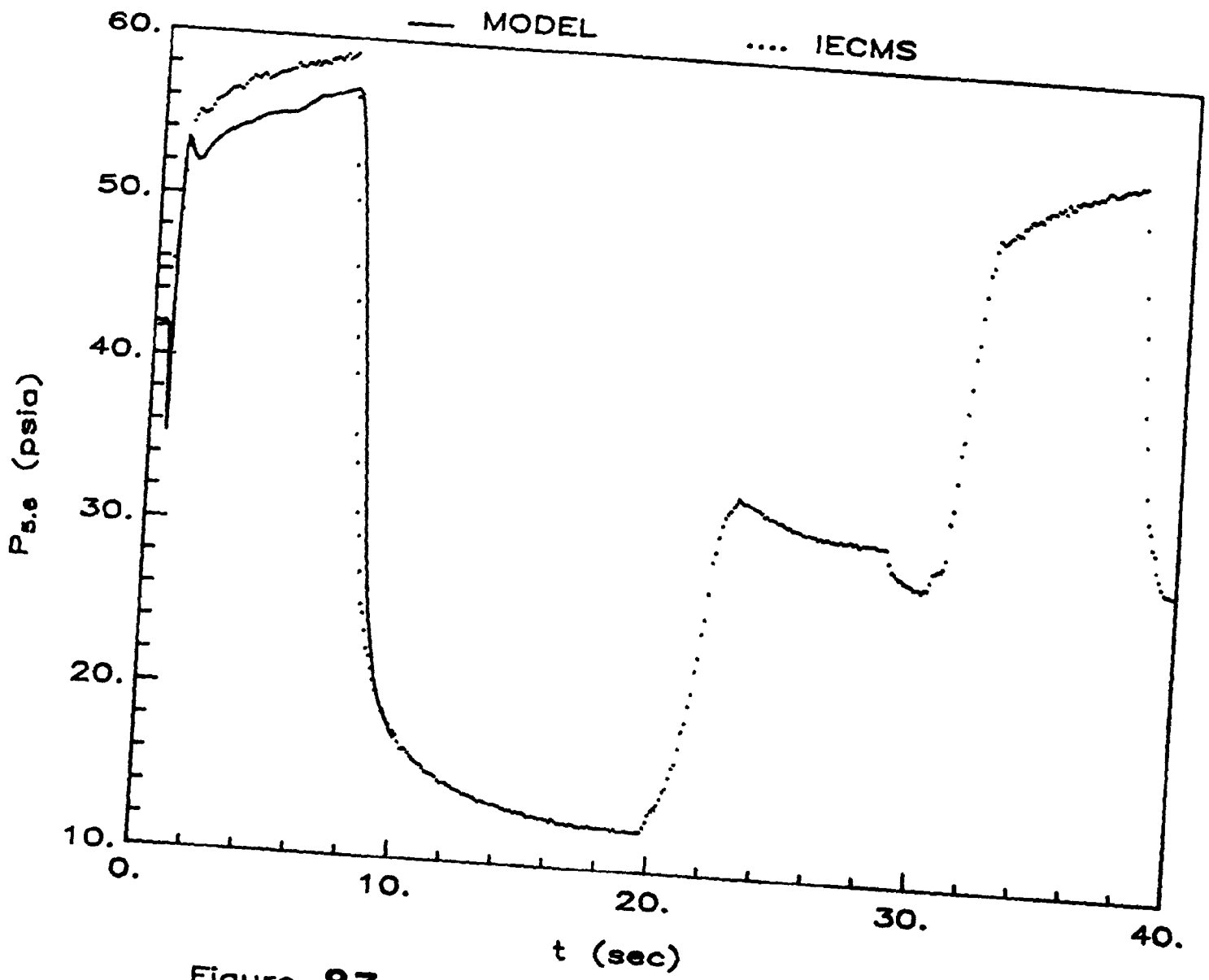

Figure **87** — P56 versus time — 912LB

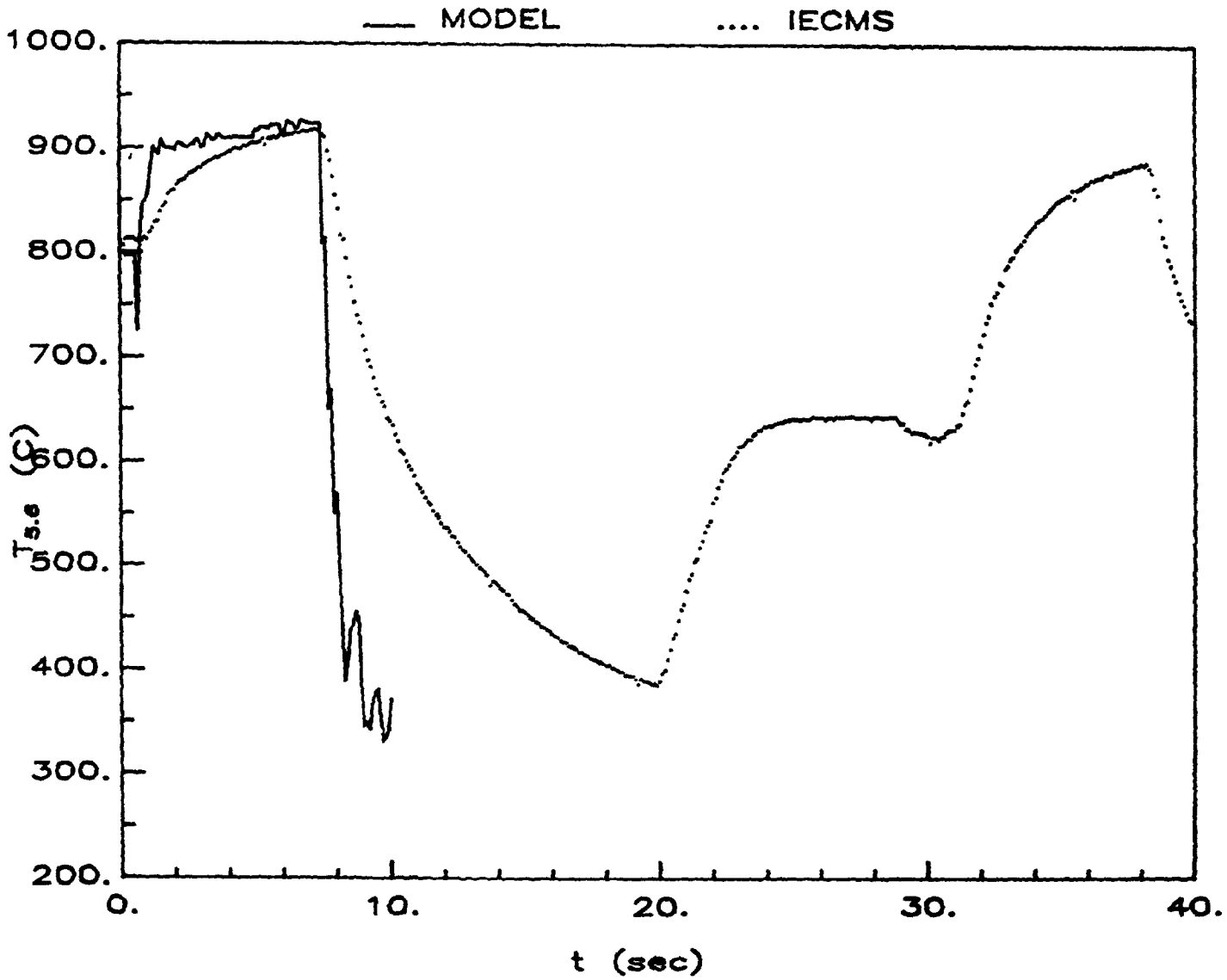

Figure 88 — T56 versus time — 912LB

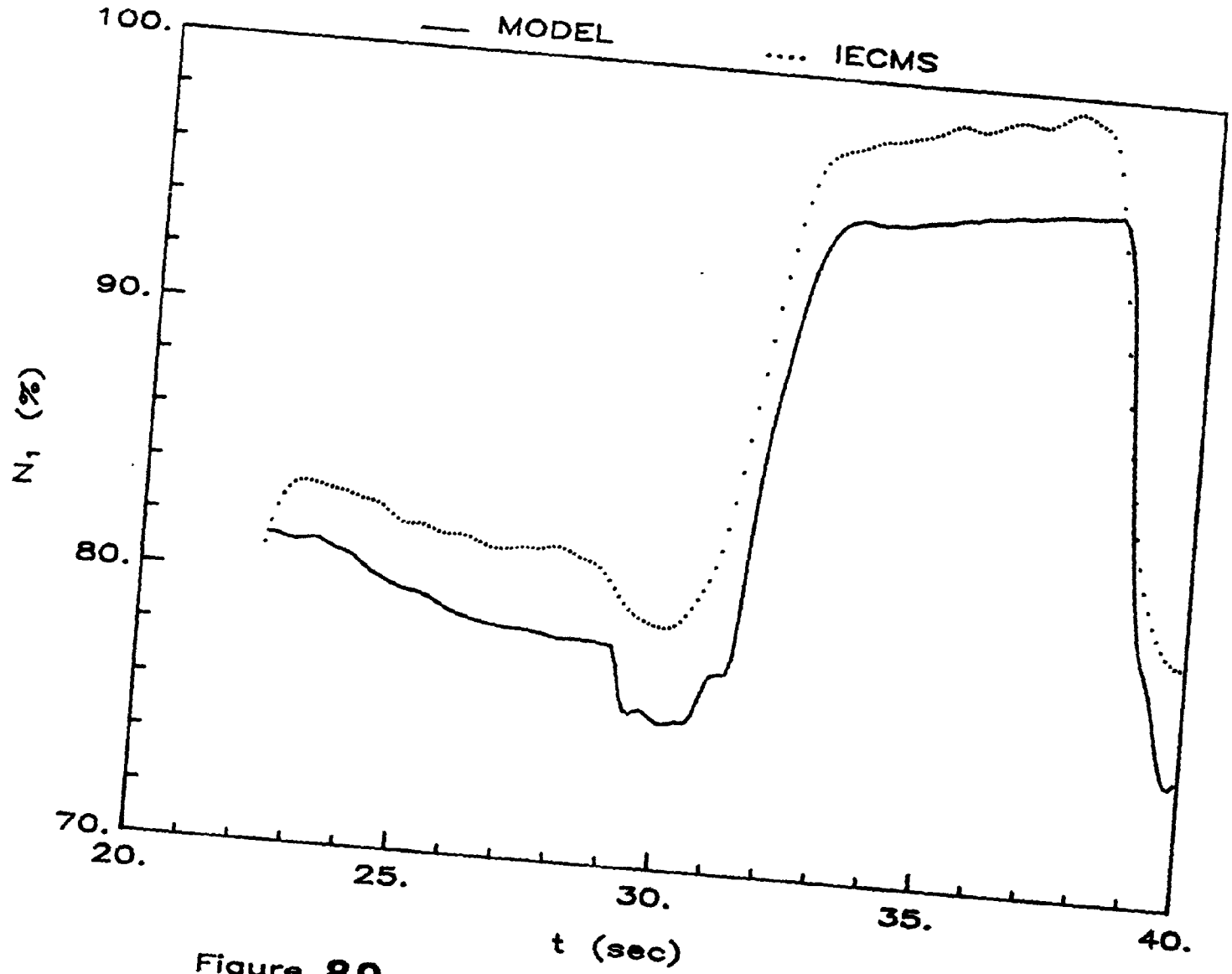

Figure **89** — N1 versus time — 912LB

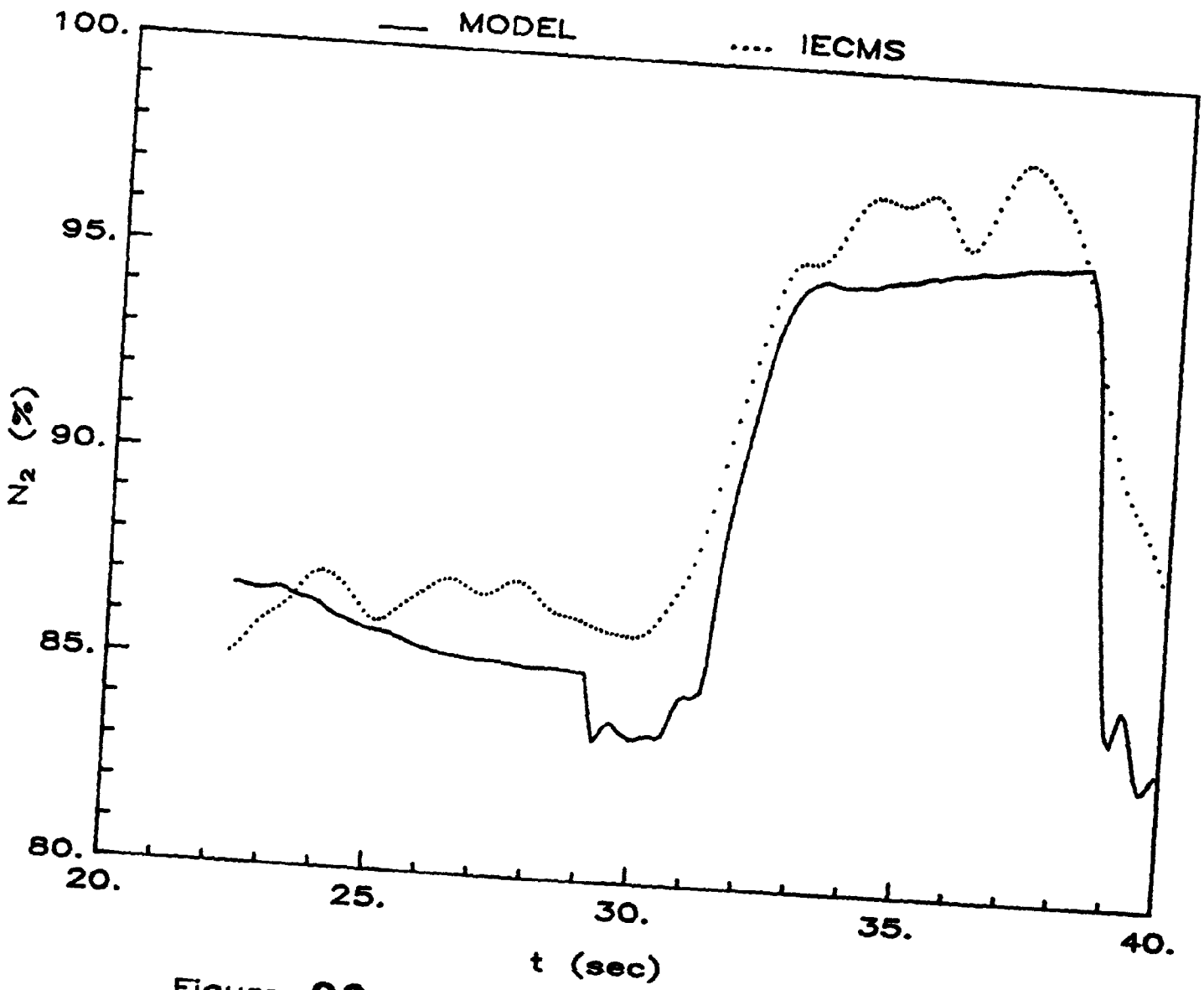

Figure **90** — N2 versus time — 912LB

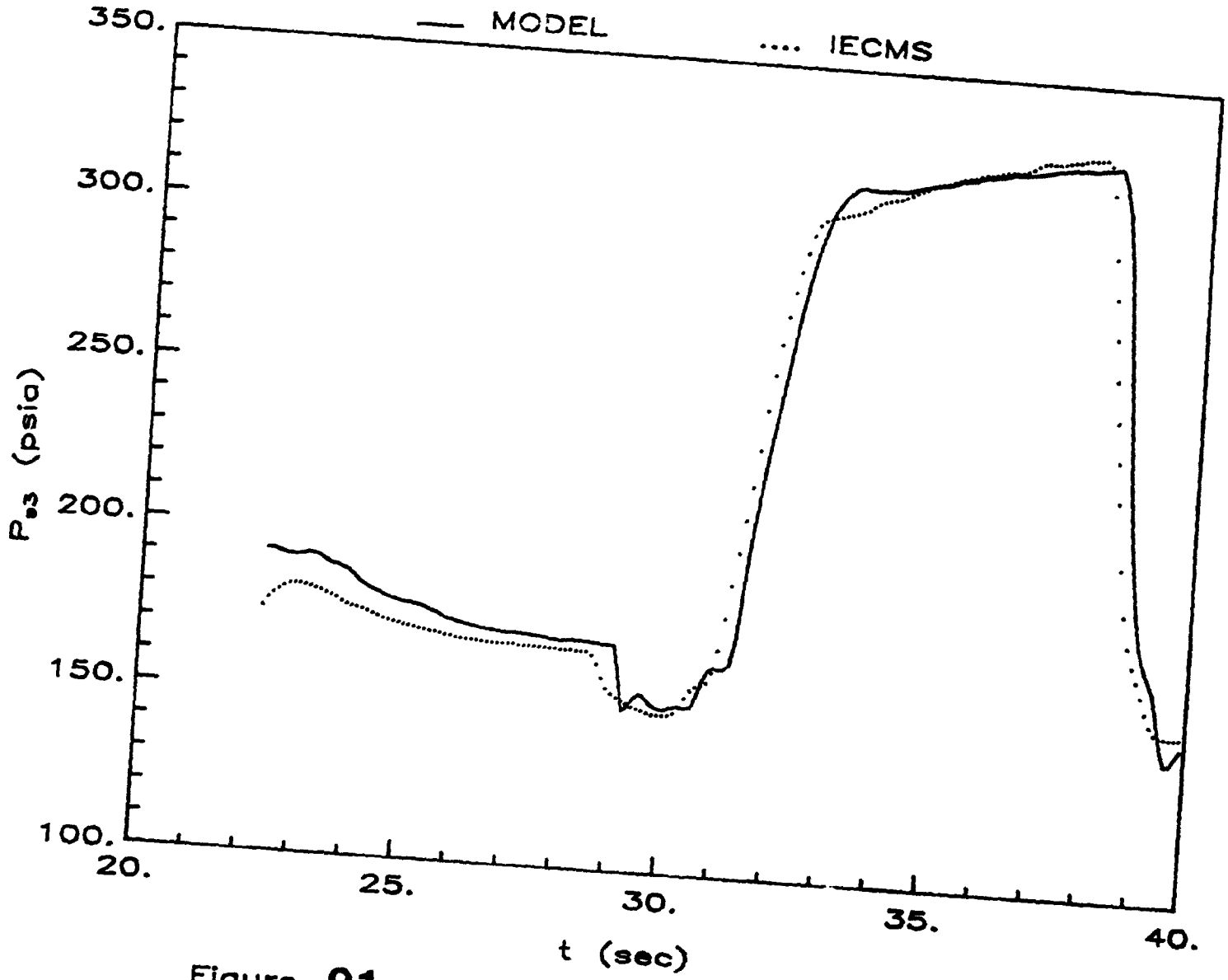

Figure **91** — PS3 versus time — 912LB

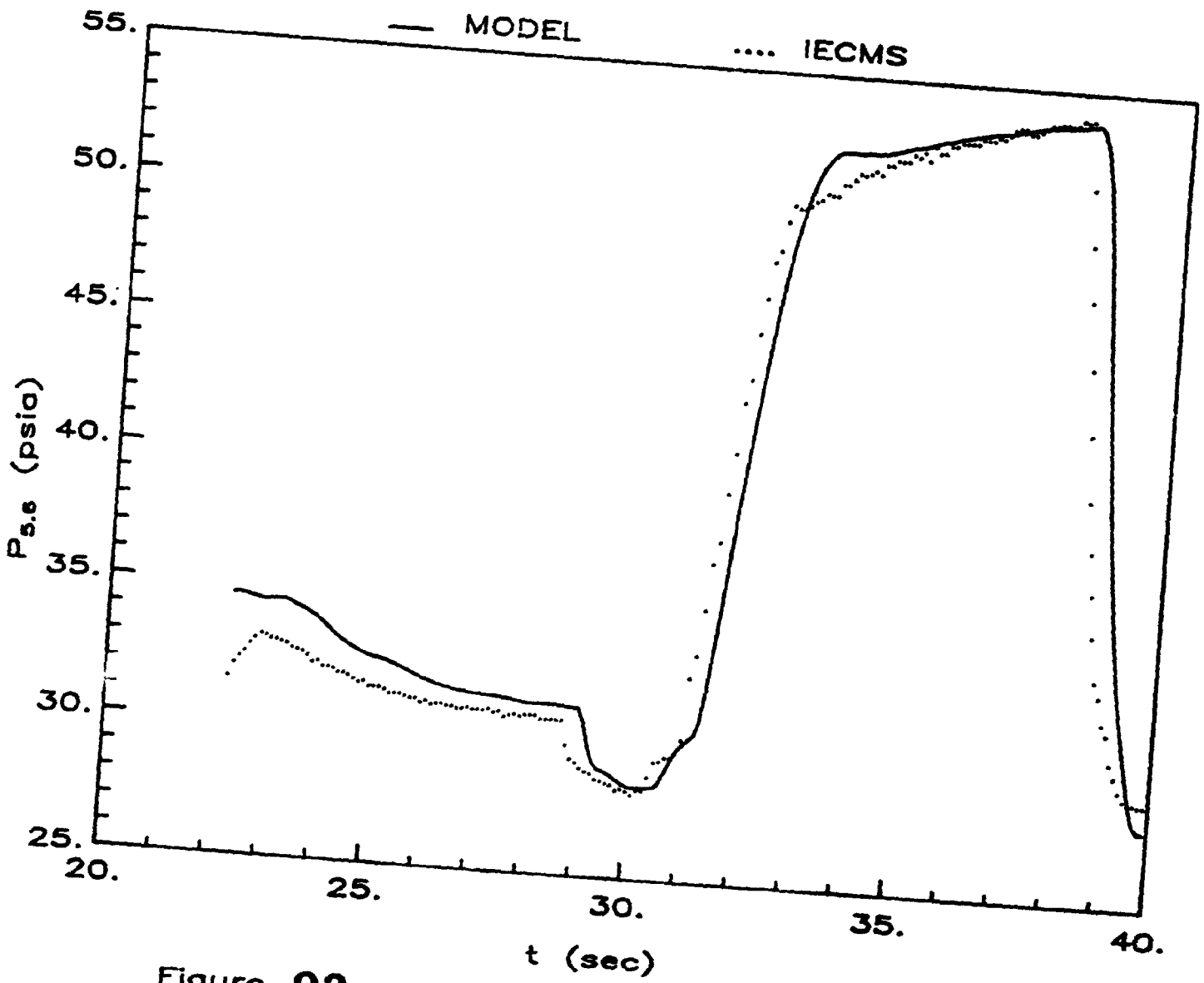

Figure 92 — P56 versus time — 912LB

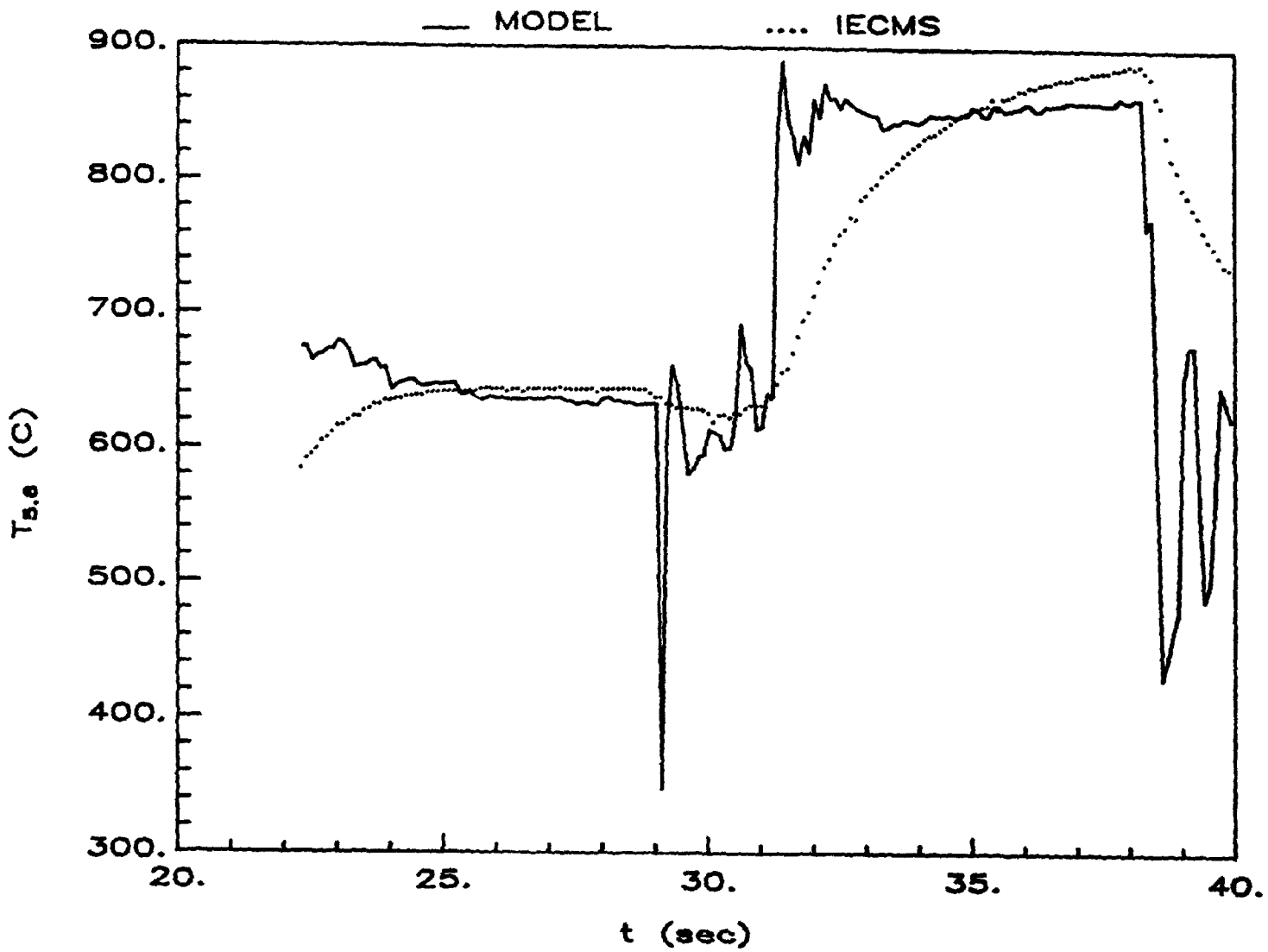

Figure 93 — T56 versus time — 912LB

END

13 09 90

FIN